Cyclic amine functionalisation by engineered cytochrome $P450_{BM3}$

A thesis submitted for the Honour School of Chemistry

DPhil 2020



Yushu Li

Hertford College
University of Oxford

Acknowledgements

I must thank my great supervisor Prof Luet Wong for his continuous support, especially during the hard time of coronavirus outbreak, discreet instructions for both work and life, and inexhaustible patience and tolerance for my intractable character. His warm personality and rigorous scholarship have refreshed my understanding of how to become a good man and an excellent academic researcher. Without him, I would not have completed my DPhil project and thesis with such alacrity. I also quite like the way he wants to bring me back to reality when I immerse myself into all the daydreaming wild research ideas.

I also would like to thank all my colleagues in Wong group. The part II students Harry Bush, Ellie Jaques, Alec Murphy and Alissa Bamford and the undergraduate students Jennifer Jackson and Yonglin Lai have contributed to this thesis. Special thanks are given to Dr Yang Cao, Dr Kouji Urata, Dr Xinkun Ren, Dr Alize Pennec, Wenyu Chen, Matthew Fisher, Yuan Zhang and Alice Wong; they are not only my comrade-in-arms over my entire doctoral period, but also my friends sharing happiness and sorrows day and night.

Many thanks to Robertson group for helping me submit NMR samples. Prof Jeremy Robertson is amongst the most helpful and agreeable organic chemists I have ever met. Chatting with Dr Jack O'Hanlon, Lucy Harwood, Jonathan Moloney, and Alethea Lee on both research topics and life things is enjoyably informative. Thanks to Dr Nick Rees, Prof Tim Claridge and Prof James McCullagh for running service NMR and MS. Many thanks to Prof Max Cryle and Prof Emily Flashman for giving precious suggestions on my thesis!

The physical and mental supports offered by my beloved parents greatly comforted me and assisted me to bravely face the difficulties occurring during my study in Oxford. I am also grateful to my intimate friends Dr Xin Zhou, Jia-hui Khoo, Xi Cao and Dr You Zhao for their companion, knowledge sharing and philosophic discussion.

Contents

Chapter 1 Introduction 1
1.1 Enzyme features of cytochromes P450 (CYPs) 2
1.1.1 Discovery of P450 enzymes 2
1.1.2 The CYP nomenclature system 2
1.1.3 The P450 catalytic cycle 3
1.1.4 General features of CYPs 6
1.1.5 P450 electron transfer chains 8
1.1.6 P450 biotechnology 10
1.2 Cytochrome $P450_{BM3}$ (CYP102A1) 16
1.2.1 Functional studies 17
1.2.2 The structure of $P450_{BM3}$ 18
1.2.3 A variant library screening methodology 27
1.3 Cyclic amine functionalisation in drug discovery 29
1.4 Objective of the thesis 35
Chapter 2 Materials and Methods 37
2.1 Materials, chemicals and equipment 38
2.1.1 Chemicals, solvents and materials 38
2.1.2 General protocols for the synthesis of the target substrates and products 39
2.1.3 Growth media and buffer components 41
2.1.4 Equipment 42
2.2 Molecular biology 42
2.2.1 Mutagenesis primer design 42
2.2.2 Site-directed mutagenesis 44
2.2.3 Agarose gel electrophoresis 45
2.2.4 Post-PCR transformation and DNA purification 45
2.3 Enzyme production in *E. coli* and purification 47
2.3.1 Competent cell preparation 47
2.3.2 DNA Transformation 47
2.3.3 Enzyme production and purification 48
2.3.4 Protein quantification 50
2.4 Activity assays 50
2.4.1 *In vitro* assays 50
2.4.2 *In vivo* assays 51
2.5 Preparative scale synthesis and product characterisation 52
2.5.1 General procedure for preparative scale biotransformation *in vitro* 52
2.5.2 Preparative scale biotransformation *in vivo* 53

2.6 Optical rotation measurements 53

Chapter 3 $P450_{BM3}$ oxidation of *N*-phenyl and *N*-benzyl pyrrolidines and piperidines: Discovery of novel enzymatic Povarov reaction 55

3.1 Introduction 56

3.2 $P450_{BM3}$ oxidation of *N*-phenyl pyrrolidine 60

3.3 $P450_{BM3}$ oxidation of *N*-phenyl piperidine 73

3.4 Attempted trapping of intermediates in enzymatic Povarov reactions 81

3.5 $P450_{BM3}$ oxidation of *N*-benzyl- and *N*-benzoyl-pyrrolidines and piperidines 90

3.6 Summary and discussion 93

Chapter 4 $P450_{BM3}$ oxidation of the fused-ring cyclic amines: Quinolines, tetrahydroquinolines and tetrahydroisoquinolines 96

4.1 Introduction 97

4.2 Oxidation of 1,2,3,4-tetrahydroquinoline (THQ) 101

4.2.1 The initial screening of THQ 101

4.2.2 The mechanisms involved in $P450_{BM3}$ oxidation of THQ 104

4.2.3 Selectivity trends in the oxidation of THQ 106

4.2.4 Engineering the selectivity of THQ oxidation 108

4.2.5 Scalability and time-course of biotransformation of THQ 109

4.2.6 Summary 111

4.3 Oxidation of 3,4-dihydro-2-quinolinone 111

4.4 Oxidation of 5,6,7,8-tetrahydroquinoline (THQ'), 5,6,7,8-tetrahydro-isoquinoline (THIQ'), 5,6,7,8-tetrahydro-quinoxaline (THQX) and 1,2,3,4-tetrahydroisoquinoline (THIQ) 114

4.5 Oxidation of quinoline 116

4.6 Summary 119

Chapter 5 Effect of substituents on the oxidation of quinoline and tetrahydroquinoline derivatives by $P450_{BM3}$ 124

5.1 Introduction 125

5.2 Substituent effects on the oxidation of the THQ core 125

5.2.1 Oxidation of 2Me-THQ 125

5.2.2 Oxidation of 6Me-THQ and 6MeO-THQ 127

5.2.3 Oxidation of 8Me-THQ 135

5.2.4 Overall perspective of substituent effects on THQ oxidation 137

5.3 Substituent effects on the oxidation of the quinoline core 139

5.3.1 Oxidation of 2Me-Q 139

5.3.2 Oxidation of 6Me-Q 141

5.3.3 Oxidation of 8Me-Q 143

5.3.4 Overall perspective of the substituent effects on quinoline oxidation 146

5.4 Summary 149
Chapter 6 The role of protecting groups in P450$_{BM3}$ oxidation of cyclic amines 151
6.1 Introduction 152
6.2 P450$_{BM3}$ oxidation of the protected THQs 153
6.2.1 Oxidation of *N*-Boc-THQ 153
6.2.2 Oxidation of *N*-Ac-THQ 156
6.2.3 Oxidation of *N*-Ms-THQ 158
6.2.4 Oxidation of *N*-Ips-THQ 160
6.2.5 The role of protecting group in P450$_{BM3}$ oxidation of THQ 161
6.3 P450$_{BM3}$ oxidation of the protected THIQs 162
6.3.1 Oxidation of *N*-Boc-THIQ 162
6.3.2 Oxidation of *N*-Ac-THIQ 165
6.3.3 Oxidation of *N*-Ms-THIQ 167
6.3.4 Oxidation of *N*-Ips-THIQ 168
6.3.5 The effect of protecting group on P450$_{BM3}$ oxidation of THIQ 170
6.4 P450$_{BM3}$ oxidation of protected single-ring cyclic amines 172
6.4.1 Oxidation of *N*-Boc-pyrrolidine 172
6.4.2 Oxidation of *N*-Boc-piperidine 175
6.4.3 Summary of P450$_{BM3}$ oxidation of *N*-Boc-pyrrolidine and piperidine 178
6.5 Protecting group effects on P450$_{BM3}$ oxidation of cyclic amines 179
Chapter 7 Remote functionalisation of lactams 182
7.1 Introduction 183
7.2 P450$_{BM3}$ oxidation of γ-butyrolactam (pyrrolidin-2-one) 187
7.2.1 Oxidation of *N*-phenyl-γ-butyrolactam 187
7.2.2 Oxidation of *N*-benzyl-γ-butyrolactam 189
7.3 P450$_{BM3}$ oxidation of δ-velarolactam (piperidin-2-one) 190
7.3.1 P450$_{BM3}$ oxidation of *N*-Boc-δ-velarolactam 191
7.3.2 Oxidation of *N*-benzyl-δ-velarolactam 192
7.4 P450$_{BM3}$ oxidation of ε-caprolactams 194
7.4.1 Oxidation of *N*-Boc-ε-caprolactam 194
7.4.2 Oxidation of *N*-benzyl-ε-caprolactam 196
7.5 Oxidation of *N*-benzyl-ζ-enantholactam 197
7.6 P450$_{BM3}$ oxidation of spirolactams 200
7.6.1 Oxidation of *N*-benzyl-2-azaspiro[4.5]decan-3-one 200
7.6.2 Oxidation of *N*-benzyl-2-azaspiro[4.6]undecane-3-one 201
7.6.3 Oxidation of 8-azaspiro[4.5]decanes and its imide derivatives 206
7.7 Summary and outlook 211

Chapter 8 Conclusion and outlook 214
8.1 Summary 215
8.2 Future work and outlook 219
Reference 221
Appendices A1

Table of figures

Figure 1 Overview of investigated cyclic amines and lactams, the highest hydroxylation selectivity at non-activated C–H bonds, and new $P450_{BM3}$ activities in this dissertation.
Figure 1.1 The catalytic pathway of P450.
Figure 1.2 The proposed catalytic pathways of P450-catalysed epoxidation and aromatisation.
Figure 1.3 The P450 fold illustrated with the structure of substrate-bound $P450_{BM3}$ (PDB code: 1jpz).
Figure 1.4 Electron-transfer in P450cam.[104–106]
Figure 1.5 Electron-transfer in Class II cytochrome P450s.[111–115,117,118]
Figure 1.6 Examples of substrate engineering in P450-catalysed biotransformations.[162,163]
Figure 1.7 Schematic workflow of rational design and directed evolution approaches for enzyme engineering.
Figure 1.8 The organisation of CYP102A1 gene. (CD: connecting domain)
Figure 1.9 Electron transfer of the BMR domain in $P450_{BM3}$.
Figure 1.10 Overlay of the SF (green) and NPG-bound (SB, orange) crystal structures of $P450_{BM3}$.
Figure 1.11 Structural differences in the I-helix region in SF (green) and SB (orange) $P450_{BM3}$.
Figure 1.12 The substrate access channel of NPG-bound wild type $P450_{BM3}$.
Figure 1.13 The water distributions close to the heme prosthetic groups in SB WT (A) and SF A82F (B).
Figure 1.14 Views of the substrate access channel in the SB WT.
Figure 1.15 The lateral wall constructed by T260/I263/A264/T436/A328/P329 and the bottom occuppied by A330 of the substrate access channel of the SB WT and the hydrogen bonding network of E267/T268.
Figure 1.16 Overlay of the crystal structures of SF A330P (yellow, water in red) and WT (grey, water in cyan).
Figure 1.17 A selection of successful research in Wong group undertaking the variant library screening methodology.
Figure 1.18 Overlay of the SF I401P (magenta) and SB WT (orange) crystal structures.
Figure 1.19 Overlay of the SF KT2 (cyan) and the SB WT (orange) crystal structures.
Figure 1.20 Simplified illustration of the principles for HTS and FBDD.
Figure 1.21 Lead identification by fragment-evolving and fragment-linking.[377]
Figure 1.22 A collection of alkaloid drugs.
Figure 1.23 Available methodologies to obtain the α-functionalised cyclic amine derivatives. (HAT: hydrogen atom transfer)
Figure 1.24 Examples of direct β- & γ-functionalisation of cyclic amines via transition metal catalysis.[411–413]
Figure 1.25 P450 oxidation of single-ring and complex cyclic amines and lactams.[220,415,419,420,422–425,447]
Figure 1.26 Proposed mechanisms for predominant P450-catalysed oxidation activities towards amines.
Figure 1.27 A collection of the investigated cyclic amines and lactams in this dissertation.
Figure 3.1 A selection of pharmaceutics containing *N*-phenyl and *N*-benzyl cyclic amines and the reaction scheme of P411 C–H functionalisation of *N*-phenyl pyrrolidine derivatives.[451,452]

Figure 3.2 Examples of microsomal, bacterial and fungal P450 oxidation of *N*-phenyl and *N*-benzyl pyrrolidines and piperidines, and their proposed mechanisms for their commonly-observed *N*-oxidation and *N*-dealkylation activities.[414,420–423,453,454,456,457,459]
Figure 3.3 Gas chromatograms for the P450$_{BM3}$-catalysed oxidation for *N*-phenyl pyrrolidine, **1**.
Figure 3.4 GC analysis for the R19/F87A/A328I-catalysed biotransformation of **1** at 7 h and 18 h.
Figure 3.5 The reaction scheme of P450$_{BM3}$ oxidation of *N*-phenyl pyrrolidine, **1**.
Figure 3.6 The comparison between the NOESY spectra for **5** and **6**.
Figure 3.7 The proposed mechanisms of aromatic hydroxylation of *N*-phenyl pyrrolidine (**1**).
Figure 3.8 The proposed mechanisms of α-oxidation of *N*-phenyl pyrrolidine (**1**) including further oxidation, dealkylation and the Povarov reaction.
Figure 3.9 Natural products with **5** as their scaffolds[468,469] and previous studies on Povarov reactions yielding **5** and **6**.[463,464,475,477–480]
Figure 3.10 The reaction scheme of P450$_{BM3}$ oxidation of *N*-phenyl piperidine, **7**.
Figure 3.11 Comparison between the COSY spectra of **10** and **11**.
Figure 3.12 The ^{1}H NMR spectrum of **12** containing <23% impurity.
Figure 3.13 The proposed mechanism of the formation of the enamine dimer **12**.
Figure 3.14 GC analysis of P450$_{BM3}$ oxidation of **7** showing titre dependence.
Figure 3.15 Binding titration of *N*-phenyl piperidine, **7**, with the GVQ mutant showing single-site binding.
Figure 3.16 The reactions involving iminium, enamine and enamine radical cation as their indispensable intermediates.[483,484,493–496,485–492]
Figure 3.17 A selection of trapping reagents and their potential cross-coupling products.
Figure 3.18 GC graphs of the cross-coupling reactions of 1,2,3,4-tetrahydroquinoline (THQ) and **1**/**7** (1 : 1).
Figure 3.19 The enzymatic cross-coupling of *N*-phenyl pyrrolidine (**1**)/1,2,3,4-tetrahydroquinoline (**13**) and *N*-phenyl piperidine (**7**)/**13**.
Figure 3.20 Comparison between the COSY spectra for **14**/**15** and **18**/**19**.
Figure 3.21 Snapshots of the ^{1}H and COSY NMR spectra for **16** and **20** which directed their assignments.
Figure 3.22 The assignment of the ^{1}H NMR of the trimer **17** (with the solvent peaks subtracted), illustrated by its COSY NMR.
Figure 3.23 The proposed mechanisms of the P450$_{BM3}$-catalysed cross-coupling of **1**/**7** and **13**.
Figure 3.24 The overlay of the substrate-free crystal structures of P450pyr (PDB: 3rwl[421], in magenta with the key regions highlighted in salmon and residues labelled in white) and P450$_{BM3}$ (PDB: 1bu7, in cyan with the key regions highlighted in yellow and residues labelled in black).
Figure 3.25 The tested substrates and the reaction schemes of P450$_{BM3}$ oxidation of **1** and **7**.
Figure 3.26 The R19/F87A/A328I-catalysed cross-coupling of **1**/**7** and **13**.
Figure 4.1 Examples of *N*-phenyl cyclic amine drugs which also contain fused-ring cyclic amine moieties.
Figure 4.2 A selection of drug molecules with fused-amine-ring scaffolds.
Figure 4.3 Examples of Pd(II)-catalysed fused-ring cyclic amine formation.[497–502]
Figure 4.4 Previous research on P450 oxidation of quinoline and isoquinoline derivatives.[264,426,427,451,506,507]
Figure 4.5 Fused-ring substrates tested in this chapter.

Figure 4.6 The reaction scheme of P450$_{BM3}$ oxidation of THQ (**13**).
Figure 4.7 Time-course monitoring of the RP/H171L/I263G-catalysed reaction oxidising 6-hydroxy-THQ, **21**, to afford 6-hydroxyquinoline, **27**.
Figure 4.8 The ^{1}H NMR spectrum of **26** with snapshots of the its COSY and HSQC NMR spectra.
Figure 4.9 The ^{1}H NMR spectra of (a) **31**, (b) **29** and **31**, and (c) **29** (subtracted spectrum).
Figure 4.10 The proposed mechanism of the formation of **21**.
Figure 4.11 The proposed mechanisms of the C2 oxidation of THQ by P450$_{BM3}$.
Figure 4.12 GC traces of the screening reactions using the variants in the TFA/B and WY3/4 plates showing highest selectivity for **21**–**25**.
Figure 4.13 GC analysis of time-course monitoring the reactions with R19/F87A/A328L at 2.3 mM, 10 mM and 20 mM of **1**, and with RP/H171L/I263G at 5 mM of **1**; all with 1 μM P450$_{BM3}$.
Figure 4.14 The time-course of the biotransformation of **25** by the R19/F87A/A328I variant.
Figure 4.15 GC analysis of THQ oxidation with peaks in monomer oxidation window by GV/A184I.
Figure 4.16 The proposed mechanism of Cα–Cβ desaturation, C3/C4 hydroxylation of **24** by P450$_{BM3}$.[516]
Figure 4.17 Reaction schemes of P450$_{BM3}$ oxidation of THIQ (**37**), THQ' (**38**), THIQ' (**42**), and THQX (**45**).
Figure 4.18 The reaction scheme of P450$_{BM3}$ of quinoline (**22**).
Figure 4.19 The ^{1}H NMR spectra of 6-hydroxy-quinoline (**27**) and 3,6-dihydroxy-quinoline (**50**).
Figure 4.20 P450$_{BM3}$ oxidation of quinoline and isoquinoline derivatives.
Figure 5.1 Overview of the oxidation activities for THQ, Q and 3,4-dihydro-2quinolinone given by P450$_{BM3}$ variants and the substrates tested in this chapter.
Figure 5.2 The reaction scheme and GC analysis of P450$_{BM3}$ oxidation of 2Me-THQ (**52**).
Figure 5.3 The reaction scheme of P450$_{BM3}$ oxidation of 6Me-THQ (**56**).
Figure 5.4 The reaction scheme of P450$_{BM3}$ oxidation of 6MeO-THQ (**64**).
Figure 5.5 GC analysis of the oxidation of 6MeO-THQ (**64**) by the variants K19/A82M/F87A and I263G.
Figure 5.6 The ^{1}H NMR spectrum of **67**.
Figure 5.7 The ^{1}H NMR spectrum of **66**.
Figure 5.8 Proposed mechanisms for the formation of the C–H amination product **66**.
Figure 5.9 The reaction scheme of P450$_{BM3}$ oxidation of 8Me-THQ (**70**).
Figure 5.10 The reaction scheme of P450$_{BM3}$ oxidation of 2Me-Q (**54**).
Figure 5.11 The reaction scheme of P450$_{BM3}$ oxidation of 6Me-Q (**57**).
Figure 5.12 The reaction scheme of P450$_{BM3}$ oxidation of 8Me-Q (**72**).
Figure 5.13 The summary of P450$_{BM3}$ oxidation of THQs and Qs.
Figure 6.1 Previous research on P450 oxidation of simple cyclic amines.[337,414–417]
Figure 6.2 General reaction scheme of P450$_{BM3}$ oxidation of *N*-protected-THQs.
Figure 6.3 NIH shift products of P450-catalysed aromatic oxidation of *N*-Boc-THIQ.
Figure 6.4 The reaction scheme of oxidation of *N*-Ms-THIQ (**143**) with RP/H171L/I263G/L437LV.
Figure 6.5 General reaction scheme of P450$_{BM3}$ oxidation of *N*-protected-THIQs.
Figure 6.6 The chiral GC analysis of the screening reactions of **155** with P450$_{BM3}$.
Figure 6.7 The proposed mechanisms of the formation of **164**.
Figure 6.8 Summary of P450$_{BM3}$ oxidation of *N*-protected piperidine, THQs and THIQs.
Figure 6.9 The comparison between C3 oxidation of the lactam **139** and the amine **131** by P450$_{BM3}$.

Figure 7.1 Examples of β-functionalisation of cyclic amines catalysed by transition metal catalysts.[551,552]
Figure 7.2 The selectivity patterns for P450$_{BM3}$ oxidation of molecules of THQ core to reveal lactams as available substrates.
Figure 7.3 An example of functionalisation of lactam and routes to functionalised cyclic amines.[553,554]
Figure 7.4 Examples of drugs and alkaloids possessing lactam and imide cores.
Figure 7.5 A selection of biohydroxylation of monocyclic,[415,419,420,422,423] fused-ring[423,424,447] and spirocyclic lactams[220,423,425] by *Beauveria bassiana* ATCC7159, *Cunninghamella elegans*, P450pyr and P450$_{BM3}$.
Figure 7.6 The reaction scheme of P450$_{BM3}$ oxidation of 2-azaspiro[4.6]undecan-3-one (**211**).
Figure 7.7 The reaction scheme of P450$_{BM3}$ oxidation of *N*-benzyl 2-azaspiro[4.6]undecan-3-one (**214**).
Figure 7.8 The ^{1}H NMR spectrum of **216** (b-OH and b*-OH).
Figure 7.9 The ^{1}H NMR of **217** (c-OH and c*-OH).
Figure 7.10 The reaction scheme of the R19/P329G/A330W-catalysed oxidation of **214**.
Figure 7.11 The ^{1}H NMR of **220**.
Figure 7.12 The reaction schemes of P450$_{BM3}$ oxidation of 8-azaspiro[4.5]decane (**221**) and 8-azaspiro[4.5]decane-7,9-dione (**222**).
Figure 7.13 The reaction scheme of the RP/F87V-catalysed oxidation of *N*-Boc-8-azaspiro[4.5]decane.
Figure 7.14 Reaction scheme of P450$_{BM3}$ oxidation of *N*-benzyl-8-azaspiro[4.5]decane-7,9-dione (**229**).
Figure 7.15 The highest P450$_{BM3}$ oxidation selectivities discovered for the lactams and imides studied in the present work.
Figure 8.1 The summary of the oxidation of all the cyclic amines and lactams tested in this thesis by engineered P450$_{BM3}$.

Table of tables

Table 2.1 Growth media components.
Table 2.2 Buffer components.
Table 2.3 Components for site-directed mutagenesis using KOD Hot Start Polymerase.
Table 2.4 Cycling conditions for KOD Hot Start DNA Polymerase.
Table 2.5 The primers for sequencing the $P450_{BM3}$ gene.
Table 2.6 Components of 10× FB_{gly} and $FB_{supplement}$.
Table 2.7 Components of the induction solution (sterilised by filtration).
Table 2.8 The preparation of the *in vitro* reaction solution.
Table 2.9 The preparation of the *in vivo* reaction solution.
Table 3.1 The TFA & TFB variant library based on K19, KT2, A330P and I401P with active site mutations introduced at R47, Y51, S72, V78, F81, A82, F87, A184, L188, I263, E267, A328, P329, Q403 and L437.
Table 3.2 The product distribution of the $P450_{BM3}$ variants (1 μM) under the condition of adding 2 mM of **1**.
Table 3.3 The product distribution of the $P450_{BM3}$ variants (1 μM) in the oxdation of **1**.
Table 3.4 The dimer fomation of the $P450_{BM3}$ variants (1 μM) oxidising **1**.
Table 3.5 The dimer ratio of the $P450_{BM3}$ variants showing constant *exo* : *endo* dimer formation.
Table 3.6 The selectivity trends for **2**, **8**–**12** under 2 mM/5 mM substrate concentrations from the screening reactions.
Table 3.7 The *exo* : *endo* dimer ratio (**10** : **11**) and the total dimer yield of $P450_{BM3}$ oxidation of **7** (2 mM and 5 mM).
Table 3.8 The conversion and product distribution of the cross-coupling of **1**/**7** and **13**.
Table 4.1 The conversion and product distributions of $P450_{BM3}$ oxidation of THQ (**13**).
Table 4.2 Engineering of the C5,C6 oxidation product, **21**, and the C2,C3 oxidation product, **23**.
Table 4.3 Summary of mutation effects promoting $P450_{BM3}$ oxidation of THQ (**13**). Further oxidation labelled in blue.
Table 4.4 Conversion and product distribution of $P450_{BM3}$ oxidation of 3,4-dihydro-2-quinolinone (**24**).
Table 4.5 Summary of mutation effects promoting $P450_{BM3}$ oxidation of 3,4-dihydro-2-quinolinone (**24**).
Table 4.6 The conversion and product distribution of $P450_{BM3}$ oxidation of THQ', THIQ', and THQX.
Table 4.7 Summary of mutation effects promoting $P450_{BM3}$ oxidation of THQ', THIQ' and THQX.
Table 4.8 The conversion and product distribution of P450BM3 oxidation of quinoline (**22**).
Table 4.9 Summary of mutation effects promoting $P450_{BM3}$ oxidation of quinoline (**22**).
Table 4.10 The correlation between substrate properties and $P450_{BM3}$ oxidation of quinoline and isoquinoline derivatives.
Table 4.11 Effect of mutations on $P450_{BM3}$ oxidation of all substrates in Chapter 4. (Major oxidation activity in red; modest and low oxidation activity in blue).
Table 5.1 Conversion and product distribution of $P450_{BM3}$ oxidation of 2Me-THQ (**52**).
Table 5.2 The mutation effects on $P450_{BM3}$ oxidation of 2Me-THQ (**52**).
Table 5.3 The conversion and product distribution of $P450_{BM3}$ oxidation of 6Me-THQ (**56**).
Table 5.4 The mutation effects on $P450_{BM3}$ oxidation of 6Me-THQ (**56**).
Table 5.5 Conversion and product distribution of $P450_{BM3}$ oxidation of 6MeO-THQ, **64**.

Table 5.6 Mutation effects on P450$_{BM3}$ oxidation of 6MeO-THQ (**64**).
Table 5.7 The conversion and product distribution of P450$_{BM3}$ oxidationof 8Me-THQ (**70**).
Table 5.8 Mutation effects on P450$_{BM3}$ oxidation of 8Me-THQ (**70**).
Table 5.9 The summary of the oxidation of THQs by the P450$_{BM3}$ variant library.
Table 5.10 The summary of the mutation effects shown in P450$_{BM3}$ oxidation of THQs.
Table 5.11 The conversion and product distribution of P450$_{BM3}$ oxidation of 2Me-Q (**54**).
Table 5.12 Mutation effects on P450$_{BM3}$ oxidation of 2Me-Q.
Table 5.13 Conversion and product distribution of P450$_{BM3}$ oxidation of 6Me-Q (**57**).
Table 5.14 Mutation effects on P450$_{BM3}$ oxidation of 6Me-Q (**57**).
Table 5.15 Conversion and product distribution of P450$_{BM3}$ oxidation of 8Me-Q (**72**).
Table 5.16 Mutation effects on P450$_{BM3}$ oxidation of 8Me-Q (**72**).
Table 5.17 The oxidation of quinoline and its derivatives by the 48 P450$_{BM3}$ variant libraries.
Table 5.18 The mutation effects on P450$_{BM3}$ oxidation of quinoline and its methyl derivatives.
Table 6.1 Conversion and product distribution of P450$_{BM3}$ oxidation of **103**.
Table 6.2 Conversion and production distribution of further oxidation of *N*-Boc-THQ (**103**).
Table 6.3 Mutation effects on P450$_{BM3}$ oxidation of *N*-Boc-THQ (**103**).
Table 6.4 The conversion and product distribution of 16-hour P450$_{BM3}$ biotransformation of *N*-Ac-THQ.
Table 6.5 The mutation effects on P450$_{BM3}$ oxidation of *N*-Ac-THQ (**113**).
Table 6.6 Conversion and product distribution of P450$_{BM3}$-catalysed oxidation of *N*-Ms-THQ (**118**).
Table 6.7 Conversion and product distribution of further oxidation of *N*-Ms-THQ by P450$_{BM3}$.
Table 6.8 The mutation effects on P450$_{BM3}$ oxidation of *N*-Ms-THQ (**118**).
Table 6.9 The conversion and product distribution of P450$_{BM3}$ oxidation of *N*-Ips-THQ (**127**).
Table 6.10 The conversion and product distribution of P450$_{BM3}$ oxidation of *N*-Boc-THIQ (**131**).
Table 6.11 Conversion and product distribution of *N*-Boc-THIQ (**131**) oxidised by the 2nd generation P450$_{BM3}$ variants. (R1 = R47L/Y51F/H171L)
Table 6.12 The conversion and further oxidation of P450$_{BM3}$ oxidation of *N*-Ac-THIQ (**137**).
Table 6.13 The conversion and product distribution of P450$_{BM3}$ oxidation of *N*-Ms-THIQ (**143**).
Table 6.14 The conversion and product distribution for oxidation of *N*-Ips-THIQ (**148**) by P450$_{BM3}$.
Table 6.15 Mutation effects on P450$_{BM3}$ oxidation of *N*-Ips-THIQ (**148**).
Table 6.16 Conversion and product distribution of P450$_{BM3}$ oxidation of *N*-Boc pyrrolidine (**155**).
Table 6.17 The conversion and product distribution of P450$_{BM3}$ oxidation of *N*-Boc-piperidine (**159**).
Table 7.1 The conversion and product distributions of P450$_{BM3}$-catalysed reactions yielding **167**–**170**.
Table 7.2 The conversion and product distribution of P450$_{BM3}$ oxidation of *N*-benzyl-γ-butyrolactam, **171**.
Table 7.3 The conversion and product distribution of P450$_{BM3}$ oxidation of *N*-Boc-δ-velarolactam, **177**.
Table 7.4 The conversion and product distribution of P450$_{BM3}$ oxidation of *N*-benzyl-δ-velarolactam, **181**.

Table 7.5 Conversion and product distribution of P450$_{BM3}$ oxidation of *N*-Boc ε-caprolactam (**188**).
Table 7.6 Conversion and product distribution of P450$_{BM3}$ oxidation of *N*-benzyl ε-caprolactam (**194**).
Table 7.7 Conversion and product distribution of P450$_{BM3}$ oxidation of *N*-benzyl ζ-enantholactam (**199**).
Table 7.8 Conversion and product profile of P450$_{BM3}$ oxidation of *N*-benzyl-2-azaspiro-[4.5]decan-3-one.
Table 7.9 The conversion and product distribution of P450$_{BM3}$ oxidation of *N*-benzyl-2-azaspiro[4.6]undecan-3-one (**214**).
Table 7.10 Conversion and product distribution of P450$_{BM3}$ oxidation of *N*-Boc 8-azaspiro[4.5]decane.
Table 7.11 The conversion and selectivity of P450$_{BM3}$ oxidation of **229**.

Abbreviations

ADH: alcohol dehydrogenase

BIA: benzylisoquinoline alkaloids

BMP: the heme domain of $P450_{BM3}$

BMR: the reductase domain of $P450_{BM3}$

CAST: combinatorial active-site saturation test

CPR: cytochrome P450 reductase

CYP: cytochrome P450

de: diastereomeric excess

dNTP: deoxynucleotide triphosphate

EDTA: ethylenediaminetetraacetic acid

ee: enantiomeric excess

FAD: flavin adenine dinucleotide

FBDD: fragment-based drug discovery

FDH: formate dehydrogenase

FID: flame ionisation detector

FMN: flavin mononucleotide

G-6P-DH: glucose-6-phosphate dehydrogenase

GC: gas chromatography

GDH: glucose dehydrogenase

GlyDH: glycerol dehydrogenase

HAT: hydrogen atom transfer

HPLC: high performance liquid chromatography

HTS: high-throughput screening

IDH: D/L-isocitrate dehydrogenase

IPTG: isopropyl-β-D-thiogalactopyranoside

ISM: iterative site-saturation mutagenesis

kan: kanamycin

LB: Luria-Bertani broth

MOPS: 3-(*N*-morpholino)propanesulphonic acid

NAD(P)(H): nicotine adenine dinucleotide (phosphate) (H = reduced form)

NIH: National Institutes of Health

NPG: *N*-palmitoylglycine

PAH: polycyclic aromatic hydrocarbon

PCR: polymerase chain reaction

PCNA: proliferating cell nuclear antigens

Pdx: putidaredoxin

PdR: puridaredoxin reductase

PDR: phthalate dioxygenase reductase

RMSD: root mean square deviation

SB: substrate-bound

SET: single electron transfer

SF: substrate-free

SOMO: singly occupied molecular orbital

SRS: substrate recognition site

TAE: tris-acetate EDTA buffer

THIQ: 1,2,3,4-tetrahydroisoquinoline

THIQ': 5,6,7,8-tetrahydroisoquinoline

THQ: 1,2,3,4-tetrahydroquinoline

THQ':5,6,7,8-tetrahydroquinoline

THQX: 5,6,7,8-tetrahydroquinoxaline

T-HYDRO: *tert*-butyl hydroperoxide

TMH: transmembrane helix

Tris: tris(hydroxylmethyl)aminomethane

TON: turnover number

TTN: total turnover number

WT: wild-type (i.e. mutation-free)

Cyclic amine functionalisation by engineered cytochrome P450$_{BM3}$

Yushu Li D.Phil. Thesis abstract

Hertford College Trinity, 2020

Cytochrome P450 enzymes are known for their characteristic activity of C–H bond oxy-functionalisation whereby one oxygen atom of atmospheric dioxygen is inserted in an available carbon-hydrogen bond of their substrates, such as drugs and natural products, to form the alcohol derivative. Cytochrome P450$_{BM3}$ from *Bacillus megaterium* has been extensively engineered to develop biocatalytic pathways to bioactive compounds due to its self-sufficiency, high expression level and promiscuity in substrate recognition. In this thesis, a high proportion of available carbon-hydrogen bonds in cyclic amines and lactams have been shown to be oxidised by engineered P450$_{BM3}$ variants with high turnover and reasonable regioselectivity (Figure 1). A combination of substrate engineering via introducing substituents (methoxy and methyl), *N*-protecting groups (phenyl, benzyl, acyl, Boc, mesyl, tosyl, and isopropylsulfonyl) and auxiliary carbocycles (cyclopentane and cycloheptane), and protein engineering by site-directed and site-saturation mutagenesis at active site residues identified by screening with a 48 P450$_{BM3}$ variant library of diverse substrate pocket topology and polarity, have enabled the oxidative diversification of these core motifs in numerous FDA-approved drugs. Unusual activities of P450$_{BM3}$ – the Povarov reaction with *N*-phenyl cyclic amines and N1-C8' coupling (amination) of 6-methoxy-1,2,3,4-tetrahydroquinoline – were also discovered. Biotransformation *in vivo* and *in vitro* of these substrates reached 1 g/L/day with 20 mM substrate conversion at turnover numbers of up to 15,000. The research has provided the basis for developing alternative routes to hydroxy and multi-functionalised cyclic amines and lactams, introducing synthetic handles

for functional group elaborations of such compounds which are frequently used in fragment-based drug discovery.

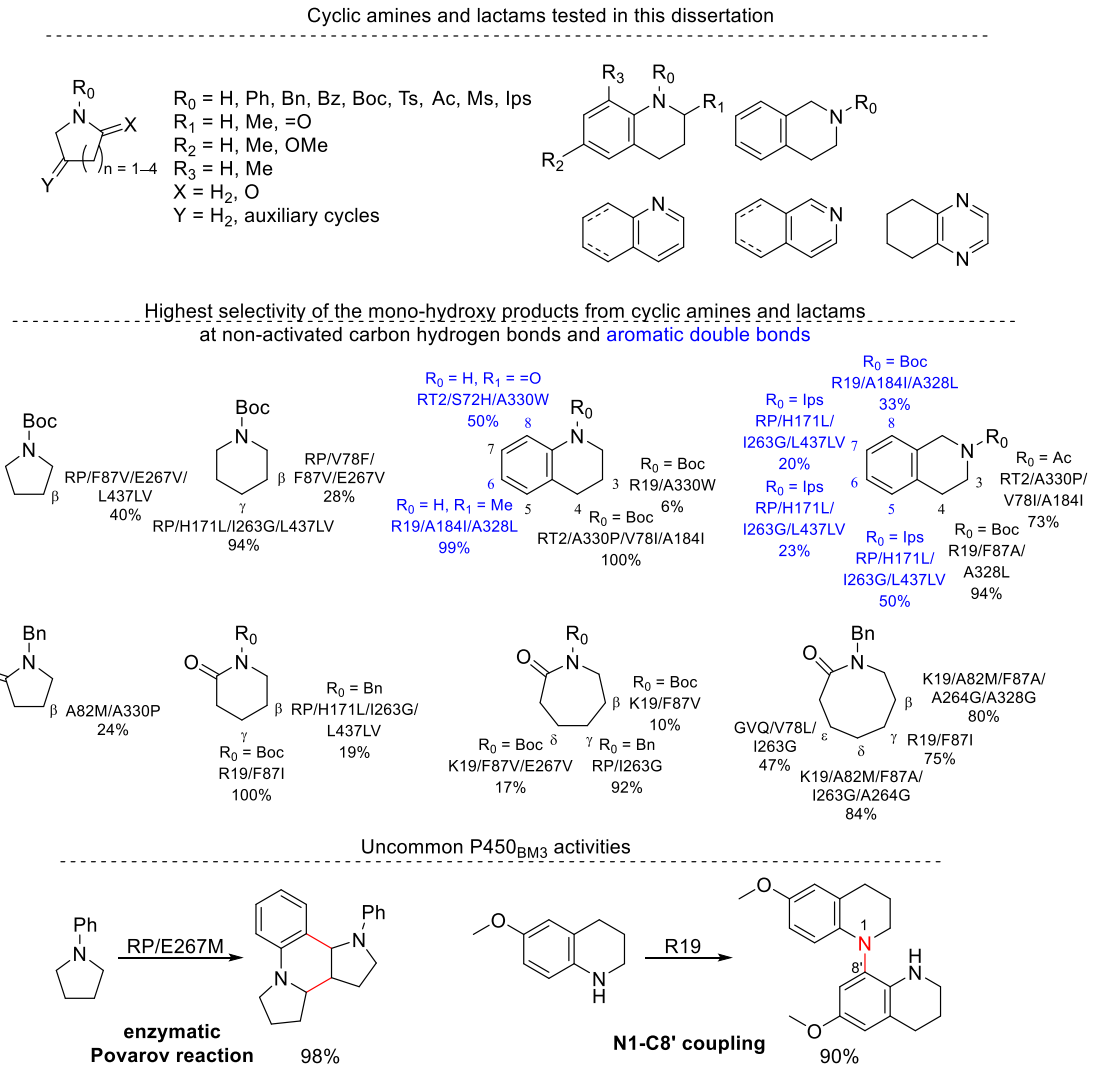


Figure 1 Overview of investigated cyclic amines and lactams, the highest hydroxylation selectivity at non-activated C–H bonds, and new $P450_{BM3}$ activities in this dissertation.

Chapter 1 Introduction

1.1 Enzyme features of cytochromes P450 (CYPs)

1.1.1 Discovery of P450 enzymes

The cytochromes P450 are a superfamily of hemoproteins which have been extensively studied for their oxidative metabolism of xeno- and endobiotics since the 1950s.[1] Maison *et al.*[2] and Hayaishi *et al.*[3] identified metalloenzymes capable of transferring one oxygen atom of atmospheric dioxygen to substrates, with the other oxygen being to water.[4] Klingenberg[5] identified a pigment in rat liver microsomes that binds carbon monoxide when reduced by either pyridine nucleotides or dithionite to give a maximum absorbance at *ca.* 450 nm, hence the name 'P450'. Omura and Sato[6] then recognised that this microsomal pigment was a hemoprotein; they found that the cysteinyl ligand to the heme was necessary for the characteristic 450 nm Soret maximum of the Fe^{II}–CO complex,[7] and named the enzyme "cytochrome P450". If the Soret absorbance is at 420 nm, the thiolate of the cysteine ligand has been protonated to form the thiol-coordinated CO complex, an inactive form of the enzyme.[8] In some cases, substrate binding or modulation of the pH could revert P420 to the active P450 form.[9–12]

1.1.2 The CYP nomenclature system

The systematic CYP nomenclature and classification of cytochromes P450 was developed by David Nelson.[13,14] CYP enzymes with >40% amino acid identity are classified into the same family (*e.g.* CYP**1**), those with >55% identity into the same subfamily (*e.g.* CYP1**A**) with each isozyme numbered (*e.g.* CYP1A**1**)[15] and each allele labelled (*e.g.* CYP1A1***1**). By 2018, >300,000 CYP sequences have been mined (21% for bacteria, 28% for fungi and the rest for animals and plants; http://drnelson.utmem.edu/cytochromeP450.html) and >41,000 sequences have been annotated.[16] This vast collection of P450s in mammals, eukaryotes, prokaryotes and even viruses,[17–19] show diverse activities ranging from steroid

demethylase,[20,21] mammalian aromatase,[22,23] fatty acid hydroxylase[24,25] to prostacyclin synthase,[26,27] C–C coupling in vancomycin biosynthesis[28] and vitamin-D hydroxylase.[29]

1.1.3 The P450 catalytic cycle

The signature C–H bond oxidation activity of P450 enzymes has the overall stoichiometry shown below:

$$R–H + NAD(P)H + O_2 + H^+ \longrightarrow R–OH + NAD(P)^+ + H_2O.$$

The two electrons required for the reductive activation of dioxygen derive from reduced pyridine nucleotides (NAD(P)H). Decades of research revealed that all CYPs function by fundamentally the same reaction cycle. However, different CYPs vary substantially in the efficiency of converting O_2 and electrons to the corresponding product.[30]

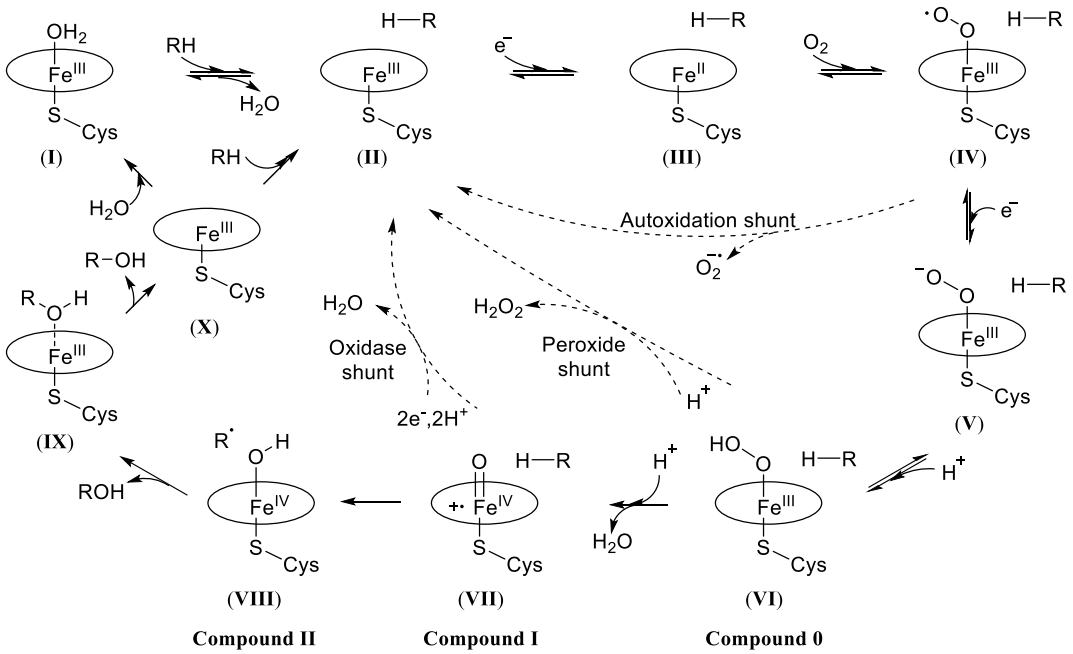


Figure 1.1 The catalytic pathway of P450.

The generally accepted catalytic cycle (Figure 1.1) is initiated by binding of a viable substrate in the active site of the enzyme to convert the low spin (S = 1/2) hexacoordinate ferric heme of the resting state **I** to the high spin pentacoordinate high spin (S = 5/2) form **II**. Loss of the water ligand is responsible for this change in the heme spin state and the

concomitant increase in the heme reduction redox potential which (a) renders heme reduction by cofactor proteins/domains thermodynamically more favourable, and (b) lowers the reorganisation energy barrier for the electron transfer step to generate the ferrous form **III**.[31] Binding of dioxygen to ferrous cytochrome P450 gives the relatively stable ferrous-oxy species **IV**.[32–34] Back-donation from iron to a π* orbital of dioxygen confers ferric-superoxide character to the complex;[35–37] the build-up of electron density on the bound oxygen is stabilised by hydrogen bonding to the side chain of a conserved Thr in the oxygen-binding groove in the I-helix.

Transfer of the second electron generates the peroxy complex **V** which is rapidly protonated to form the ferric hydroperoxy species **VI**, also known as Compound 0. Protonation of the distal oxygen of **VI** facilitates heterolytic O–O bond scission; the distal oxygen is lost as water while the proximal oxygen atom becomes an oxo ligand to the heme iron which is oxidised from the ferric form to a formal oxidation state of +5; however, this ferryl, Compound I species **VII** is more appropriately described as an Fe^{IV}=O group with a π-cation radical delocalised on the porphyrin. The ferryl oxygen abstracts a hydrogen atom from a C–H bond of the bound substrate, leading to the Fe^{IV}–OH, Compound II species **VIII** and a substrate radical, which undergoes a "rebound" reaction with hydroxyl to yield the alcohol product weakly ligated to the ferric heme iron (**IX**). Displacement of the alcohol product by water regenerates the resting state of the enzyme and completes the cycle.

There are some subtle details in the steps of the cycle. P450 enzymes can turn over NAD(P)H in the absence of a viable substrate. This metabolically wasteful activity is typically low because of slow first electron transfer, which arises from the high reorganisation energy associated with breaking the Fe–OH_2 bond to form the pentacoordinate ferrous state. Binding of a viable substrate causes the water ligand to dissociate, thus lowering the reorganisation energy to increase of rate of electron transfer.

This is commonly referred to as "gating" of the catalytic cycle. Moreover, although the first electron transfer is accelerated by substrate binding it remains the slowest step and is often rate-limiting for many CYP enzymes. In the case of $P450_{BM3}$ (CYP102A1), the subject of this thesis, the 1st electron transfer is not rate-limiting; the 2nd electron transfer and perhaps subsequent steps also contribute to the overall observed rate. Dioxygen binding to the ferrous form of the enzyme triggers changes to the number and position of ordered water molecules within the active site, especially within the oxygen-binding groove in the I helix. An acid-alcohol pair (Asp251 and Thr252 for CYP101A1) within this groove is proposed play a key role in proton delivery, firstly to the peroxo species **V** and then the hydroperoxy group of Compound 0 (**VI**) for O–O bond cleavage.[34,38,39] Some P450 enzymes, *e.g.* P450cin and P450eryF, utilise the substrate for proton delivery.[40,41] In addition to Compound I, Compound 0 has been proposed to participate directly in P450-catalysed epoxidation (P450 PimD),[42] aromatisation (*e.g.*, CYP19A1)[43] and C–C bond cleavage (*e.g.*, CYP125A1),[44–48] revealing the possibility of substrate-specific selection of the appropriate 'active oxygen' for catalysis.

The P450 catalytic cycle is susceptible to uncoupling of NAD(P)H consumption from product formation. The ferrous-oxy complex can undergo autoxidation to lose superoxide, which dismutates into hydrogen peroxide and dioxygen in aqueous solution, especially if the substrate weakens the binding.[49–51] Protonation of Compound 0 at the proximal oxygen generates hydrogen peroxide which readily dissociates (the peroxide shunt).[30] Compound I can be reduced by two electrons and protonated twice to afford the ferric species, which is known as oxidase shunt as four electrons were utilised to reduce dioxygen to waters.[52]

Other catalytic pathways also exist. For example, P450-catalysed epoxidation involves initial attack by the ferryl oxygen on the π bond, followed by ring-closure (Figure 1.2 A);[53–56] P450-catalysed aromatic oxidation follows the epoxidation pathway to form the arene

oxide intermediate, which then undergoes ring-opening, NIH shift, and enolisation to afford the phenol product (Figure 1.2 B).[57–59]

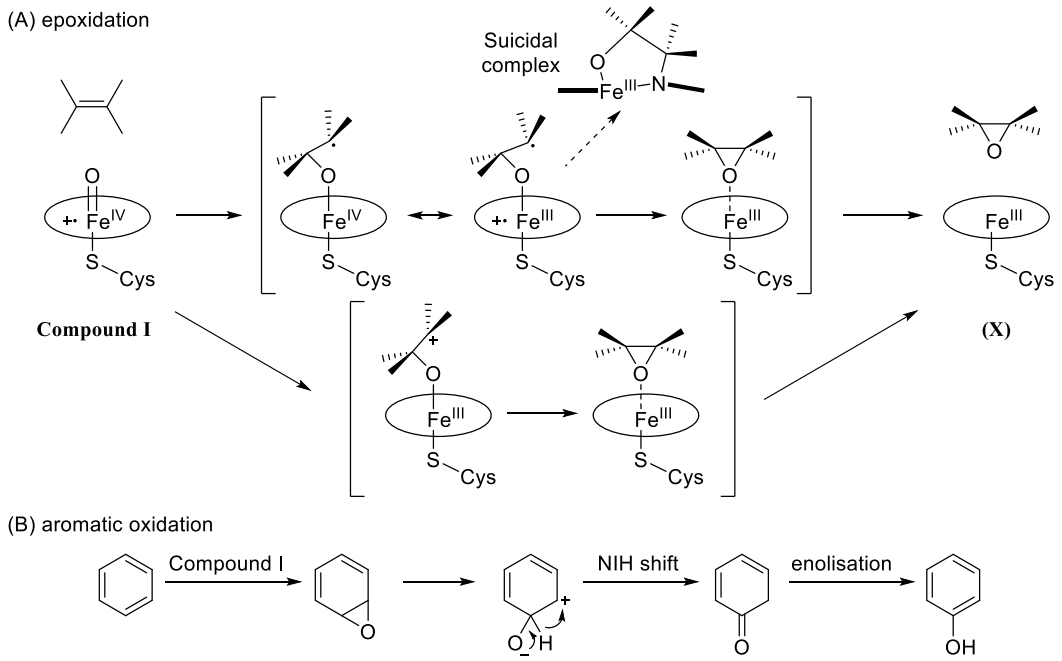
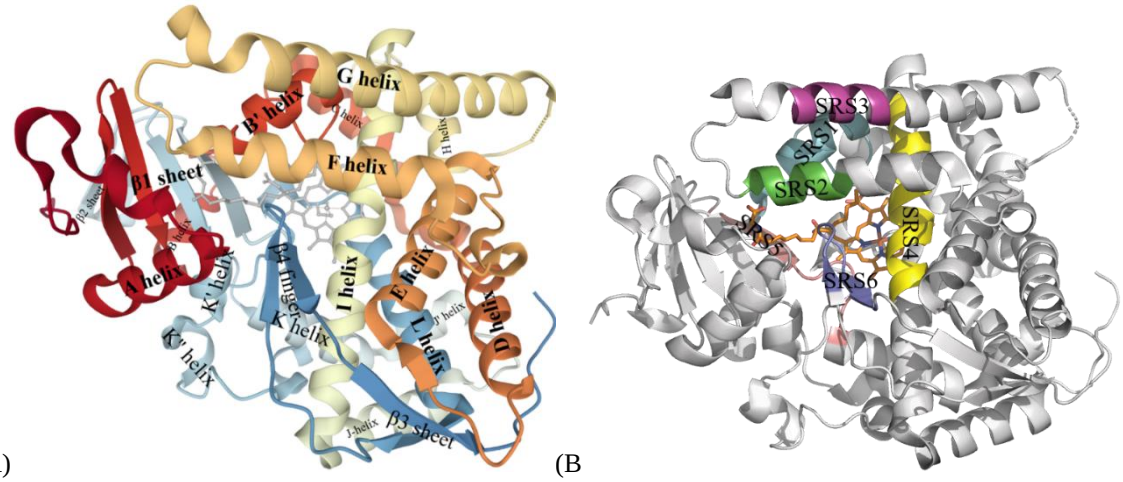


Figure 1.2 The proposed catalytic pathways of P450-catalysed epoxidation and aromatisation.

1.1.4 General features of CYPs

Although numerous phylogenetic tree branches[16] have been established, the resemblance in the three-dimensional structures of bacterial and microsomal P450s is striking despite the low sequence identity (<20%) amongst different subfamilies.[60–65] CYP enzymes are hemoproteins of *ca.* 500 amino acids. The characteristic "P450 fold" consists of a series of helices (A–L) and β-sheets (β1–β5). As the structure of substrate-bound $P450_{BM3}$ (Figure 1.3 A) demonstrates, the conserved structural core consists of a four-helix bundle with three parallel helices (D, L and I) and one antiparallel E-helix.[66] The heme prosthetic group lies between the distal I-helix and the proximal L-helix; the loop to N-terminal side (signature amino acid sequence: **F**XX**G**X(**H**/**R**)X**C**X**G**) of this proximal helix harbours the β bulge (Cys-Pocket) containing the unique strictly conserved heme-ligated Cys.[67] In addition to this Cys ligand, the **E**XX**R** pattern in the K-helix is also conserved.[68] The crucial I-helix on the heme distal side forms one wall of the substrate pocket with a characteristic kink in

the middle (signature amino acid sequence (**A**/**G**)**G**X(**E**/**D**)**T**) which stabilises dioxygen binding and facilitates proton delivery.[50,67] For the CYP152 peroxygenase family, the (E/D)T sequence in the I-helix evolves into R/P (R241/P242 for SPα, R242/P243 for BSβ and R245/P246 for OleT), in which the positively-charged Arg anchored the fatty acid carboxylate group at the catalytic site for the mechanistic shift towards decarboxylation.[9] Of the less conserved parts of the structure, the B-C the F-G blocks are part of the active site and show considerable variations.[60]



(A) (B

Figure 1.3 The P450 fold illustrated with the structure of substrate-bound $P450_{BM3}$ (PDB code: 1jpz).

Six substrate recognition sequence (SRS) regions have been identified by sequence alignment techniques to highlight the P450 subdomains which generally affect substrate specificity and binding the most.[69,70] SRSs are deemed to be flexible domains, shifting upon substrate binding in an induced-fit mechanism to favour substrate binding and ensuing catalysis.[70,71] The B'-helix region (SRS1), part of the F- and G-helices (SRS2 and SRS3), part of the I-helix (SRS4), the contact region between the K-helix and β2-sheet (SRS5), and the β4-finger (SRS6) encompass the active site of P450 (Figure 1.3 B).[60,69,70,72]

Eukaryotic P450s are membrane-bound enzymes with a N-terminus transmembrane helix (TMH) of roughly 20 amino acid residues,[73,74] linked to their catalytic domains with a *ca.* 10-residue linker.[75,76] Such regions of mitochondrial P450s are cleaved off during the

protein-importing process,[77] whilst microsomal P450s retain this feature. The TMH is not required for enzymatic catalysis, as TMH-cleaved microsomal P450s maintain their activity.[78,79] The N-terminus portion of the catalytic domain, from the linker to the B-C loop, shifts down towards the heme proximal side and drags the A-propionate, commonly situated on the distal face in prokaryotic P450s, to the proximal side.[80–83] This movement of the A-propionate brings N-terminal/β-sheet domain residues closer to the F/G loop, and the exceptionally variable F- and G-helices often exhibit two auxiliary F'- and G'-helices, collectively forming the hydrophobic surface inserted into the membrane.[84–89] The A'-, A-, B'-, F-, F'- and G-helices, the B/C and F'/G' loops control the accessibility of the substrate channel to molecules entering the active site from the membrane.[80] For soluble P450s, the B'-, F- and G-helices and the F/G loop are responsible for opening and closing of the substrate entrance, as revealed by the substrate-free and substrate-bound crystal structures and relevant conformation dynamics.[90–93]

1.1.5 P450 electron transfer chains

For each turn of the catalytic cycle, a P450 enzyme receives two electrons from a redox partner protein, which include diflavin reductases,[94,95] flavodoxins,[96,97] ferredoxins,[98,99] and phthalate dioxygenase reductase (PDR)-type proteins.[100–105] According to the composition of the redox partners, cytochromes P450 have been classified into ten classes (Class I–X),[106] with Class I and Class II P450s being the most extensively studied.

Class I P450s have two redox partners: a FAD-containing reductase (ferredoxin reductase), which receives two electrons from NAD(P)H and transfer these one at a time to a [Fe_2S_2] protein (ferredoxin) which transfers the electron to the P450 monooxygenase.[107] The electron shuttle process of its prototype CYP101A1 (P450cam) is shown in Figure 1.4.

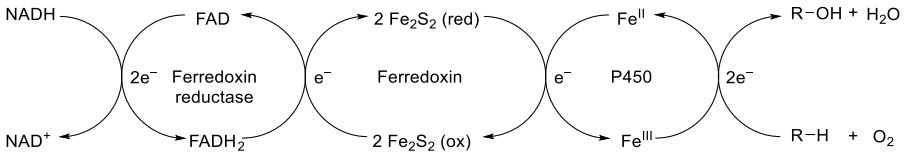


Figure 1.4 Electron-transfer in P450cam.[107–109]

Class II P450s are located in the endoplasmic reticulum of eukaryotes. The membrane-bound NADPH-cytochrome P450 reductase (CPR) serves as the redox partner of the corresponding membrane-bound P450. It consists of a NADPH/FAD binding domain, a linker domain, a FMN binding domain and a N-terminal transmembrane domain.[110–113] Alternatively, the NADH-driven cytochrome b_5/b_5 oxidoreductase pair can supply two electrons from NADH to these P450 isozymes.[114] The CPR component can transfer both the first and the second electron to the P450 by a 1-3-2-1 electron cycle,[115–118] whereas cytochrome b_5 transfers the second electron only (Figure 1.5);[114,119–121] examples include CYP2A6, CYP2B1, CYP2B4, CYP2C9, CYP2E1, and CYP3A4.[122–124]

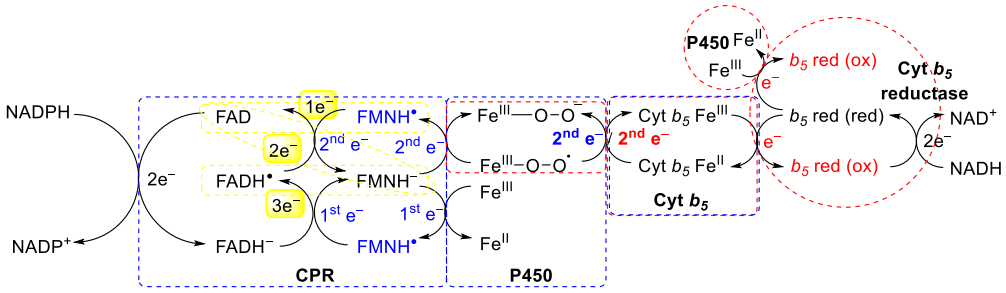


Figure 1.5 Electron-transfer in Class II cytochrome P450s.[114–118,120,121]

Class III P450s are 3-component systems where a NAD(P)H-dependent FAD-containing ferredoxin reductase and a FMN-containing flavodoxin transfer electrons to the P450 enzyme; P450cin is one example.[125–127] The thermophilic CYP119[128] is a Class IV P450 with its redox partner comprising of a ferredoxin[129] and a 2-oxoacid:ferredoxin oxidoreductase;[130] this was the first P450 to be found not to utilise NAD(P)H as cofactors.[131,132] For the Class V 14α-demethylase CYP51, a [Fe_3S_4] type ferredoxin is fused at the N-terminus of the P450 domain, and a putative NAD(P)H-dependent reductase may

supply reducing equivalents to this ferredoxin.[133] The flavodoxin of Class VI is fused to the N-terminus of heme domain, and supported by a putative NAD(P)H-dependent flavoprotein reductase, *e.g.* CYP177A1.[96,97,134] Both Class VII and Class VIII P450s are self-sufficient, but an P450-unassociated phthalate dioxygenase reductase constructed with NADH-, FMN-binding and [Fe_2S_2] ferredoxin domains is fused to P450 in Class VII, *e.g.* CYP116B2 (P450RhF),[100–104] whilst a CPR-like diflavin reductase partner containing NADPH-, FAD- and FMN-binding domains is fused in Class VIII, *e.g.* CYP102A1 ($P450_{BM3}$).[95,135–140] P450nor, a Class IX P450, converts two NO molecules into N_2O with NADH as electron donor.[141,142] The CYP74 subfamily makes up Class X, which incorporate the acyl hydroperoxide of the substrate as oxygen source, by independent intramolecular transfer system, to form a new C–O bond with no need for NAD(P)H.[143–146]

1.1.6 P450 biotechnology

P450 enzymes catalyse C–H bond oxidation at ambient temperatures in aqueous solution using oxygen from air as the oxidant to yield products of biological and pharmacological activities, which is rarely achievable for classical organic synthesis under similar, environmentally friendly conditions. Physiologically, P450s show very broad substrate range and catalyse numerous reaction types. They play key roles in the biosynthesis and metabolism of natural products in microorganisms, insects and plants.[147–154] The potentially huge number of processes that could be made greener by the use of P450 enzymes made them attractive targets for biotechnological applications. However, the barriers to general commercial applications are also evident and challenging: low turnover numbers, insufficient selectivity for target products, the requirement of NAD(P)H for reaction *in vitro*, the reconstitution of multi-protein electron transfer chains,[155,156] the presence of uncoupling pathways impairing catalytic efficiency,[157–159] and technical issues of substrate uptake and product efflux in whole-cell reactions.[160,161] Therefore, P450 biotechnology research has

focused on (a) substrate and protein engineering for higher activity and selectivity, (b) engineering of higher turnover number, stability and improved electron transfer, (c) electron source engineering by the design of P450 fusion proteins and substitution of cofactors, (d) metabolic engineering to mimic natural biosynthesis of pharmacological compounds and establish *de novo* synthesis of plant metabolites.[162,163]

1.1.6.1 Substrate engineering

For substrate engineering, introduction of auxiliary groups and use of decoys are approaches for improving regio- and enantioselectivity.[164] A recognition moiety is attached to the substrate, and the modified form is used for biotransformation with improved selectivity and yield (Figure 1.6).[165,166] Decoy molecules are chemically inert and fill the active site of the enzyme, hence increasing the selectivity due to consistent substrate binding orientation; the approach has been successfully applied to olefination, benzene oxidation and sulfoxidation.[167–170]

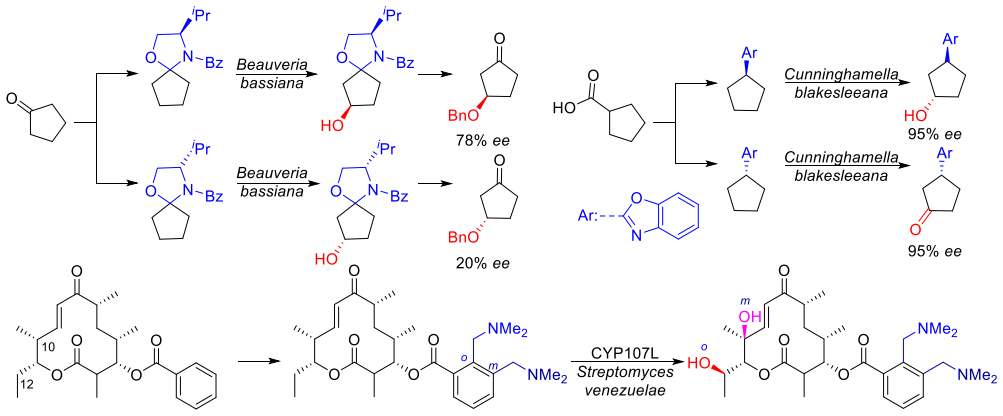


Figure 1.6 Examples of substrate engineering in P450-catalysed biotransformations.[165,166]

1.1.6.2 Protein engineering: rational design *vs.* directed evolution

The general strategies for protein engineering of CYPs for the oxidation of unnatural substrates can be divided into “rational design” and “directed evolution” (Figure 1.7).[171] Rational design requires structural knowledge of the protein from X-ray crystallography or

molecular modelling to identify residues for mutagenesis to improve activity, selectivity, stability, *etc.*[171] Directed evolution resembles natural evolution; random mutagenesis of a whole gene or domains, insertions, deletions, or recombination of homologous genes[172] are applied to seek the "dream variant" out of the potentially countless variants.[173,174] Efficient screening protocols, *e.g.* by a phenotype, are absolutely required for larger scale random mutagenesis efforts.

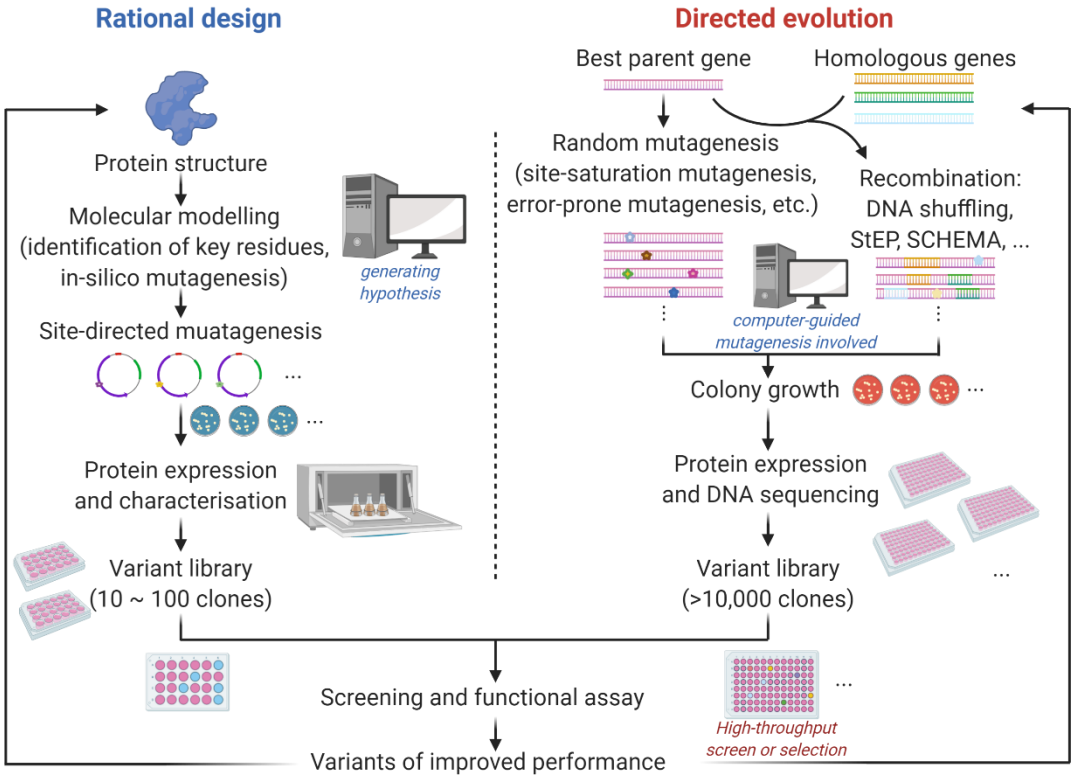


Figure 1.7 Schematic workflow of rational design and directed evolution approaches for enzyme engineering.

The limitation of rational design is that the hypothesis may be incorrect, whilst the harsh truth for directed evolution is that the hit rates for new activities rarely reach high levels. In essence, rational design can be slow and inefficient as few mutants are made by site-directed mutagenesis and there is always the possibility that a different mutation at the target residue would give better results. Moreover, mutations that exert their effects by allosteric effects would not be proposed. By contrast, a random mutagenesis approach could reveal such long-range effects if the screening method covers enough variants. A

limitation of error-prone PCR – the most common approach for introducing random mutations – is that it might not cover all possible mutations as the technique typically introduces a single nucleotide change.

There are continuing efforts to develop compromise approaches to provide better coverage of the sequence space of the enzyme without invoking random mutagenesis and high-throughput screening. In iterative site-saturation mutagenesis (ISM), amino acid residues are subjected to site-saturation mutagenesis one at a time, in each case the best mutant from the previous round serves as the template. In the combinatorial active-site saturation test (CAST) approach, residues in different regions of the substate pocket are selected for mutations covering a reduced number of mutations at each, and the combined library (typically thousands of variants in size) is screened for the desired outcome.[175] Small, focused libraries of combinations of 3–5 mutations at 2–3 residues known or proposed to affect activity and selectivity have been used. One example is the use of a two-residue library of $P450_{BM3}$ constructed for F87 and A328, which led to enhanced activity but most notably altered product profile for the oxidation of sesquiterpenes, as well as linear and cyclic alkanes.[176–178] Larger libraries of up to 500 $P450_{BM3}$ variants have been used as a "training set" to identify residues affecting product selectivity that were then subjected to site-saturation mutagenesis to optimise the variants. A good example is the synthesis of human as well as novel metabolites of artemisinin.[179] On the scope of evolving enzymes via the recombination of homologous genes, the DNA shuffling approach established the variant libraries from the CYP1A and the CYP3A subfamilies, rendering the new variants capable of oxidising non-natural substrates; and the staggered extension process (StEP) created the variant library of CYP2A6, which figured out the sequence determinants for indole hydroxylation. Shuffling of non-homologous CYP sequences, *e.g.* incremental truncation of hybrid enzymes (ITCHY) and sequence homology-independent protein

recombination (SHIPREC), was also explored.[180] Secondary structural exchange of homologous P450s, *e.g.* the incorporation of large P450 structural elements of $OxyB_{van}$ into $OxyB_{tei}$ to build the catalytically-competent OxyB chimera, was reported, to illuminate that the unusual *in vitro* behaviour of OxyB in vancomycin biosynthesis was not originated from the major regions of P450.[181]

Using $P450_{BM3}$ oxidation of testosterone as an example, both strategies were taken to explore higher regio- and enantioselectivity.[182–185] Since WT $P450_{BM3}$ showed no activity for testosterone oxidation, rational design of the enzyme, underpinned by previous research on the oxidation of other substrates, selected R47 and L188 in the hydrophobic channel of the substrate entrance,[186] F87, E267 and A328 which are close to the heme,[91,187] A82 which lies deep into the substrate pocket and may sequester a substrate molecule,[188,189] along with S72 and L437 identified from *in silico* modelling,[190] for site-directed and site-saturation mutagenesis. It turned out that RP/F87V/E267V/A328I offered 80% 2β-alcohol, K19/F87V/Q403P 96% 15β-alcohol,[185] M01/A82W 86% 16β-alcohol, and M01/A82W/S72I 82% 16α-alcohol[183] from screening a few hundred enzyme variants. For directed evolution, R47, T49, V78, A82, F87, M185 and A330 were mutated by site-saturation mutagenesis on the base variant F87A, which finally gave 97% of the 2β-alcohol (F87A/A330W) and 96% of 15β-alcohol (R47Y/T49F/V78L/A82M/F87A) by screening 10^5 variants.[182] High regio- and stereoselectivity were achieved but altered regioselectivity was not found until a recent 15-residue site-saturation mutagenesis and high-throughput screening led to mutants giving 95% 7β-hydroxy-testosterone.[191]

1.1.6.3 Strategies for accelerating electron transfer

Two approaches have been reported for constructing P450 fusion proteins. Hybrid enzymes are constructed by genetic fusion of P450 and reductase domains from different P450

systems to generate self-sufficient P450s. The most commonly used reductase domains are the diflavin BMR domain from $P450_{BM3}$[192,193] and the reductase domain of P450RhF.[194,195] The length and nature of the linker between fused domains are the crux of the desired function. Both helical and nonhelical linkers can rigidly separate the connected domains with helical ones containing mainly P, T and F, whereas non helical ones are abundant in L, R, E, M and Q of variable length (4.5 ± 0.7 residues for short linker, and 21 ± 7.6 for long linker).[196] Flexible and cleavable linkers are the other two types.[197] Such techniques facilitate the establishment of eukaryotic,[198,199] plant,[200,201] bacterial,[198,202] and mixed P450 fusionproteins.[203,204] The "PUPPET" approach exploit the propensity for three distinct proliferating cell nuclear antigens (PCNAs) to self-assemble into a heterotrimer. Thus, the 3 components of the CYP101A1 system were fused to different PCNAs, *e.g.* PCNA1-PdR, PCNA2-Pdx , and PCNA3-P450cam; the self-assembled heterotrimers brought the three enzymes closer to each other for more efficient electron transfer.[205,206] A related approach fused PdR to P450cam, enabling more rapid and productive binding and electron transfer by a freely diffusing Pdx.[108]

Chemical cofactors, such as dithionite[207,208] and peroxides,[209,210] can either replace NADPH or circumvent the need for $2e^-/2H^+$ activation of dioxygen. There are two types of electrochemical cofactors. Indirect electrochemical cofactors,[211,212] organometallic[213,214] and biological mediators,[215,216] enable electron transfer from an electrode to the linked P450. Direct electrochemical cofactors modify the electrode surface and immobilise the P450 on the electrode,[217] and include detergents,[218] conductive polymers,[219,220] hydrophilic gels,[221,222] and biofilms.[223,224] Highly efficient cofactor regeneration systems have been developed using D/L-isocitrate dehydrogenase (IDH),[225] glycerol dehydrogenase (GlyDH),[226,227] formate dehydrogenase (FDH),[228–230] alcohol dehydrogenase (ADH),[231] glucose dehydrogenase (GDH), and glucose-6-phosphate dehydrogenase (G-6P-DH).[232]

Light-driven cofactor regeneration can be accomplished by either mimicking photosynthesis to transfer electrons by photochemical reduction, *e.g.* the hybrid Ru^{II}-L407C-Fe^{III} $P450_{BM3}$ enzyme,[233,234] or directly adding to the P450 reaction system the plant chloroplast mixture, which oxidises water to dioxygen by photosystem II,[235] and reduces $NADP^+$ into NADPH by photosystem I.[236–238]

1.1.6.4 Whole-cell biosynthesis

Whole-cell reactions have been a routine approach for synthesising drug metabolites,[239–242] small molecules,[243–247] and plant secondary metabolites[248] including terpenoids,[249–254] flavonoids,[255–257] glucosinolates,[258] and alkaloids.[259–261] Synthetic biology and metabolic engineering approaches have been applied for some targets. The biosynthesis pathway of benzylisoquinoline alkaloids (BIA) with varied pharmacological activities involves multiple P450-catalysed steps; the entire pathway has been assembled in microorganisms, with CYPs co-expressed with other enzymes to produce the target alkaloids.[259–262]

1.2 Cytochrome $P450_{BM3}$ (CYP102A1)

$P450_{BM3}$ was identified as a soluble NADPH-dependent medium- to long-chain fatty acid sub-terminal (ω–1, ω–2, ω–3) hydroxylase,[263–266] but its physiological role remains unknown. It was the first single-polypeptide, catalytically self-sufficient P450 to be characterised,[267] with a 55 kDa P450 domain (BMP) fused to a 65 kDa diflavin reductase domain (BMR)[95,136,268] to form the 120 kDa full-length enzyme.[269,270] This self-sufficiency leads to high activity (>4,000 turnovers/min with fatty acids). The enzyme is readily expressed in *Escherichia coli*, reaching >30 μmol/L in industrially relevant scale (>10 m^3) fed-batch fermentations.[271–273] In addition, biotransformation at >10 kg scale per batch with good isolated yields has been reported.[274] These properties make $P450_{BM3}$ an excellent candidate for biotechnological applications.

1.2.1 Functional studies

Within the CYP102A subfamily (A1–A15), the A2, A3, A5, and A7 isozymes were more active fatty acid hydroxylases than $P450_{BM3}$ (CYP102A1), whilst A14 accepted 1,4-naphthoquinone as a better substrate than fatty acids.[66] The A5 isozyme demonstrated faster electron transfer.[275] The heme domain of A3 was less stable than BMP,[276] but its reductase domain was more tolerant of temperature and DMSO than BMR.[277,278] Within the subfamily, the F/G, G/H, J/J' loops and the N-terminus of the G-helix in BMP were poorly conserved,[91] unlike the B'/C and E/F loops, C-, E- and I-helices and the β5-sheet.[66] Within the subfamily, SRS4 (residues 253–271) is fully conserved; SRS6 (residues 434–441) shows some variations; SRS1 (residues 69–92) is well conserved; SRS2 and SRS5 (residues 181–188 and 325–335) show several variable sites; SRS3 (residues 200–208) shows little residue conservation.[66]

At the C-terminus of the BMP domain, a short linker connects to BMR at the N-terminus the FMN-binding domain (Figure 1.8). The linker region is required since mixing of separately expressed BMP and BMR domains did not reconstitute activity.[279–281] Deleting linker residues one by one disabled hydroxylase activity gradually,[282] whilst Pro/Gly-substitutions increased the catalytic activity, perhaps by loosening this relatively rigid helix.[283]

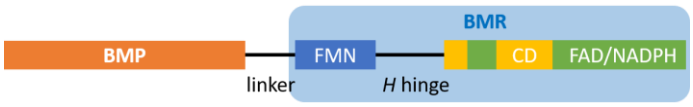


Figure 1.8 The organisation of CYP102A1 gene. (CD: connecting domain)

The BMR domain resembles CPR in structure. Its FMN-subdomain[284] shares great similarity with bacterial flavodoxin,[285] and the FAD-subdomain[286,287] might originate from spinach FdR.[288] It is difficult to express separately from BMP[289,290] due to its susceptibility to thermal inactivation.[291] Electron transfer in BMR follows a 0-2-1-0 cycle (Figure 1.9)

rather than the 1-3-2-1 cycle of CPR, without any priming reactions, forming the FMN semiquinone FMNH• (rather than the hydroquinone $FMNH^-$ in CPR)[292] which was detected by EPR when the FAD was reduced.[286,287,293] It was proposed that such divergence arose from the lack of a Gly residue between Y536 and N537 in the FMN-binding loop to stabilise FMNH•.[61]

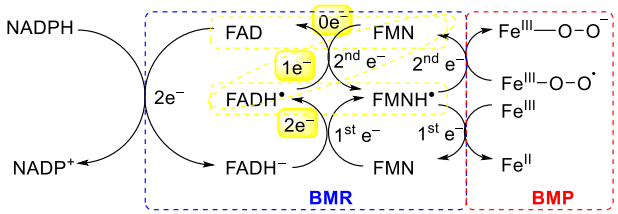


Figure 1.9 Electron transfer of the BMR domain in $P450_{BM3}$.

$P450_{BM3}$ functions as a dimer,[294] as evidenced by enhanced activity with increased protein concentration.[207,295] The first electron travelled from the FAD domain of one monomer to the FMN domain of the other, and thence to either heme domain.[296,297] Disulfide bridges assisted the dimerisation of BMR and BMP,[288,298] which was also dependent on ionic strength.[296] Increased ionic strength slightly increased the binding of BMR to BMP,[299] and too low or high buffer concentration might impair the activity of $P450_{BM3}$.[300,301]

1.2.2 The structure of $P450_{BM3}$

Cryo-EM at 7.6 Å resolution revealed conformational changes involved in redox partner recognition in the *trans* configuration of the dimeric $P450_{BM3}$.[302] The open state of the dimer showed the FMN domain of one monomer rotated away from its FAD domain, whereas in the closed state the FMN domain moved closer to its FAD domain, improving FAD-to-FMN and FMN-to-heme electron transfers.

1.2.2.1 Open and closed forms

Overlay of the crystal structures of substrate-free (SF, the open structure, PDB code: 1bu7) and *N*-palmitoylglycine-bound (SB, the closed structure, PDB code: 1jpz) $P450_{BM3}$

revealed conspicuous shifts in the regions of the F-, G-, H-, I-helices, the F/G and G/H loops (Figure 1.10) and the residues F87, F261 and L437.[71] Two salt bridges, K224(G-helix)–D251(I-helix) and Q229(G/H loop)–N239(H-helix), were broken in the SB structure, and the rotated D217(G-helix)–R255(I-helix) salt bridge was further stabilised by a new hydrogen bond with N213, leading to the tilt and half-turn rotation of the F- and G-helices that closed the substrate access channel and the disruption of the I-helix. The heme water ligand (Wat1020, Fe–O distance 2.5 Å) in the SF form, which was hydrogen bonded to the A264 carbonyl oxygen, was lost. A new ordered water, Wat502, appeared in the oxygen-binding groove and was hydrogen bonded with both A264 and T268 (Figure 1.11). The I-helix kink angle went from 13° in the SF form to 5° in the SB form.[66] The F87 and F261 side chains in the SB form were rotated by *ca.* 90° compared to the SF structure; the movement of F87 might have led to the retreat of L437 in the β4-finger from the heme.[303]

In all fatty acid-bound crystal structures of $P450_{BM3}$ (PDB codes: 1jpz, 1fag, 2uwh and 4kpa), the carbon scaffolds of the substrates located beyond (≥6.9 Å) the reach of the heme iron for oxidation, casting doubt on the validity of using such structures for identifying enzyme–substrate contacts for mutagenesis.[66] Conformational changes after heme reduction, oxygen binding, the 2nd electron transfer and steps beyond could move the substrate closer to the heme. Alternatively, the SB structure could be a snapshot or local minimum within the binding positions for the flexible fatty acid substrate, and the natural dynamics of the substrate in the active site might lead to productive binding conformations.

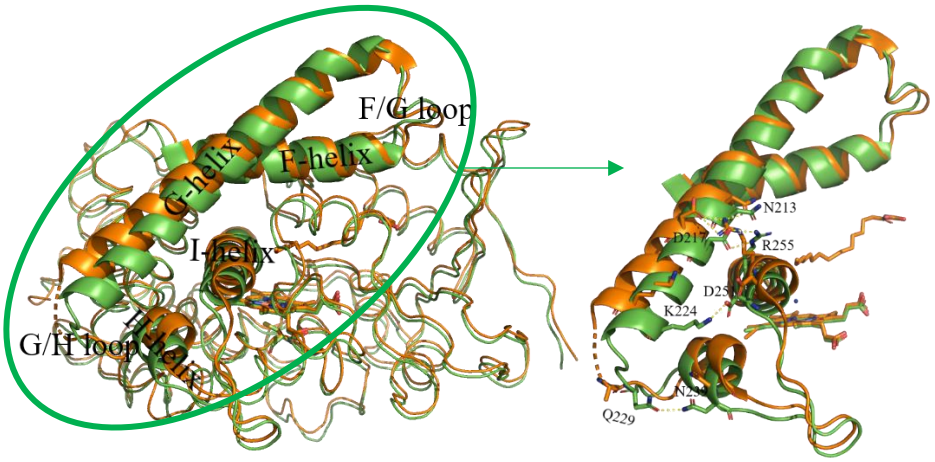


Figure 1.10 Overlay of the SF (green) and NPG-bound (SB, orange) crystal structures of $P450_{BM3}$.

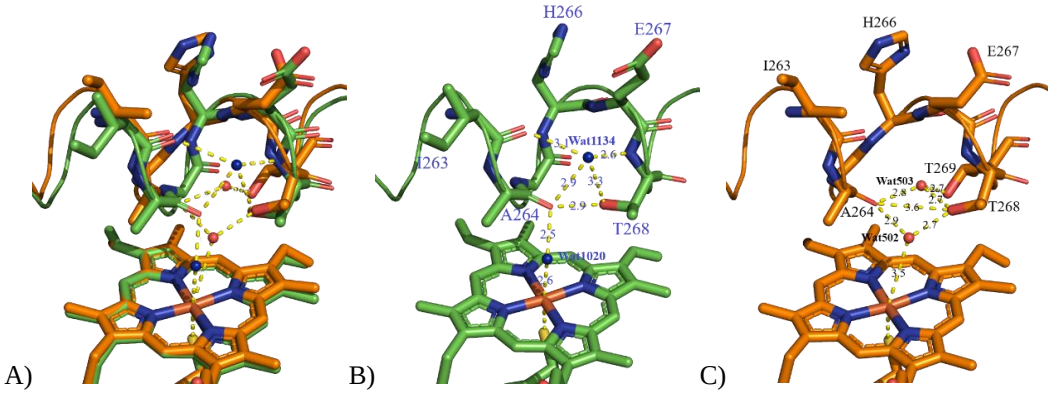


Figure 1.11 Structural differences in the I-helix region in SF (green) and SB (orange) $P450_{BM3}$.

1.2.2.2 The role of $P450_{BM3}$ active site residues

The crystal structure of SF $P450_{BM3}$ revealed a clear substrate channel extending from the surface to the active site. All residues within 5 Å of NPG in the NPG-bound WT structure were identified to establish the substrate access channel and binding pocket to be comprised of the residues P25, V26, L29, R47, L51, Q73, A74, L75, V78, A82, F87, T88, T260, I263, A264, A328, P329, A330, M354, L437 and T438 (Figure 1.12). Every one of these has been subjected to site-directed and site-saturation mutagenesis.

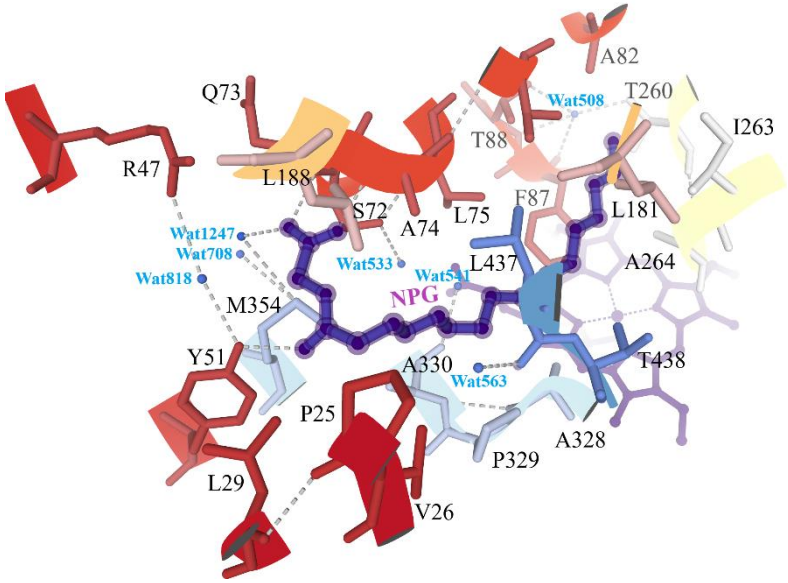
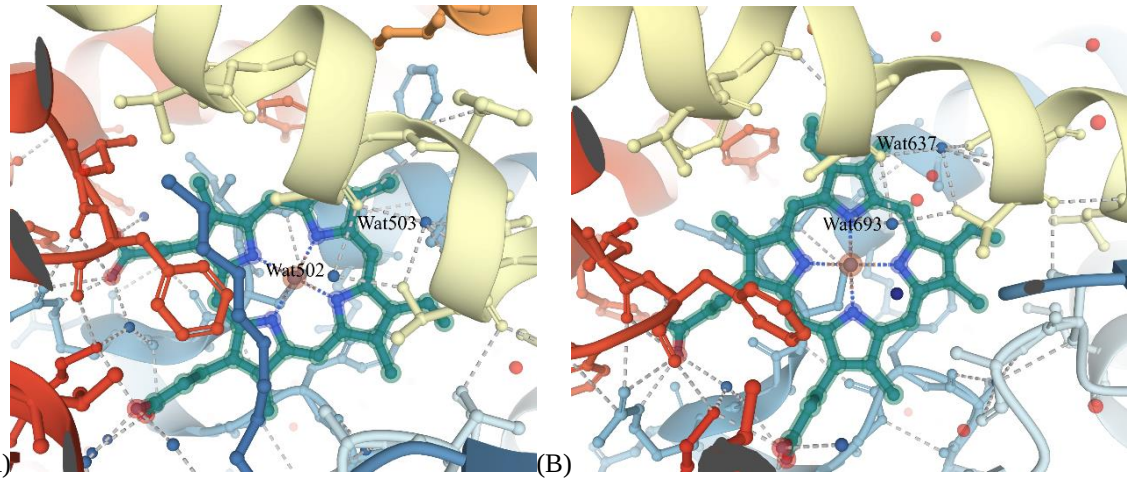


Figure 1.12 The substrate access channel of NPG-bound wild type $P450_{BM3}$.

The residues R47 and Y51 at the entrance of the channel are proposed to be the initial binding site for the carboxylate group of the fatty acid to guide the entrance and sequestration of these substrates into the active site.[278,304] The charge-reversal mutation R47E suppressed oxidation of fatty acids, but C12–C16 trimethylammonium compounds became good substrates.[136,305] The non-polar double-mutation variant R47A/Y51F showed inhibited oxidation of fatty acids,[306] whilst the R47Q/S mutants capable of developing hydrogen bonds indicated enhanced *N*-myristoyl-L-methionine binding affinity.[307] The couplet R47L/Y51F was found active for the oxidation of less polar substrates, *e.g.* polycyclic aromatic hydrocarbons (PAHs) and terpenes,[304,308] since the increase in hydrophobicity improved the initial recognition of the less polar substrates.[304]

The residues S72/Q73/A74/L75/V78/A82 in the B' helix constituted one lateral wall of the substrate pocket. The middle region (A74/L75/V78/A82) was less polar and made the substrate pocket more hydrophobic. The residues S72/Q73/A74, along with Y51, form hydrogen bonds with polar and charged termini of the linear substrates, *e.g.* NPG, decoy molecules and drugs.[309–311] The mutations S72V/I/F, V78M/C/D and A82W/F/M enhanced the conversion and altered the regioselectivity of $P450_{BM3}$-catalysed steroid oxidation;[312]

S72W/H/Y/D/E, V78I/L and A82M either enhanced the oxidation of amine drugs or altered the product distributions.[185,274,313] A74G enhanced *O*-dealkylation of coumarin derivatives[314] and improved the regio- and enantioselectivity of allylic oxidation of ω-alkenoic acids/esters.[315] Mutations at L75 were found to adjust the flexibility of the B'-helix.[316] The SF A82F/W showed 20%–25% high-spin heme content;[189] the two characteristic water molecules (Wat693/Wat637) of the SF A82F (PDB code: 4kf0) mirrored the arrangement of Wat502/Wat503 in the SB WT structure (Figure 1.13).[317]



(A) (B)

Figure 1.13 The water distributions close to the heme prosthetic groups in SB WT (A) and SF A82F (B).

F87 and T88 protruded deeply into the active site. The hydrogen bonding network amongst Wat508, T88 and T260 constituted the terminal of the substrate access channel, and the rotation of F87 could affect enzyme activity and regioselectivity due to its perpendicular orientation and being only 3.1 Å above the heme (Figure 1.14 A).[309] The bulky and non-polar nature of F87 shielding the termini of medium chain fatty acids was proposed as a plausible explanation for the subterminal hydroxylating property of $P450_{BM3}$.[318] However, the F87V/A mutations with their reduced side-chain volumes did not improve terminal hydroxylation of fatty acids; more of the internal carbons were attacked instead.[66] Another P450 isozyme, $P450_{BioI}$, oxidised the middle carbons of the fatty acid moiety linking to acyl carrier protein (*e.g.*, pimeloyl-ACP) by forcing the carbon chain into a U-shape to expose

C7/C8 for hydroxylation,[319] the product of which could be further oxidised via the mechanism of C–C bond cleavage.[320,321] Mutations at F87 expanded the substrate range of $P450_{BM3}$ significantly: F87A/V/G mutations were found to enhance the oxidation of PAHs, β-ionone and monoterpenes,[176,178,187,231,269,322–327] and F87L/V/Y assisted drug metabolism.[177,326,328–331] T88C improved the activity of octane oxidation but showed little effect on product selectivity.[332]

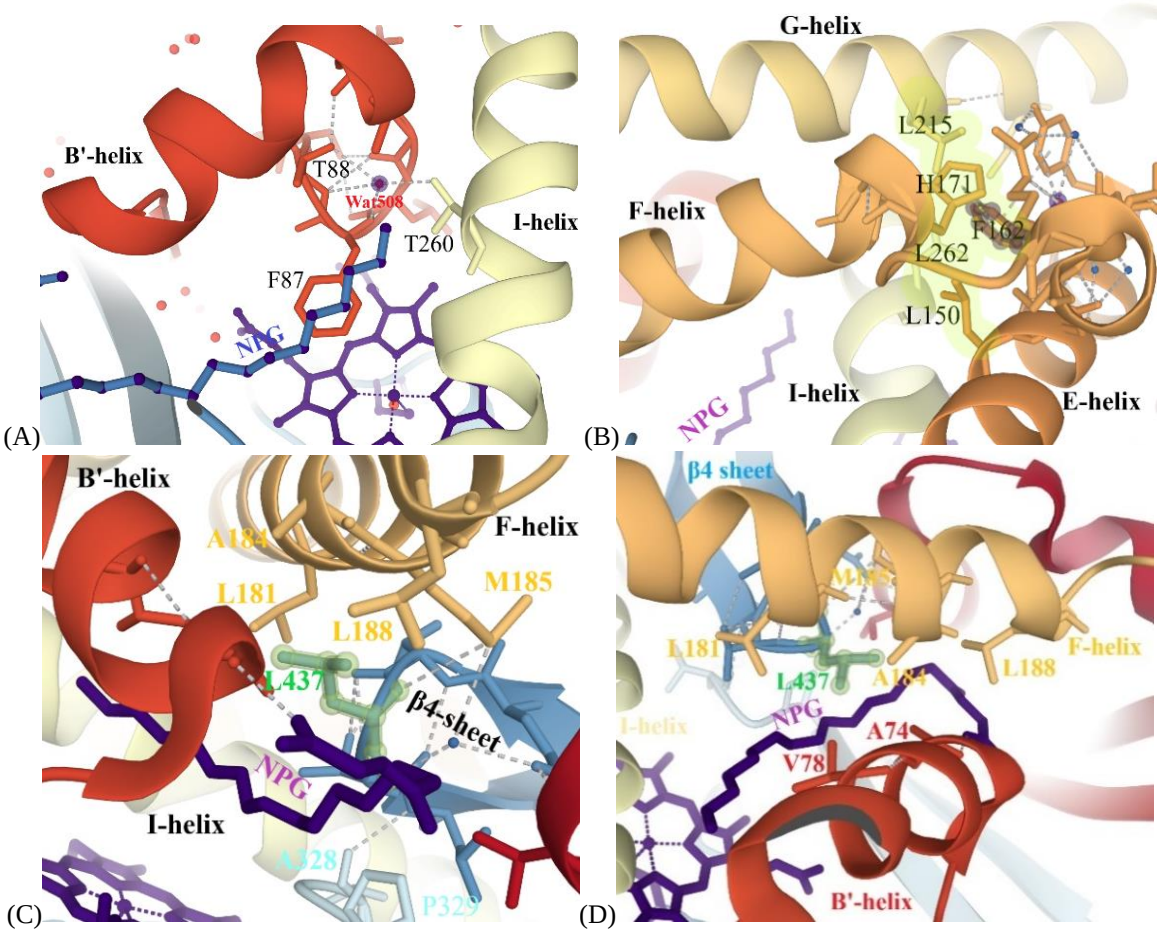


Figure 1.14 Views of the substrate access channel in the SB WT.

The N-terminal residue H171 of the F-helix developed π-π interaction with F162, both of which resided in the knot region of the E-/F-/G-/I-helices (Figure 1.14 B). Either H171L[333] or F162I,[334] disrupting this π-π interaction, showed enhanced catalytic efficiency, perhaps because non-polar substitutions increased the flexibility of E-/F-/G-/I-helices. The H171L mutation, in combination with F87A,[333] Q307H identified from random mutagenesis[300] and

N319Y adjacent to the putative FMN-domain binding sites,[335] led to the variant K19/F87A (K19 = H171L/Q307H/N319Y) which has been reported to oxidise non-natural substrates such as PAHs,[333] drugs,[185] and natural products.[336]

Three Leu residues, L181 and L188 in the F-helix and L437 in the β4-sheet, constituted the roof of the access channel; the interval between L181 and L188 was occupied by L437 protruding right below A184 and M185 (Figure 1.14 C & D).[337] L181K significantly enhanced the oxidation of short chain fatty acids, presumably playing a similar role to the R47/Y51 tether at the channel entrance.[306] L181A, in combination with Ala mutations at L75, T260 and L437, expanded the size of the substrate pocket, enabling the variants to oxidise non-linear and bulky substrates, *e.g.* the alkaloids thebaine and dextromethorphan and steroids.[338] From the crystal structure of A184K/R, a new salt-bridge between the F- and B'-helices (K/R184:D80) was formed, with the F-helix lifted up to create a more spacious active site.[339] Site-saturation mutagenesis was carried out at L188; L188W/E suppressed the peroxide shunt, and L188D/C increased the NADPH oxidation rate.[340] MD simulation of L188Q suggested that this mutation loosened the contact with the β-sheets, destabilising the variant to trigger catalysis.[337] The triple-mutation variant GVQ (A74G/F87V/L188Q),[341] with L188Q destabilising the enzyme and F87V increasing the size of substrate pocket, showed high catalytic activities towards aliphatic compounds,[176,269,327,342,343] PAHs[324,344,345] and drug fragments.[269,274,346]

The I-helix residues T260, I263 and A264, the β4-sheet residue T438, and the loop residues A328 and P329 formed the other lateral wall of the substrate pocket; A330 in the β1-sheet is below the bound NPG substrate (Figure 1.15 A). The I-helix acid-alcohol pair E267/T268, though not contacting the substrate directly, regulated the hydrogen bond network close to the heme group and other substrate-contacting residues, hence adjusting the polarity of the substrate pocket. The hydroxy group of T438 formed a hydrogen bond with the carboxylate

group of E267 (Figure 1.15 B). T268 is crucial for dioxygen binding and proton delivery.[50,347,348] T268A disrupted such process, and facilitated carbene transfer to yield almost enantiopure cyclopropanes.[349] However, the T268A variant showed excellent efficacy (comparable to wild type) for the hydroxylation of the fatty acids with 14 and 15 carbons, whereas the fatty acids with 12 and 16 carbons were less active.[321] This suggested that the deleterious effect of T268A on molecular oxygen activation was also substrate-dependent.[321] Mutation of E267 (to Q or V) did not cause loss of activity,[350,351] suggesting that other residues could also assist proton delivery. Ala264 was close to the heme; its carbonyl oxygen forms a hydrogen bond with the heme sixth ligand in the SF structure. The A264G mutation enhanced PAH oxidation significantly and altered product distributions.[304] I263A was found to alter valencene oxidation activity and selectivity,[323] and the enantioselectivity of terminal epoxidation of linear alkenes,[231] while I263G altered the regioselectivity of fatty acid oxidation towards the internal carbons.[325]

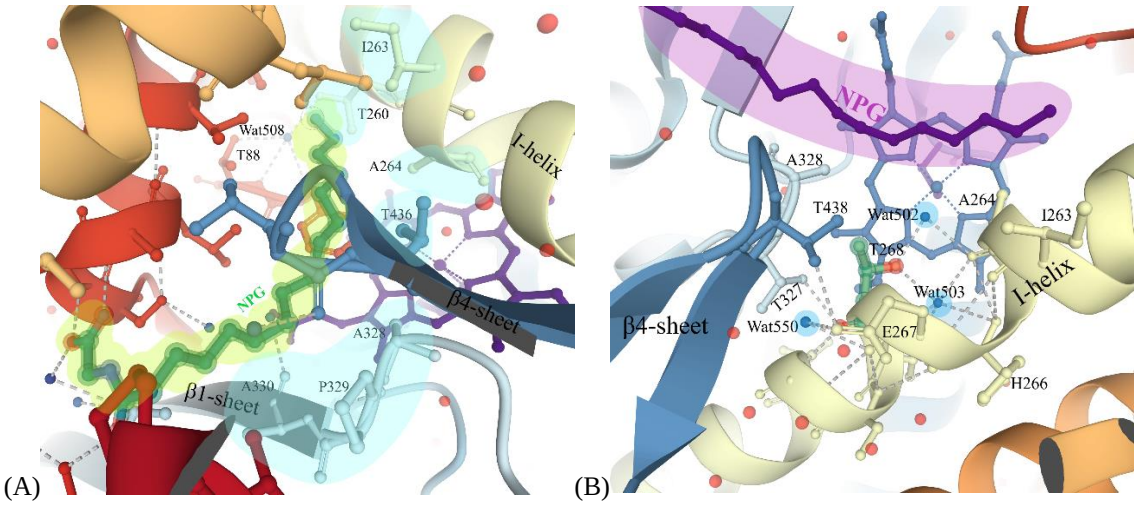


Figure 1.15 The lateral wall constructed by T260/I263/A264/T436/A328/P329 and the bottom occuppied by A330 of the substrate access channel of the SB WT and the hydrogen bonding network of E267/T268.

A328 was another frequently mutated residue in $P450_{BM3}$. The NPG-bound A328V crystal structure showed little difference from NPG-bound WT (RMSD = 0.12 Å), but the activity pattern was altered to favour ω–1 hydroxylation of fatty acids.[352] Directed evolution at

A328/P329 engineered the enantioselectivity of the allylic hydroxylation of 1-methyl-cyclohexenecarboxylate with both V/N/I and Y/C/H/I/G/D/S at the 328 and 329 sites favouring the *R*-enantiomer;[353] A328L was reported enhancing silane hydroxylation after site-saturation mutagenesis;[354] A328F was found to improve benzene dihydroxylation by developing a "triple-Phe" barricade inside the active site (F82/F87/F328) to stabilise the substrate and its intermediates.[248] The structure of the SF A330P variant (PDB code: 3m4v) showed disrupted arrangement of the A328–A330P loop of the WT and P329 intruded inward by 2.6 Å, constricting the F87, I-helix and A328–A330P enclosure;[355] the distal water (Wat1020) of the heme in the SF WT was displaced to Wat562 in the SF A330P, and fewer water molecules remained in the active site (Figure 1.16). This more restricted active site was apt to accommodate smaller molecules that the A330P variant enhanced turnover and altered activity for pentane[333] and alkylbenzenes.[356]

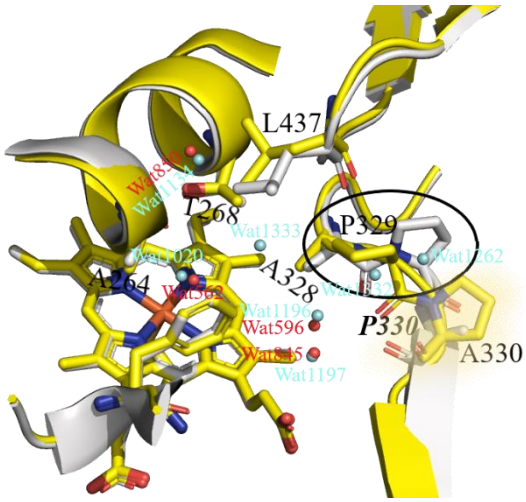


Figure 1.16 Overlay of the crystal structures of SF A330P (yellow, water in red) and WT (grey, water in cyan).

Mutations at L437 impacted the catalytic efficiency and product profile in drug metabolism. L437E, via a hydrogen bond with L188Q to reorient the substrate inside the active site, enhanced conversion and C5'-hydroxylation of flucloxacillin, whereas L437 and L437N/S/T/A gave lower conversion and different product profiles.[311] The bulky side-chain of L437 implied that mutations that reduced the side-chain volume might enlarge the

substrate pocket hence expanding the substrate range towards large molecules. However, this was not true in $P450_{BM3}$ oxidation of the precursor to Nigelladine A: the L437A mutation showed impaired activity in contrast with the WT.[357] L437K/R decreased the catalytic efficiency for linear substrates.[306] L437I slightly improved the oxidation of 3-methulanisole and shifted the regioselectivity.[358] L437V/F altered the enantioselectivity of sulfoxidation of 1-thiochroman-4-ones.[359] L437N/T/S showed similar regioselectivity in the incubation with the racemic α-ionone, whereas these three mutations favoured the *S*-enantiomer of 3-hydroxy product regardless of incubating with pure *S*- or *R*-α-ionone.[360] The insertion mutation L437LV promoted *p*-phenol formation in the oxidation of *N*-protected anilines.[361] T438V/I/L/F were added into the A82F variant to engineer the stereoselectivity of styrene epoxidation, with T438F/V favouring the *R*-styrene oxide.[362]

1.2.3 A variant library screening methodology

The methodology adopted in this thesis used a small library of 48 $P450_{BM3}$ variants in two 24-well plates to screen selected substrates for oxidation. These variants are a subset of a library of >400 variants established on the base variants A330P, RP (R47L/Y51F/I401P), RT2 (R47L/Y51F/KT2), GVQ (A74G/F87V/L188Q), K19/F87A (F87A/H171L/Q307H/N319Y) and R19 (R47L/Y51F/K19). Mutations at two or more active site residues including R47, Y51, S72, A74, V78, F81, A82, F87, H171, A184, L188, I263, A264, E267, A328, P329, Q403, and L437 were introduced to reshape the substrate pocket by altering its polarity and topology, which in theory would offer greater product diversity and wider substrate specificity. Activity and selectivity analysis of the screening data, assisted by crystal structure analysis, provided guidance for designing new generation variants aiming at higher catalytic efficiency and regio- and stereoselectivity for the target products. Such methodology have been used in oxidation of PAHs,[333] steroids,[363] natural products,[336] and amine drugs (Figure 1.17).[185,345,361]

Of the base variants, K19 contains the activity-enhancing F87A and H171L mutations. The crystal structure of the A330P variant showed repositioning of P329 into the substrate pocket, disrupting the arrangement of active site waters and reducing the active site volume (Figure 1.16). The crystal structure of SF I401P showed that the proline mutation caused the heme to drop away from the substrate pocket to a position similar to that in the SB WT structure (Figure 1.18). The water "ligand" was 3.6 Å from the heme iron and thus readily displaced even by non-natural substrates that fit less well into the active site to initiate the catalytic cycle, leading to enhanced activity towards numerous compounds.[364] The KT2 variant (A191T/N239H/I259V/A276T/L353I) showed enhanced activity with a wide range of compounds.[303,333] Its SF crystal structure (PDB code: 3psx) was superimposable on that of the SB WT. The N239H mutation likely initiated the conformational change by breaking the Q229–N239 salt bridge, thus freeing G-helix movements that cascaded to cleavage of the K224–D251 salt bridge between the G- and I-helices.[303] The only remaining D217–R255 salt bridge between these helices adopted the conformation of the SB WT (Figure 1.19).[303] Both the I401P and KT2 mutants could be considered to be in more catalytically-ready conformations, such that the kinetic gating of the P450 catalytic cycle by slowing down the 1st electron transfer without a viable substrate being bound, no longer operated. These structural and biochemical features made the base variants excellent platforms for enzyme engineering.

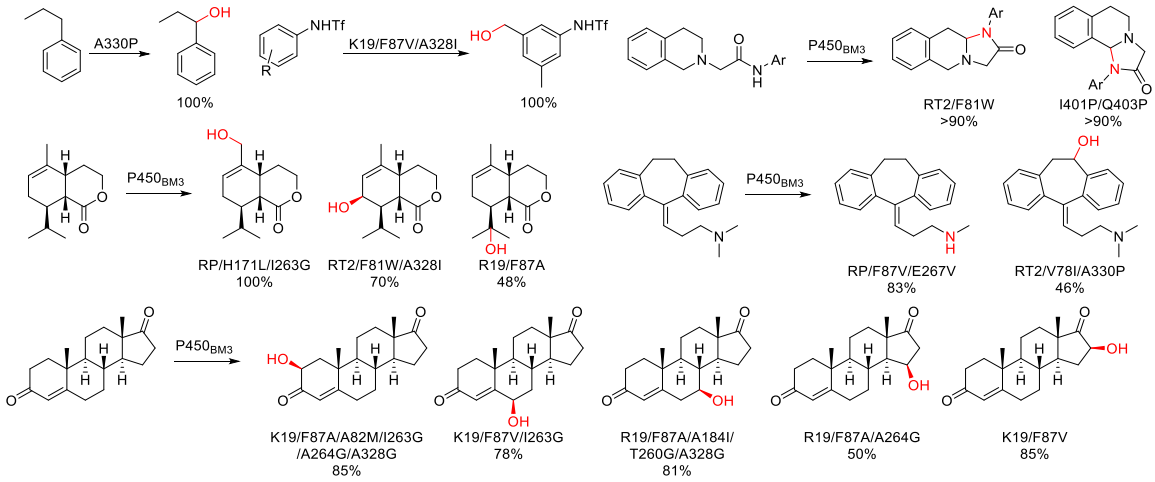


Figure 1.17 A selection of successful research in Wong group undertaking the variant library screening methodology.

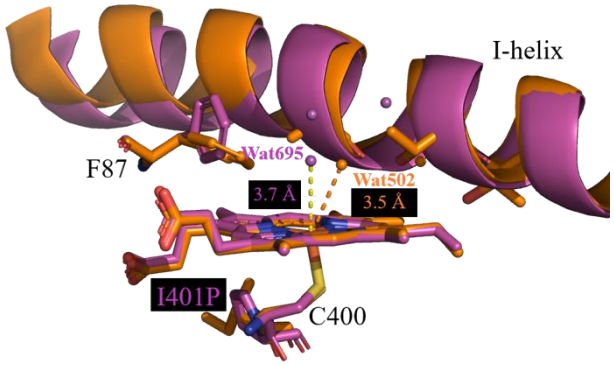


Figure 1.18 Overlay of the SF I401P (magenta) and SB WT (orange) crystal structures.

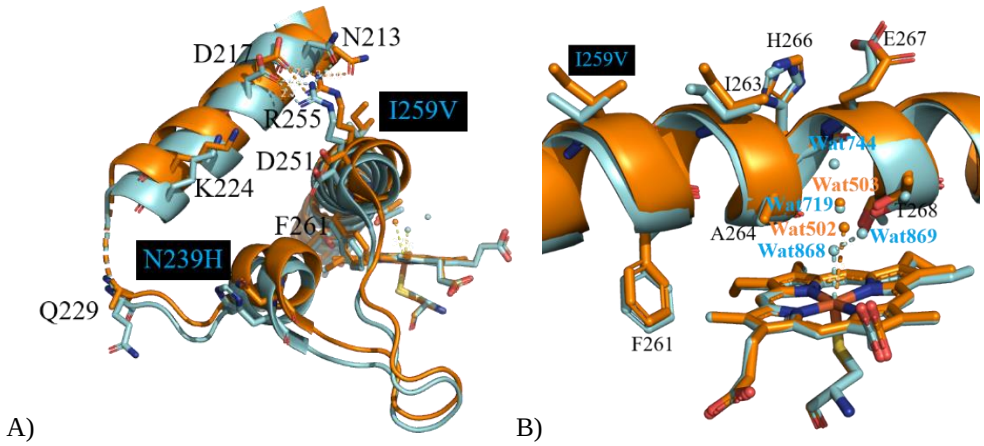


Figure 1.19 Overlay of the SF KT2 (cyan) and the SB WT (orange) crystal structures.

1.3 Cyclic amine functionalisation in drug discovery

Six strategies[365,366] have been developed to obtain hits and leads in drug discovery, including (a) modification of existing active molecules, (b) systematic high-throughput

screening (HTS) of natural products and synthetic compounds,[367] (c) retroactive analysis of biological information for drug optimisation, (e) rational design based on molecular pathological mechanisms, and (f) identification of small molecules with low efficacy that are then linked together to provide lead compounds. The last approach is also known as fragment-based drug discovery (FBDD).[368,369] In contrast to HTS which suffers from huge screening efforts (10^5–10^6 compounds), inadequate diversity, low hit rates, and poor druggability,[366] FBDD screens smaller numbers of compounds of high structure diversity (~10^3 compounds) to search for low-affinity fragments (K_d in the μM–mM range), avoiding the drawbacks of HTS.[368] The combination of both strategies in practice gave rise to numerous FDA-approved drugs.[370–380] The general principles of HTS and FBDD can be illustrated by simplified ligand-protein binding models (Figure 1.20).[381] For HTS, ~10^6 drug-like molecules (up to 30 heavy atoms) are screened for leads with high affinity (K_d <1 μM),[368] whilst only ~10^3 drug fragments (up to 20 heavy atoms, MW <300 Da) are tested to find low-affinity fragments (K_d >1 mM).[382–385] Less complex molecules showed higher hit rates,[384] especially when fragments are selected by the 'rule of 3' principle, that is, a molecule of MW <300 Da, with a cLogP of ≤3, and 3 or fewer hydrogen bond donors/acceptors.[386]

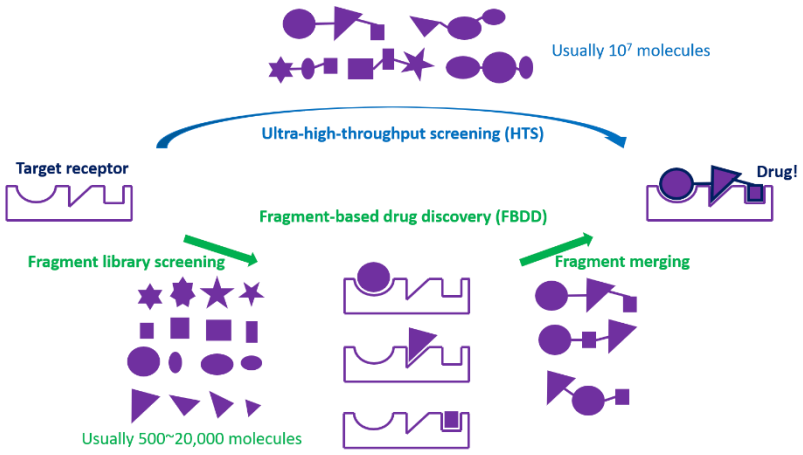


Figure 1.20 Simplified illustration of the principles for HTS and FBDD.

Since cyclic amines are common cores of drugs and natural products, with 59% of FDA-approved drugs containing nitrogen heterocycles,[387] all fragment libraries for FBDD include such molecules. A selection of fragment-to-lead examples is shown in Figure 1.21.[386] The most common cyclic amine drug cores are pyrrolidine and piperidine, often with multiple substitutions.[387,388] Simple 2D-rings (*e.g.* pyridine or benzene) are more frequently used than 3D-rings (pyrrolidine or cyclopentane, *etc.*), and mono- and bi-cyclic compounds predominate the cyclic fragments of drugs.[388] These cores are also the scaffolds of alkaloids with a variety of pharmacological activities (Figure 1.22).[389] Methods for cyclic amine functionalisation at all available carbon/nitrogen atoms are hence of interests.

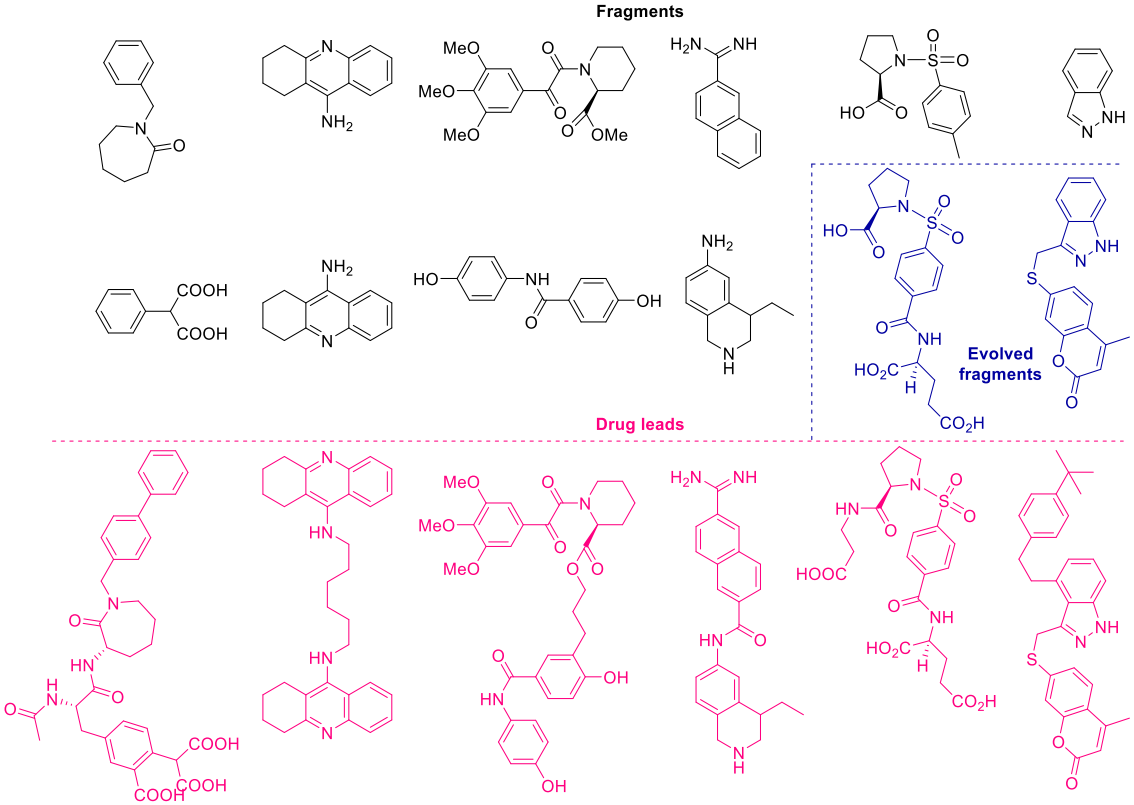


Figure 1.21 Lead identification by fragment-evolving and fragment-linking.[386]

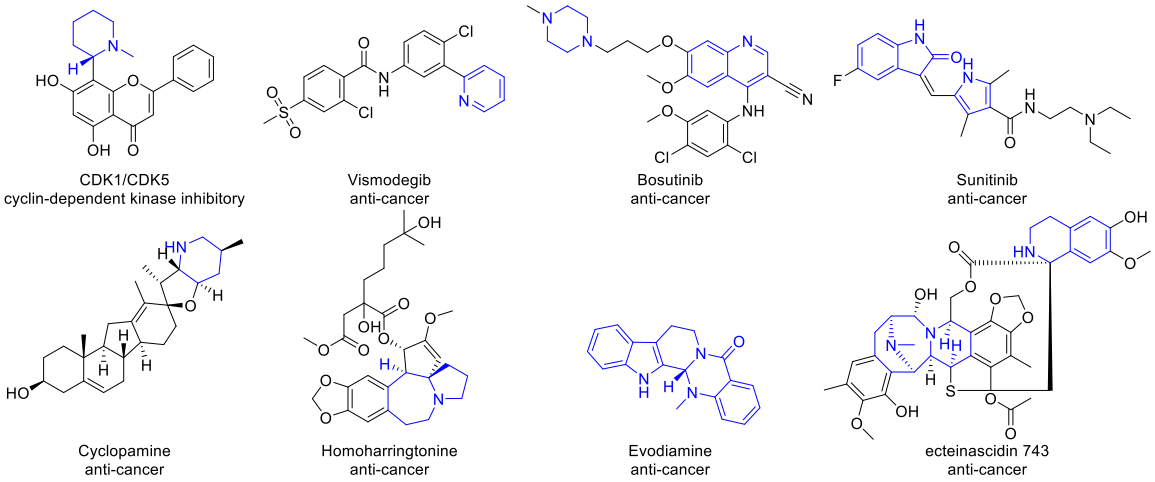


Figure 1.22 A collection of alkaloid drugs.

Routine methodologies are well established for α-C–H activation. α-Substituted saturated cyclic amines are prepared, either by direct sp^3 C–H activation[390–397] or by the construction of the α-functionalised heterocycle from the corresponding acyclic amine derivatives (Figure 1.23).[397,398] Direct sp^3 C–H activation can be divided mechanistically into four major groups: (a) α-amino anion species reacting with nucleophiles,[395,399,400] (b) α-amino cation species (iminium) reacting with nucleophiles, subdivided into transition-metal (Cu[401–404], Pt[405], *etc.*) catalysed oxidation, chemical oxidation,[406] thermal oxidation,[390] electrochemical oxidation[407] and visible light-induced photocatalytic oxidation,[392] (c) α-amino radical rebound with radicophiles,[408] and (d) transition metal-catalysed C–H activation (Pd[394] or Ru[409,410]).[391,393] Establishment of pyrrolidine/piperidine rings can be accomplished by *N*-centred radical mediated reactions via N–X (X = F, Cl, Br or I) or N–H bond cleavage,[411,412] which would generate α-functionalised products but also β-[413] and multi-functionalised cyclic amines,[414,415] by transition-metal catalysts (Pd[416] and Rh[417–419]).[397]

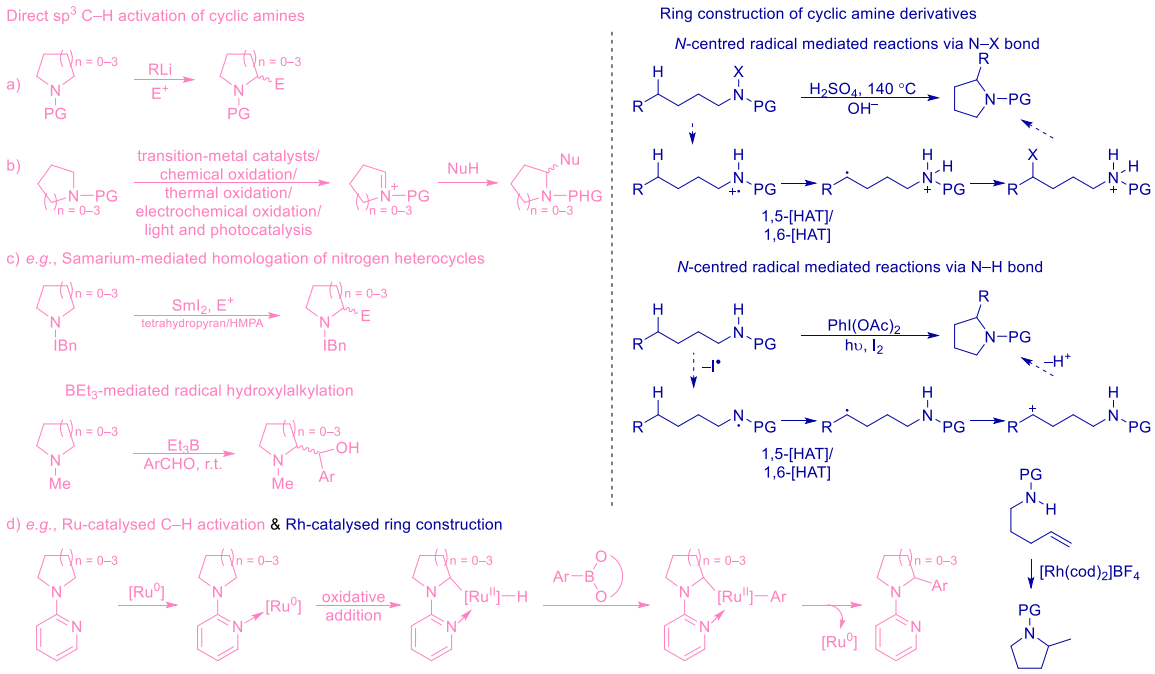


Figure 1.23 Available methodologies to obtain the α-functionalised cyclic amine derivatives. (HAT: hydrogen atom transfer)

Direct β-C–H activation is also possible (Figure 1.24). Ru^{II}-catalysed coupling of cyclic amines and aldehydes led to β-alkylation with good regioselectivity.[420,421] γ-Functionalisation was reported via Pd-catalysed transannular C–H arylation of alicyclic amines affording reasonable yields of the target enantiomers.[422] Nevertheless, remote functionalisation of cyclic amines remains challenging in classical synthesis.

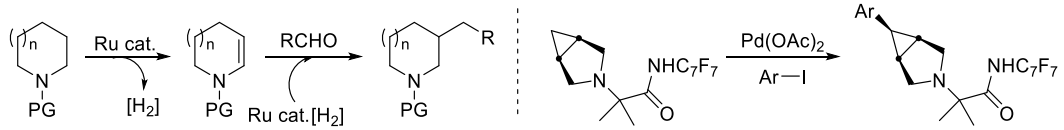


Figure 1.24 Examples of direct β- & γ-functionalisation of cyclic amines via transition metal catalysis.[420–422]

Biocatalysts such as cytochrome P450 enzymes may provide a controllable approach for remote functionalisation of cyclic amines. Li and co-workers[423–429] reported β- and γ-C–H bond activation of cyclic amines and lactams by engineered P450pyr with high regio- and enantioselectivity;[430] *Beauveria bassiana* ATCC 7159 produced the β-/γ-/δ-alcohols of five-, six-, and seven-membered ring amines (Figure 1.25).[431,432] *Beauveria bassiana* ATCC 7159,[431,432] *Cunninghamella elegans*[433] and *Streptomyces antibioticus* ATCC

14890[434] showed C–H activation at non-activated sites of complex cyclic amines and lactams. Quinoline and isoquinoline were metabolised by microsomal CYPs[435] and P450cam.[436]

Although microbial oxidation had been used extensively, it was notable that cyclic amine oxidation by defined, recombinant P450 enzymes remained poorly explored. Previous studies showed that common P450 oxidation activities for amines were *N*-dealkylation and *N*-oxidation.[437–439] These were common outcomes from drug metabolism by human CYPs. Two possible mechanisms were proposed for *N*-dealkylation: hydrogen atom transfer (HAT) for conjugated amines,[440–444] and single electron transfer (SET) for non-conjugated amines (Figure 1.26).[445–449] *N*-oxidation occurred primarily for neutral nitrogen atoms to form either N–OH from N–H or *N*-oxide from tertiary nitrogen atom by SET.[450–455] Although these are mechanistically interesting in the context of P450 activity, there were few examples of controlled remote functionalisation of cyclic amines and lactams with high selectivity.

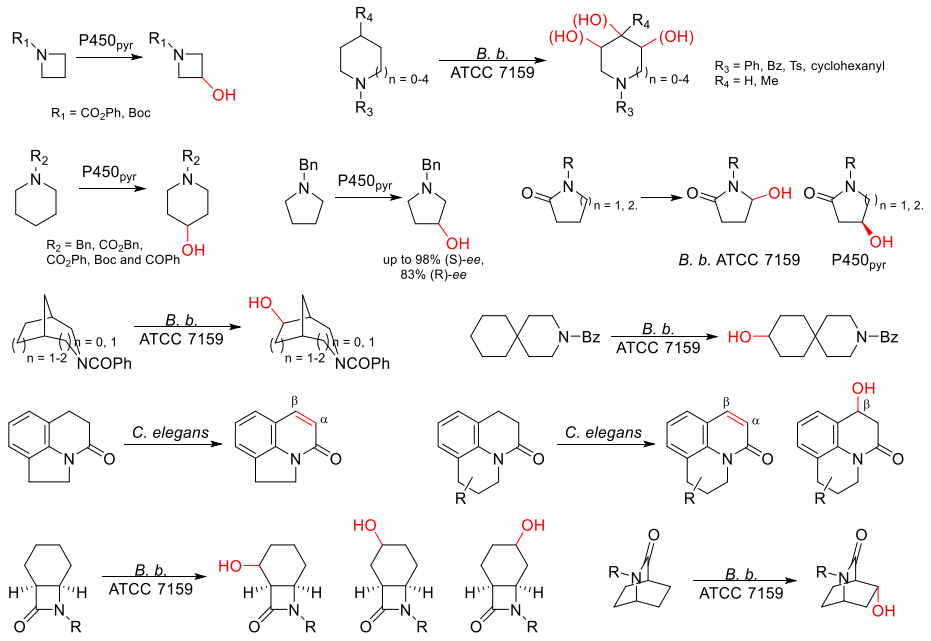


Figure 1.25 P450 oxidation of single-ring and complex cyclic amines and lactams.[225,424,428,429,431–434,456]

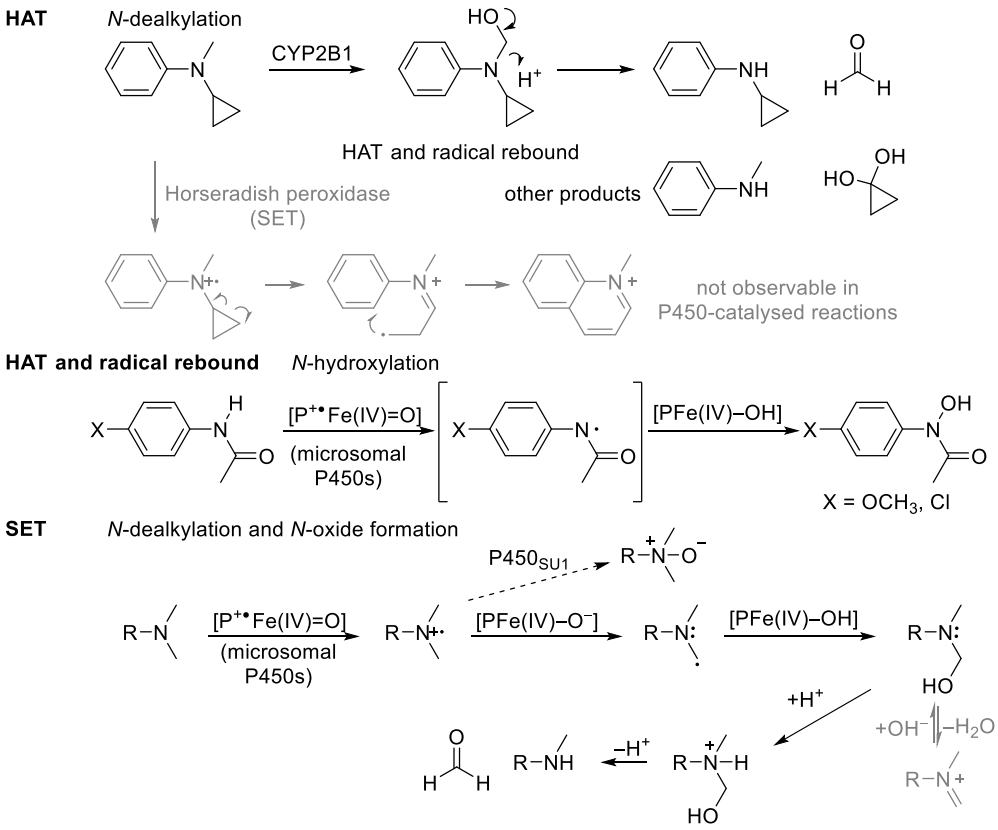


Figure 1.26 Proposed mechanisms for predominant P450-catalysed oxidation activities towards amines.

1.4 Objective of the thesis

The work described in this dissertation set out to explore remote C–H bond oxy-functionalisation of cyclic amines and lactams by engineered P450$_{BM3}$ with high product diversity and selectivity, and to identify variants and mutations which show similar effects on the selectivity of oxidation across related compounds. New P450$_{BM3}$-catalysed reaction types are also of interest. The ultimate goal of the research is to expand the usage of these enzymes in drug synthesis.

The substrates explored in this thesis are shown in Figure 1.27. Two methodologies are adopted: (a) protein engineering via rational design/evolution under the guidance of mutation-activity correlations observed from screening with a 48 P450$_{BM3}$ variant library; and (b) substrate engineering through the introduction of substituents (*e.g.* methyl and methoxy), *N*-protecting groups (*e.g.* phenyl, benzyl, acyl, Boc, mesyl, tosyl, and

isopropylsulfonyl), functional group (*e.g.* carbonyl) and auxiliary carbocycles (*e.g.* cyclopentane, cyclohexane and cycloheptane). The effect of substrate aromaticity on $P450_{BM3}$ oxidation of fused-ring cyclic amines is also studied.

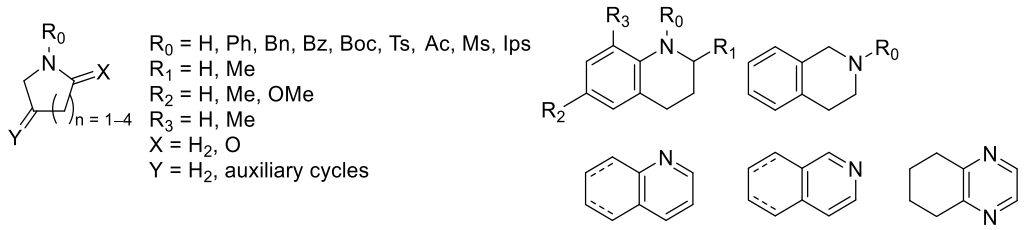


Figure 1.27 A collection of the investigated cyclic amines and lactams in this dissertation.

In the thesis, Chapter 3 describes the oxidation of *N*-phenyl pyrrolidine and piperidine, leading to the discovery of the enzymatic Povarov reaction with examples of cross-coupling of cyclic amines. Chapters 4, 5 and 6 respectively explore the mutation, substituent and *N*-protecting group effects on the oxidation of the fused-ring quinoline, tetrahydroquinoline and tetrahydroisoquinoline cores, showing high product diversity for their lactam derivatives and evidence for remote functionalisation. Therefore, Chapter 7 investigates the remote functionalisation of monocyclic and spirocyclic lactam derivatives, with examples of high product diversity and selectivity for some of the hydroxy-lactam products. Chapter 8 gives a summary of the results of the thesis and suggestions for further work.

Chapter 2 Materials and Methods

2.1 Materials, chemicals and equipment

2.1.1 Chemicals, solvents and materials

General reagents and chemicals were from Alfa-Aesar, Fisher Scientific, Sigma-Aldrich, and Fluorochem, UK, and Tokyo Chemical Industry, Japan. *N*-Phenyl pyrrolidine, 1,2,3,4-tetrahydroquinoline, 8-methyl-1,2,3,4-tetrahydroquinoline, 6-methyl-1,2,3,4-tetrahydro-quinoline, quinoline, quinaldine, 6-methylquinoline, 8-methylquinoline, 5,6,7,8-tetrahydro-quinoline, 5,6,7,8-tetrahydroisoquinoline, 5,6,7,8-tetrahydroquinoxazaline, 6-methoxy-1,2,3,4-tetrahydroquinoline, pyrrolidine, piperidine, *N*-Boc-pyrrolidine, *N*-Boc-piperidine, *N*-phenyl-pyrrolidin-2-one, *N*-benzyl-pyrrolidin-2-one, *N*-benzyl-piperidin-2-one, ε-caprolactam, ζ-enantholactam, *N*-Boc-2-piperidone, *N*-Boc-ε-caprolactam, glutarimide, 1-(2-bromophenyl)-piperidine, 1-(4-amino-phenyl)-piperidine, 4-phenyl-piperidine, and 4-(1-pyrrolidinyl)-piperidine were from Sigma-Aldrich. *N*-Vinyl-ε-caprolactam, 1,2,3,4-tetrahydro-quinaldine, 3-hydroxyquinoline, 3,4-dihydro-(2*H*)-quinoline, 3*S*-hydroxy-pyrrolidine, 3*R*-hydroxy-pyrrolidine, 3*S*-hydroxy-piperidine and 3*R*-hydroxy-piperidine were from Fluorochem. All spirolactams and heptamethyleneimine were acquired from Tokyo Chemistry Industry. *N*,*N*-Diethylaniline, *N*-ethylaniline, aniline and 1,2,3,4-tetrahydroisoquinoline were from Alfa-Aesar. The reagents di-tert-butyl-bicarbonate, mesyl chloride, tosyl chloride, ipsyl chloride, acetyl chloride, DMAP, benzyl bromide, sodium hydride, β-mecaptoethanol, lithium aluminium hydride and pyridine were from Sigma-Aldrich and Fisher Scientific.

HPLC grade solvents were from Sigma-Aldrich and Merck. Media components were from Melford Laboratories, Sigma-Aldrich and Fisher Scientific. Kanamycin was from Melford Laboratories. Glucose dehydrogenase was from Codexis, USA. NADPH was from Apollo Scientific. $NADP^+$ monosodium salt was from Prozomix. Isopropyl-β-D-thiogalacto-

pyranoside (IPTG) was from Fisher Scientific. Lysozyme and catalase were from Sigma-Aldrich. Oligonucleotides were supplied by Eurofins Genetic Services, UK.

2.1.2 General protocols for the synthesis of the target substrates and products

2.1.2.1 Synthesis of the *N*-Boc amines and amides

To a solution of amine or amide (0.2 M, 1 eq) in anhydrous tetrahydrofuran was added 4-dimethylaminopyridine (DMAP, 0.21 M, 1.05 eq). Di-tertbutyl-di-carbonate (0.26 M, 1.3 eq) dissolved in anhydrous tetrahydrofuran was added dropwise into the mixture so that the temperature was maintained ≤25 °C and the reaction mixture was then stirred at ambient temperature for 4 hours (monocyclic amines) or 16 hours (fused-ring amines and lactams). The solvent was thereafter removed *in vacuo* and the residue re-dissolved in ethyl acetate. The organic layer was washed sequentially with the same volume of 0.1 M HCl, saturated $NaHCO_3$ and brine, dried over sodium sulfate, filtered and evaporated to give the crude mixture. This mixture was then purified by silica gel chromatography using petrol:ethyl acetate (from 6:1 to 1:1 *v/v*, according to the substrate) as eluent to afford a yellow oil in most cases.

2.1.2.2 Synthesis of the *N*-Ms-, *N*-Ts-, and *N*-Ips-amines

A fused-ring amine (0.1 M, 1.0 eq) was dissolved in dry pyridine. The sulfonyl chloride (0.14 M, 1.4 eq) was added dropwise and the reaction mixture was stirred overnight at room temperature. Monitoring by gas chromatography and TLC indicated that the reaction was completed. The solvent was removed *in vacuo* to afford the crude to which a solution of 1 N HCl (50 mL) and ethyl acetate (50 mL) were added. The organic layer was separated, and the aqueous phase was extracted twice with ethyl acetate (2× 50 mL). The combined organic phase was dried over sodium sulfate and the solvent was removed *in vacuo*. The product was purified by silica gel chromatography using petrol:ethyl acetate as eluent.

2.1.2.3 Synthesis of the *N*-benzyl lactams

To the solution of a lactam (0.1 M, 1 eq) in DCM was added NaH (0.105 M, 1.05 eq) and the mixture was stirred for 0.5 h to allow the mixture to cool to room temperature. Benzyl bromide (0.15 M, 1.5 eq) was added to the mixture which was stirred overnight. The reaction was treated with 1/5 volume of saturated ammonium chloride solution and the aqueous layer was extracted with ethyl acetate. The combined organic extracts were dried over anhydrous sodium sulfate and concentrated *in vacuo*. The crude was then purified by silica gel chromatography using petrol:ethyl acetate (1:1 *v/v* mixture) as eluent to afford the *N*-benzyl lactam.

2.1.2.4 Reduction of lactams

Lithium aluminium hydride (0.5 M, 5 eq) was dissolved in 50 mL of anhydrous tetrahydrofuran and cooled to 0 °C in an ice bath under argon. After it was completely dissolved, the lactam (0.1 M, 1 eq) was dissolved in 20 mL anhydrous tetrahydrofuran and added dropwise to the lithium aluminium hydride solution. After the addition was completed, the reaction mixture was stirred at room temperature for 0.5 hour, and then heated to reflux for 4.5 hours. After TLC monitoring showed that the reaction was completed, the mixture was cooled to 0 °C, followed by successive slow addition of water (1/50 of the reaction volume), 15% sodium hydroxide solution (1/50 of the reaction volume) and water (3/50 of the reaction volume) and stirring for 0.5 hour. Into the mixture was added sodium sulfate, and the mixture was filtered over Celite. For non-protected lactams, the same volume of 1 N HCl in diethyl ether was added to the filtrate at 0 °C, and the mixture was stirred for 1 hour, then concentrated to obtain its hydrochloride salt. For protected lactams, the filtrate was concentrated *in vacuo* to afford the crude mixture which was further purified by silica gel chromatography using DCM:MeOH as eluent to yield the target product.

2.1.3 Growth media and buffer components

Water used for bacterial growth was purified using Millipore Elix systems. Type 1 water (resistivity ≥12 MΩ cm) was used for the preparation of media, general enzyme manipulations and biotransformation reactions; type 2 ultrapure water (≥18 MΩ cm) was utilised in molecular biology experiments such as PCR, DNA purification, electrophoresis and primer dilution. The components of media (per L) are listed in Table 2.1 and the components of the buffers (per L) in Table 2.2. All media were steam sterilised at 120 °C for 20 mins. LB_{kan} and FB_{gly} included 30 mg L^{-1} kanamycin, which was added after cooling to ambient temperature. The pH of the media and the buffers was adjusted according to the principle of introducing no new components into the system.

Table 2.1 Growth media components.

Medium	Components (per L)
LB	10 g tryptone, 5 g yeast extract, 10 g NaCl.
LB_{agar}	10 g tryptone, 5 g yeast extract, 10 g NaCl, 15 g bacto-agar.
SOC	20 g tryptone, 5 g yeast extract, 0.5 g NaCl, 10 mL 250 mM KCl. Adjust to pH 7.0 using 10 M NaOH, then add 20 mL of filter-sterilised 20% (*w*/*v*) glucose.
FB_{gly}	19.2 g $K_2HPO_4 \cdot 3H_2O$, 3.6 g $NaH_2PO_4 \cdot 3H_2O$, 2.5 g $(NH_4)_2SO_4$, 2.0 g Na_2SO_4, 1.2 g $Na_3C_3H_5O(COO)_3 \cdot 2H_2O$, 0.5 g NH_4Cl, 5.0 mL glycerol. Autoclave and then add 2.0 mL 1 M $MgSO_4 \cdot 7H_2O$, 3.0 ml trace elements solution, 1.0 mL 10% *w*/*v* thiamine-HCl.
Trace elements	20.1 g Na_2EDTA, 16.7 g $FeCl_3 \cdot 6H_2O$, 0.74 g $CaCl_2 \cdot H_2O$, 0.25 g $CoCl_2 \cdot 6H_2O$, 0.18 g $ZnSO_4 \cdot 7H_2O$, 0.132 g $MnSO_4$, 0.1 g $CuSO_4 \cdot 5H_2O$.

Table 2.2 Buffer components.

Buffer	Components (per litre)
50× TAE, pH 8.5	242.2 g Tris, 57.1 mL glacial acetic acid, 100 mL 0.5 M Na_2EDTA. Supplied by manufacturer and diluted 50 folds before use.
TFB1, pH 5.8	100 mM RbCl, 50 mM $MnCl_2$, 30 mM KOAc, 10 mM $CaCl_2$. Adjusted to pH 5.8 using 1 M acetic acid, filter sterilised prior to use.
TFB2, pH 6.8	10 mM MOPS, 10 mM RbCl, 75 mM $CaCl_2$, 30% *v*/*v* glycerol. Adjusted to pH 6.8 using 1 M KOH, filter sterilised prior to use.
100 mM phosphate, pH 8.0	16.28 g K_2HPO_4, 0.89 g KH_2PO_4. Adjusted to pH 8.0 using either 1 M K_2HPO_4 or 1 M KH_2PO_4.

TFB1, TFB2 = Transformation buffers 1 and 2

2.1.4 Equipment

Sonication was carried out using a Misonix 3000 sonicator and Fisher Scientific FB-505 ultrasonic processor. PCR experiments were completed in a Techne thermocycler. UV-visible spectra were acquired on an Agilent Cary 50 spectrophotometer. Chiral phase gas chromatography analyses were performed on a Thermo Finnigan Trace instrument equipped with a flame ionisation detector (FID) and an AS3000 autosampler using a CYCLOSIL-B fused silica column (30 m × 0.25 mm × 0.25 μm film thickness) and Thermo Finnigan Trace1300 GC fitted with an FID, a DB-1 fused silica capillary column (30 m × 0.25 mm × 0.25 μm film thickness) and an AI 1310 autosampler. Helium was used as the carrier gas at a flow rate of 1.5 mL min^{-1}. The injectors were maintained at 200 °C, 250 °C or 280 °C and the FID at 250 °C. ^{1}H and ^{13}C NMR spectra were recorded on Bruker Avance AVII 400 (400.2 MHz for ^{1}H and 100.6 MHz for ^{13}C) or AVIII 500 (499.9 MHz for ^{1}H and 125.7 MHz for ^{13}C <AVD500>, 500.3 MHz for ^{1}H and 125.8 MHz for ^{13}C <AVC500>) spectrometers in $CDCl_3$ or MeOD, internally referenced to the residual protio solvent. Mass spectra (MS) were acquired on a Bruker microTOF spectrometer operating in electrospray ionisation (ESI) mode.

2.2 Molecular biology

2.2.1 Mutagenesis primer design

For each mutagenesis reaction, two staggered complementary oligonucleotides comprising 30 to 50 bases were designed using SnapGene Viewer, including at least 10 bases to the 5'-side of the mutated nucleotide(s) and 15 bases after its 3'-side with normally 21 bases complementary to each other and the rest specifically binding to the corresponding template DNA during the annealing process. Oligonucleotide sequences are listed in Appendix 2. Melting temperatures (T_m) were calculated and shown by SnapGene Viewer which were 2

to 3 °C lower than the value calculated by the equation in the Stratagene mutagenesis protocol (Eq. 2.1):

$$T_m\ (°C) = (675/N) + (0.41 \times GC) - M + 81.5 \qquad \text{(Equation 2.1)}$$

where N is the primer length (in bases), GC the guanine/cytosine percentage, and M the percentage of mismatching nucleotides. Therefore, the experimental annealing temperatures ($T_{a\text{-}exp}$) were calculated as (T_m – 2.5) °C.

The double-mutation primers at the residues I263 and E267 were designed according to the back-to-back principle which had nine complementary overlapping base pairs at the unmutated interval region of A264/G265/H266, particularly with the 5' of the forward primer starting from the first nucleotide of A264 and containing the E267 mutation, and the 5' of the reverse primer initiating from the first complementary 5' nucleotide of T266 and mutating at the I263 residue. The length of each primer followed the common rule of primer design which should be within 30 to 50 base pairs and the T_m was calculated by SnapGene and should be kept within the range from 55 °C to 65 °C with the difference between the forward and the reverse primers less than 2 °C. The usage of these back-to-back primers could introduce 2 mutations in one PCR reaction.

The degenerate primers were designed according to the principle of the staggered primers, using NDT (N = A, G, C, T; D = A, G, T) as degenerate codon at the mutated residue which could generate Asn, Asp, His, Tyr, Ser, Gly, Cys, Thr, Iso, Val, Leu and Phe, and the melting temperature of the degenerate primers in site-saturation PCR reactions was calculated individually for the entire 12 primer pairs and the touch-down PCR-running program was operated.

2.2.2 Site-directed mutagenesis

Site-directed mutagenesis was performed by a polymerase chain reaction (PCR)-based method using the KOD Hot Start Polymerase kit from Merck. Based on the manufacturer's guidelines, the reaction components are listed in Tables 2.3 and the cycling conditions are given in Table 2.4 for the set-temperature and the touch-down programs. The template DNA in each PCR reaction was digested for 1 h at 37 °C using 1 mL of Dpn I.

Table 2.3 Components for site-directed mutagenesis using KOD Hot Start Polymerase.

Component	**Volume / µL**
10× KOD Hot Start buffer	5
10 mM dNTPs	5
25 mM $MgSO_4$	3
DMSO	2
10 µg µL−1 template DNA	0.5
10 µM forward primer (5'−3')	1.5
10 µM reverse primer (3'−5')	1.5
KOD Hot Start polymerase	1
dd H_2O	30.5

Table 2.4 Cycling conditions for KOD Hot Start DNA Polymerase.

Program	**Description**	**Time/s**	**Temperature/°C**	**No. of cycles**
Set-temperature	Initial denaturation	180	95	5
	Denaturation	20	95	35
	Annealing	10	T_m – 2.5	
	Extension	160	70	
Touch-down	Initial denaturation	180	95	5
	Denaturation	20	95	5
	Annealing	10	T_m + 2.5	($T_{a\text{-}exp}$ = T_m + n – 2.5 °C for the n cycle, n = 5)
	Extension	150	70	
	Denaturation	20	95	5
	Annealing	10	T_m – 2.5	($T_{a\text{-}exp}$ = T_m – n + 3.5 °C for the n cycle, n = 5)
	Extension	150	70	
	Denaturation	20	95	25
	Annealing	10	T_m – 5	($T_{a\text{-}exp}$ = T_m – 5 °C, for all cycles)
	Extension	150	70	

2.2.3 Agarose gel electrophoresis

Agarose (0.5 g) was dissolved in 50 mL 1× TAE buffer by microwave heating for 2 min using a defrosting program. RedSafe (2 µL, 10 mg/mL) was added, and the gel was poured into the mould with the cell comb and left to solidify for 30 min after which the cell comb was removed. 250 mL of 1× TAE was used as running buffer. Samples were loaded into 25 µL wells created at the cathodic end of the cell, with one being reserved for 4 µL of Promega 1 kbp DNA reference ladder. Diagnostic samples (12 µL) of PCR reaction mixtures included 2 µL Promega 6× loading dye, and were run for 20 min at 120 V, after which the separated DNA fragments were visualised under ultraviolet light. Diagnostic samples (4 µL) of DNA miniprep products included 2 µL Promega 6× loading dye, and were run for 20 min at 120 V, and the separated DNA plasmids were visualised under ultraviolet light.

2.2.4 Post-PCR transformation and DNA purification

After an hour of digestion of the 40 µL PCR reaction mixture using 1 µL Dpn I and 5 µL 10× Dpn I working buffer, 10 µL of the digested mixture was added into 40 µL *E. coli* DH5α or *E. coli* Acella competent cells freshly thawed from storage at −80 °C in a 1.5 mL microcentrifuge tube. After 30 min incubation on ice, the cells were heat-shocked at 42 °C for 45 seconds and placed back on ice for 5 min. 500 µL filter-sterilised SOC medium preheated to 37 °C was added, and the cells were incubated at 37 °C, 200 rpm for 2 hours before being spread onto an LB_{agar} plate containing 30 mg L^{-1} kanamycin. The LB_{agar} plate was then incubated for 16 hours in a 37 °C incubator and 5 mL LB_{kan} (containing 30 mg L^{-1} kanamycin) was inoculated by the single colony harbouring the target plasmid from the LB_{agar} plate. The inoculated LB_{kan} was left for overnight growth at 37 °C, 200 rpm.

DNA was purified using solutions supplied by the Thermo Scientific GeneJET Plasmid Miniprep kit (#K0503) according to manufacturer's protocol. The overnight LB_{kan} culture

was centrifuged at 10,000 *g* for 10 min; the supernatant was decanted, and the cell pellet was resuspended in 250 µL of the Resuspension Solution (100 µg/mL RNase A) then transferred to a 1.5 mL microcentrifuge tube. 250 µL of Lysis Solution was added and mixed by inverting the tube 4−6 times until the solution became viscous and slightly clear prior to incubation for 2−3 minutes. 350 µL of Neutralisation Solution was added and mixed carefully and thoroughly by reverting the tube 4−6 times. Cell debris and chromosomal DNA were removed by centrifugation at 14,800 *g* for 10 min. The cleared lysate from each tube was transferred to a GeneJET spin column by decanting or pipetting with no disturbance of the white precipitate. Spin columns were centrifuged at 14,800 *g* for 1 min and the flow-through was discarded. 500 µL of Wash Solution was added into the spin column, eluted by centrifugation at 14,800 *g* for 1 min and discarded. A further 500 µL wash solution was added, eluted by centrifugation at 14,800 *g* for 1 min and discarded. The column was then centrifuged for 2 min to ensure thorough solution clearance and left open in air at room temperature for 30 min in order to fully evaporate any remaining ethanol in the Wash Solution left on the column. 40 µL of Elution Buffer was added to the centre of the GeneJET spin column membrane and left incubating for 2 min, after which the DNA product was eluted by centrifugation for 1 min. The DNA solution was analysed by agarose gel electrophoresis and quantitated by UV spectroscopy. Each absorbance unit at 260 nm corresponded to a concentration of 5 µg/µL after 100-fold dilution.

The mutated $P450_{BM3}$ gene was sequenced by Source BioScience, UK using two primers, T7F and BM3FP2 (Table 2.5), to ensure the presence of the desired mutation(s).

Table 2.5 The primers for sequencing the $P450_{BM3}$ gene.

Primer	**Sequence**
T7F	TAATACGACTCACTATAGG
BM3FP2	CTGCAGCGAGCAAATCCAGACGAC

2.3 Enzyme production in *E. coli* and purification

2.3.1 Competent cell preparation

Cells of the desired strain (BL21 DE3, DH5α and Acella) were streaked onto an antibiotic-free LB plate and incubated at 37 °C for 16 h. A single colony was grown overnight at 37 °C in 2.5 mL of antibiotic-free LB in a sterile 50 mL centrifuge tube, shaking at 200 rpm. The overnight culture was transferred to 250 mL freshly-prepared antibiotic-free LB supplemented with 20 mM $MgSO_4$ and grown for a further 4−6 h at 37 °C, 120 rpm until OD_{600} reached 0.4–0.6. Cells were pelleted by centrifugation in sterile 50 mL tubes at 5,000 *g* for 5 min at 4 °C. The supernatant was discarded, and the tubes were centrifuged for a further 1 min, after which the remaining supernatant was removed with a sterile pipette. Each cell pellet was gently resuspended in 20 mL TFB1 on ice, and left for at least 20 min before centrifugation at 4,500 *g* for 5 min at 4 °C. Each cell pellet was then gently resuspended in 2 mL TFB2 on ice and left for 1 h. The cells were then placed as 100 µL aliquots into freshly sterilised 0.5 mL microcentrifuge tubes, flash-frozen in liquid nitrogen and kept in storage at −80 °C.

2.3.2 DNA Transformation

For plasmid DNA transformation, 1 µL of plasmid DNA was pipetted into 40 µL *E. coli* BL21 DE3 or Acella competent cells thawed from storage at −80 °C. After 30 min on ice, the cells were heat-shocked at 42 °C for 45 seconds and then placed back on ice for 5 min. 500 µL filter-sterilised SOC medium was added, and the cells were incubated at 37 °C, 200 rpm for 2 h before being spread onto an LB_{agar} plate containing 30 mg L^{-1} kanamycin. The plate was incubated at 37 °C for 16 h to afford single colonies.

2.3.3 Enzyme production and purification

A single colony of *E. coli* BL21 DE3 or Acella transformed with the $P450_{BM3}$ plasmid was inoculated into a 15 mL centrifuge tube containing 5 mL LB_{kan} media and grown at 37 °C, 200 rpm for 6 h. 500 µL of 66% *v/v* autoclaved glycerol was combined with 500 µL of this culture in a freshly-autoclaved 1.5 mL microcentrifuge tube, flash frozen in liquid nitrogen, and kept in storage at –80 °C as a cell stock.

For enzyme production, 10× FB_{gly} and $FB_{supplement}$ were prepared using Milli-Q water, following the recipe in Table 2.6. 1 mL of cells in the LB_{kan} culture was inoculated into a 2 L sterile conical flask containing 50 mL of 10× FB_{gly} and 450 mL Milli-Q water and 1.5 mL of $FB_{supplement}$ and grown at 37 °C, 160 rpm for 16 h. The incubator temperature was lowered to 20 °C and the shaking speed to 120 rpm, and the cultures were left to shake for at least 1 hour. Enzyme expression was then initiated and continued by adding 1 mL of induction solution (Table 2.7) and 0.5 g tryptone power every 12 h. The expression time could be two days if the colour of the cell culture turned red quickly (~24 hours) or three days if the red colour was light after 24 h of induction.

Table 2.6 Components of 10× FB_{gly} and $FB_{supplement}$.

Solution	**Component**	**Mass or Volume**
10× FB_{gly}	K_2HPO_4	147 g
	NaH_2PO_4	31 g
	$(NH_4)_2SO_4$	25 g
	Na_2SO_4	20 g
	$Na_3Citrate{\cdot}2H_2O$	12 g
	NH_4Cl	5 g
	glycerol	63 g
	Milli-Q water	1 L
$FB_{supplement}$ (sterilised by filtration through a 0.2 µm microbiological filter, added into 500 mL 1× FB_{gly})	Kanamycin	15 mg
	$MgSO_4{\cdot}7H_2O$	250 mg
	Thiamine·HCl	50 mg
	Trace Element	1.5 mL

Table 2.7 Components of the induction solution (sterilised by filtration).

Component	Mass or Volume
IPTG	380 mg
δ-ALA·HCl	672 mg
$FeSO_4 \cdot 7H_2O$	112 mg
Kanamycin	600 mg
Milli-Q water	40 mL

Cells of each 500 mL culture were harvested after 48 h or 72 h by centrifugation at 5,250 *g* for 10 min at 4 °C, and wet-cell-weight (wcw) per 500 mL was recorded for comparison of the per unit mass expression level of various mutants. The red cell pellet from each 500 mL culture was resuspended in 40 mL of 50 mM potassium phosphate, pH 8.0, with the addition of 10 mg lysozyme, by shaking at 160 rpm, 25 °C for 1 h.

The cell suspension was transferred to a 100 mL beaker and the cells are lysed by sonication on ice. The sonication procedure consisted of 20 cycles of 15-second pulses followed by a 30-second cooling period at 55% amplitude. The lysate was centrifuged for 15 min at 9,500 *g*, 4 °C to remove the cell debris. The supernatant containing the P450 enzyme was poured into a 100 mL beaker and subjected to ammonium sulfate fractionation. The amount of solid ammonium sulfate to achieve 40% saturation (calculated by the ammonium sulfate calculator http://encorbio.com/protocols/AM-SO4.htm) was added and the mixture stirred at 4 °C until the solid was fully dissolved. The mixture was centrifuged for 15 min at 9,500 *g*, 4 °C. The supernatant was retained and ammonium sulfate was added to achieve 60% saturation in order to precipitate the P450 enzyme. After stirring to dissolve the solid, the mixture was centrifuged at 9,500 g, 4 °C for 20 minutes. The supernatant was discarded, and the enzyme pellet redissolved in 5 mL phosphate buffer (50 mM, pH 8.0).

2.3.4 Protein quantification

The concentration of the enzyme solution was determined by the CO-difference assay in which the 20-fold diluted enzyme solution was reduced by a few crystals of sodium hydrosulphite. The UV-vis spectrum (200–700 nm) of this reduced form was recorded as the baseline, and CO was slowly bubbled through the solution (50 bubbles would normally be enough) to give the difference spectrum of the CO-bound enzyme showing the characteristic absorption at 450 nm. If the concentration of the enzyme solution was unexpectedly high, the CO-saturation step was repeated until there was no further change in the spectrum. The concentration of the protein is estimated using the following equation:

$$[\text{P450}]\ (\mu\text{M}) = (A_{450} - A_{490}) \times 20 \times 10^6 / \varepsilon \qquad \text{(Equation 2.2)}$$

where ε (91,000 M^{-1} cm^{-1}) is the extinction coefficient.[457]

The total amount of recovered enzyme was calculated from the concentration and volume of the enzyme solution, from which the biomass yield from the culture in μmol/g-wcw was calculated.

2.4 Activity assays

2.4.1 *In vitro* assays

2.4.1.1 Substrate binding titration of $P450_{BM3}$ heme domain

The substrate was added as different stock solutions to a 5 μM solution of the $P450_{BM3}$ enzyme in 50 mM Tris (pH 7.4, 2% DMSO *v/v*) at 30 °C to achieve final substrate concentrations of 1, 2, 3, 4, 5, 6, 7, 8, 10, 15, 20, 25, 30, 35, 40, 45, 50, 55, 60, 75, 80, 85, 90, 95, 100 μM. After the addition of each aliquot of substrate solution the difference spectrum 350 nm to 500 nm was recorded and the peak-to-trough difference ($\Delta A = A_{388} - A_{420}$) was calculated and plotted to produce the binding-titration curve. This was fitted with

1-, 2- or 3-substrate-binding models to identify the number of substrate molecules binding to the ferric form of the enzyme.

2.4.1.2 *In vitro* screening-scale biotransformation

The stock of each enzyme variant was diluted to 10 μM, 100 μL of which was pipetted into each well of 24-well plate to prepare the variant library for *in vitro* screening reactions. The components and the volume of each for a 1 mL scale reaction are listed in Table 2.8. The plates were shaken at 20 °C, 160 rpm for 2–6 hours (varying on account of the biotransformation rate of individual substrates). A 500 μL aliquot of the reaction mixture was removed and extracted with 300 μL ethyl acetate, 100 μL of which was analysed by either gas chromatography or TLC. The remainder of the reaction mixture was left shaking overnight, extracted and analysed to determine if further oxidation occurred.

Table 2.8 The preparation of the *in vitro* reaction solution.

Component	Stock concentration	Volume / μL
Glucose	1 M	100
GDH	2 U/μL	10
$NADP^+$	40 mM	10
Substrate	200 mM	10
Cyclodextrin (optional)	200 mM	100 (used in turnover of insoluble substrate)
Phosphate buffer (pH 8.0)	100 mM	770 (no cyclodextrin) or 670 (with cyclodextrin)

2.4.2 *In vivo* assays

2.4.2.1 Screening-scale biotransformation in whole cells

A single *E. coli* BL21 DE3 or Acella colony harbouring the appropriate plasmid was inoculated into 5 mL LB_{kan} and grown for 16 h at 37 °C, 200 rpm. 100 μL of this seed culture was mixed with 900 μL of 1× FB_{gly} ($FB_{supplement}$ added) and shaken at 160 rpm, 37 °C for 8 h and induced at 20 °C for another 48 h with 10 μL induction solution added

every 6 h. The FB_{gly} culture was transferred to a 1.5 mL microcentrifuge tube and centrifuged at 14,800 *g* for 1 min. The reddish cell pellet was resuspended by 1 mL of the reaction solution shown in Table 2.9. The mixture was transferred to a well in a 24-well plate and shaken at 20 °C for 2–6 h, after which it was centrifuged at 14,800 *g* for 1 min and 500 μL of the supernatant was extracted with 300 μL ethyl acetate and analysed by GC. The pellet was resuspended in the remaining supernatant and returned to the 24-well plate to be shaken for another 10 h to study the product distribution over prolonged incubation.

Table 2.9 The preparation of the *in vivo* reaction solution.

Component	**Stock concentration**	**Volume / μL**
Glucose	1 M	100
GDH	2 U/μL	10
$NADP^+$	40 mM	10
Substrate	200 mM	10
Cyclodextrin (optional)	200 mM	100 (used in turnover of insoluble substrate)
Phosphate buffer (pH 8.0)	100 mM	870 (no cyclodextrin) or 770 (with cyclodextrin)

2.5 Preparative scale synthesis and product characterisation

2.5.1 General procedure for preparative scale biotransformation *in vitro*

Preparative scale reactions were performed in 50 mL 100 mM phosphate buffer (pH 8.0) in a 250 mL conical flask containing 5 μM enzyme, 10 mM substrate (200 mM stock in ethanol), 8 U/mL glucose dehydrogenase (2 U/μL stock in 100 mM phosphate, pH 8.0), and 100 mM glucose. $NADP^+$ monosodium salt was added to a final concentration of 80 μM, to initiate the reaction which was shaken at 160 rpm at 20 °C until completion. The reaction mixture was extracted with ethyl acetate (3× 50 mL), the combined organic phase was dried over Na_2SO_4, filtered and solvent was removed *in vacuo*. The crude mixture was

purified by silica gel column chromatography to afford products which were fully characterised by 1D/2D NMR and high-resolution MS.

2.5.2 Preparative scale biotransformation *in vivo*

A single colony of *E. coli* BL21 DE3 or Acella harbouring the appropriate plasmid was inoculated into 100 mL FB_{gly} ($FB_{supplement}$ added) and grown for 16 h at 37 °C with shaking at 160 rpm. The temperature was lowered to 20 °C. Enzyme production was induced by adding 200 µL induction solution at 6-h intervals for 48 h. After harvesting, the reddish cell pellet was resuspended in 20 mL 50 mM phosphate buffer (pH 8.0), 10 mL of which was used for enzyme quantification. The other 10 mL was diluted to 50 mL with 100 mM phosphate (pH 8.0) containing 1.8 g glucose, 10 mg GDH (5 U/mg) and 10 mg $NADP^+$ for cofactor regeneration, and 10 mM substrate. The reaction was monitored by TLC and GC by using 300 µL ethyl acetate to extract 500 µL of the supernatant of the whole cell reaction. On completion, the reaction mixture was centrifuged at 9,500 *g* for 5 min to collect the supernatant, which was extracted by 3× 50 mL ethyl acetate. Solvent was removed *in vacuo* and the crude mixture was purified by silica gel chromatography with all products fully characterised by 1D/2D NMR and high-resolution MS.

2.6 Optical rotation measurements

The pure and dry sample was dissolved in 1 mL $CHCl_3$ (10 mg/mL). The polarimeter was left to warm up for 30 min with the water bath set to 25 °C. The sample cell was removed from the polarimeter, washed three times with solvent (3× 1 mL $CHCl_3$) and then filled with solvent to the half-height of the vertical tube keeping the horizontal tube free from any bubbles. The stoppers were then placed in and the cell was put back into the polarimeter. The pure solvent was set to be calibrated as 0.000°. The cell was then emptied and dried with compressed air. The sample to be tested was injected into the cell as described above

and measured for 10 readings, of which the average value was recorded as <α>. The $[\alpha]_D$ was calculated as follows:

$$[\alpha]_D = (100 \times \langle\alpha\rangle) / (l\ [\text{dm}] \times c\ [\text{g}/100\ \text{mL}])$$

where l is the path length in dm (1 for the polarimeter used for the measurements) and c is the concentration of the sample, 1 g per 100 mL in this case.

Chapter 3 $P450_{BM3}$ oxidation of *N*-phenyl and *N*-benzyl pyrrolidines and piperidines: Discovery of novel enzymatic Povarov reaction

3.1 Introduction

The *N*-phenyl and *N*-benzyl protected cyclic amines are common motifs in pharmaceutics such as delafloxacin, ombitasvir, repaglinide and besifloxacin with a phenyl protecting group, and siponimod, revefenacin and clopidogrel with a benzyl protecting group (Figure 3.1). These possess assorted pharmacological activities varying from anticoagulant, anticonvulsant, antiplatelet, antibiotic, anti-tumour and anti-viral (HIV or Hepatitis C) properties for treating high cholesterol, diabetes, acute myeloid leukemia, non-small cell lung cancer and chronic obstructive pulmonary disease. The core of these drugs consists of α-, β- or γ-functionalised cyclic amine rings incorporated with *ortho*-, *meta*- and *para*-substituted phenyl rings, which implies that functionalisation at any C–H bond of these cores will be of interest for drug discovery and synthesis.

In this chapter, the oxidation of *N*-phenyl pyrrolidine, *N*-phenyl piperidine, *N*-benzyl pyrrolidine and *N*-benzyl piperidine by engineered variants of $P450_{BM3}$ are described. Previous research revealed different pathways for the oxidation of *N*-phenyl and *N*-benzyl alicyclic amines by the biomimetic system of tetraphenylporphyriniron(III) chloride/PhIO (FeTPP/PhIO).[458,459] For *N*-benzyl piperidine, it only gave *N*-dealkylation, possibly by single electron transfer (SET) rather than the classical hydrogen atom transfer (HAT).[458] The HAT mechanism yielded negligible amount of the lactam and the dimeric product of *m/z* 290 (<1% in total) for *N*-phenyl piperidine, whereas SET gave no product due to the lack of the exocyclic benzylic CH_2 which rotates freely to be eclipsed to the nitrogen-centred radical cation facilitating deprotonation.[458] As for the P450-related oxidation, Zhang and Arnold have reported the functionalisation of *N*-phenyl pyrrolidine derivatives using cytochrome P411 derived from CYP102A1 by replacing Cys400 with Ser, which changed the activity from monooxygenase to carbene transferase, to afford α-alkylated products with reasonable enantioselectivity (Figure 3.1).[460,461]

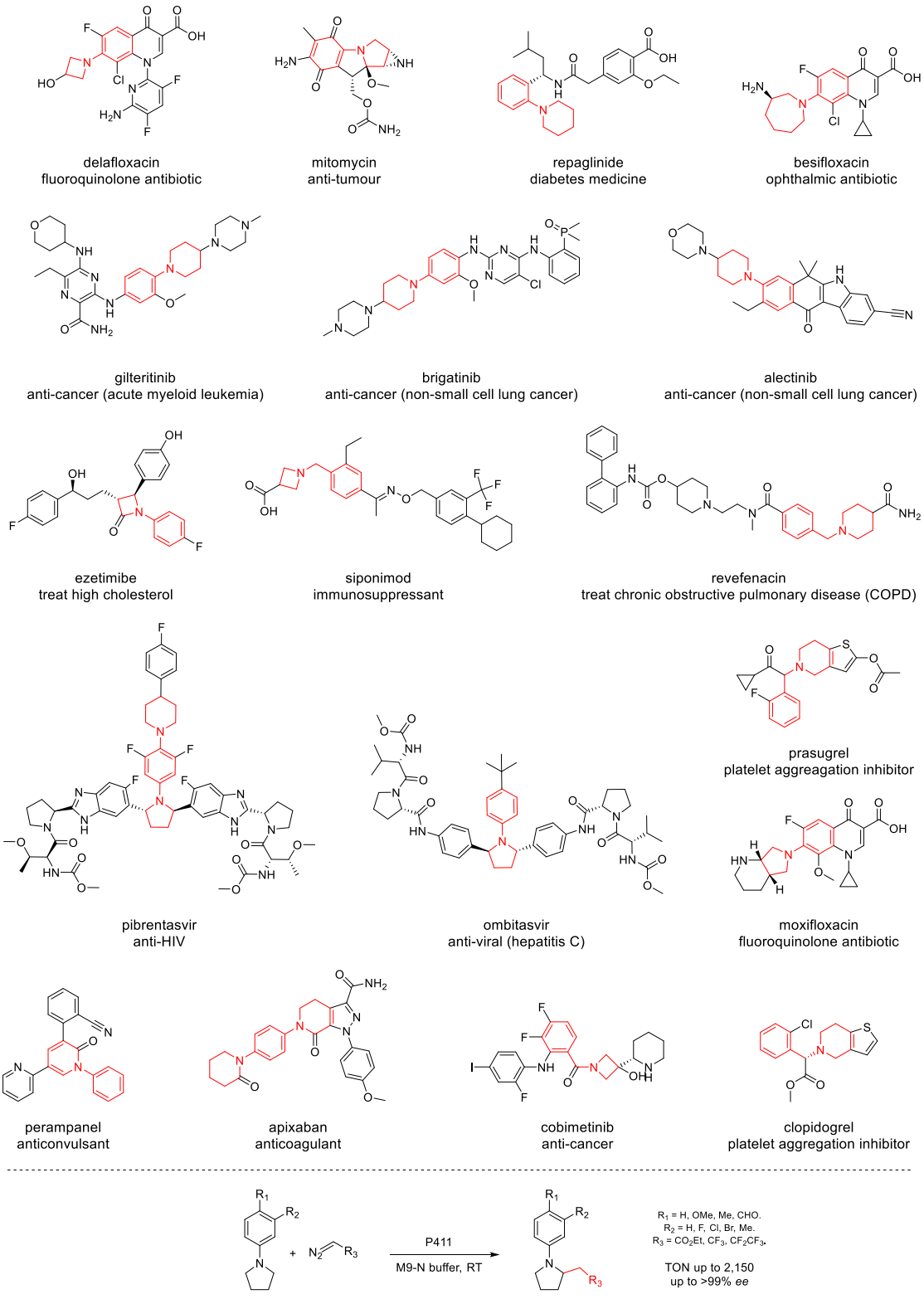


Figure 3.1 A selection of pharmaceutics containing *N*-phenyl and *N*-benzyl cyclic amines and the reaction scheme of P411 C–H functionalisation of *N*-phenyl pyrrolidine derivatives.[460,461]

Other CYPs have already been reported to be active for these substrates (Figure 3.2). CYP2B1 gave the iminium and *N*-oxide (140 : 1) for *N*-phenyl pyrrolidine.[462–464] Rat liver microsomal P450s converted *N*-phenyl piperidine into the iminium and *N*-oxide.[465] Incubation of *N*-benzyl pyrrolidine and cyanide with rabbit liver microsomes yielded the lactam, the *N*-oxide, the iminium, the enamine, and the iminium-trapped *N*-benzyl-2-cyanopyrrolidine.[466] The *N*-benzyl piperidine drug derivative, phencyclidine, was oxidised by liver microsomal P450s at C3 of the cyclohexane ring, C3 and C4 of the piperidine ring, and to the *meta*-phenol.[467] For bacterial and fungal P450s, engineered P450pyr from *Sphinomonas* sp. HXN-200 has been evolved to hydroxylate *N*-benzyl pyrrolidine at the β carbon with 100% regioselectivity and 98% *ee* to (*S*)- and 83% *ee* to (*R*)-enantiomers,[429,430,468] and to convert *N*-benzyl piperidine to the γ-alcohol.[423] *Beauveria sulfurescens* ATCC 7159 oxidised *N*-phenyl piperidine to the *para*-phenol,[431] *p*-substituted *N*-phenyl piperidines at C4(γ)–H,[431] and phencyclidine at C3 of the cyclohexane ring and C4(γ) of the piperidine ring.[432] However, *N*-benzyl alicyclic amines were not oxidised by this organism.[432]

Remote functionalisation, *e.g.*, at the β-position, already proven viable by P450pyr, is of interest as it is most difficult for classical synthesis to achieve. It is also worth noting that the unstable carbinolamine intermediate leads to ring-opening *N*-dealkylation to form the linear amino-aldehyde (Figure 3.2). The SET mechanism yields the *N*-radical cation to form *N*-oxide and the iminium intermediate, which has been trapped by the nucleophilic CN^-. (The HAT mechanism only provided the iminium from the carbinolamine.) Such trapping reactions may be expanded to generate α-functionalised alicyclic amines. *N*-dealkylation and *N*-oxidation are commonly shown by human CYP enzymes, and have to be suppressed by engineering the CYP102A1 enzyme.

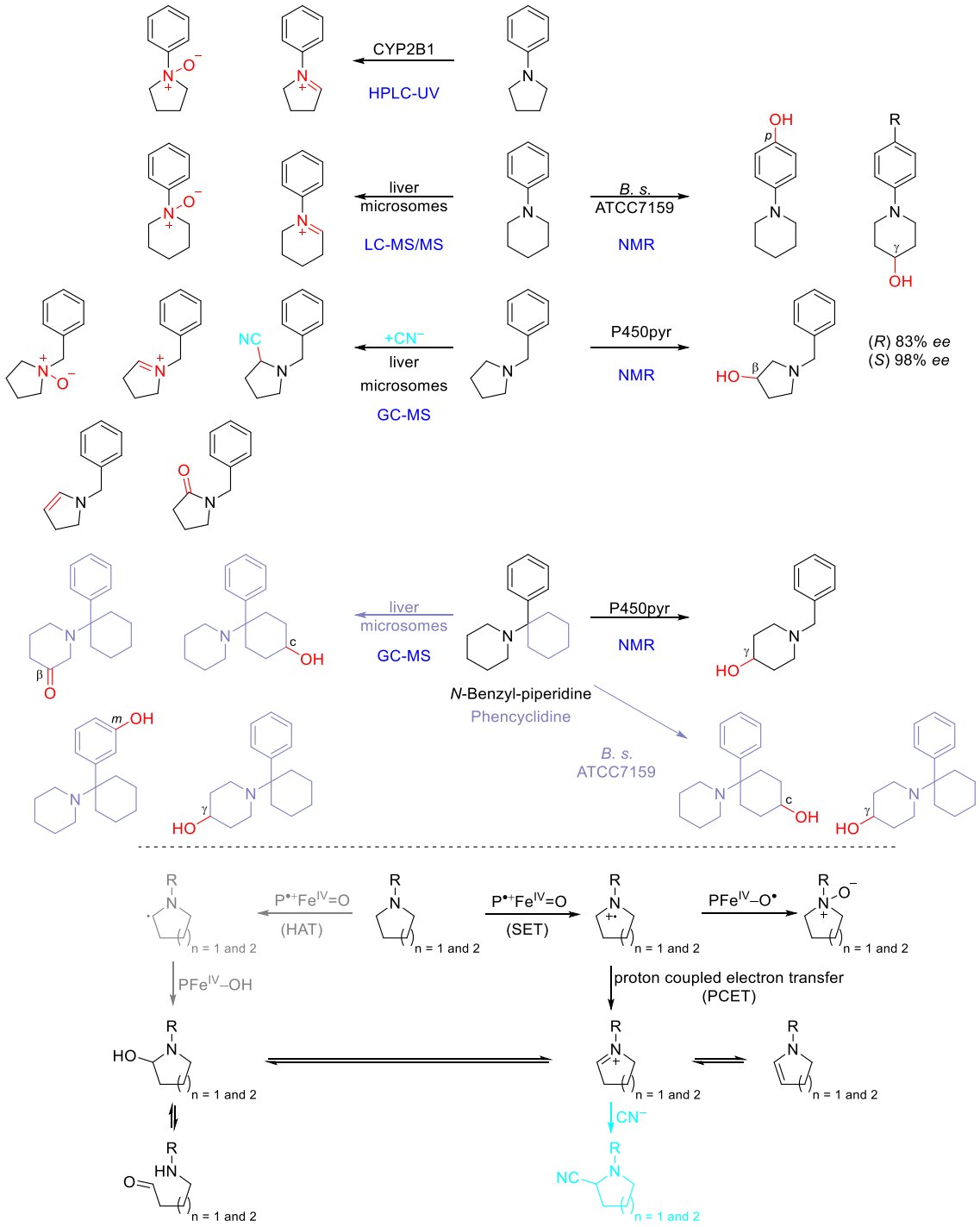


Figure 3.2 Examples of microsomal, bacterial and fungal P450 oxidation of *N*-phenyl and *N*-benzyl pyrrolidines and piperidines, and their proposed mechanisms for their commonly-observed *N*-oxidation and *N*-dealkylation activities.[423,429–432,462,463,465,466,468]

3.2 $P450_{BM3}$ oxidation of *N*-phenyl pyrrolidine

N-Phenyl pyrrolidine (**1**) was screened against the initial library of 48 variants (1 μM, the TFA/TFB plates <Table 3.1>, Appendix 3.1) at low (2 mM) and high (5 mM) substrate concentration in 1 mL of 100 mM phosphate buffer (pH 8.0) containing 40 μM $NADP^+$, 100 mM glucose, and 0.2 U/ml GDH to regenerate the cofactor NADPH. The 24-well plates were shaken at 20 °C, 120 rpm for 16 hours (Appendix 3.1). Surprisingly, the screening reactions of 2 mM and 5 mM substrate gave different product distribution around the shorter retention time window in GC chromatographs (Figure 3.3), suggesting the change of titre influenced the activity pattern via affecting substrate binding. Preparative reactions with the R19/F87A/A328I and RP/H171L/I263G variants using 10 mM substrate and 5 μM enzyme in 100 mL of phosphate buffer (100 mM, pH 8.0) were monitored (Figure 3.4), and the pH dropped to 6.5 when no further conversion occurred. The pH drop had little impact on these reactions. Variants like R19/F87A showed multiple peaks within the GC retention time window of monomer oxidation (Figure 3.3).

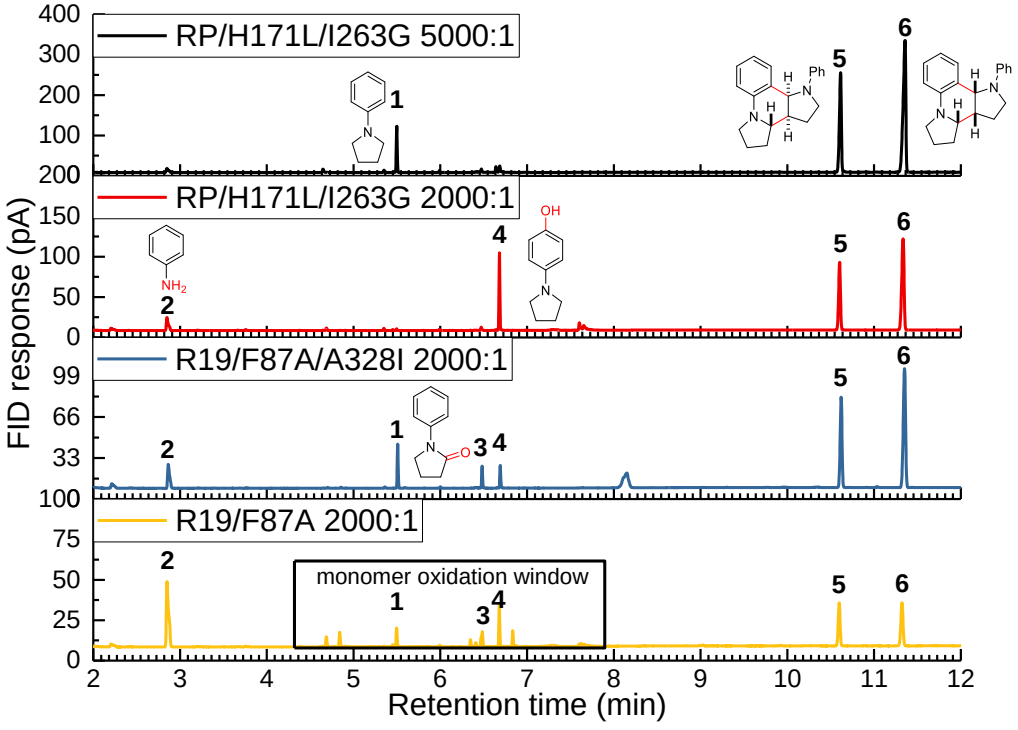


Figure 3.3 Gas chromatograms for the $P450_{BM3}$-catalysed oxidation for *N*-phenyl pyrrolidine, **1**.

Table 3.1 The TFA & TFB variant library based on K19, KT2, A330P and I401P with active site mutations introduced at R47, Y51, S72, V78, F81, A82, F87, A184, L188, I263, E267, A328, P329, Q403 and L437.

TFA plate	**TFB plate**
R19/F87A/A328I	A330P
K19/A82M/F87A	RP/F81W
K19/Y51L/F87A/A328I	RT2/S72A/A328I/A330P
K19/F87A/A184I/A328I	RP/H171L/I263G
RP/F87V/E267V/L437VL	RT2/P329V/A330P
K19/F87A/I263A	GVQ
RP	RT2/A330W
RP/E267V	F87A
RT2/F81W	R19/F87A
RP/F87V/E267V	RP/A82M/I263A
K19/F87V/A328I	RT2/V78F
RP/F87V/E267V/L437LV	R47L/Y51F
K19/V78I/F87A/A328I	K19/A82M/F87A/E267F
RT2/A330P/I401M	RP/H171L
RT2/A82M/A330P	RP/E267G
RT2/I401P	KSK48
RT2/A330P	K19/F87V/Q403P
RT2/A184I/A330P	RT2/V78I/A184I/A330P
RT2/V78I/A330P	RP/F87V/L188Q/E267V
RT2	RP/V78F/F87V/E267V
RP/I263A/E267V	RT2/F81W/A328I
WT	RP/E267M
RP/A330P	K19/F87V/I263A/A328I
RP/F87V	RT2/S72W/A330W

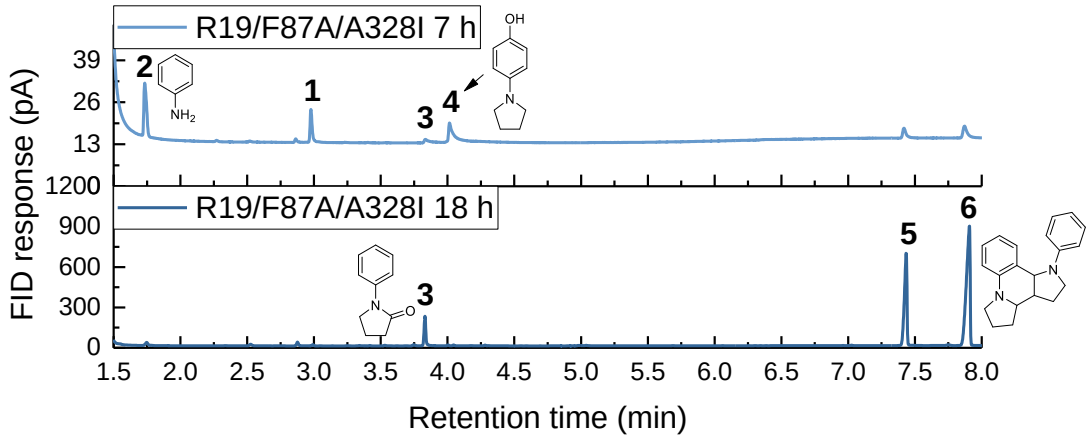


Figure 3.4 GC analysis for the R19/F87A/A328I-catalysed biotransformation of **1** at 7 h and 18 h.

Five major products, aniline (**2**), *N*-phenyl γ-butyrolactam (**3**), the *para*-phenol (**4**), and the dimers **5** and **6** (Figure 3.5), were purified and characterised from the reactions with R19/F87A/A328I and RP/H171L/I263G. All characterisation data are listed in Appendix 4.1 and consistent with literature.[469–473] The colour of the reactions yielding **4** became dark brown, from pale orange solutions. Therefore, screening reactions were carried out for the 2nd and 3rd generation variant libraries (Appendix 3.2) in the dark to prevent photo-catalysed decomposition of **4**. The relative stereochemistry of **5** and **6** were confirmed by NOESY spectra (Appendix 4.1, Spectra 5 and 10).[473] The H10 (δ 4.45 ppm) of **5** showed an nOe to H9 but not H8, whereas the H10 (δ 5.11 ppm) of **6** showed nOe with both H9 and H8 (Figure 3.6).

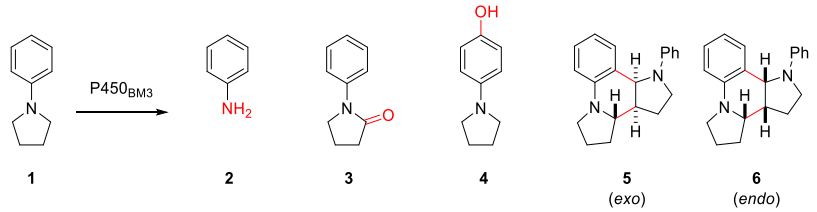


Figure 3.5 The reaction scheme of P450$_{BM3}$ oxidation of *N*-phenyl pyrrolidine, **1**.

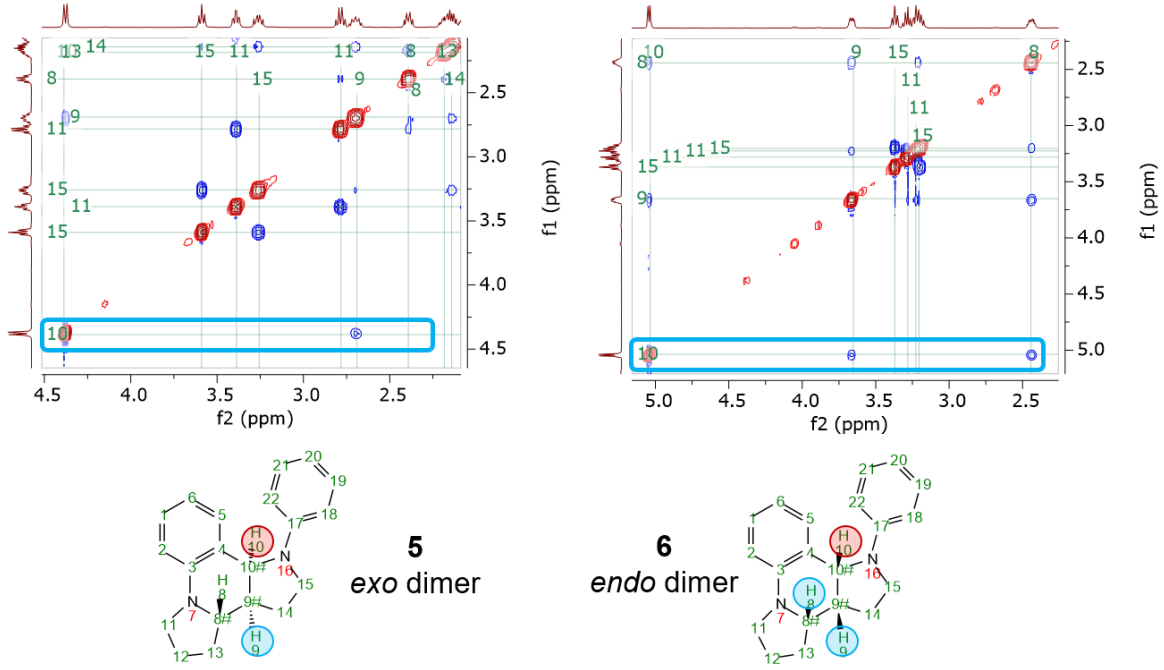


Figure 3.6 The comparison between the NOESY spectra for **5** and **6**.

The products **2** and **3** were both active substrates for $P450_{BM3}$. Some of the unidentified peaks in Figure 3.3 originated from oxidation of **2** and **3**, as the screening reaction with 5 mM of **1** with R19/F87A gave 80% of **2** and 11 % of **3** (55% conversion) while 32% of **2** and 2% of **3** (full conversion) were observed in the screening reaction with 2 mM of **1**. There was no evidence of **4** in the screening tests with 5 mM of **1** (Appendix 3.1). This suggested that there are other substrate molecule(s) inside the active site which inhibited the substrate being bound with its phenyl ring orienting to the ferryl compound I species.

The reaction with R19/F87A/A328I (10 mM substrate and 5 μM enzyme, ratio = 2,000) showed quite different product distribution at 7 h and 18 h in the dark (Figure 3.4). After 7 h incubation, most of the substrate was consumed (as judged from the peak height of **1**), but the product peaks were small. The ^{1}H NMR of the 7 h crude extraction of the reaction showed no substrate or product. Nevertheless, the major products **3**, **5** and **6** appeared at 18 h. This observation might stem from the slow reaction of the carbinolamine, which might not be extractable and hence undetectable by GC at 7 h. This also explained the nearly 100% regioselectivity of α-oxidation (giving **3**, **5** & **6**) shown at 18 h. Other methods, *e.g.*, LC and SFC capable of detecting hydrophilic species, can be utilised to monitor the reaction. The contrast between 2 mM and 10 mM substrate addition (Figure 3.3 & 3.4) for R19/F87A/A328I also revealed the substrate concentration influenced the product profile.

The formation of *para*-phenol **4** can be rationalised by the NIH shift mechanism whereby the initially formed 3,4-arene oxide undergoes ring-opening to the C3 carbocation preferentially due to the stabilisation by the nitrogen lone pair (Figure 3.7).

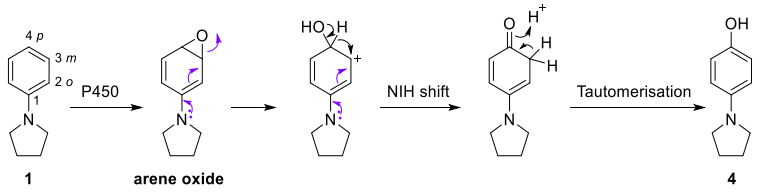


Figure 3.7 The proposed mechanisms of aromatic hydroxylation of *N*-phenyl pyrrolidine (**1**).

The formation of aniline **2**, the lactam **3** and dimers **5** and **6** can be rationalised by α-hydroxylation via HAT, since **1** was known to be totally inert to the Compound I biomimetic reagents FeTPP/PhIO and the *bona fide* electron transfer reagent $Co^{III}W$.[458] The HAT reagents *t*BuOOH/FeTPP giving <1% of the lactam and the dimeric product of *m/z* 290 matched the characterisation of **3**, **5** and **6** herein. The unstable carbinolamine is their common precursor. It is hydroxylated by P450 again, followed by dehydration to form the lactam **3**. It can also undergo C–N bond cleavage to form the amino aldehyde. Another cycle of C–N bond cleavage gives aniline **2**. For dimerisation, the carbinolamine loses OH^- to afford the iminium species which is in equilibrium with the enamine tautomer. There are two possible mechanisms of dimer formation, the process of which is known as the Povarov reaction,[474] the concerted Diels-Alder reaction *vs.* the stepwise Mannich reaction. In the Diels-Alder reaction, the enamine serves as a dienophile to react with the positively-charged iminium s-*cis* diene under inverse electron demand to form **5** and **6**. In this process, the interaction of the HOMO of the enamine and the LUMO of the iminium forms the dimeric iminium adduct (Figure 3.8).[475] The regiochemistry is arranged by electrostatic attraction, since the β-carbon of the enamine is more electron rich than its α-carbon, therein attacking the electron-deficient iminium carbon of the diene. For the stereochemistry, the enamine can either approach the diene from the less sterically-hindered side to form the *exo* **5**, or develop π-stacking interaction with the phenyl group of the iminium so that the *endo* **6** is given. However, in the stepwise Mannich reaction, the enamine attacks the iminium by nucleophilic attack to form the dimeric iminium, which then undergoes intramolecular cyclisation by electrophilic substitution (Figure 3.9). Theoretically, the 1st step of the stepwise Mannich reaction controls the absolute stereochemistry of Cα' and Cβ', and the 2nd step could generate both *cis*- and *trans*-diastereoisomers. Formation of **5** and **6** is the first example of an enzymatic Povarov reaction.

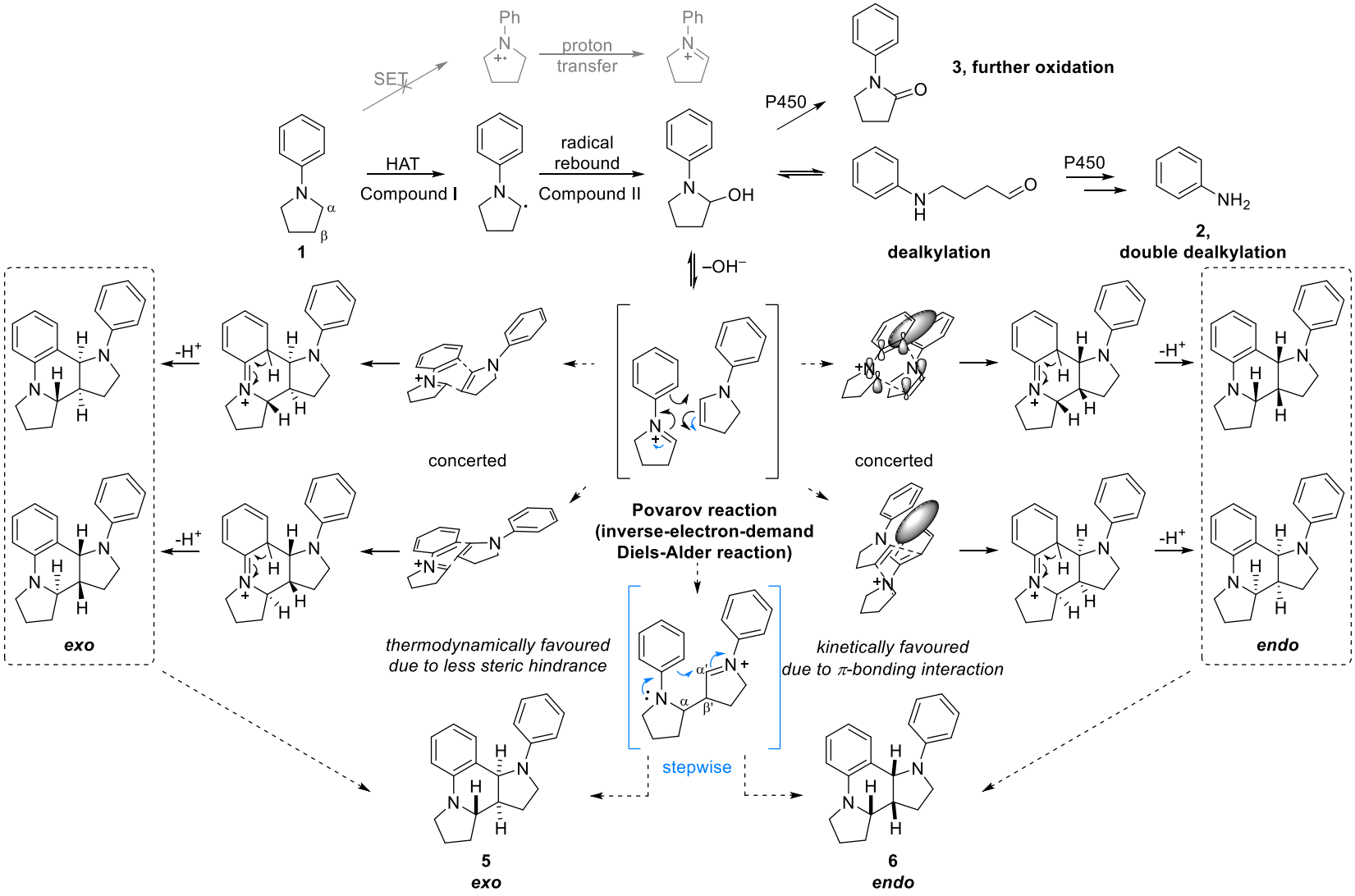


Figure 3.8 The proposed mechanisms of α-oxidation of *N*-phenyl pyrrolidine (**1**) including further oxidation, dealkylation and the Povarov reaction.

The *exo* dimer is the scaffold of the plant alkaloids incargranine B,[476] which was wrongly assigned to have a unique indolo-[1,7]naphthyridine core when it was firstly purified in 2010, and seneciobipyrrolidine.[477] The total synthesis of incargranine B was reported utilising 2 M HCl to convert the monoalkylated aniline to the dimers via the stepwise Mannich reaction (*endo* : *exo* = 2 : 1, and each diastereomer is racemic, Figure 3.9).[478]

Long before the total synthesis of incargranine B, the dimeric core had been discovered and thoroughly studied. After the report of its chemical structure in 1955,[479] the reduction of the lactam derivatives of *N*-phenyl pyrrolidine (**1**) by $LiAlH_4$ and $NaBH_4$ followed by acid treatment,[480,481] the ozonation/hydrazination of **1** with diethyl azodicarboxylate/ozone,[482] and the dehydrogenation of **1** by γ-radiolysis and by dibenzoyl peroxide were found to produce the dimeric core.[483] Amongst these papers, the concerted Diels-Alder reaction was proposed for dimer formation,[482] which was also adopted by the silylation of the lactam, **3**, by $PhMe_2SiLi$ yielding **5** and **6**.[484] A rhodium catalyst with H_2 and CO was found to convert *o*-cyanoallylanilines to the dimers.[485]

As for the research after 2000, the *endo* dimer (72%) was given by *tert*-butyl hydroperoxide (T-HYDRO) with $NaOAc{\cdot}3H_2O$ in cyclohexane (70 °C, 24 h) from *N*-phenyl pyrrolidine (Figure 3.9).[486] Under different conditions (70 °C, 24 h, *t*-BuOK in MeOH), T-HYDRO also gave the lactam **3** (85% yield).[486] $PhMe_2SiLi$ (2.4 equiv.) reacted with the lactam **3** by warming from –78 °C to –20 °C, then treatment with $NaHCO_3$ and water, to generate 31% of the *endo* and 16% of the *exo* dimers with 42% of **3** left unconverted (Figure 3.9 in orange).[473,484] The photocatalyst $Ru(bpy)_3(PF_6)_2$ also converted **1** into the dimers in 10% yield under visible-light (Figure 3.9 in blue).[487] The cell-divided control reaction in the TEMPO-mediated electrolysis of **1** and 1,4-dicyanobenzene also generated **5** and **6** (35% in total, *exo* : *endo* = 4 : 1), with **5** (*exo*) as the dominant dimer (Figure 3.9 in magenta).[472] The utilisation of bis(2,2,2-trichloroethyl)azodicarboxylate for α-functionalisation of

pyrrolidine derivatives also showed that the phenyl group steered the reaction to the Povarov reaction (Figure 3.9 in green) rather than direct α-C–H activation which was given from *N*-Ts, *N*-Boc, *N*-Bz and *N*-Troc pyrrolidines.[488]

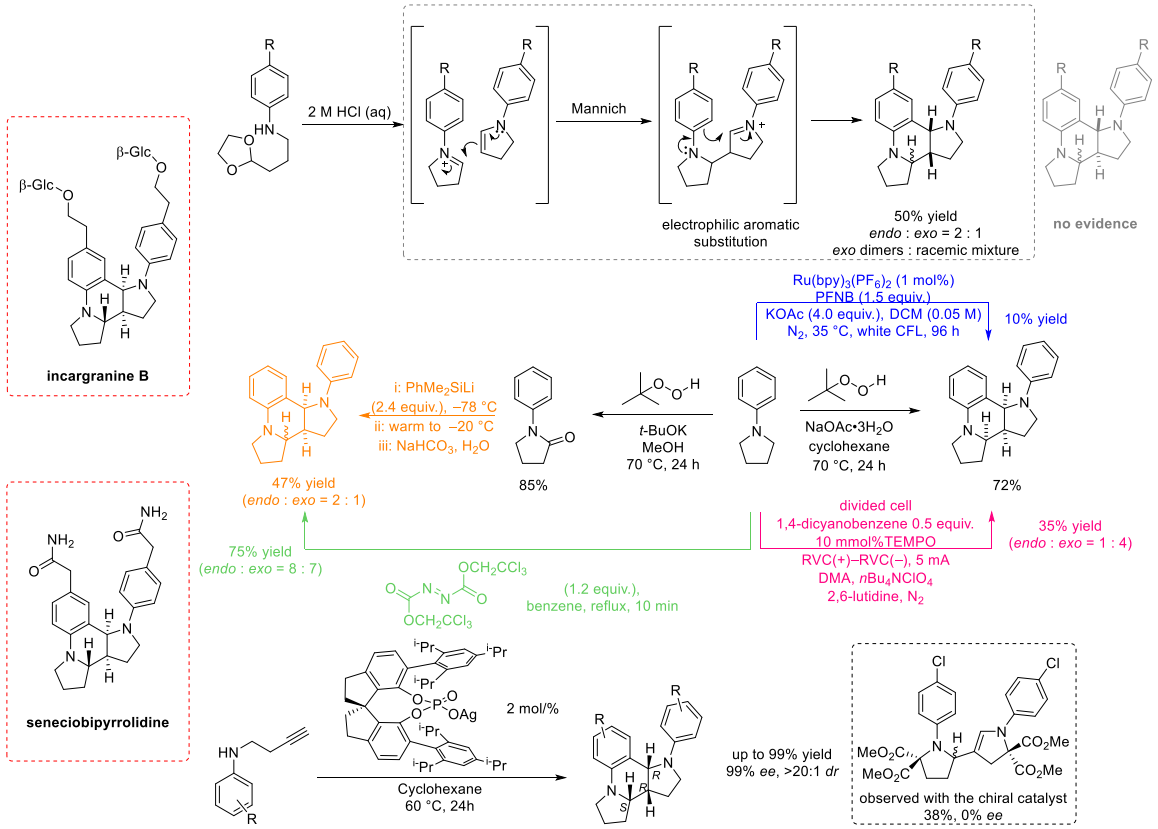


Figure 3.9 Natural products with **5** as their scaffolds[477,478] and previous studies on Povarov reactions yielding **5** and **6**.[472,473,484,486–489]

Secondary aminoalkynes were oxidised to the *endo* dimers (*e.g.* 99% yield of the *endo* dimer **6**, 83% *ee* to the *R,R,S*-epimer) by metal-phosphate catalysts via counteranion-controlled tandem formal Povarov reaction (Figure 3.9).[489] One intermediate in the stepwise mechanism, the dimeric enamine, was purified from the reaction with the chiral metal-phosphate catalyst. However, it was confusing that this intermediate was racemic whilst the resultant dimer forming from this intermediate showed high diastereomeric excess (≥90%) and enantiomeric excess (≥93%), which was hardly justified by a reversible Mannich reaction.[489] Another interesting observation was that the dimers generated by all the aforementioned reactions were either in the *endo* or in the *exo* configuration, without

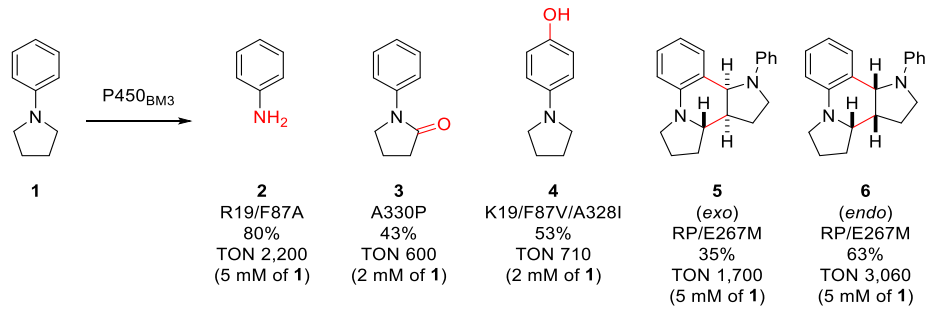
any evidence of other diastereoisomers. Therefore, the debate over the actual process of dimer formation in the Povarov reaction remains. Moreover, high regio- and enantioselectivity were only achieved for the *endo* dimers, whilst incargranine B and seneciobipyrrolidine were both in the *exo* configuration. This observation hinted at the possibility that there might be enzymes in plants that favour the formation of the 'unfavoured' *exo* dimer.

After 16 h incubation at a substrate concentration of 2 mM, all TFA/B library variants gave ≥50% conversion (TTN ≥1,000), whereas wild type $P450_{BM3}$ showed 40% conversion (TTN 800, Appendix 3.1). For the reactions at a substrate concentration of 5 mM, 28 variants showed >50% conversion (TTN >2,500) after 16 h incubation (Appendix 3.1). The base variants RP and RT2 showed excellent activities (66% and 91% conversion, TTN 3,300 and 4,550) at the substrate concentration of 5 mM. The mutations H171L, E267V/M and I401P enhanced the activity to 94%, 87%, 97% and 97% conversion (TTN 4,700, 4,350, 4,850 and 4,850) given by the variants RP/H171L, RP/E267V, RP/E267M and RT2/I401P.

The overnight incubation with the R19/F87A variant showed the highest activity towards dealkylation (32% for 2 mM substrate, TTN 640, and 80% for 5 mM substrate, TTN 2,200, Table 3.2 & 3.3). A330P gave the most of the lactam **3** with 43% selectivity (TON 600) from 5 mM substrate (Table 3.2 & 3.3). The variant K19/F87V/A328I gave 53% of **4** (TON 710) from 2 mM substrate (Table 3.2). RP/E267M generated the most of dimers from 5 mM substrate, with 35% of the *exo*-dimer **5** and 63% of the *endo*-dimer **6** (TON 1,700 and 3,060 respectively, Table 3.2). In the library, the dimers were prevalently formed in most reactions (>50% selectivity in 46 reactions of 2 mM substrate and 44 reactions of 5 mM substrate), and the *endo* dimer was favoured. The *exo* : *endo* ratio remained around 4–6 : 10 by 2 mM substrate screening, whilst it fluctuated from 2 : 10 to 6 : 10 in 5 mM substrate screening.

The screening reactions of 5 mM substrate gave no **4**, but the mutations A82M, F87V, A184I, I263G and A328I improved the formation of **4** in 2 mM substrate screening reactions. Mutagenesis was carried out at these sites on the base variants K19, K19/F87A, GVQ, R19 and R19/F87A. The 2nd generation variants K19/F87V/A328V, R19/F87A/A328L, R19/A184I/A328L and GVQ/I263G/A328L promoted the selectivity of **4** to various extent in reactions with 2 mM substrate (Table 3.2). The combination F87V/I263G/A328L in GVQ/I263G/A328L exclusively favoured **4** (96%, TON 1,310).

Table 3.2 The product distribution of the $P450_{BM3}$ variants (1 μM) under the condition of adding 2 mM of **1**.



1

2 R19/F87A 80% TON 2,200 (5 mM of **1**)

3 A330P 43% TON 600 (2 mM of **1**)

4 K19/F87V/A328I 53% TON 710 (2 mM of **1**)

5 (*exo*) RP/E267M 35% TON 1,700 (5 mM of **1**)

6 (*endo*) RP/E267M 63% TON 3,060 (5 mM of **1**)

Mutant	**Conv.**	**Selectivity pattern**						*exo* : *endo*
		2	**3**	**4**	**5**	**6**	dimers	
WT	40%	3%	2%	**9%**	22%	63%	85%	4/10
R19/F87A	100%	32%	2%	9%	17%	20%	38%	8/10
RT2/A330P	63%	3%	13%	**1%**	25%	59%	83%	4/10
RT2/A184I/A330P	74%	3%	4%	**9%**	30%	54%	83%	6/10
RT2/A82M/A330P	88%	1%	1%	**34%**	22%	42%	64%	5/10
RP	97%	5%	2%	–	34%	59%	93%	6/10
RP/F87V	90%	19%	3%	**14%**	23%	41%	64%	6/10
RP/H171L	98%	5%	–	–	35%	59%	94%	6/10
RP/H171L/I263G	100%	6%	1%	**16%**	28%	49%	77%	6/10
K19/F87V/A328I	67%	3%	7%	**53%**	11%	26%	37%	4/10
K19/A82M/F87A/I263G*	68%	38%	15%	–	16%	31%	47%	5/10
GVQ/A82M/I263G*	48%	44%	21%	–	11%	24%	34%	4/10
K19/F87V/A328V*	88%	17%	3%	**59%**	8%	13%	21%	6/10
GVQ/I263G/A328L*	68%		4%	**96%**	–	–	–	–
R19/F87A/A328L*	78%	10%	10%	**49%**	13%	18%	31%	8/10
R19/A184I/A328L*	92%	0%	0%	**90%**	5%	5%	10%	9/10

*: the 2nd generation variants

Nα-oxidation was the only activity observed in the screening of 5 mM substrate. F87A favoured the dealkylation pathway, whilst I263A, E267F, A328I and A330P slightly enhanced lactam formation (Table 3.3). This showed that the I-helix residues I263–E267 and the loop of A328–A330 were crucial for the formation of lactam **3**. Mutagenesis around these regions produced two types of new variants. One type, including the variants KU3/A328I/A330P and I263G, converted the substrate into **3** mainly (100% and 86% selectivity) after 8 hours of biotransformation under 2 mM substrate concentration, but prolonged incubation (24 h) led to dimer formation (61% and 70% of dimers). The other type included the I-helix-mutated variants R19/F87A/I263G/A264G and R19/F87A/G265GG. These maintained the selectivity pattern with the consumption of the substrate. R19/F87A/I263G/A264G also lifted the selectivity of **3** to 67% (TON 900).

Table 3.3 The product distribution of the $P450_{BM3}$ variants (1 μM) in the oxdation of **1**.

Substrate Conc.	**Mutant**	**Conv.**	**Selectivity pattern**					*exo* : *endo*
			2	**3**	**4**	**5**	**6**	
5 mM	WT	20%	4%	11%	–	11%	39%	3/10
	F87A	43%	57%	11%	–	5%	24%	2/10
	R19/F87A	55%	**80%**	11%	–	2%	6%	3/10
	A330P	28%	6%	**43%**	–	7%	34%	2/10
	RT2	91%	2%	–	–	36%	61%	6/10
	RT2/A330P	38%	3%	29%	–	13%	48%	3/10
	K19/F87A/I263A	32%	21%	30%	–	7%	27%	2/10
	K19/A82M/F87A	63%	7%	1%	–	29%	59%	5/10
	K19/A82M/F87A/E267F	20%	53%	36%	–	–	–	–
	K19/F87V/A328I	36%	4%	27%	–	10%	42%	2/10
2 mM	KU3/A328I/A330P* *8 h*	10%	–	**100%**	–	–	–	–
	KU3/A328I/A330P* *24 h*	86%	9%	12%	19%	25%	36%	7/10
	I263G* *8 h*	19%	14%	**86%**	–	–	–	–
	I263G* *24 h*	83%	7%	15%	8%	28%	42%	7/10
	R19/F87A/I263G/A264G* *8 h*	24%	33%	**67%**	–	–	–	–
	R19/F87A/I263G/A264G* *24 h*	75%	40%	**60%**	–	–	–	–
	R19/F87A/G265GG* *8 h*	42%	50%	**50%**	–	–	–	–
	R19/F87A/G265GG* *24 h*	85%	58%	**42%**	–	–	–	–

From Table 3.3, it was also noticed that the lactam-yielding variants of lower conversion (<40%, TON <2,000) with 5 mM substrate addition tended to favour the *endo* dimer substantially, since the *exo* : *endo* ratio varied from 2 : 10 to 3 : 10, whilst the other variants showed ratios of 5–6 : 10. Their corresponding product distributions for the reactions with 2 mM substrate addition also showed higher ratio for the *exo* dimer (Table 3.4). The I-helix mutations I263G and E267G, and the A328/P329/A330 loop mutations A328I and A330P, favoured the *endo* dimer as the wild type enzyme and chemical Povarov reaction did.

Table 3.4 The dimer fomation of the $P450_{BM3}$ variants (1 μM) oxidising **1**.

Substrate Conc.	**Mutant**	**Conv.**	**Selectivity pattern**						*exo* : *endo*
			2	**3**	**4**	**5**	**6**	dimers	
5 mM	WT	20%	4%	11%	–	11%	**39%**	50%	3/10
	K19/F87A/I263A	32%	21%	30%	–	7%	**27%**	34%	2/10
	K19/F87V/A328I	36%	4%	27%	–	10%	**42%**	52%	2/10
	A330P	28%	6%	43%	–	7%	**34%**	41%	2/10
	RT2/A330P	38%	3%	29%	–	13%	**48%**	61%	3/10
	RP/E267G	24%	9%	8%	–	11%	**40%**	51%	3/10
2 mM	WT	40%	3%	2%	9%	22%	**63%**	85%	4/10
	K19/F87A/I263A	64%	21%	7%	11%	18%	**43%**	61%	4/10
	K19/F87V/A328I	67%	3%	7%	53%	11%	**26%**	37%	4/10
	A330P	64%	4%	13%	–	27%	**57%**	84%	5/10
	RT2/A330P	63%	3%	13%	1%	25%	**59%**	83%	4/10
	RP/E267G	50%	9%	4%	2%	24%	**62%**	85%	4/10

The proportion of the *exo* dimer, the scaffold of incargranine B[478] and seneciobipyrrolidine,[477] in the dimer mix (*exo* : *endo* = 6 : 10) was maintained by F81W, H171L, I263G, E267V/M and I401P regardless of the change in substrate concentration (Table 3.5). These mutations also maintained higher conversion (>80%, TTN >4,000) and dimer formation (>95% selectivity for **5** and **6**, TON >3,900) with 5 mM substrate. No variant managed to get more *exo* **5** than *endo* **6**, but lower concentration of the added substrate did improve the formation of the *exo* dimer (Appendix 3.1).

Table 3.5 The dimer ratio of the $P450_{BM3}$ variants showing constant *exo* : *endo* dimer formation.

Mutant	2 mM substrate				5 mM substrate			
	Conv.	**5**	**6**	*exo* : *endo*	**Conv.**	**5**	**6**	*exo* : *endo*
RT2/F87W	99%	34%	60%	6/10	96%	35%	62%	6/10
RP/F81W	98%	35%	59%	6/10	81%	35%	62%	6/10
RP/H171L	98%	35%	59%	6/10	94%	35%	62%	6/10
RP/H171L/I263G	100%	28%	49%	6/10	93%	34%	62%	6/10
RP/E267V	99%	36%	61%	6/10	87%	35%	61%	6/10
RP/E267M	99%	37%	61%	6/10	97%	35%	63%	6/10
RT2/I401P	99%	34%	59%	6/10	97%	35%	61%	6/10

To sum up, the engineered $P450_{BM3}$ variants oxidised *N*-phenyl pyrrolidine (**1**) at the α C–H bond of the pyrrolidine ring (up to 100% selectivity, TON 4,850) and the C3=C4 double bond of the phenyl ring (up to 96% selectivity, TON 1,310). No Nβ-hydroxylation product was observed. The substrate : enzyme ratio affected the selectivity between these two activities; only low substrate concentration (2 mM) reactions showed the formation of the *para*-phenol **4**, which was enhanced by the F87V, A184I, I263G and A328I/V/L mutations.

The downstream product distribution of α-hydroxylation depended on substrate concentration. Except for the RT2, RT2/F81W, RP/F87W, RP/H171L(/I263G), RP/E267V(M) and RT2/I401P variants, the other variants showed inhibited dimerisation under high substrate concentration (5 mM). For the variants in the reactions with 5 mM substrate, the mutation F87A favoured dealkylation whilst the I263A, E267F, A328I and A330P tuned the activity towards lactam formation. The 2nd generation variants containing the double mutation I263G/A264G or the insertion mutation G265GG favoured lactam formation at both low and high substrate concentrations. For the enzymatic Povarov reaction herein discovered, the *endo* dimer was favoured to various extents (*exo* : *endo* = 6 : 10 in most cases). Higher substrate concentration, along with the mutations I263G/A, E267G, A328I, and A330P, increased the percentage of the *endo* dimer in the dimer mix

but with modest selectivity for the dimers, whilst the reactions showing increased *exo* dimer formation generated more dimers in total.

The F87 loop, the I-helix (particularly the I263–E267 region) and the A328–A330P loop were found to be key to engineer the regioselectivity of $P450_{BM3}$ oxidation of *N*-phenyl pyrrolidine (**1**), but it was beyond prediction that the substrate concentration impacted the enzymatic oxidation process. In contrast with the CYP2B1 oxidation of **1**, *N*-oxidation was diminished, and the enzymatic Povarov reaction was firstly found for engineered $P450_{BM3}$.

3.3 $P450_{BM3}$ oxidation of *N*-phenyl piperidine

N-Phenyl piperidine **7** was screened against the 48 variant library (TFA1/TFB, Appendix 3.3) using substrate concentrations of 2 mM and 5 mM with 1 μM enzyme. The screening reactions were carried out using the same protocol as for **1**. Preparative reactions with the variants R19/F87A/A328I, RP/H171L/I263G and RT2/S72W/A330W were conducted at 10 mM substrate and 5 μM enzyme in 100 mL of 100 mM phosphate buffer. Products **2** and **8**–**12** (Figure 3.10) were purified and characterised by NMR and MS. The NMR and MS data for **2**, **8** and **9** were consistent with literature data.[469,490,491] Three dimers **10**–**12** were characterised in mixture forms, herein tentatively assigned by NMR and MS data. Both the mixture of **10** and **11** and the sample mainly containing **12** gave the definitive $[(2M_7 - 4) + H]^+$ peak at 319. The dimers **10** and **11** were fully assigned around the newly formed tetrahydroquinoline core, and the stereochemistry (*endo* or *exo*) was determined by the coupling between H25 and H26 in the COSY spectrum (Figure 3.11). The product **12** was assigned to the enamine dimer (Figure 3.12), as all aromatic hydrogens remained and a narrow doublet at δ 6.48 (H13) suggested a β-substituted enamine structure. The double doublet at δ 3.71 (H5) was shifted to lower field due to the substitution of the enamine, and the coupling pattern in the COSY spectrum confirmed it was coupled to a CH_2 (C4) group.

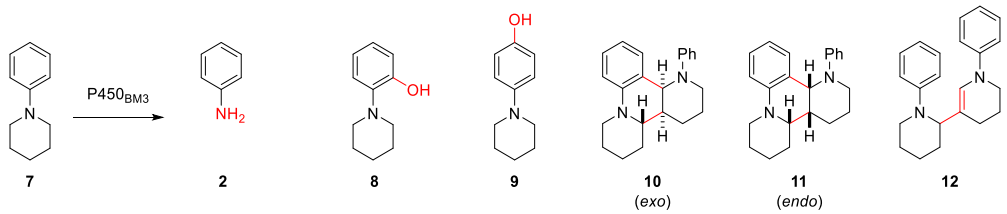


Figure 3.10 The reaction scheme of $P450_{BM3}$ oxidation of *N*-phenyl piperidine, **7**.

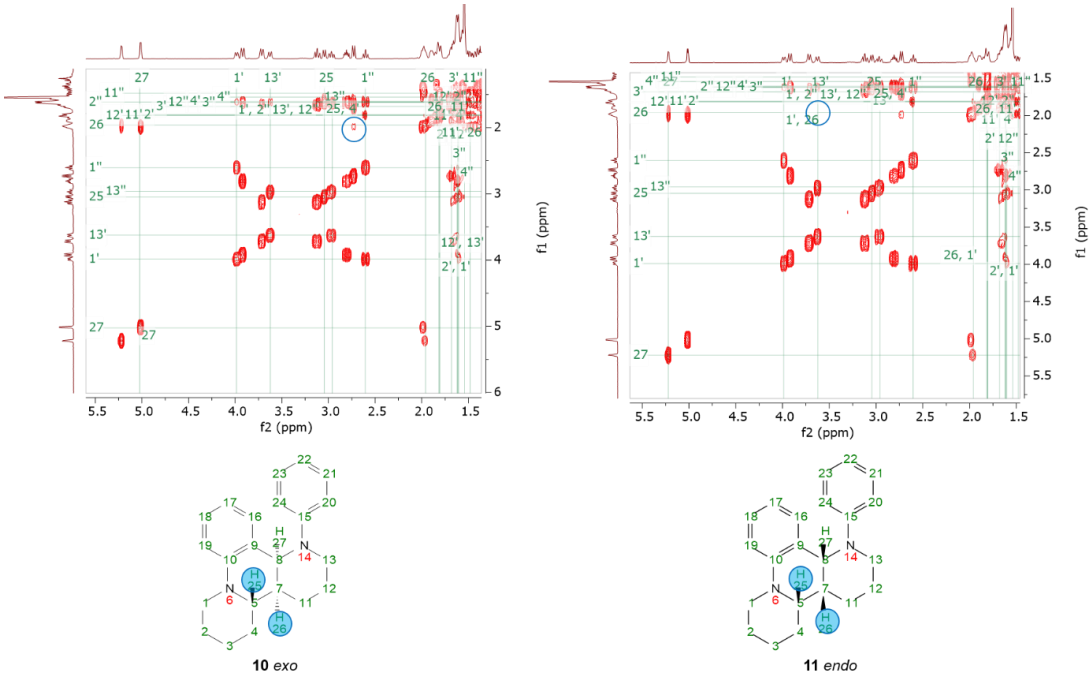


Figure 3.11 Comparison between the COSY spectra of **10** and **11**.

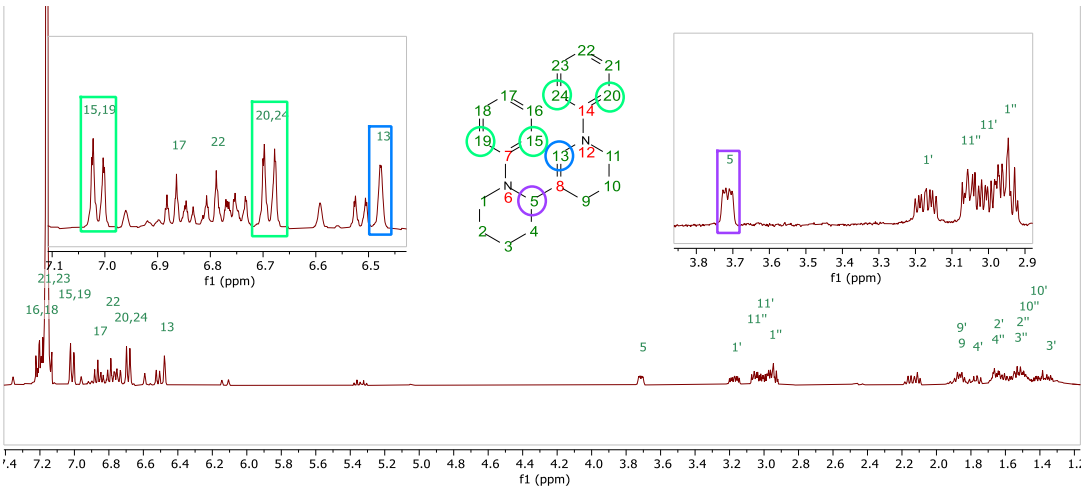


Figure 3.12 The ^{1}H NMR spectrum of **12** containing <23% impurity.

The formation of **2**, **10**, **11** and **12** are rationalised by $P450_{BM3}$-catalysed α-hydroxylation, followed by similar pathways as their pyrrolidine counterparts in Figure 3.8, and **12** is generated by nucleophilic attack by the enamine monomer and deprotonation (Figure 3.13). The formation of **12** coincided with the dimeric enamine formed in the counteranion-controlled tandem formal Povarov reaction.[489] However, the amount of **12** was not enough for mechanism testing or confirmation of absolute stereochemistry. Hence, it remains unknown whether **12** was the intermediate in enzymatic Povarov reaction or the product from a divergent pathway initiated by Nα hydroxylation. Unlike its pyrrolidine analogue, the *exo* dimer **10** was dominant across the entire variant library.

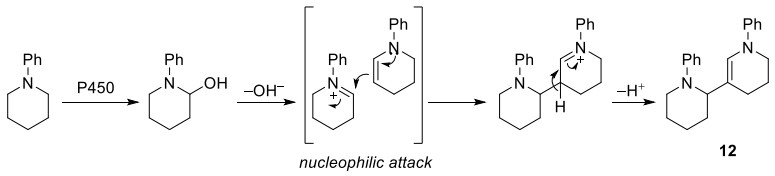


Figure 3.13 The proposed mechanism of the formation of the enamine dimer **12**.

The two sets of screening data in Appendix 3.3 showed that the titre of the reaction affected the product distribution (Figure 3.14). For instance, the K19/F87V/Q403P variant converted **7** to 15% of **8**, 80% of **9** and 5% of dimers in the reaction with 5 mM substrate, whilst the reaction with 2 mM substrate gave 12% of **2**, 7% of **8**, 31% of **9** and 29% of dimers along with several uncharacterised products. RP/I263A/E267V yielded no **9** at 2 mM substrate but 36% of **9** at 5 mM substrate, whereas R19/F87A gave 29% of **9** and 49% of dimers at 2 mM substrate and 20% of **9** and 80% of dimers at 5 mM substrate. RT2 gave 15% of **8** at 2 mM substrate but 34% of **8** at 5 mM substrate.

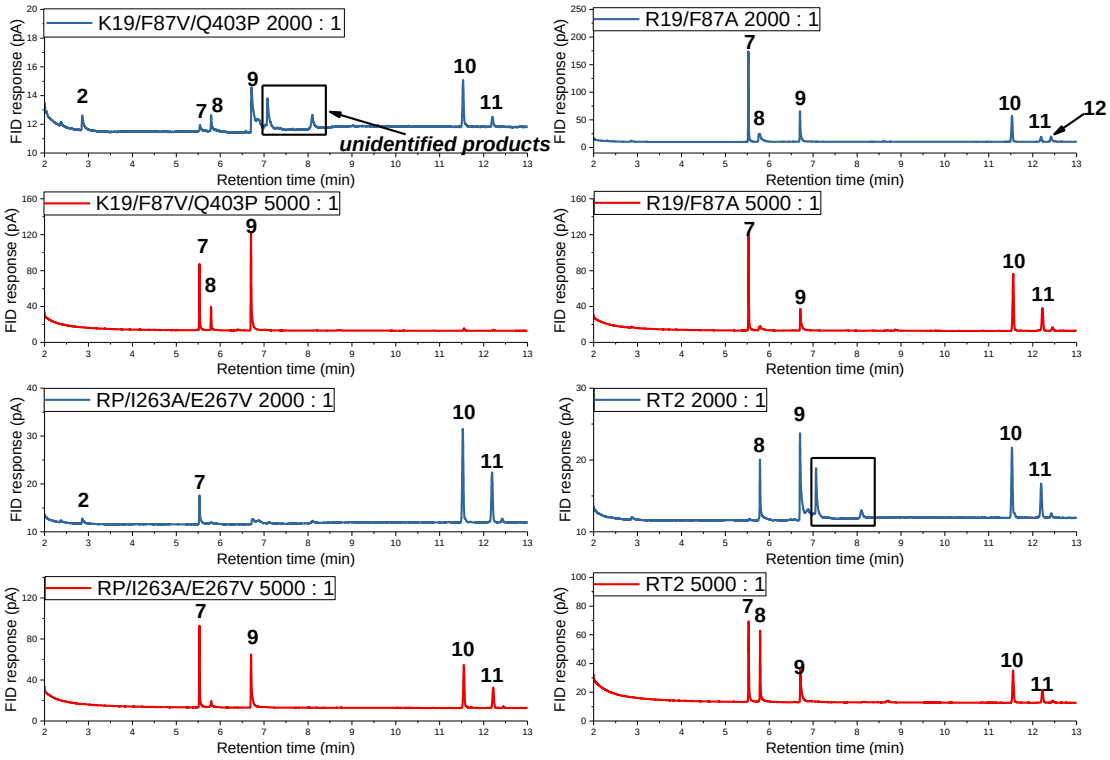
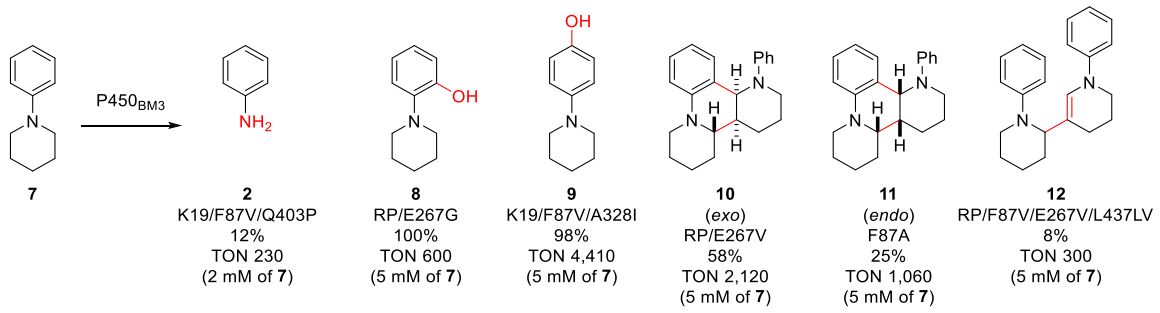


Figure 3.14 GC analysis of $P450_{BM3}$ oxidation of **7** showing titre dependence.

Amongst the overnight screening reactions with 5 mM substrate, 44 out of 48 variants showed >50% conversion (TTN >2,500). Wild type $P450_{BM3}$ gave the phenol products with modest conversion (79% of **8** at 24% conversion of 2 mM substrate, and 41% of **8** and 40% of **9** at 44% conversion of 5 mM substrate). The variants R19/F87A/A328I, K19/F87V/A328I, RT2/A184I/A330P, and RT2/P329V/A330P gave ≥90% conversion (TTN ≥4,500). This suggested that the A328/P329/A330 loop was important for promoting conversion. The mutations F87A/V and I263G also lifted the enzymatic activity.

For aromatic oxidation, RP/E267G gave 100% of *ortho*-phenol **8** at 5 mM substrate (TON 600), but its reaction with 2 mM substrate gave less (53% of **8**). An opposite example was given by wild type, which gave the higher proportion of **8** in the reaction with 2 mM substrate (79%) than with 5 mM substrate (41%). The variant K19/F87V/A328I gave 98% of *para*-phenol **9** (TON 4,410) with 5 mM substrate while RP/F87V/H171L/I263G provided 93% of **9** (TON 3,950) at 5 mM substrate (Table 3.6).

Table 3.6 The selectivity trends for **2**, **8**–**12** under 2 mM/5 mM substrate concentrations from the screening reactions.



7

2
K19/F87V/Q403P
12%
TON 230
(2 mM of **7**)

8
RP/E267G
100%
TON 600
(5 mM of **7**)

9
K19/F87V/A328I
98%
TON 4,410
(5 mM of **7**)

10
(*exo*)
RP/E267V
58%
TON 2,120
(5 mM of **7**)

11
(*endo*)
F87A
25%
TON 1,060
(5 mM of **7**)

12
RP/F87V/E267V/L437LV
8%
TON 300
(5 mM of **7**)

Mutant	**Selectivity & TON for 2**		**Mutant**	**Selectivity & TON for dimers**	
	2 mM	**5 mM**		**2 mM**	**5 mM**
K19/F87A/I263A	8% 110	–	WT	21% 100	20% 440
K19/F87V/Q403P	12% 230	–	F87A	66% 1,250	81% 3,440
	Selectivity & TON for 8		R19/F87A	49% 650	80% 2,800
RP/E267G	53% 150	100% 600	RP	47% 900	49% 2,160
	Selectivity & TON for 9		RP/E267V	92% 1,800	81% 2,960
RP	18% 350	32% 1,410	RP/I263A/E267V	95% 1,690	58% 2,150
RP/F87V	42% 810	88% 3,830	RP/F87V/E267V/L437VL	88% 1,300	66% 2,340
RP/H171L	31% 480	29% 910	RP/F87V/E267V/L437LV	82% 1,200	56% 2,100
RP/H171L/I263G	92% 1,690	90% 3,920	RP/F87V/E267V/L188Q	30% 520	72% 2,880
RP/H171L/I263G/F87V	100% 1,380	93% 3,950	GVQ (Q: L188Q)	44% 700	75% 3,230
RT2/A330P	32% 630	43% 1,850	RT2	35% 700	39% 1,460
RT2/A330P/A82M	86% 1,570	96% 4,180	RT2/A330P	45% 880	50% 2,150
RT2/A330P/P329V	71% 1,020	73% 3,290	RT2/A330P/V78I	82% 1,610	64% 2,820

As to dimer formation, the variant RP/I263A/E267V afforded 95% of dimers (TON 1,620) at 2 mM substrate, whilst F87A gave highest proportion of the dimers (81% selectivity, TON 3,440) at 5 mM substrate (Table 3.6).

To summarise, the selectivity trends shown in Table 3.6, dealkylation was a minor pathway for most variants; formation of the *ortho* phenol **8** was enhanced by the E267G mutation at 2 mM substrate concentration; the *para* phenol **9** was promoted by the mutations A82M, F87V, I263G, A328I and P329V at both 2 and 5 mM substrate; the mutations V78I, F87A, E267V favoured dimerisation at both substrate concentrations; L437VL, L437LV and I263A maintained high selectivity for dimers with 2 mM substrate, and L188Q improved the dimer formation at 5 mM substrate.

Table 3.7 The *exo* : *endo* dimer ratio (**10** : **11**) and the total dimer yield of $P450_{BM3}$ oxidation of **7** (2 mM and 5 mM).

Mutant	2 mM of **7**		5 mM of **7**	
	10 : 11	dimers	**10 : 11**	dimers
WT	10/5	21%	10/3	20%
F87A	10/6	66%	10/5	81%
K19/F87A/A82M	10/7	86%	10/5	42%
K19/A82M/F87A/E267F	10/2	30%	10/5	57%
K19/F87A/I263A	10/7	45%	10/4	42%
K19/F87A/A328I/I263A	10/3	25%	10/5	44%
K19/F87A/A328I/A184I	10/6	69%	10/5	14%
RP/E267V	10/6	92%	10/4	81%
RP/E267M	10/2	52%	10/4	5%
GVQ	10/2	44%	10/4	75%
RP/F87V/E267V/L188Q	10/3	30%	10/5	72%
RP/F87V/E267V/L437LV	10/7	82%	10/3	56%
RP/F87V/E267V/L437VL	10/6	88%	10/4	66%
RT2/A330W	10/3	41%	10/5	68%
RT2/A330P	10/6	45%	10/5	50%
RT2/A330P/V78I	10/7	82%	10/6	64%

For the diastereomeric pair of dimers, all variants preferentially formed the *exo* dimer **10** to the *endo* dimer **11** with the ratio of **10** : **11** ranging from 10 : 7 to 10 : 1. Comparing the screening results of wild type with those for the variants (Table 3.7), the mutations V78I, A82M, F87A, A184I, I263A, E267V, A330P and L437VL increased the proportion of the *endo* dimer **11** in the dimer mix at both 2 and 5 mM of **7**, and L437LV enhanced the formation of **11** only at 2 mM of **7**. In contrast, the mutations L188Q, E267F/M, A328I and A330W pushed higher the proportion of the *exo* dimer **10** at 2 mM of **7**, but slightly promoted the formation of the *endo* dimer **11** at 5 mM of **7**. These suggested that the regions V78–A82, I263–E267, and A328–A330 and the residues F87, A184, L188, L437 affected the stereochemistry of the Povarov reaction.

The bulkier mutations Phe, Met, and Trp at the residues E267 and A330 were found to strongly favour the *exo* dimer **10** at 2 mM of **7** (Table 3.7) perhaps due to their steric demands, rendering the transition state for the *endo* dimer less favourable. The variants giving >50% of dimers revealed the convergence of keeping the *exo* : *endo* ratio at around 10 : 4 in the reactions with 5 mM substrate. This observation implied that the *endo* and the *exo* dimer formation could reach a stage where the active site of the enzyme was fully 'saturated' with a couple of substrate molecules, leaving the two reacting intermediates binding in similar relative orientation, thence yielding a dimer mix of constant distribution.

R19/F87A and R19/F87A/A328I yielded 4–10% and 2–3% of **12**, suggesting alterations at A328 changed the selectivity of **12**. Other R19/F87A/A328X variants were hence made for the promotion of **12**. R19/F87A/A328G improved the selectivity of **12** to 14% (TON 180). Mutagenesis to engineer the stereoselectivity of **10** and **11** were not productive thus far.

The variation between the dimer ratio of the reactions yielding **10** and **11** suggested binding of mutiple substrate molecules inside the active site of variants. The change of the substrate

concentration altering the ratio of **10** : **11** also added support for this assumption. Therefore, substrate binding titration was carried out using GVQ (44% and 75% selectivity of the dimers, TON 700 and 3,230 at 2 mM and 5 mM of **7**, respectively) as the test enzyme. Single-site binding behaviour was observed (Figure 3.15), which oddly suggested that dimerisation occurred in solution. It is possible, however, that a second molecule of substrate is inside the substrate access channel but does not interfere with the binding of the substrate close to the heme. Hence, the single-site binding titration curve did not rule out dimerisation inside the active site. Other methods, *e.g.* isothermal titration calorimetry[492] and NMR,[493] could be also attempted to allow for a better understanding of substrate binding.

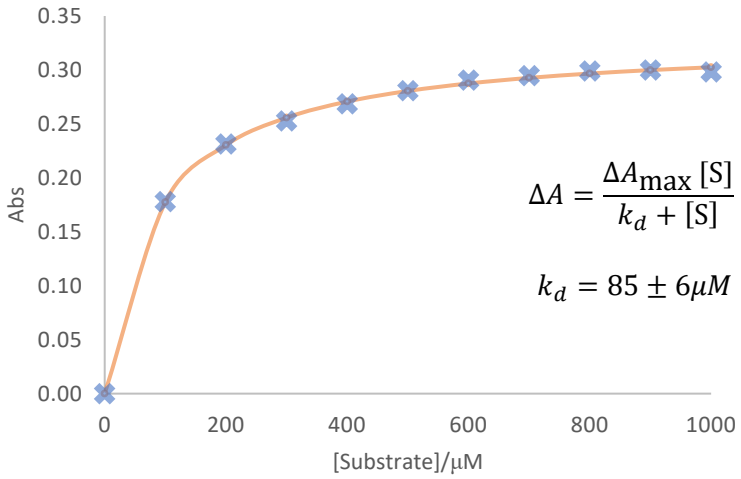


Figure 3.15 Binding titration of *N*-phenyl piperidine, **7**, with the GVQ mutant showing single-site binding.

The oxidation of **1** and **7** shared some similarities, but also varying in product distribution. For similarities, no direct evidence for remote functionalisation in both $P450_{BM3}$-catalysed biotransformation; aromatic oxidation and α oxidation were the activities shown by the variant library; enzymatic Povarov reactions were observed in both cases with high total yield achieved (97% of **5** and **6**, TON 4,660; 81% of **10** and **11**, TON 3,440); the substrate concentration altered the product profile; and the regions of V78–A82, I263–E267, A328–A330 and the residues F87 and L437 were crucial for activity engineering. The differences

were also obvious. Dealkylation was far less common for the piperidine substrate **7**. No lactam was formed in $P450_{BM3}$ oxidation of **7** while no *ortho* phenol and enamine dimer was given from **1**. Wild type converted less **7** into the dimers, and the substrate concentration change mainly influenced the regioselectivity for aromatic oxidation. The *endo* dimer was favoured for **1**, but the *exo* dimer for **7**. Formation of the enamine/iminium dimer **12** in oxidation of **7** was of significance, since it hinted that the addition of nucleophile or electrophile might be able to trap the iminium or the enamine intermediate to form α-derivatised or β-derivatised *N*-phenyl pyrrolidine/piperidine. The enzymatic Povarov reaction established the biocatalytic pathway to construct the multi-substituted 1,2,3,4-tetrahydroquinoline (THQ) core.

3.4 Attempted trapping of intermediates in enzymatic Povarov reactions

The generation of the enamine dimer **12** from **7** broadened the scope of $P450_{BM3}$ oxidation of **1** and **7**. This suggested that the iminium and the enamine intermediates could be mutually trapped by each other. Previous research on enantioselective α-functionalisation of aldehydes,[494–500] enantioselective Diels-Alder reaction with α,β-unsaturated ketones,[501,502] the enantioselective construction of pyrrolidines by cascade addition-cyclisation,[503] and enantioselective Mukaiyama-Michael reaction[504] by secondary amine catalysts revealed the catalytic mechanisms involving the formation of the iminium, the enamine, and the SOMO intermediate (the enamine radical cation).[500] All of these reactions commenced from the aldehyde or the α,β-unsaturated ketone reacting with a 2° amine catalyst to form the iminium, the enamine, the enamine cation, or the SOMO intermediate to catalyse the rest of the reaction with the other component (Figure 3.16). Some small-molecule iron catalysts, such as Fe(PDP)[505] and $Fe(dibm)_3$,[506] also brought about α-functionalisation of cyclic amines via the enamine or the iminium intermediate (Figure

3.16). These reactions formed C–C bonds by either electrophilic substitution[505] or radical olefin hydrofunctionalisation.[506] Other P450s, *e.g.* CYP719B1[507] and CYP80G2,[508] were also reported to catalyse C–C bond formation. These examples validated that trapping the intermediates generated in enzymatic Povarov reaction was feasible. Three types of trapping experiments were planned for $P450_{BM3}$-catalysed biotransformation: a) using other diene/dienophile to trap the iminium/enamine to construct the tetrahydroquinoline core, b) using a nucleophile to trap the iminium to obtain the α-functionalised cyclic amine, and c) using an electrophile to trap the enamine to generate the β-substituted iminium.

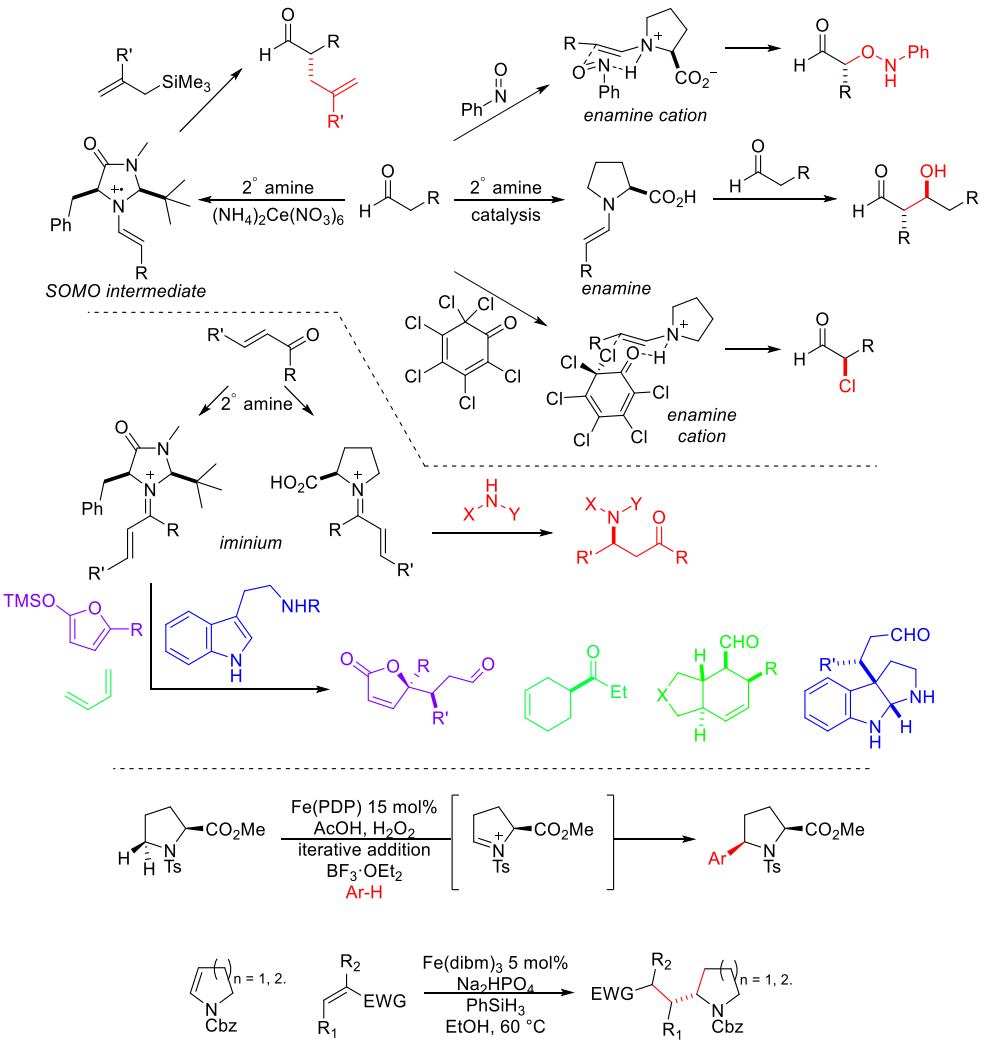


Figure 3.16 The reactions involving iminium, enamine and enamine radical cation as their indispensable intermediates.[494,495,504–506,509,496–503]

A selection of trapping reagents (Figure 3.17) were tested by mixing with **1** or **7** in the ratio of 1 : 1 and 4 : 1 (2.5 mM : 2.5 mM and 10 mM : 2.5 mM) via the catalysis of the R19/F87A/A328I variant (1 μM). The initial trial showed that only the cross-coupling reactions of 1,2,3,4-tetrahydroquinoline (**13**, THQ) and **1**/**7** (1 : 1) successfully generated the heterodimers (Figure 3.18). Other trapping attempts were fruitless so far.

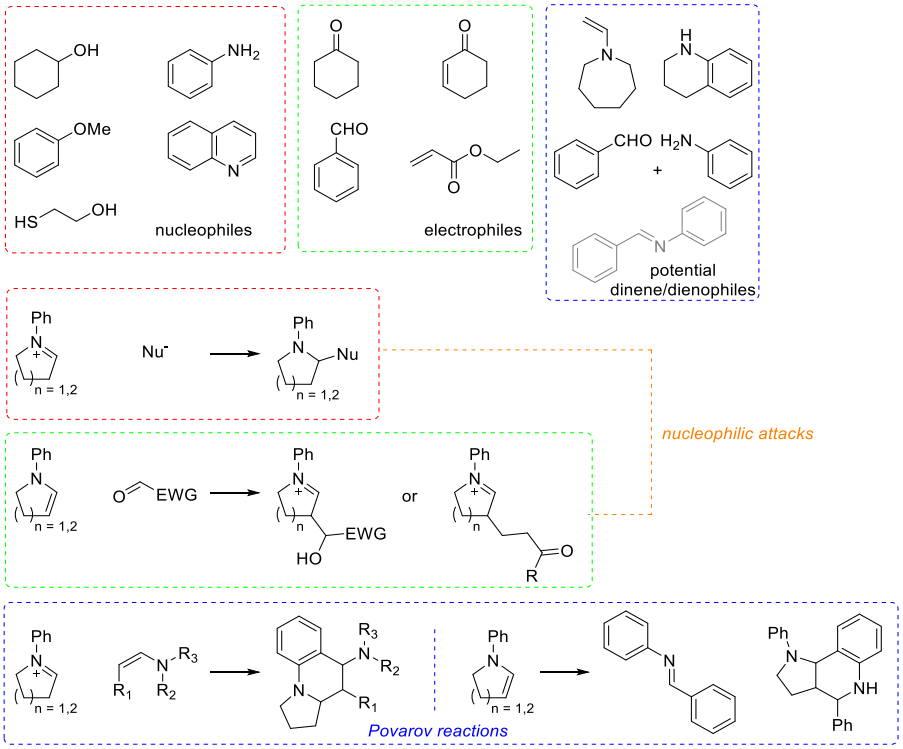


Figure 3.17 A selection of trapping reagents and their potential cross-coupling products.

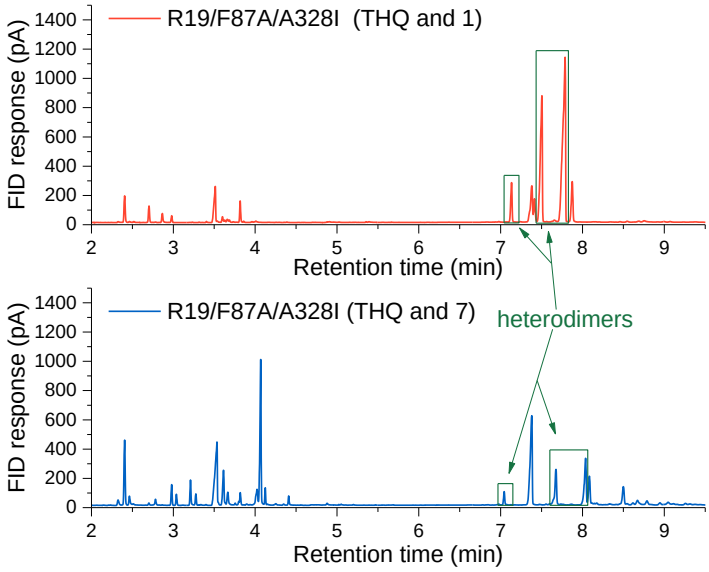


Figure 3.18 GC graphs of the cross-coupling reactions of 1,2,3,4-tetrahydroquinoline (THQ) and **1**/**7** (1 : 1).

The lack of the cross-coupling products from nucleophilic attack implied that the enzymatic Povarov reactions might occur inside the active site, hence manageable by protein engineering. For the cross-coupling of **1**/**13** and **7**/**13** (Figure 3.18), the R19/F87A/A328I variant (5 μM in 100 mL phosphate buffer, pH 8.0) was used to scale up the cross-coupling reactions of **13** and **1**/**7** (5 mM for each) for product purification. The heterodimers and the heterotrimer **14**–**20** were purified and characterised by NMR and MS (Figure 3.19, Appendix A 4.1, Spectra 25–46).

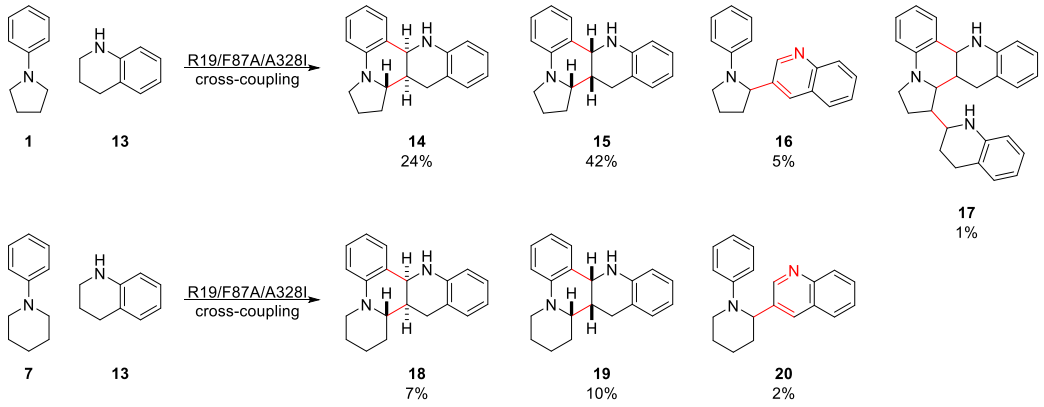


Figure 3.19 The enzymatic cross-coupling of *N*-phenyl pyrrolidine (**1**)/1,2,3,4-tetrahydroquinoline (**13**) and *N*-phenyl piperidine (**7**)/**13**.

The relative stereochemistry of **14**/**15** and **18**/**19** was determined by the coupling between the two hydrogens linking to the two carbons of the newly formed C–C bonds (Figure 3.20). For both cross-coupling reactions, the *endo* dimers were dominant over the *exo* dimers, following the general principle for normal Diels-Alder reactions. The mass of **16** and **20** were found to be [$M_{1/7} + M_{13} - 6$], which were different from the mass of the dimers **14**/**15** and **18**/**19** ([$M_{1/7} + M_{13} - 4$]) generated from the enzymatic Povarov reactions. The two hydrogens at δ 8.81 (H17) and 7.83 (H13) in **16**, both of which were narrow doublets (J = 2.2–2.3 Hz), were coupled to each other by the aromatic W-shaped long-range coupling (Figure 3.21). This portrayed that **13** was oxidised to a 3-substituted quinoline (losing 5 hydrogen atoms), and a doublet at δ 4.87 suggested that the α-C of the pyrrolidine ring was

substituted (losing one hydrogen). The structure of **16** was hence confirmed, as was the assignment of the structure of **20** (Figure 3.21).

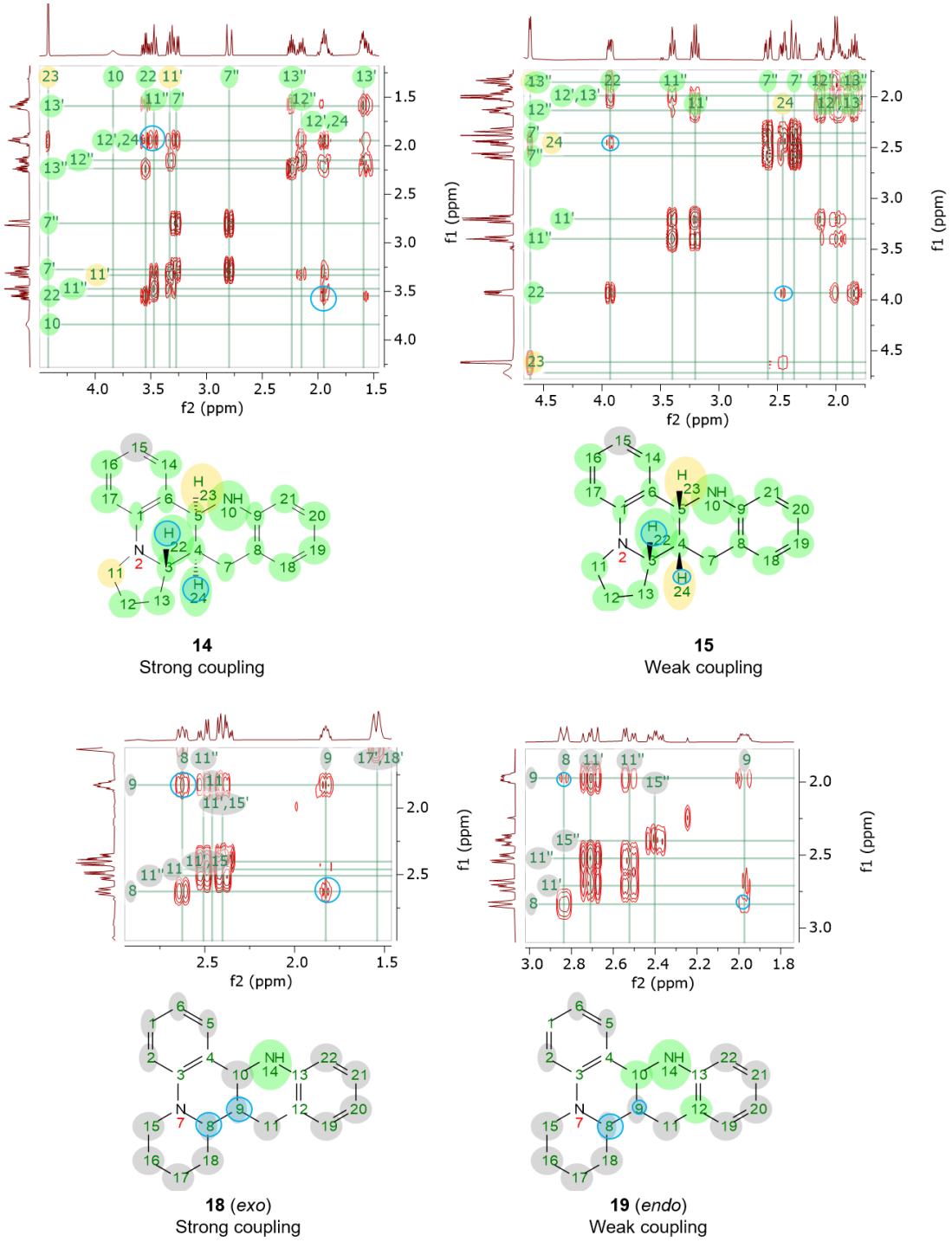


Figure 3.20 Comparison between the COSY spectra for **14**/**15** and **18**/**19**.

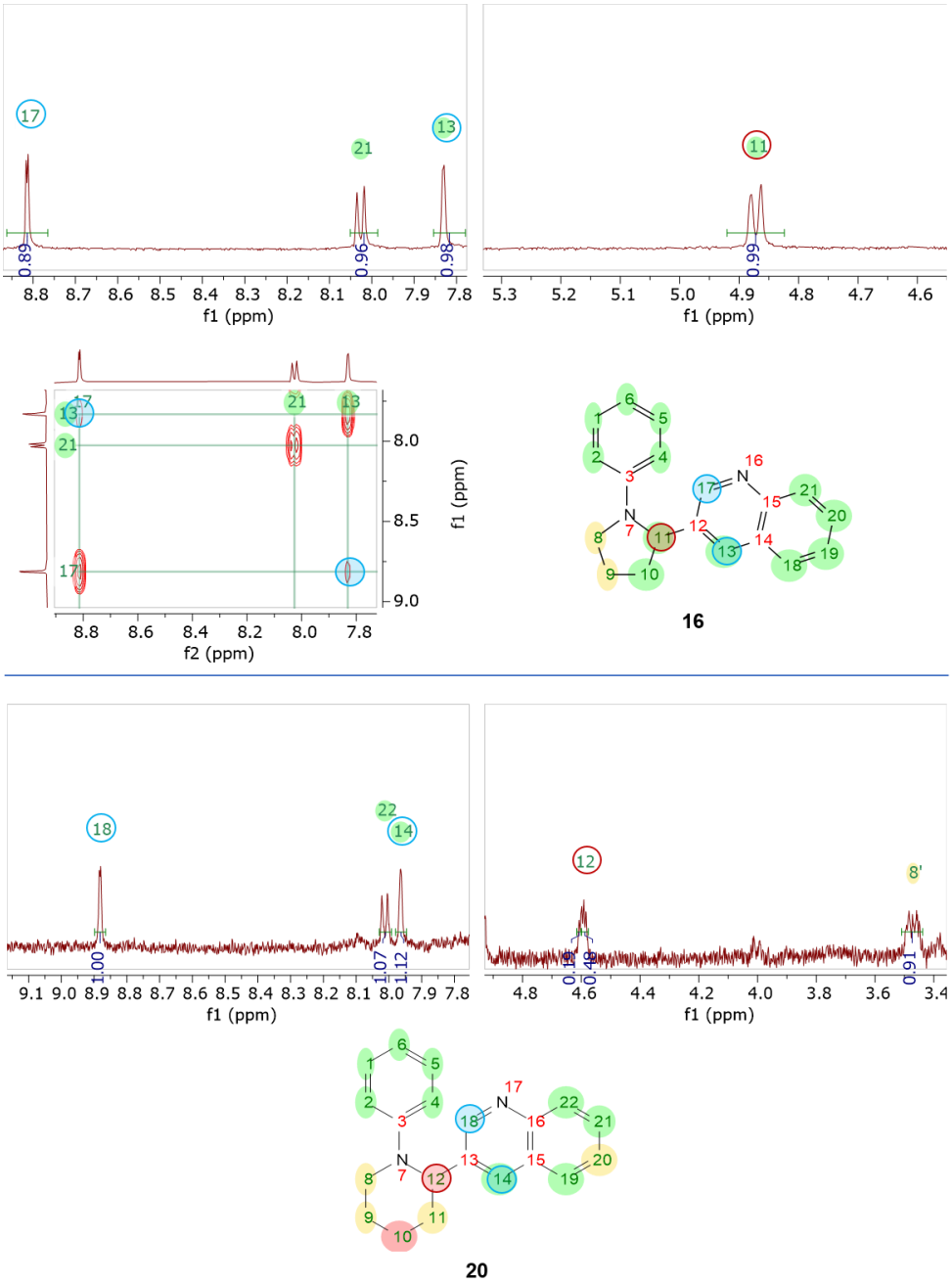


Figure 3.21 Snapshots of the ^{1}H and COSY NMR spectra for **16** and **20** which directed their assignments.

The arrangement of the heterotrimer **17**, whose mass was [M_1 + 2M_{13} – 6] (HMRS <ESI^{+}> 408.2437), was traced from the low-field hydrogen (H18 at δ 4.44, doublet) in the ^{1}H NMR spectrum (Figure 3.22). The COSY spectrum showed this proton to be linked to the double-quartet at δ 2.52 (H19) which further extended the linkage to the α C31–H31 of the pyrrolidine ring at δ 3.76 (dd). This α C–H was coupled to β C30–H30 (δ 2.30, m, 1H) and

H19 at δ 2.52. This β proton also demonstrated coupling to the α C8–H8 (δ 3.30, td) of the piperidine ring of the 2nd THQ motif, and the linkage of the trimer core was established.

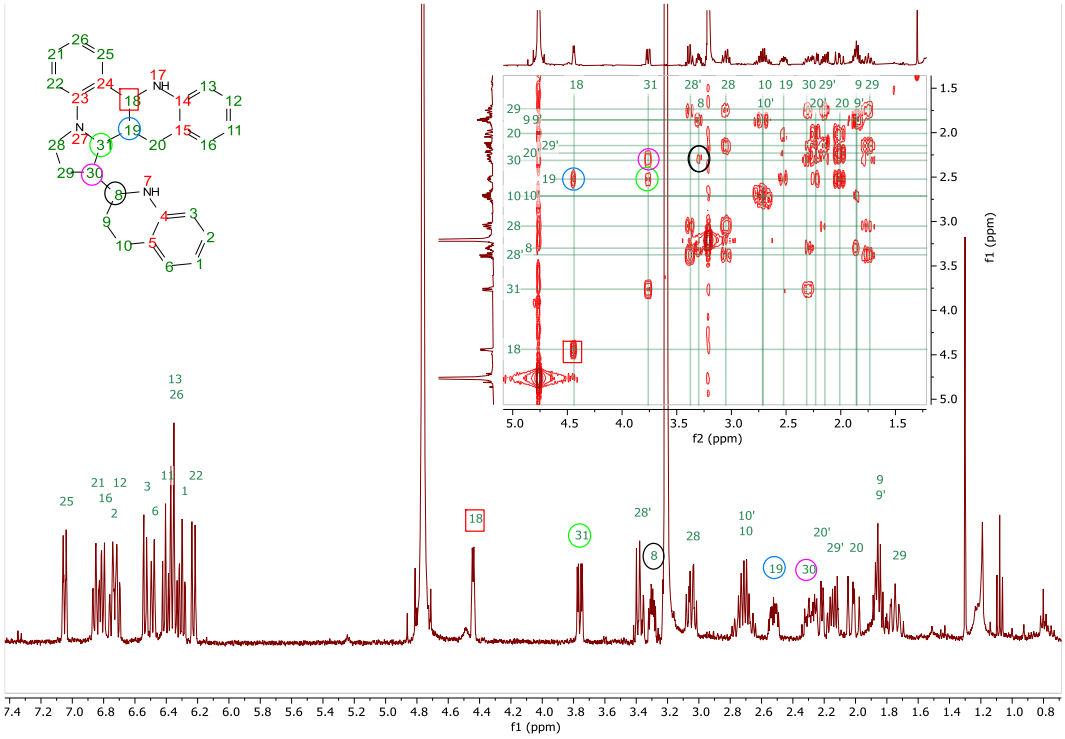


Figure 3.22 The assignment of the ^{1}H NMR of the trimer **17** (with the solvent peaks subtracted), illustrated by its COSY NMR.

The rationale of dimer and trimer formation is supported by enamine/iminium chemistry (Figure 3.23). In the initial stage of the reaction, both substrates are hydroxylated at their α C–H bonds to form the carbinolamine intermediates, which eliminate the hydroxy ion to form the iminium intermediates in equilibrium with the enamine tautomers. Therefore, 2 pairs of iminium/enamine could occur inside the active site. The iminium diene of **1**/**7** and the enamine dienophile of **13** complete the enzymatic Povarov reaction (Figure 3.23 a). The nucleophilic enamine of **13** attacks the iminium of **1**/**7** to form the heterodimeric imine. Its allylic/benzylic C–H bond is activated, and thence hydroxylated by P450$_{BM3}$ again. The allylic alcohol dehydrates due to the strong driving force of aromatisation, yielding **16**/**20** (Figure 3.23 b). Such a mechanism, rather than electrophilic substitution, is more plausible, as the attempted cross-coupling of quinoline and **1**/**7** gave no cross-coupling products, even

though quinoline was a common product in P450$_{BM3}$ oxidation of **13** (Chapter 4, Figure 4.6). The observation of **16**/**20** at least proved that the heterodimeric imine could be oxidised quickly by P450 hence against a stepwise mechanism of Povarov reaction via reversible Mannich reaction. The enamine of **1** can also attack the iminium of **13** to afford the β-substituted diene, which finishes the enzymatic Povarov reaction with the enamine of another molecule of **13** to form the heterotrimer **17** (Figure 3.23 c).

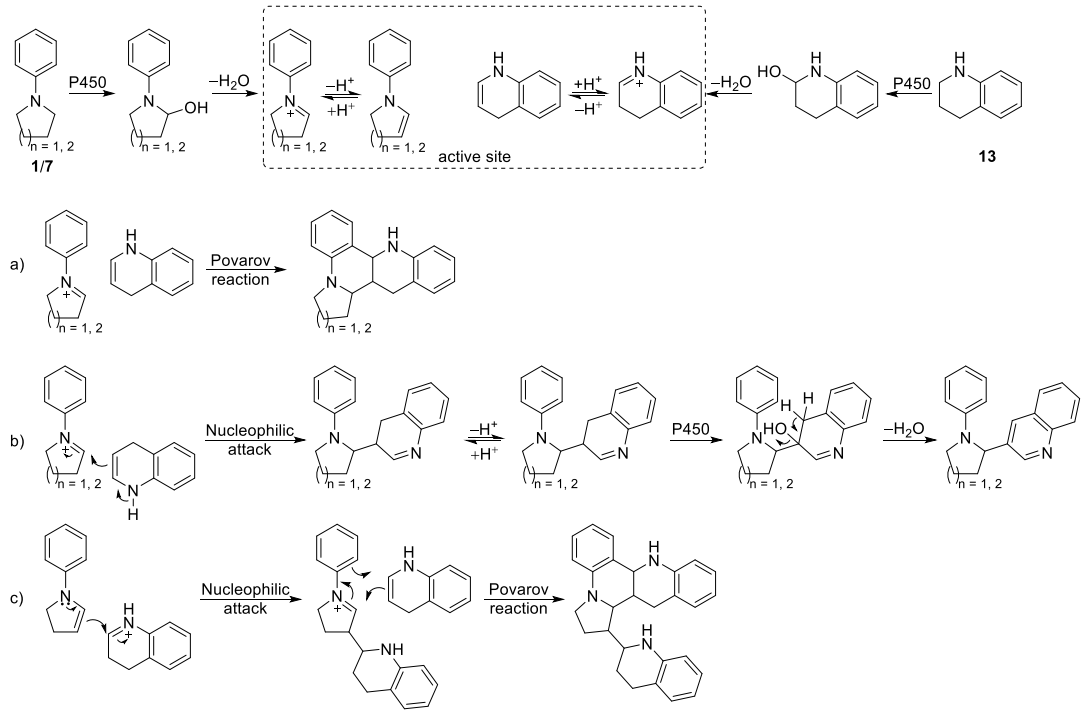


Figure 3.23 The proposed mechanisms of the P450$_{BM3}$-catalysed cross-coupling of **1**/**7** and **13**.

The mutation effects in the cross-coupling reactions of **1**/**7** and **13** were explored by the screening reactions using 2.5 mM of **1**/**7** and 2.5 mM of **13** with 1 μM of the enzymes in the 48 variant library (TFA/A1 and TFB). The reactions were shaken in the dark for 16 hours at 120 rpm, 20 °C. The screening results (Appendix 3.4) suggested that the R19/F87A/A328I gave the most of the cross-coupling products for both **1** and **7** with **13**.

Scrutinising the screening results (Table 3.8), it was noticeable that wild type showed uncommonly low activity when the mixture of **1**/**7** and **13** was added (6% and 22% conversion, TTN 300 and 1,100, mainly oxidising **1**/**7** but inert to **13**). The mutations A82M,

F87V, A328I, A330P and the combination of F87V/E267V promoted the oxidation activity in general (conversion up to 97%, TTN up to 4,850). They also increased the formation of the heterodimers substantially for **1** and **13** and slightly for **7** and **13**, giving highest proportion of the heterodimers 79% of **14**–**16** in total (TON 3,440 offered by RP/F87V/E267V/L188Q) and 27% of **18**–**20** in total (TON 1,280 provided by R19/F87A/A328I).

Table 3.8 The conversion and product distribution of the cross-coupling of **1**/**7** and **13**.

Mutant name	**conv.**	**Selectivity (1 and 13)**				**conv.**	**Selectivity (7 and 13)**			
		14	**15**	**16**	**14:15**		**18**	**19**	**20**	**18:19**
WT	6%	11%	17%	0%	6/10	22%	0%	0%	0%	
R19/F87A	19%	27%	46%	0%	6/10	66%	7%	11%	2%	7/10
R19/F87A/A328I	95%	31%	45%	1%	7/10	95%	10%	14%	3%	8/10
K19/F87A/A82M	77%	27%	41%	1%	6/10	89%	8%	8%	2%	9/10
K19/F87A/A328I/Y51L	91%	28%	44%	1%	6/10	91%	10%	16%	1%	6/10
K19/F87A/A328I/A184I	94%	28%	41%	2%	7/10	77%	7%	12%	2%	6/10
GVQ	85%	26%	43%	1%	6/10	20%	0%	11%	0%	
K19/F87V/Q403P	74%	26%	42%	1%	6/10	76%	5%	6%	1%	8/10
K19/F87V/A328I/I263A	33%	32%	37%	2%	9/10	79%	7%	13%	2%	5/10
RP/F87V/E267V/V78F	73%	28%	48%	2%	6/10	77%	4%	3%	5%	13/10
RP/F87V/E267V/L188Q	87%	30%	47%	2%	6/10	89%	7%	8%	4%	9/10
RP/F87V/E267V/L437LV	97%	24%	42%	1%	6/10	82%	8%	11%	2%	7/10
RP/A330P	93%	25%	39%	1%	6/10	87%	8%	12%	2%	7/10

Unlike the cross-coupling of **1** and **13**, the cross coupling of **7** and **13** was the side reaction of the biotransformation of the 1 : 1 mixture of **7** and **13**, which mainly gave the products from the oxidation of **7** or **13** individually. The ratio of the *exo* : *endo* dimers remained constant for the reactions of high conversion and selectivity (>70% conversion and >65% selectivity of dimers, TON >2,550) in the enzymatic cross-coupling of **1** and **13** (Table 3.8). A328I slightly increased the ratio of the *exo* dimer (**14**). In contrast, the ratio for the cross-coupling of **7** and **13** varied from 5 : 10 to 13 : 10 (Table 3.8). The mutation V78F favoured

the *exo* dimer, whereas the mutations Y51L and I263A increased the ratio of the *endo* dimer with limited enhancement. For **16** and **20**, A328I and the combinations of V78F/E267V and L188Q/E267V could nudge the enzyme to generate small amount from nil.

To sum up, the cross coupling of **1** and **13** behaved consistently with regard to the propensity to favour the *endo* dimer, whereas the cross coupling of **7** and **13** generated less dimer and the dimer ratio fluctuated drastically. This can be the consequence of the insensitive FID response shown by GC due to the material constraint in each reaction extract. *N*-Phenyl pyrrolidine showed greater propensity for cross-coupling than *N*-phenyl piperidine, perhaps due to their ring structures of different flexibility. Like the oxidation of **1**/**7**, the V78–A82, I263–E267 and A328–A330 regions and F87 were key to engineer the cross-coupling reactions.

The absence of cross-coupling of **1**/**7** with other trapping reagents posed the question of how the molecules of **13** reacted with **1**/**7** inside the active site. *N*-Vinyl-ε-caprolactam was also an enamine, but unable to trap the iminium diene herein. The mechanism behind this phenomenon remains unknown. If such question can be solved, the trapping reactions via nucleophilic attack or electrophilic substitution would be feasible and manageable.

3.5 P450$_{BM3}$ oxidation of *N*-benzyl- and *N*-benzoyl-pyrrolidines and piperidines

In contrast with **1** and **7**, *N*-Bn and *N*-Bz-cyclic amines were less active a substrate. The 48 P450$_{BM3}$ variant library showed no activity towards *N*-Bn- and *N*-Bz-pyrrolidines and piperidines, in stark contrast with the oxidation of *N*-Bn-pyrrolidine by WT P450pyr affording β-alcohols as the only product with good yield.[430] Moreover, *Sphingomonas* sp. HXN-200 harbouring P450pyr also converted *N*-Bz-, *N*-Cbz- and *N*-Boc-pyrrolidines and piperidines, phenylpyrrolidine-1-carboxylate, and *N*-Bn- and *N*-Boc-γ-butyrolactams and δ-velarolactams to β-alcohols only,[428,468] with *N*-Ac- and *N*-methoxycarbonyl-pyrrolidines

not oxidised though.[468] They were inactive substrates perhaps because of their smaller size and higher substrate mobility exposing nitrogen binding to heme.

Comparison of the overlaid structure of $P450_{BM3}$ and P450pyr (Figure 3.24 A and A1–A4) showed that a) the F-/G-helices of P450pyr were 2–3 turns shorter than those of $P450_{BM3}$, which were responsible for opening/closing the substrate access channel; b) the B'-helix in $P450_{BM3}$ was a free loop in P450pyr and both propionates of P450pyr were located on the proximal side; c) the I-helix of P450pyr was slightly closer than $P450_{BM3}$ with the the Cα of its closet residue G255 to I-helix move 0.3 Å towards the iron centre in contrast with that of A264. The characteristic F87 loop in $P450_{BM3}$ was disrupted in P450pyr, the I102 of which occupied the corresponding region; and I82 and M305 in P450pyr protruded to the A-propionate position in $P450_{BM3}$ (displaced to A330 in $P450_{BM3}$) and thence pushed the A-propionate to relocate to the proximal side. The L302 residue of P450pyr (aligned with A328 in $P450_{BM3}$) reached 0.9 Å closer to the iron centre than A328 in $P450_{BM3}$. F403 in P450pyr (aligned with L437 in $P450_{BM3}$) protruded towards the heme ion, which perhaps stabilised the phenyl motif in the tested cyclic amine substrates.

The ‘fastened bag’ topology of the substrate pocket of P450pyr (comprising of M305, L302, T259, G255, L251 and I102, Figure 3.24 B1) distinctly differs from the protruding linear substrate channel in $P450_{BM3}$ (constructed by A330, A328, T268, A264, the A-propionate and F87, Figure 3.24 B1). The higher-up residues N100, I82, F403, D258, V254 and T186 protruding into the active site of P450pyr were bulkier and more polar than A74, L75, V78, L437 and M185 that form the roof of the substrate channel of $P450_{BM3}$ (Figure 3.24 B2). Therefore, engineering $P450_{BM3}$ to oxidise cyclic amines and lactams at Nβ might be achieved by grafting the features of the active site of P450pyr, *e.g.* disrupting the B'-helix and the adjacent loop and introducing bulky mutations to push down the A-propionate, onto $P450_{BM3}$.

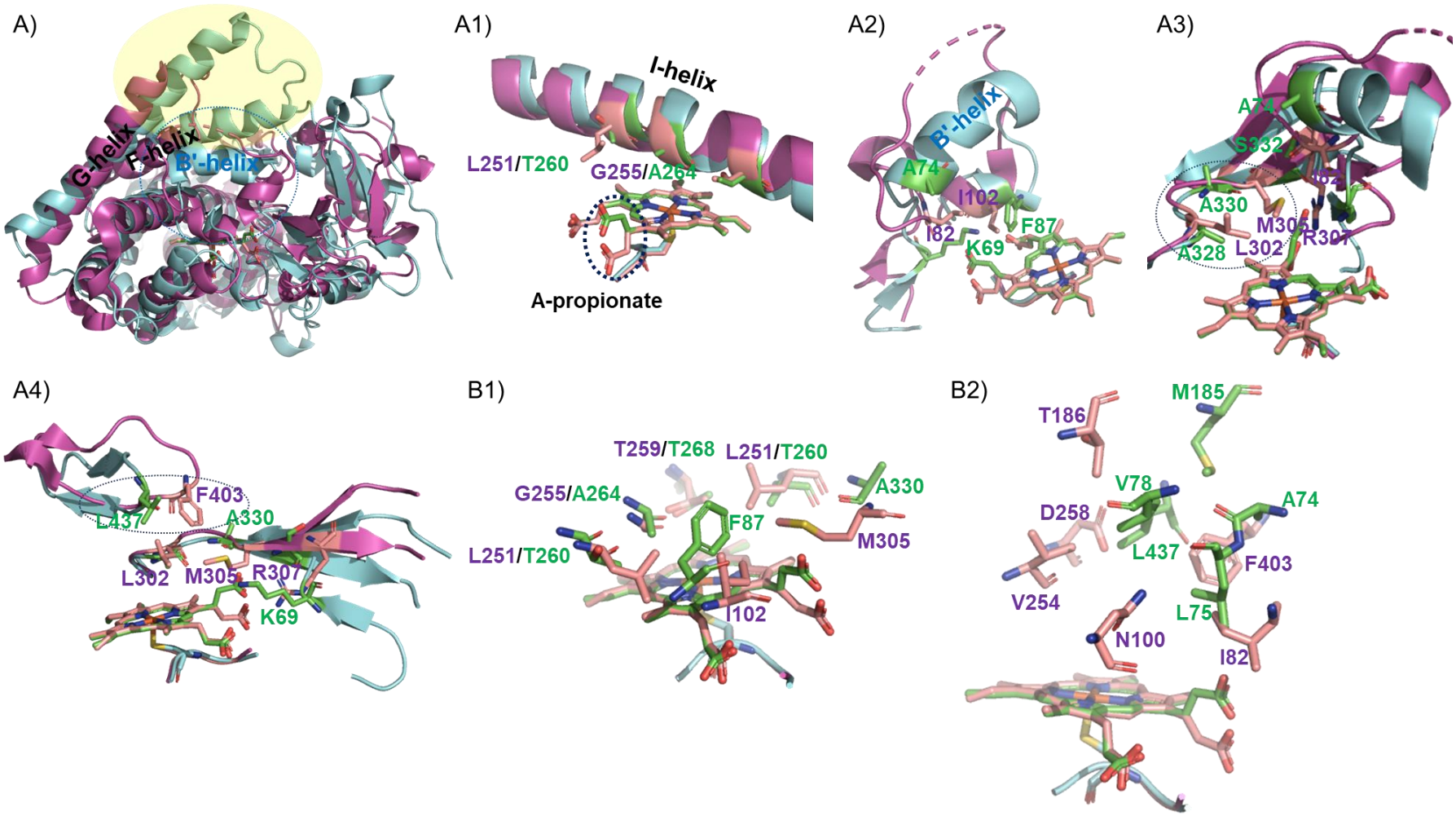


Figure 3.24 The overlay of the substrate-free crystal structures of P450pyr (PDB: 3rwl[430], in magenta with the key regions highlighted in salmon and residues labelled in purple) and $P450_{BM3}$ (PDB: 1bu7, in cyan with the key regions highlighted in green and residues labelled in green).

3.6 Summary and discussion

In this chapter, *N*-phenyl and *N*-benzyl-pyrrolidines and piperidines, and *N*-benzoyl piperidine (Figure 3.25) were tested against the P450$_{BM3}$ variant library. The current variant library gave no oxidation for *N*-Bn- and *N*-Bz-cyclic amines. The active substrates *N*-phenyl pyrrolidine and piperidine (**1** and **7**) were oxidised on the aromatic ring to form *para*- and *ortho*-phenols **4**, **8** and **9** up to >95% selectivity. The α-oxidation of **1** and **7** was the other prevalent activity observed for most variants. The common α-oxidation activities of *N*-dealkylation and amide formation were controlled by altering the substrate concentration and monitoring the reaction over the entire process to reach reasonable yields (80% of **2** and 60% of **3**). The unexpected dimers **5**, **6**, **10** and **11** were formed from the enzymatic Povarov reaction, in which iminium and enamine intermediates were generated from α-hydroxylation. Although the alkaloids incargranine B and seneciobipyrrolidine were identified from plant extracts long ago, the biosynthetic pathways are unknown. The unprecedented enzymatic Povarov reaction discovered here offers a reasonable pathway.

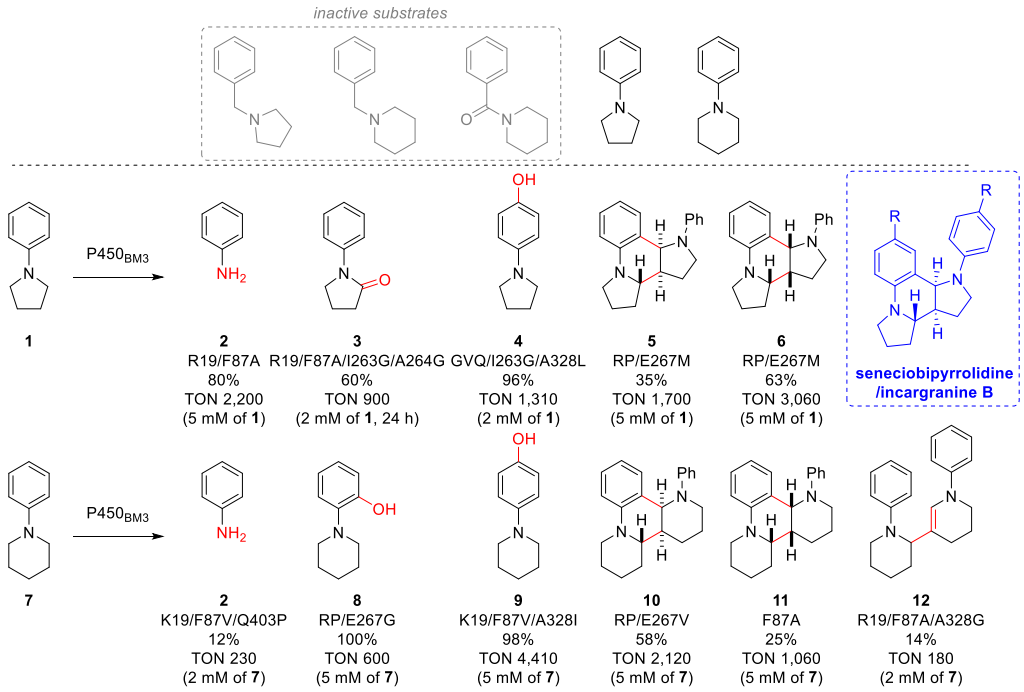


Figure 3.25 The tested substrates and the reaction schemes of P450$_{BM3}$ oxidation of **1** and **7**.

The substrate : enzyme ratio and the incubation time of the biotransformation, along with the mutations, affected the enzymatic Povarov reaction. The mutation E267V was found to promote dimer formation for both **1** and **7** regardless of changing substrate concentration. The regioselectivity for dimers could be engineered up to 98% and 92% selectivity in the biotransformation of **1** and **7** individually. However, the absolute stereochemistry has not been established and remains to be determined. In the oxidation of **1**, dimer formation followed the common rule of Diels-Alder reaction favouring the *endo* dimer, **6**, and the ratio of the *exo* : *endo* dimer was maintained at *ca.* 6 : 10. On the contrary, **7** was converted to the *exo* dimer **10** predominantly, and the *exo* : *endo* ratio fluctuated from 3 : 10 to 10 : 10. Mutations at F87, L437 and the V78–A82, I263–E267, A328–A330 regions can modestly alter the stereoselectivity, but unable to reverse the *exo* (*endo*) preference.

The enzymatic Povarov reaction and the formation of the uncommon dimer **12** suggested the possibility of trapping the enamine/iminium and diene/dienophile intermediates. Successful examples revealed that the biotransformation of the 1 : 1 mixture of **1**/**7** and 1,2,3,4-tetrahydroquinoline (**13**) produced the Povarov dimers **14**/**15** and **18**/**19**, the nucleophilic-attack dimers **16** and **20**, and a trimer **17** (Figure 3.26). The *endo* dimers were dominant. The selectivity for cross-coupling reached 79% for **1**/**13**, but only 27% for **7**/**13**. The mutations F87V, E267V, A328I and A330P were crucial for promoting the formation of heterodimers, whereas V78F, A82M, L188Q, I263A and L437LV influenced the stereoselectivity of the cross-coupling process.

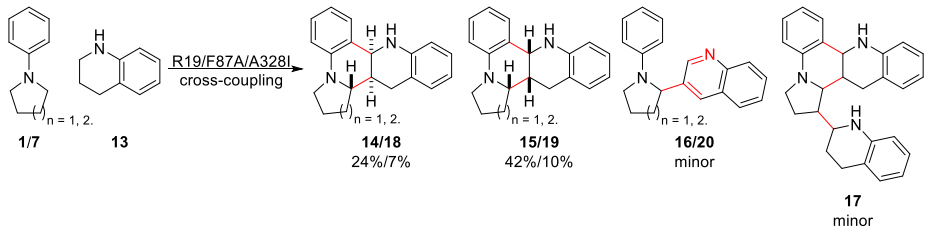


Figure 3.26 The R19/F87A/A328I-catalysed cross-coupling of **1**/**7** and **13**.

The substrate-binding titration based on the observation of spin-state shift was less informative to determine whether the enzymatic Povarov reaction occurred inside/outside the active site. However, the approach of linking two substrate molecules chemically, either by a flexible linear carbon chain of proper length or by a "soft" ring structure, might clear the confusion. Echoed with CYP121 catalysing the intramolecular C–C bond formation of cyclodityrosine,[510] if the enzyme yielding high proportion of Povarov dimers with **1** and **7** is also observed to produce the analogue of the Povarov dimers in the biotransformation of the newly synthesised substrate, the enzymatic Povarov reaction should occur inside the active site.

The β- and γ-alcohols were not observed in any of these reactions. Substrate-bound crystal structures of $P450_{BM3}$ and P450pyr should be obtained to provide reliable guide for further protein engineering. Structural overlay of the substrate-free P450pyr (the only available one so far) and $P450_{BM3}$ offered hints on how to evolve $P450_{BM3}$ towards this target. Introducing polar and bulky mutations (N/Q/Y/W/H/F/L/M) into the active site and disrupting the B'-helix and the F87 loop of $P450_{BM3}$ might be conducive. The trapping reactions can probably be diversified by shortening the gate-keeping F/G-helices and introducing charged amino acids at key residues, the latter of which might extend the lifetime of the enamine/iminium intermediates thence facilitating the trapping process.

Chapter 4 $P450_{BM3}$ oxidation of the fused-ring cyclic amines: Quinolines, tetrahydroquinolines and tetrahydroisoquinolines

4.1 Introduction

Scrutiny of some FDA-approved drugs in Chapter 3 which contain phenyl cyclic amines, shows that their fused-ring analogues are also common in amine drugs (Figure 4.1).

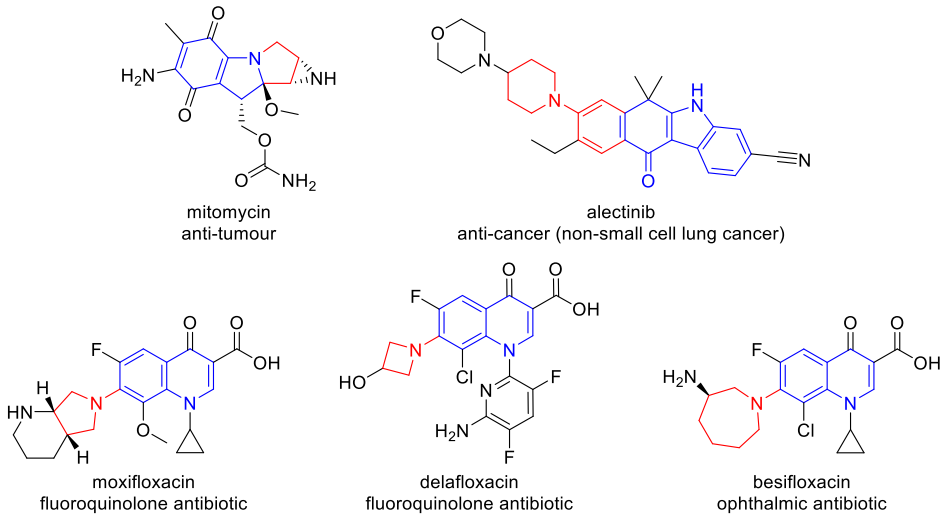


Figure 4.1 Examples of *N*-phenyl cyclic amine drugs which also contain fused-ring cyclic amine moieties.

A more detailed survey (Figure 4.2) shows that a benzene ring fused with pyrrolidine, pyrrole, piperidine, pyridine and azepane constitutes the scaffolds of numerous drugs and the linkages between different drug fragments, which are the moieties showing affinity towards drug targets. The pharmacological effects of these molecules cover a wide spectrum, including anti-cancer, anti-depression, anti-Alzheimer's, antihypertension, anti-Parkinsonism, antipsychotic, and antiviral (HIV and Hepatitis C) activities. Synthetic approaches to these derivatives of indole, isoindole, quinoline, isoquinoline, and 1-, 2- and 3-benzazepine derivatives normally utilise transition metal catalysts; some examples using Pd(II) are given in Figure 4.3; these either constructed the fused rings or directly functionalised the cores at the aromatic sites.[511–516]

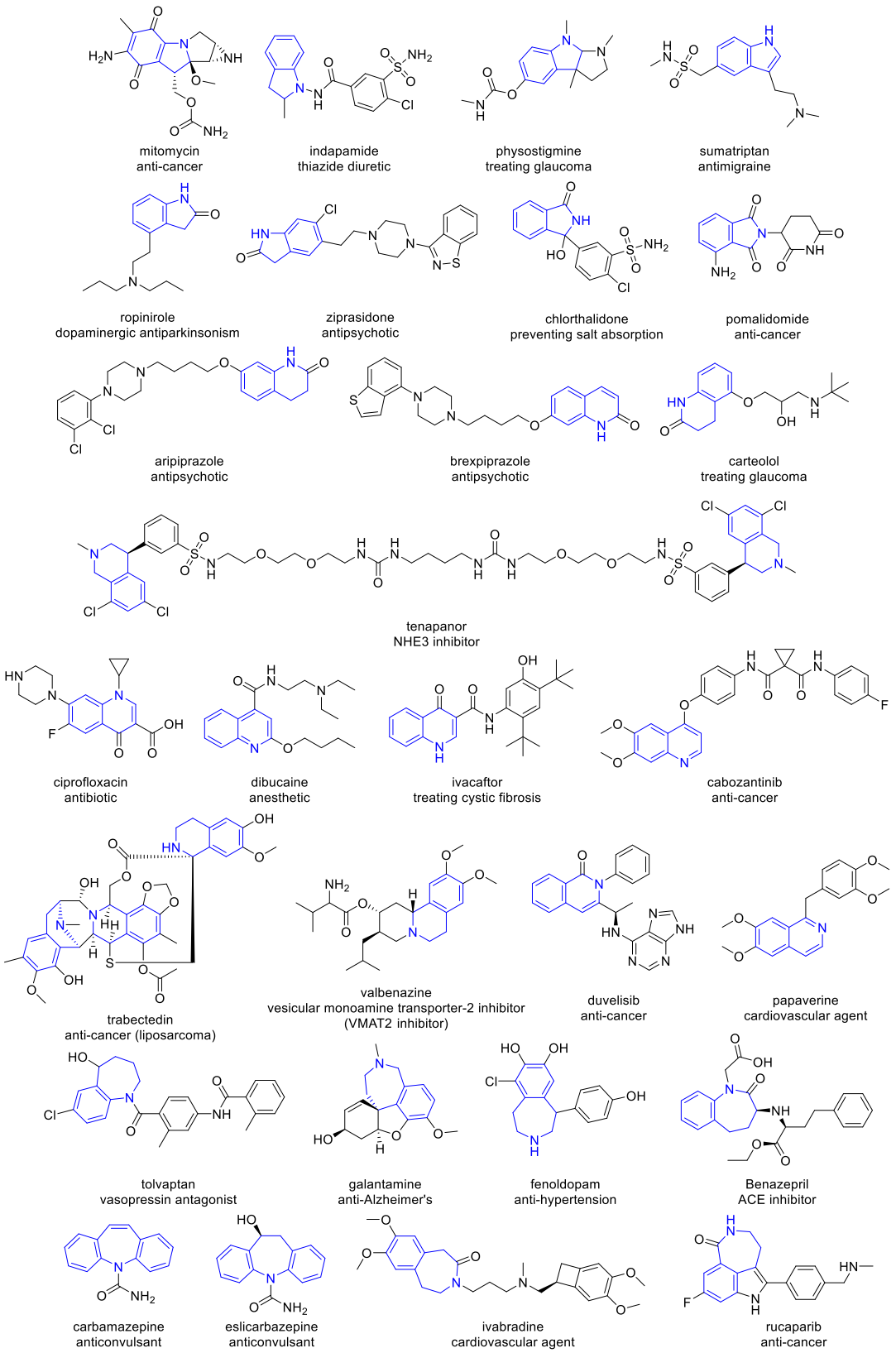


Figure 4.2 A selection of drug molecules with fused-amine-ring scaffolds.

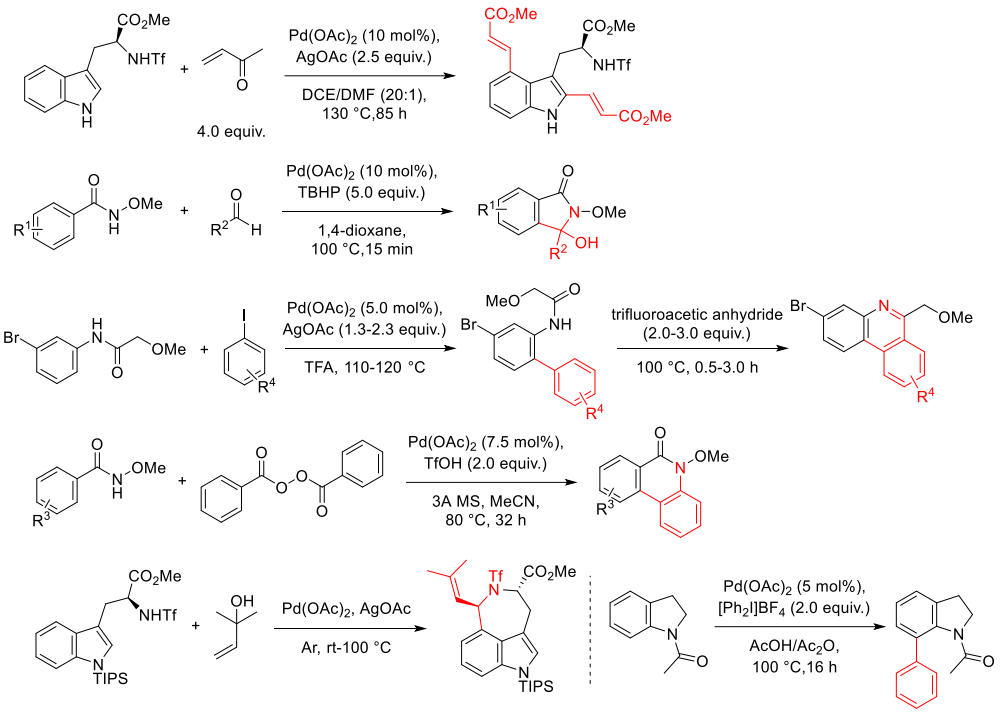


Figure 4.3 Examples of Pd(II)-catalysed fused-ring cyclic amine formation.[511–516]

Fused-ring five-membered and six-membered cyclic amine derivatives are synthesised by ring closure involving the formation of one, two and even three C–C bonds,[517] or via the hydrogenation of their heterocyclic aromatic counterparts[518] whose formation also rely on ring construction.[519] Each derivative would require a repeat of the synthesis route, with the attendant need to optimise conditions and potential issues with applicability of the reactions.

Direct oxidation of quinoline and tetrahydroquinoline derivatives has been reported. Zhang *et al.*[460] reported α-functionalisation of *N*-methyl-1,2,3,4-tetrahydroquinoline catalysed by the engineered carbene-transferase P411 in whole-cell reactions with reasonable turnover and enantioselectivity (Figure 4.4 A). Quinoline was oxidised by human CYPs to *N*-oxide, and 3-, 5-, 6- and 8-hydroxyquinolines (Figure 4.4 B).[435] Benzylic and C5 hydroxylation have been reported for the oxidation of 8-methylquinoline by the GVQ (A74G/F87V/L188Q) variant of $P450_{BM3}$ (Figure 4.4 C).[269] Human CYPs converted isoquinoline to its *N*-oxide (Figure 4.4 D).[436] P450cam formed both the *N*-oxide and 5-hydroxy derivatives with quinoline (Figure 4.4 B).[436] 1,2,3,4-Tetrahydroisoquinolines were

oxidised by rat liver microsomes to form C4-alcohols,[520] and by human liver microsomes to form the C1-alcohol and the corresponding iminium mainly (Figure 4.4 E).[521] Drug molecules of 1,2,3,4- and 5,6,7,8-tetrahydroisoquinoline cores, which are capable of treating Parkinson's disease and hypertension, were generally reported to be inhibitory of CYP enzymes including 1A2, 2D6, 2C9, 2C19, 3A4 and 11B1.[522,523]

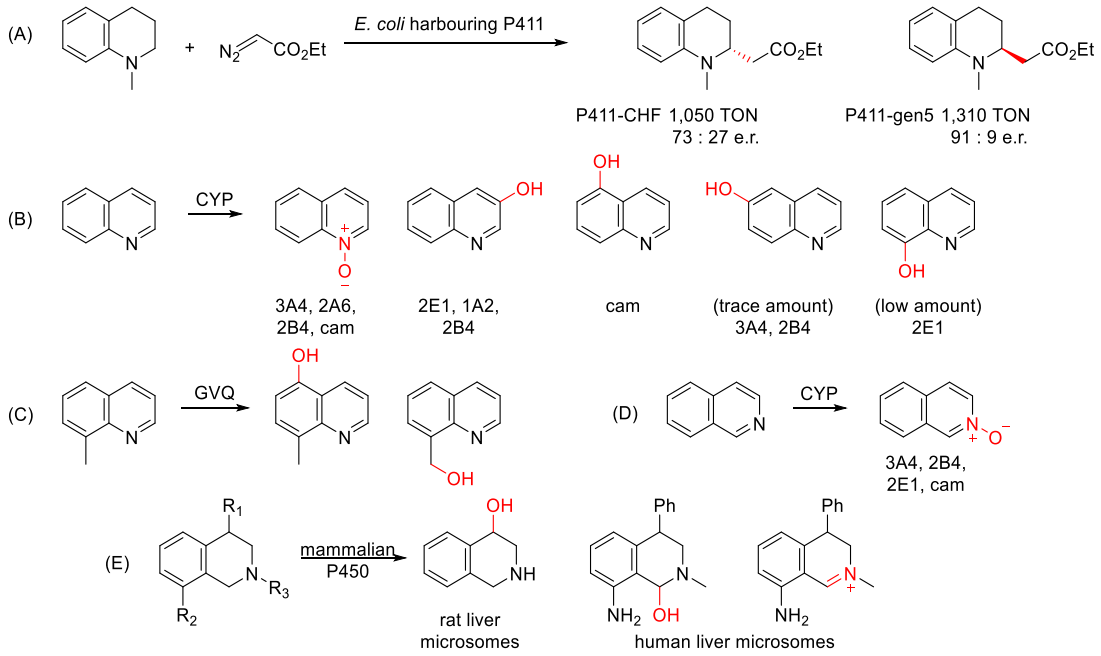


Figure 4.4 Previous research on P450 oxidation of quinoline and isoquinoline derivatives.[269,435,436,460,520,521]

In this chapter, the compounds quinoline (Q), 1,2,3,4-tetrahydroquinoline (THQ), 5,6,7,8-tetrahydroquinoline (THQ'), 1,2,3,4-tetrahydroisoquinoline (THIQ), 5,6,7,8-tetrahydro-isoquinoline (THIQ') and 5,6,7,8-tetrahydroquinoxaline (THQX) were studied for their oxidation by $P450_{BM3}$ (Figure 4.5). The oxidation of THQ, 3,4-dihydro-2-quinolinone and Q by $P450_{BM3}$ demonstrated in this chapter has been published.[274]

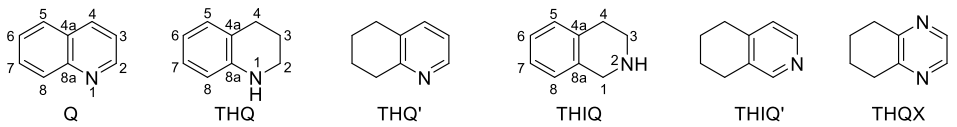


Figure 4.5 Fused-ring substrates tested in this chapter.

4.2 Oxidation of 1,2,3,4-tetrahydroquinoline (THQ)

4.2.1 The initial screening of THQ

Screening scale reactions for an initial library of 48 variants (the WY3/4 plates, Appendix 3.5) were carried out in 24-well plates for 16 h at 20 ºC, shaking at 120 rpm. Products were isolated from preparative scale reactions (20–100 mg) by silica gel column chromatography and characterised by NMR and MS data in consistent with literature (Appendix 4.2).[274,524–528] The variant library oxidised THQ (**13**) to a mixture of products (Figure 4.6), including 6-hydroxy-THQ (**21**), the aromatisation product quinoline (**22**), 3-hydroxy-quinoline (**23**), and 3,4-dihydro-2-quinolinone (**24**); in addition, the dimer **25**, and trace amount of the trimer **26** were observed. After a prolonged incubation of 8 h, the THQ derivative **21** was fully converted by most of the variants to the aromatised product, 6-quinolinol (**27**, Figure 4.7). The dimer **25** was further oxidised to **28**–**31** by R19/F87A/A328I.

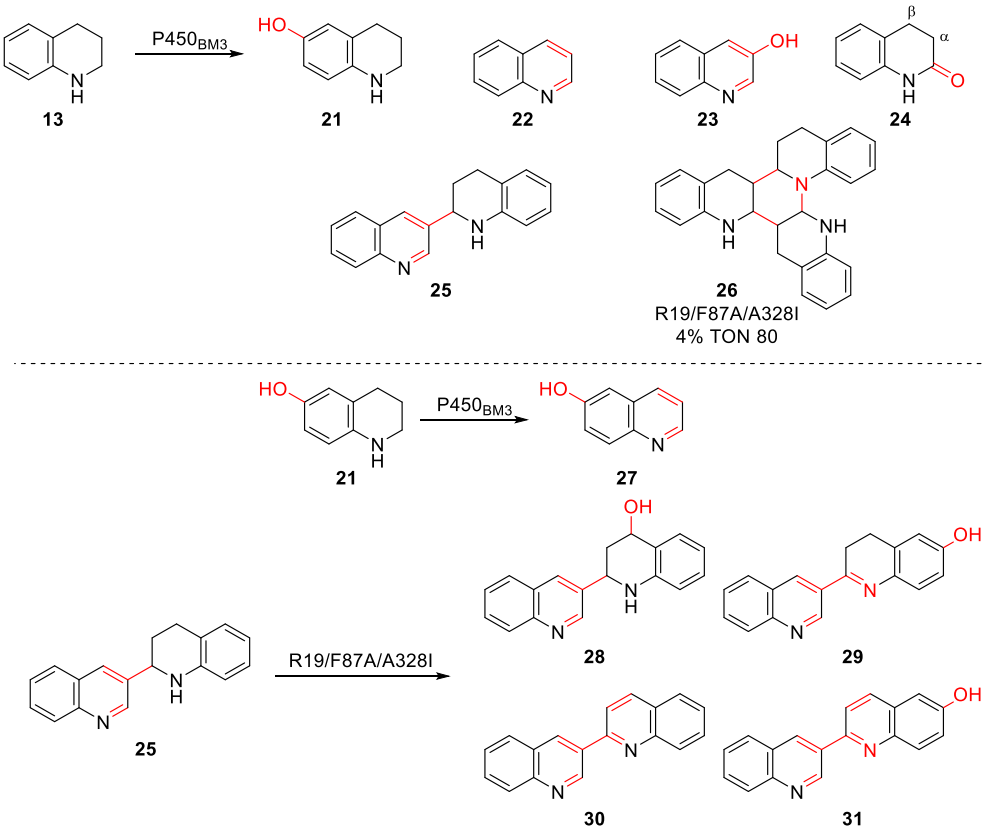


Figure 4.6 The reaction scheme of $P450_{BM3}$ oxidation of THQ (**13**).

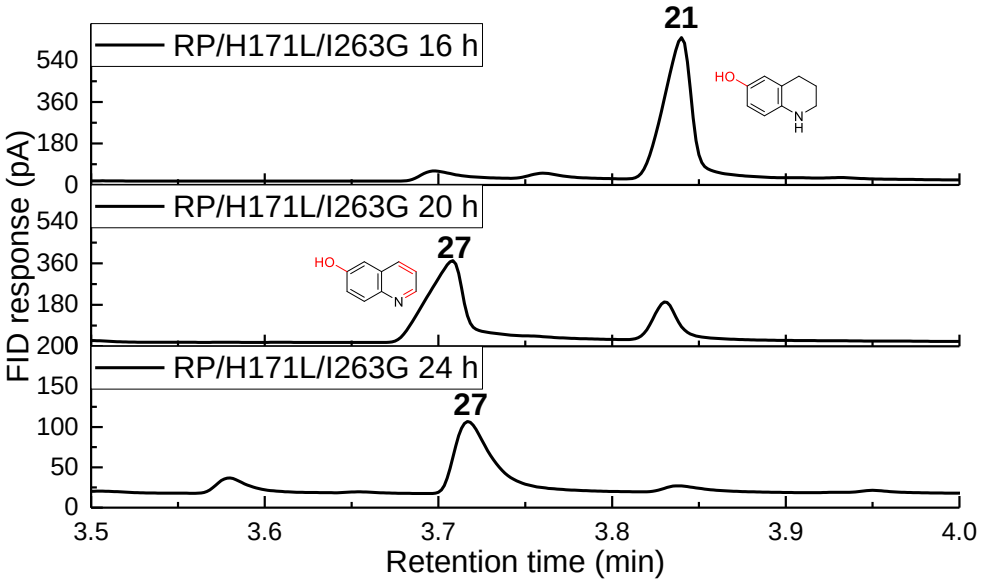


Figure 4.7 Time-course monitoring of the RP/H171L/I263G-catalysed reaction oxidising 6-hydroxy-THQ, **21**, to afford 6-hydroxyquinoline, **27**.

The mass of the trimer (**26**, 4% yield, TON 80) was shown as [$3M_{13}$ – 6], with five CH and four CH_2 signals identified in the HSQC spectrum (Spectrum 50, Appendix 4.2). The linkage of the C11–C12–C13–C14–C8–N7 ring of **26** was tracked by the coupling pattern in the COSY spectrum from the characteristic doublet at δ 5.72 (H11, Figure 4.8).

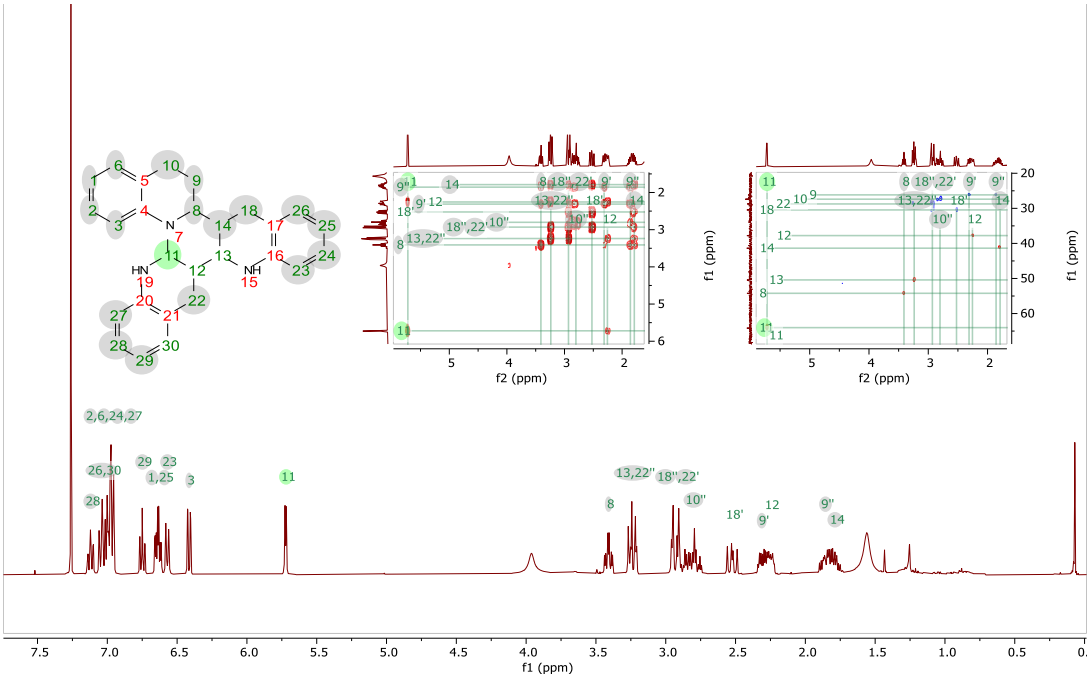


Figure 4.8 The ^{1}H NMR spectrum of **26** with snapshots of the its COSY and HSQC NMR spectra.

The NMR spectra of the mixture of **29** and **31**, and of pure **31** itself were used for identifying **29** and **31**. Their ^{1}H NMR overlay (Figure 4.9 b) distinguished the signals for **29** and **31** (Figure 4.9 c & a). The mass of **29** was [2M$_{13}$ + 8] (mass of **25** + O – 2H), and the only two CH_2 signals at δ 2.90 and 3.00 were in the aliphatic region (Figure 4.9 c). The coupling pattern of three aromatic CH peaks at δ 7.30 (d, *J* = 8.4 Hz), 6.72 (dd, *J* = 8.4, 2.8 Hz) and 6.66 (d, *J* = 2.8 Hz) suggested that C19 was hydroxylated. The other two hydrogens were hence absent from C11 and N12 of **29**, compared to **25**. The mass of **31** was [2M$_{13}$ + 6] (mass of **29** – 2H); no aliphatic hydrogens remained (Figure 4.9 a), and the C19-substituted coupling pattern shifted to lower field showing peaks at δ 8.04 (d, *J* = 9.1 Hz), 7.39 (dd, *J* = 9.1, 2.7 Hz), 7.19 (d, *J* = 2.7 Hz). This revealed that the imine moiety in **29** was fully aromatised to **31**.

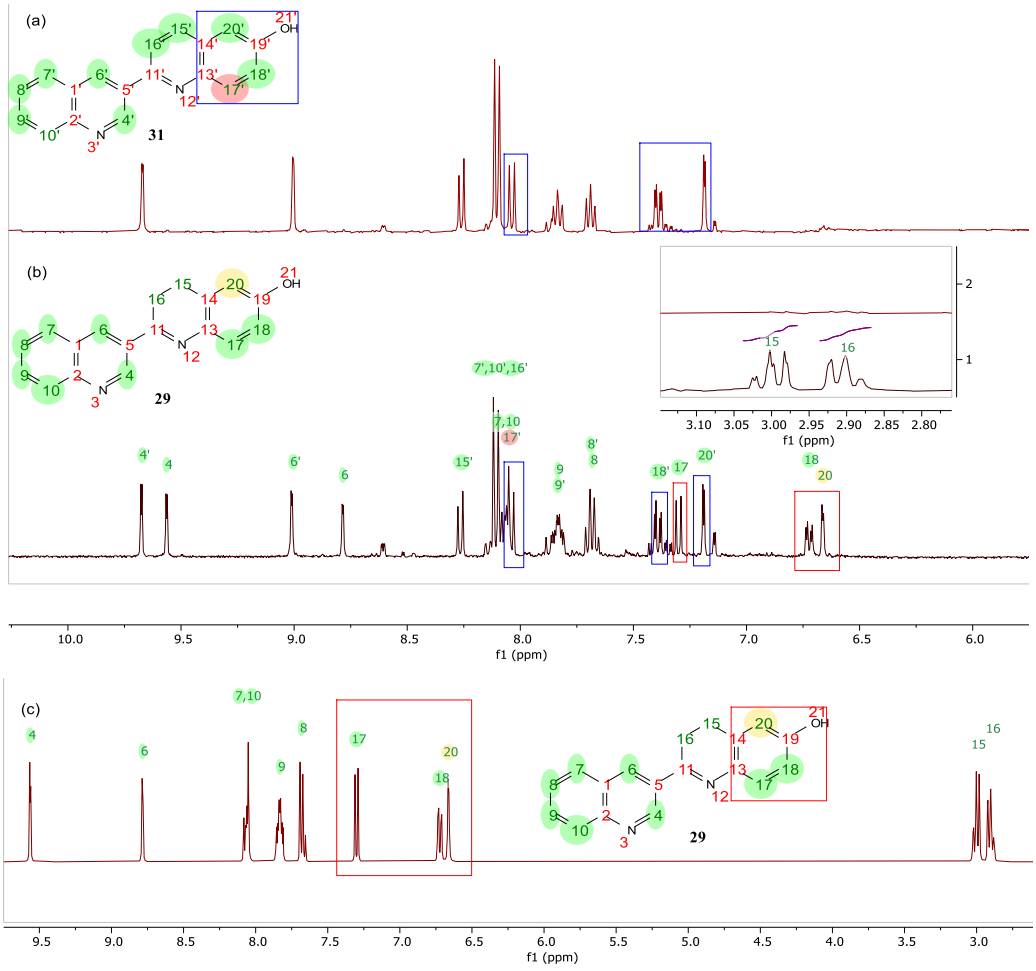


Figure 4.9 The ^{1}H NMR spectra of (a) **31**, (b) **29** and **31**, and (c) **29** (subtracted spectrum).

4.2.2 The mechanisms involved in P450$_{BM3}$ oxidation of THQ

Mechanistically, formation of 6-hydroxy-THQ **21** is consistent with an NIH shift whereby the initially formed 5,6-arene oxide undergoes ring-opening to form the C5 carbocation preferentially because of stabilisation by the nitrogen lone pair (Figure 4.10).

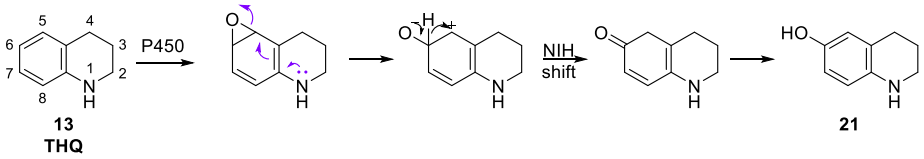


Figure 4.10 The proposed mechanism of the formation of **21**.

3,4-Dihydroquinolin-2-one (**24**) is formed by C2 oxidation to the alcohol and then the ketone (Figure 4.11). The formation of **23** is initialised by C2 oxidation of **13** rather than further oxidation of quinoline **22**, because the oxidation of **22** by the same variant gave no **23**. In the proposed mechanism in Figure 4.11, the C2 hydroxylation of THQ by P450 forms the carbinolamine, which readily generates the imine/iminium/enamine intermediates by losing hydroxy ion or dehydration. The H3 of the imine is abstracted by Compound I to form the allylic radical and Compound II. The hydroxy radical offered by Compound II can thus rebound either with one H4 (in blue) to form a water molecule leaving the rest of the imine radical aromatised via intramolecular radical rebound to form **22**, or with the imine radical to form the allylic alcohol (in red). Another H3 of the allylic alcohol is abstracted by Compound I to form the hydroxyalkyl radical and Compound II, which abstracts the C4-hydrogen aromatising to form **23**. Three cycles of oxidation by P450 are implicated in the formation of **23** from **13**, even though multi-cycles of oxidation by P450 was more commonly observed for hydrophobic substrates, *e.g.* the demethylation of steroids by CYP51.[529]

For the dimerisation process, the iminium and the enamine intermediates interact with each other by a nucleophilic attack to yield the dimeric imine, whose imine moiety is further

aromatised by P450 to form **25**. The THQ moiety of **25** can be then activated at the C4, C2 and C5,C6 positions to form **28**–**31**. The observation of **29** and **31**, in contrast with the fact that **30** was an inert substrate to P450, revealed useful insights for the aromatisation process catalysed by P450, confirming the imine to be the intermediate. For trimer formation, one imine and two enamine intermediates cyclise via stepwise self-condensation[530] to form **26**.

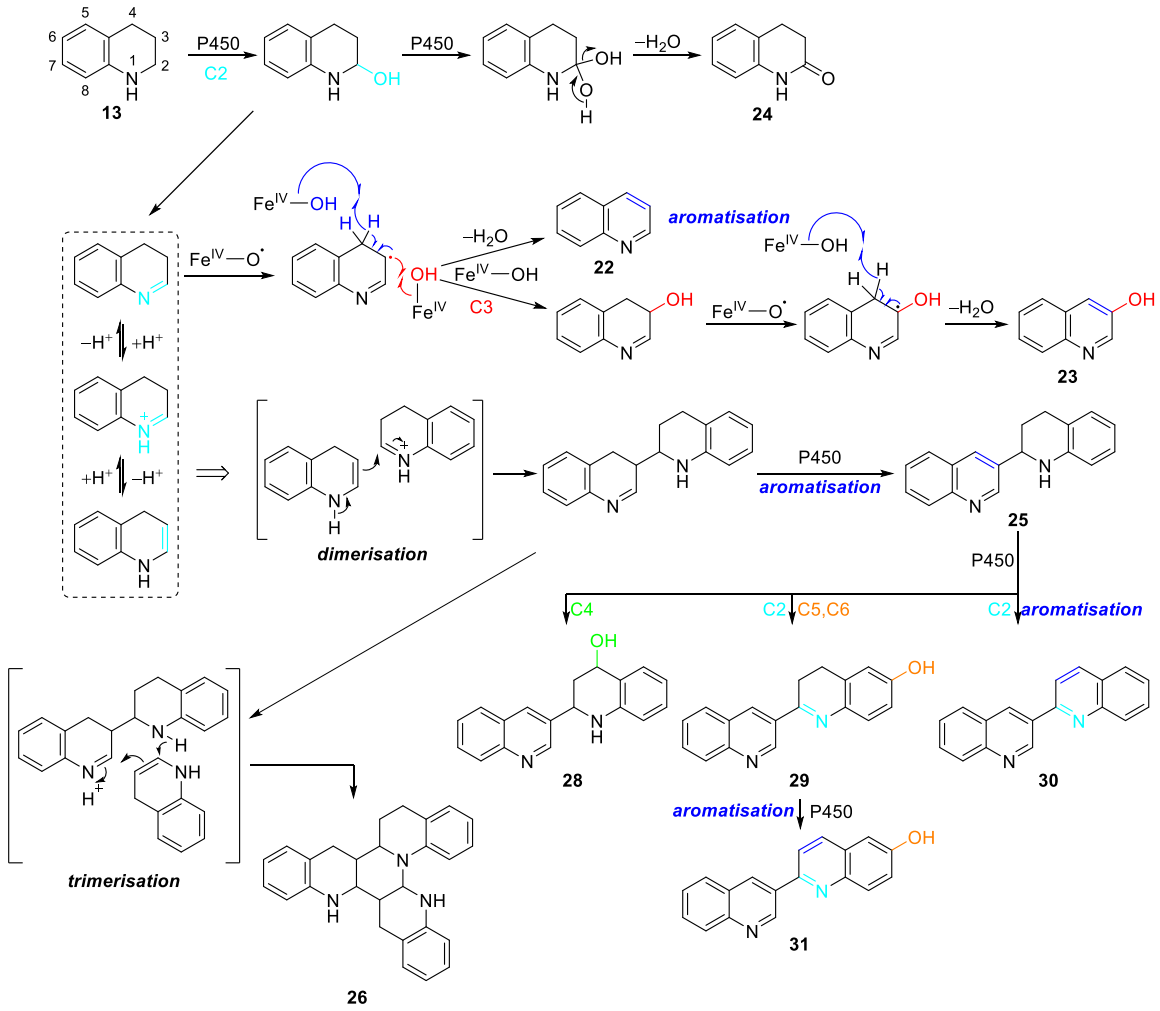


Figure 4.11 The proposed mechanisms of the C2 oxidation of THQ by $P450_{BM3}$.

In sum, the $P450_{BM3}$ variant library oxidised the THQ core at C2 showing aromatisation, dimerisation and trimerisation activities, and at C5,C6 to give 6-hydroxy-THQ derivatives. The oxidation of the dimer **25** also occurred at C4 of its THQ moiety. No direct C3 (β) hydroxylation was observed, nor C7,C8 oxidation.

4.2.3 Selectivity trends in the oxidation of THQ

Within the screening library, 30 out of 48 variants (WY3/4 plates, Appendix 3.5) gave ≥50% conversion of **13** while the wild type enzyme showed negligible activity. Of the products (Table 4.1 and Figure 4.12), the 2nd generation variant R19/I263G/A328L gave the highest proportion of the 6-phenol **21** (79%, TON 1,390), which was then fully converted to the aromatised 6-quinolinol (**27)** after 8 h incubation. The variant RP/V78F/F87V/E267V in the TFA/TFB plates gave the most of quinoline **22** (94%, TON 1,730). The highest proportion of **23** (14%, TON 260) was given by R19/F87A/A328I. RP/V78I/E267V produced the highest amount of **24** (20%, TON 350), and R19/F87A yielded the most of the dimer **25** (60%, TON 1,160).

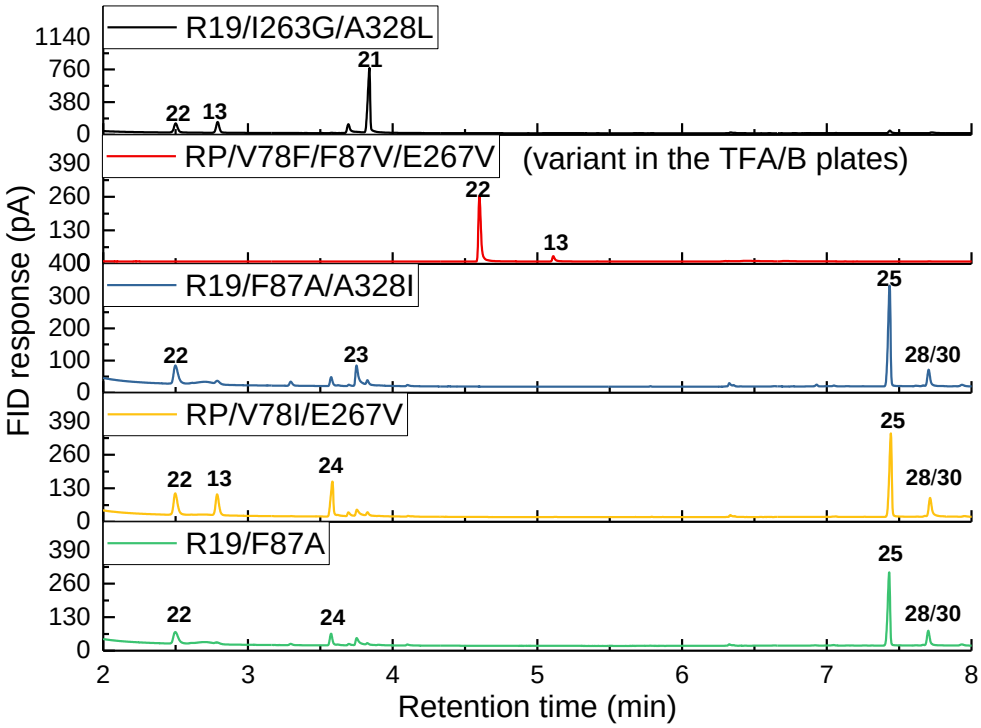
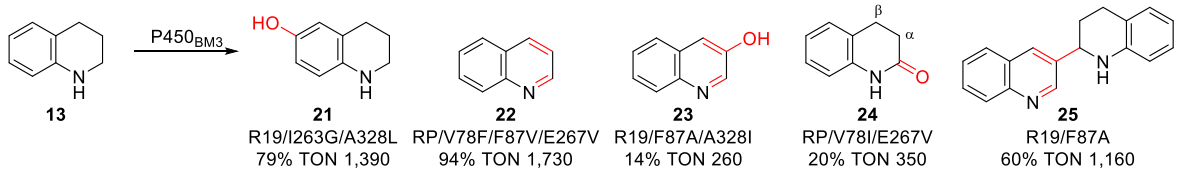


Figure 4.12 GC traces of the screening reactions using the variants in the TFA/B and WY3/4 plates showing highest selectivity for **21**–**25**.

The mutations F87A, A184I and A328I/V/L promoted the conversion dramatically with R19/A184I/A328L and R19/F87A/A328I showing 99% conversion (TON 1,980, Table 4.1). The addition of A328L to GVQ/I263G promoted the formation of **21** from nil to 48%

selectivity. The unmutated F87 also maintained reasonable selectivity for C5,C6 oxidation at 40% (TON 420 given by R19), due to its bulkier size. For C2 oxidation, F87A and F87V were necessary. It was also noted that these two mutations favoured C2(α) oxidation of all the tested cyclic amine and lactam substrates in this thesis, since they opened up the active site of $P450_{BM3}$ and the increased substrate mobility tended to expose the most activated position to the ferryl oxygen of Compound I. V78F, F87V and E267V enhanced the aromatisation selectivity; the mutations F87A and A328I/F slightly improved the formation of **23**; lactam formation was improved by F87V and A184I; dimerisation was favoured by F87A, A184I and I263G (Table 4.1).

Table 4.1 The conversion and product distributions of $P450_{BM3}$ oxidation of THQ (**13**).



Plates	Mutant name	Conversion	Selectivity				
			21	**22**	**23**	**24**	**25**
WY3/4	WT	10%	31%	47%	5%	13%	3%
	GVQ	3%	–	82%	–	–	18%
	GV/A184I	**91%**	11%	16%	5%	**15%**	**53%**
	GVQ/I263G	12%	–	69%	–	–	**31%**
	GVQ/I263G/A328L	**62%**	**48%**	12%	3%	3%	35%
	R19	52%	**40%**	18%	3%	8%	31%
	R19/F87A	**97%**	4%	17%	8%	10%	**60%**
	R19/F87A/A328I	**99%**	6%	16%	**13%**	4%	58%
	R19/F87A/A328F	**94%**	11%	19%	**12%**	5%	51%
	R19/A184I/A328L	**99%**	39%	12%	1%	–	47%
	K19/F87V	69%	12%	18%	4%	**18%**	48%
	K19/F87V/A328V	**89%**	25%	13%	3%	4%	54%
TFA/B	RP	93%	59%	**10%**	–	–	31%
	RP/F87V	100%	–	**31%**	–	–	49%
	RP/E267V	85%	6%	**43%**	–	–	25%
	RP/F87V/E267V	100%	–	**56%**	–	–	44%
	RP/V78F/F87V/E267V	92%	–	**94%**	–	–	6%

4.2.4 Engineering the selectivity of THQ oxidation

As A328L and unmutated F87 showed enhancing effect for C5,C6 oxidation, A328L was introduced to RP/H171L/I263G and R19 whose 87F remained (Table 4.2). The 2nd generation variant RP/H171L/I263G/A328L raised the selectivity to 84% of **21** (TON 1,680), and R19/A328L also showed improvement. The 2nd generation variant R19/I263G itself gave 85% of **21** (TON 1,700). These showed that both the single mutations I263G and A328L and the combination I263G/A328L favoured C5,C6 oxidation when F87 was maintained. For the base variant R19/F87A, addition of A328L or I263G individually showed no improvement; only the combination I263G/A328L increased the selectivity of **21** by 24%, showing that the I263G/A328L combination favoured C5,C6 oxidation regardless of the size of the 87 residue.

Table 4.2 Engineering of the C5,C6 oxidation product, **21**, and the C2,C3 oxidation product, **23**.

Mutant	**conv.**	**21**	**22**	**23**	**24**	**25**
R19	52%	40%	18%	3%	8%	31%
R19/A328L*	100%	60%	13%	–	–	26%
R19/I263G*	100%	**85%**	4%	–	–	12%
R19/I263G/A328L*	88%	79%	14%	3%	–	4%
RP/H171L	93%	33%	54%	–	1%	10%
RP/H171L/I263G	97%	54%	9%	6%	1%	31%
RP/H171L/I263G/A328L*	100%	**84%**	10%	0%	–	6%
R19/F87A/A328L	100%	6%	12%	3%	5%	62%
R19/F87A/I263G	100%	5%	46%	3%	4%	31%
R19/F87A/I263G/A328L*	100%	**28%**	40%	**6%**	–	23%
GVQ/I263G/A328F*	83%	7%	19%	34%	–	41%
GLQ/I263G (F87L)*	19%	7%	62%	0%	**13%**	19%
GLQ/I263G/A328L*	22%	–	26%	**58%**	–	16%
GLQ/I263G/A328F*	20%	–	23%	**61%**	–	16%

*: 2nd generation variant.

For C2 oxidation of THQ, the selectivity for aromatisation (**22**) and dimerisation (**25**) has already reached excellent levels. The engineering work focused on the promotion of 3-

quinolinol **23** and the lactam **24**. The substrate was screened against the 2nd generation library based on GVQ/I263G with the F87 and A328 residues mutated to nonpolar amino acids (A/V/I/L/F, developed by Yang Cao and Nelson Kondia-Yema), since F87A and A328I/F favoured **23** and F87V promoted **24**. The base variant GVQ/I263G/A328L gave 3% selectivity for both **23** and **24**. The 2nd generation variant GVQ/I263G/A328F lifted the selectivity of **23** from 3% to 34% (TON from 40 to 560, Table 4.2), and the GLQ/I263G/A328F (L: F87L) improved it to 61%, though with low conversion. GLQ/I263G/A328L also gave 58% of **23**. GLQ/I263G slightly increased the selectivity of **24** from nil given by GVQ/I263G to 13% (Table 4.2).

4.2.5 Scalability and time-course of biotransformation of THQ

The scalability of biotransformation of THQ (**13**) was also explored using the variants RP/H171L/I263G, R19/F87A/A328L, and R1/I263G (R1 = R47L/Y51F/H171L). The reaction could be carried out at 100 mL scale in shake flasks, without active aeration, agitation or pH control, and afforded 62% yield of the products from 20 mM substrate with 1 μM of the R1/I263G variant (164 mg products purified out of 266 mg substrate, TON 12,300). The 1 h incubation with R19/F87A/A328L at the titre of 2.3 mM substrate : 1 μM enzyme reached total conversion (TON 2,300, Figure 4.14), and the 18-hour incubation consumed all substrate at the titre of 10 mM substrate : 1 μM enzyme by sequential addition of 2 mM substrate over 10 hours (TON 10,000, 1.76 g/L/day, Figure 4.13). One-off addition of 20 mM substrate with the same variant gave full conversion after 6-day incubation (TON 20,000, 0.44 g/L/day, Figure 4.13). Whole-cell reactions were attempted with RP/H171L/I263G at similar scale and reacting condition offering TON >5,000 with retarded further oxidation (Figure 4.13).

As the prolonged incubation of THQ with R19/F87A/A328I offered further oxidation products **28**–**31** from **25**, the oxidation of this bulkier substrate **25** itself (THQ-Q dimer,

MW 260.13) with R19/F87A/A328I was monitored over 4 days at the titre of 0.5 mM substrate : 1 μM enzyme, reaching >50% conversion after 4 days (TON >250, >0.016 g/L/day, Figure 4.14). The dimers **29** and **31** were not GC-detectable, creating issues for data analysis. Nevertheless, the biotransformation of **25** was much slower than that of THQ. Therefore, the screening reactions of THQ (**13**) extracted within the time window of 8–16 h incubation at 2 mM of **13** could minimise the oxidation of **25** and guarantee the accuracy of the screening data analysis.

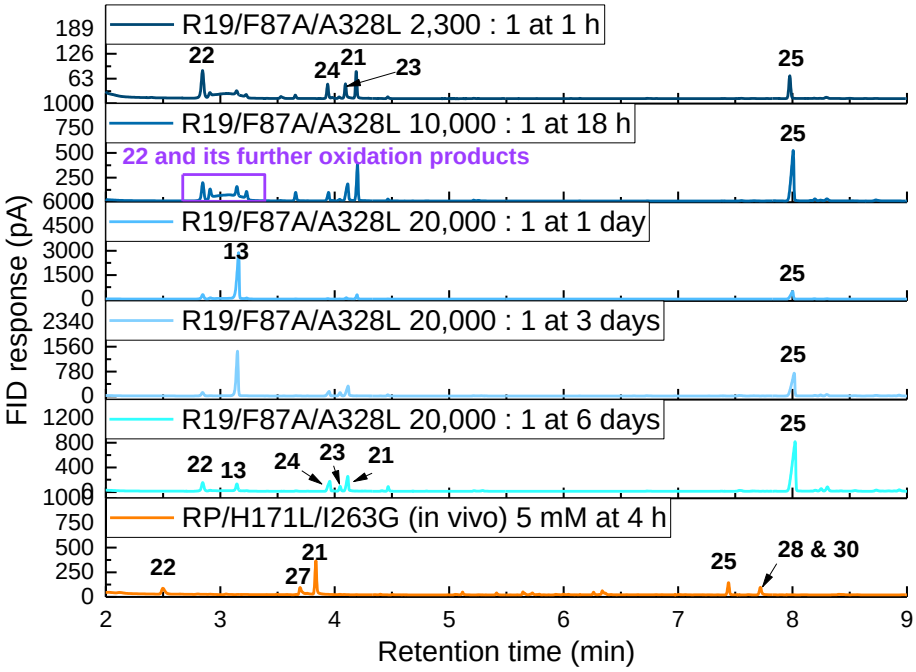


Figure 4.13 GC analysis of time-course monitoring the reactions with R19/F87A/A328L at 2.3 mM, 10 mM and 20 mM of **1**, and with RP/H171L/I263G at 5 mM of **1**; all with 1 μM $P450_{BM3}$.

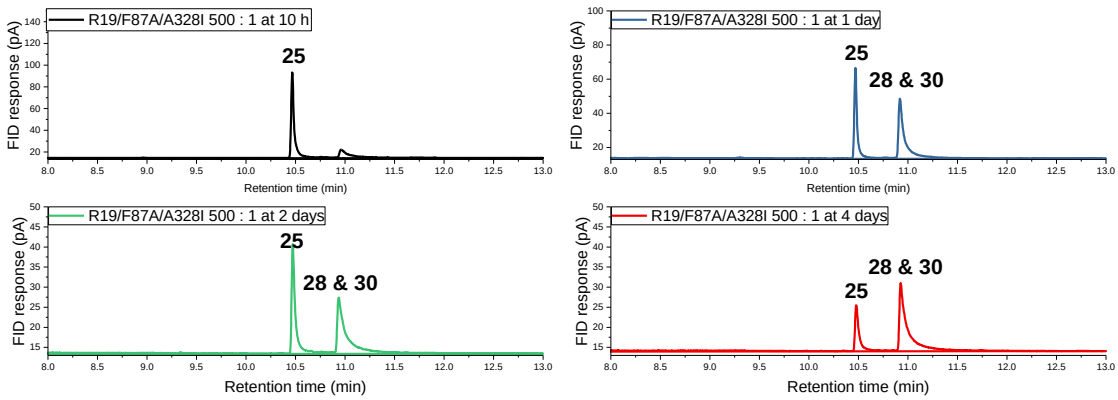
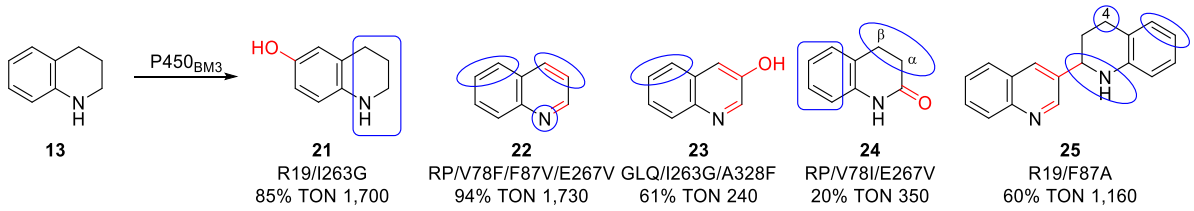


Figure 4.14 The time-course of the biotransformation of **25** by the R19/F87A/A328I variant.

4.2.6 Summary

The oxidation of THQ gave products from C2 and C5,C6 oxidation, both showing high selectivity. The unmutated F87 and the combination of I263G/A328L favoured C5,C6 oxidation, whilst F87A/V/L promoted C2 oxidation. No direct oxidation at C3,C4 or C7,C8 was observed. After initial C2 oxidation to the carbinolamine, aromatisation, stepwise C2,C3 oxidation, lactam formation and dimerisation were observed and engineered to ≥60% selectivity of **22**, **23** and **25**. The effect of mutations on THQ oxidation selectivity are summarised in Table 4.3. Control of reaction time is important for suppressing further oxidation of all the products, which can also be achieved by *in vivo* reactions.

Table 4.3 Summary of mutation effects promoting $P450_{BM3}$ oxidation of THQ (**13**). Further oxidation labelled in blue.



conversion	C2 oxidation				C5,C6 oxidation
	aromatisation	C2,C3 oxidation (23)	lactam	dimerisation	
F87A A184I A328V/I/L	V78F F87V E267V	F87A/L A328I/F/L	F87V/L A184I	F87A A184I I263G	F87-unmutated I263G/A328L

4.3 Oxidation of 3,4-dihydro-2-quinolinone

Similar to THQ (**13**), the lone pair on the nitrogen atom of 3,4-dihydro-2-quinolinone, **24**, is delocalised, in particular with the carbonyl group. Moreover, in THQ oxidation screening, reactions yielding **24** in prolonged incubation showed more products (Figure 4.15).

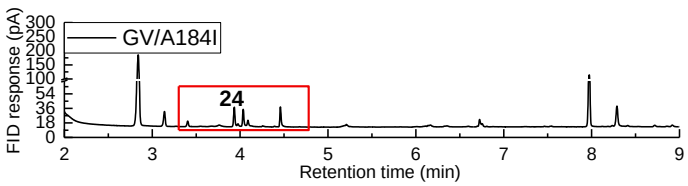


Figure 4.15 GC analysis of THQ oxidation with peaks in monomer oxidation window by GV/A184I.

These suggested the lactam **24** was probably oxidised by the P450$_{BM3}$ variants. Therefore, pure **24** was screened against the 48 variant library (WY3/4, Appendix 3.6) at the titre of 2 mM of **24** : 1 μM of enzyme. Hydroxylation at the α-position to the carbonyl group (**32**), desaturation of the Cα–Cβ bond (**33**), benzylic oxidation (**34**), C5,C6 oxidation (**35**), and C7,C8 oxidation (**36**) were observed (Table 4.4). Therefore, all C–H/C=C bonds in **24** were herein activated.

The Cα–Cβ desaturation reaction can be initialised at either C3–H or C4–H via HAT to form the radical, which is rapidly captured by Compound II for electron transfer and deprotonation or another HAT to form a water molecule and the alkene product **33** directly (Figure 4.16).[531]

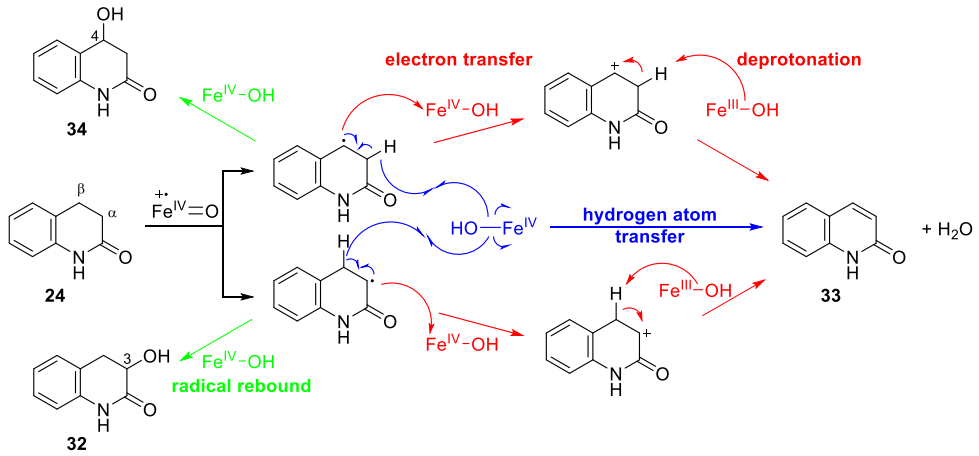
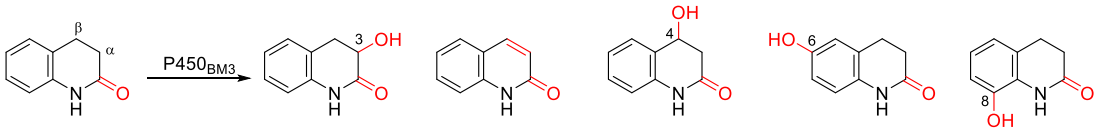


Figure 4.16 The proposed mechanism of Cα–Cβ desaturation, C3/C4 hydroxylation of **24** by P450$_{BM3}$.[531]

The conversion and TON showed that **24** was less active than **13**, for which the low solubility of **24** might be a key factor. The wild type enzyme was not active for **24** at all. The screening results in Table 4.4 showed that the mutations V78I, A82M, F87A and I263G improved the conversion, and the RP/H171L/I263G was the only variant giving >50% conversion (66%, TON 1,320). As for the lactam moiety, C3 hydroxylation was slightly improved by the A82W and I263G/A mutations, and C4 hydroxylation was favoured by V78I and A330P. The mutation F87A favoured Cα–Cβ desaturation, *e.g.*, R19/F87A

showed 63% of **33** compared to 25% given by R19. For aromatic oxidation, the combination of I263G/A328L gave 100% selectivity for C5,C6 oxidation, and the residues S72 and V78 in the B'-helix and A330 steered the oxidation towards C7,C8 oxidation.

Table 4.4 Conversion and product distribution of $P450_{BM3}$ oxidation of 3,4-dihydro-2-quinolinone (**24**).



24 | **32** RP/H171L/I263G 6% TON 80 | **33** R19/F87A/A328I 65% TON 530 | **34** RT2/V78I/A184I/A330P 76% TON 670 | **35** R19/I263G/A328L 100% TON 520 | **36** KU3/A330P 25% TON 210

Mutant	**conv.**	**32**	**33**	**34**	**35**	**36**
K19/A82M/F87A	44%	–	52%	48%	–	–
RP/A82W/I263A	6%	15%	36%	49%	–	–
RP/A82M/I263A	32%	9%	22%	39%	30%	–
RP/H171L/I263G	**66%**	**6%**	19%	27%	48%	–
RP/F87V	11%	–	56%	44%	–	–
RP/V78I/F87V	30%	–	31%	53%	6%	10%
R19	18%	–	25%	37%	16%	23%
R19/F87A	34%	–	63%	37%	–	0%
R19/F87A/A328I	41%	–	**65%**	35%	–	0%
R19/I263G/A328L	26%	–	–	–	**100%**	–
KU3/A330P	42%	–	13%	60%	2%	**25%**
RT2/V78I/A184I/A330P	44%	–	15%	**76%**	2%	7%
RT2/S72W/A330W	12%	–	33%	54%	–	13%
RT2/A330W	7%	–	11%	36%	15%	38%
RT2/S72R/A330W*	1%	–	25%	30%	4%	40%
RT2/S72L/A330W*	1%	–	27%	29%	–	44%
RT2/S72W/A330W	12%	–	33%	54%	–	13%
RT2/S72H/A330W*	70%	–	6%	38%	6%	**50%**
RT2/S72Y/A330W*	66%	–	9%	44%	7%	39%
RT2/S72V/A330W*	7%	–	14%	38%	25%	22%

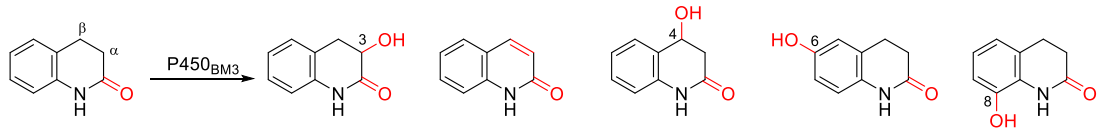
*: 2nd generation variant.

The highest selectivity for **33**–**35** exceeded 60% and were not targeted for protein engineering. Attempts to improve the yield of **32** were fruitless, perhaps due to fast trapping of the C3 radical during the desaturation process. On the basis of the observed selectivity trends, the residue S72 was selected to engineer C7,C8 oxidation based on RT2/A330W

(Table 4.4). The amino acids R, L, H, Y and V were introduced at S72, and RT2/S72H/A330W improved the selectivity of **36** to 50%, TON 700.

In summary, the lactam **24**, whose nitrogen is more sp^2 hybridised than in THQ, showed modest conversion. Nonetheless, all C–H and C=C double bonds were activated. The mutation effects are summarised in Table 4.5. The greater product diversity for **24** compared to THQ, **13**, suggested that the NH group in THQ might be involved in restricting substrate binding within the active site, and/or the lactam carbonyl group led to different binding orientations.

Table 4.5 Summary of mutation effects promoting $P450_{BM3}$ oxidation of 3,4-dihydro-2-quinolinone (**24**).



24 | **32** RP/H171L/I263G 6% TON 80 | **33** R19/F87A/A328I 65% TON 530 | **34** RT2/V78I/A184I/A330P 76% TON 670 | **35** R19/I263G/A328L 100% TON 520 | **36** RT2/S72H/A330W 50% TON 700

conversion	C3	C4	Cα–Cβ desaturation	C5,C6	C7,C8
V78I A82M F87A I263G	A82W I263G/A	V78I A330P	F87A	I263G/A328L	S72H/Y V78I A330W/P

4.4 Oxidation of 5,6,7,8-tetrahydroquinoline (THQ'), 5,6,7,8-tetrahydro-isoquinoline (THIQ'), 5,6,7,8-tetrahydro-quinoxaline (THQX) and 1,2,3,4-tetrahydroisoquinoline (THIQ)

The pyridine and pyrazine derivatives THQ' (**38**), THIQ' (**42**) and THQX (**45**) containing sp^2 nitrogen atoms, and THIQ (**37**) whose nitrogen is sp^3 hybridised, were screened against the 48 variant library (WY7/8) at the titre of 2 mM substrate : 1 μM enzyme. Unlike the rat liver microsomes showing C4-hydroxylation,[520] THIQ (**37**) was not oxidised by this $P450_{BM3}$ variant library, similar to *N*-Bn-cyclic amines whose nitrogen atoms are also sp^3 hybridised (Figure 4.17). The sp^2-N containing **38**, **42** and **45** were all oxidised by the

variant library at the benzylic positions (C5/C8, Figure 4.17). NMR and MS of the products matched literature data.[532–537]

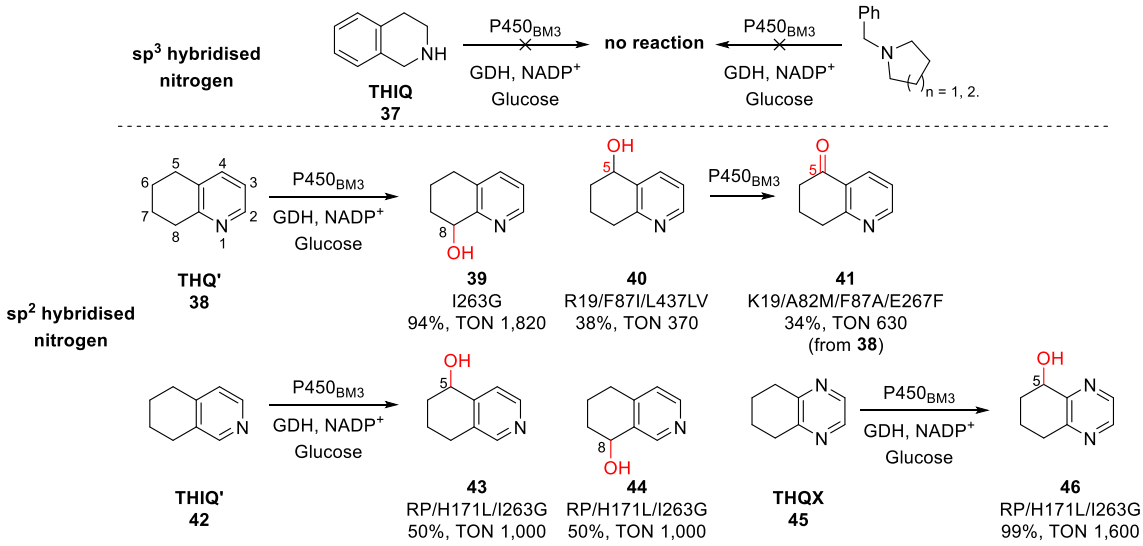


Figure 4.17 Reaction schemes of $P450_{BM3}$ oxidation of THIQ (**37**), THQ' (**38**), THIQ' (**42**), and THQX (**45**).

Table 4.6 The conversion and product distribution of $P450_{BM3}$ oxidation of THQ', THIQ', and THQX.

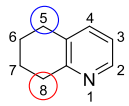
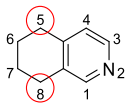
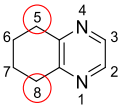
Mutant	**THQ' (38)**					**THIQ' (42)**		**THQX (45)**	
	Conv.	**39**	**40**	**41**	***40 & 41***	**Conv.**	**43 & 44**	**Conv.**	**46**
WT	10%	92%	8%	–	*8%*	–	–	3%	100%
I263G	**97%**	94%	2%	4%	*6%*	–	–	12%	100%
RP/H171L/I263G	**95%**	76%	–	19%	*19%*	**100%**	100%	**80%**	99%
RP/I263A/E267V	**100%**	93%	3%	2%	*4%*	**72%**	100%	**66%**	100%
RP/F87V	3%	81%	19%	0%	*19%*	1%	100%	7%	92%
RP/V78I/F87V	**99%**	91%	6%	2%	*8%*	**53%**	100%	32%	100%
RT2/V78I/A184I/A330P	**96%**	89%	6%	5%	*11%*	5%	100%	**52%**	100%
K19/A82M/F87A	**97%**	54%	7%	**29%**	***36%***	1%	100%	30%	94%
R19/F87A	86%	60%	19%	8%	*27%*	–	–	5%	100%
R19/F87A/A184I	**96%**	52%	7%	**28%**	***36%***	2%	100%	20%	93%
R19/F87A/A328L	**100%**	77%	7%	4%	*11%*	1%	100%	**65%**	95%
R19	84%	90%	8%	1%	*10%*	–	–	16%	100%
R19/F87I	**95%**	59%	28%	2%	***29%***	–	–	8%	89%
R19/F87I/L437LV	49%	54%	**38%**	1%	***39%***	–	–	2%	100%

THQ' (**38**) was an active substrate, with 19 variants giving >90% conversion (TTN >1,800). THIQ' (**42**) and THQX (**45**) were less active, with 3 and 6 variants giving >50% conversion (TTN >1,000, Appendix 3.7). The variants RP/H171L/I263G and RP/I263A/E267V were

very active for all these substrates (>65% conversion, TTN >1,300). As shown in Table 4.6, the mutations V78I and I263G promoted the conversion of **38**; V78I and the combinations H171L/I263G and I263A/E267V improved the oxidation of **42** and **45**; and A328L increased the conversion of **45**. For THQ' (**38**), C8-hydroxylation was dominant, with even WT showing 92% selectivity. The C5 oxidation products **40** and **41** were minor components, and F87I/A and L437LV promoted C5 oxidation. For THIQ' (**42**), the three active variants gave 1 : 1 ratio of the 5- and 8-alcohols, **43** and **44**. For the symmetric **45**, C5 (C8) hydroxylation was the only observed activity.

The position of the nitrogen atom in THIQ' (**42**) strongly affected the benzylic oxidation by $P450_{BM3}$, reversing the preference for C8-hydroxylation shown by THQ' (**38**). The contrast in conversion for THQ' (**38**) and THQX (**45**) showed that more nitrogen atoms in the substrate molecule inhibited the oxidation activity. The mutation effects are summarised in Table 4.7.

Table 4.7 Summary of mutation effects promoting $P450_{BM3}$ oxidation of THQ', THIQ' and THQX.

C5 : C8 <2 : 3  THQ'		C5 : C8 1 : 1  THIQ'	C5 = C8  THQX
conversion	**C5 oxidation (minor)**	**conversion**	**conversion**
V78I I263G	F87I/A L437LV	V78I H171L/I263G I263A/E267V	V78I H171L/I263G I263A/E267V A328L

4.5 Oxidation of quinoline

Quinoline (**22**), possessing full aromaticity and a sp^2 nitrogen, was a modest substrate for the 48-variant library (WY1/2, Appendix 3.8). It was oxidised to the *N*-oxide (**47**), 3-hydroxy-quinoline (**23**), and a stable 5,6-arene oxide (**48**, Figure 4.18). Acid treatment of **48** led to the formation of 5-quinolinol (**49**). Using the purified products **23** and **48** to

incubate with selected variants, 3,6-dihydroxy-quinoline (**50**), 5-quinolinol (**49**) and *cis*-5,6,7,8-diepoxy-quinoline (**51**) were obtained. NMR and MS of **47**–**49** and **51** matched literature.[274,538,539]

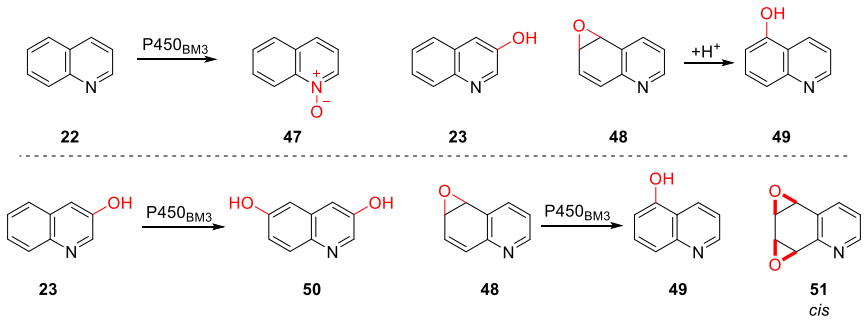


Figure 4.18 The reaction scheme of $P450_{BM3}$ of quinoline (**22**).

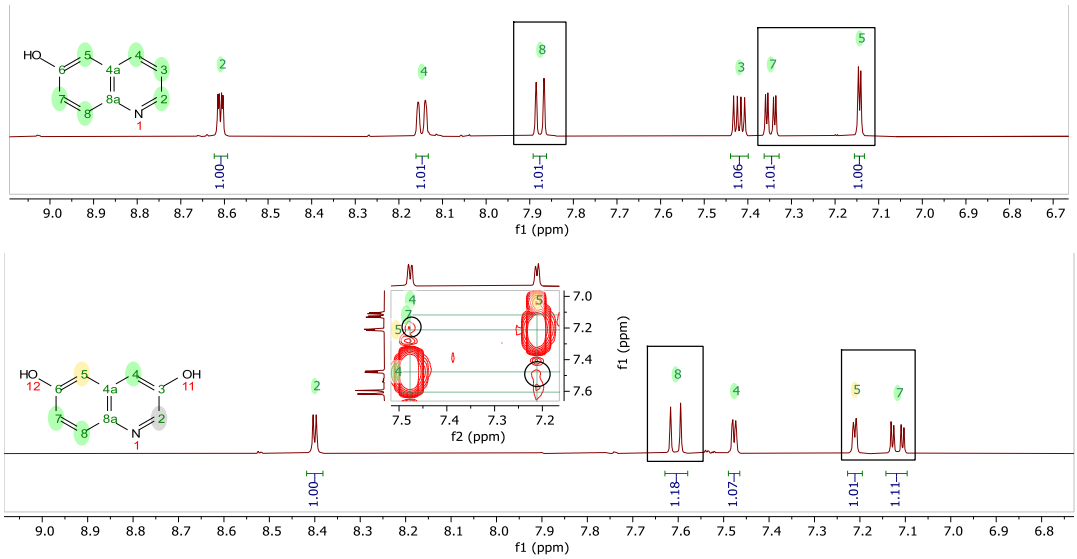
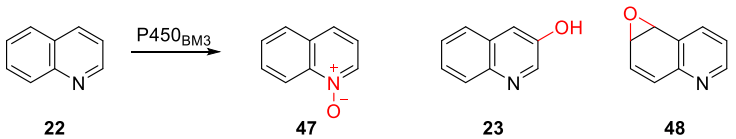


Figure 4.19 The ^{1}H NMR spectra of 6-hydroxy-quinoline (**27**) and 3,6-dihydroxy-quinoline (**50**).

The mass of **50** was [M_{22} + 2O]. Comparison of the coupling patterns of the hydrogens in the benzene rings of 6-hydroxy-quinoline (**27**) and 3,6-dihydroxy-quinoline (**50**) confirmed that C6 of **50** was hydroxylated, along with the long-range coupling between H4 and H5 in the COSY spectrum of **50** (Figure 4.19). The 3-hydroxyl group accelerates the ring-opening of its 5,6-arene oxide intermediate, which should have led to the 3,5-diphenol. The unexpected formation of **50** suggested the active site residues played a role in the ring-opening process.

Across the variant library (WY1/2), 8 out of 48 variants gave >50% conversion (TTN >1,000). The mutations V78I, I263G and A328I/L enhanced the conversion (Table 4.8). For *N*-oxidation, the mutation F87A increased the selectivity of **47** from nil (R19) to 77% (R19/F87A), and the further addition of A328I/L pushed the selectivity to up to 99% (TON 1,540). C3,C4 oxidation was a minor activity, with V78I and I263G/A328L slightly increasing **23**. C5,C6 oxidation was substantially enhanced by the addition of V78I, I263G and A330P to achieve 97% selectivity of **48** (TON 1,010 given by KU3/A330P, Table 4.8).

Table 4.8 The conversion and product distribution of P450BM3 oxidation of quinoline (**22**).

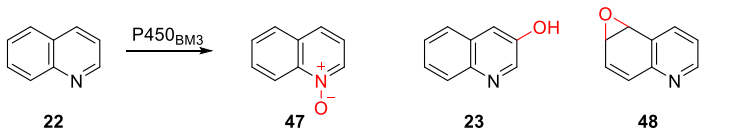


Mutant	Conv.	47	23	48
K19/F87V	37%	65%	–	34%
K19/F87V/A328I	**79%**	91%	–	–
R19/F87A	18%	77%	–	–
R19/F87A/I263G	25%	2%	**9%**	81%
R19/F87A/A328L	**78%**	99%	–	–
R19/F87A/A328I	**77%**	98%	–	–
R19/F87A/E267F/A328I	**80%**	**99%**	–	–
R19/I263G/A328L*	5%	–	**35%**	65%
KU3/A330P	**52%**	–	–	**97%**
RP/F87V	29%	54%	4%	37%
RP/V78I/F87V	41%	3%	**9%**	86%
RP/V78I/F87V/I263G*	**100%**	–	–	**100%**
RP/H171L/I263G	**64%**	–	3%	79%

*: 2nd generation variant.

The yield of **48** was improved by introducing I263G into R19/V78I/F87V, and this 2nd generation variant gave 100% selectivity with full conversion (TON 2,000). The mutation effects on quinoline oxidation are summarised in Table 4.9.

Table 4.9 Summary of mutation effects promoting $P450_{BM3}$ oxidation of quinoline (**22**).



22 → **47** R19/F87A/E267F/A328I 99%, TON 1,580; **23** R19/I263G/A328L 35% TON 40; **48** RP/V78I/F87V/I263G 100% TON 2,000

conversion	N1,C2	C3,C4	C5,C6
V78I I263G A328I/L	F87A A328L/I	V78I I263G/A328L	V78I I263G A330P

4.6 Summary

Amongst the tested quinoline and isoquinoline derivatives in Table 4.10, THQ and THQ' were active substrates for the current $P450_{BM3}$ variant library. Q and THQX were modest substrates, and the lactam **24** and THIQ' were less active. THIQ was totally inactive, perhaps due to its electron richness and substrate mobility exposing the sp^3 nitrogen atom to bind to heme. This suggested the position of the nitrogen atom, the extent of the aromaticity of substrate and the number of the heteroatoms influenced the oxidation of these fused-ring scaffolds: N2 evidently lowered the activity, whereas N1 was active; full aromaticity tended to retard oxidation; more heteroatoms, either the introduction of a carbonyl group or a nitrogen atom, hampered the oxidation by $P450_{BM3}$. One variant, RP/H171L/I263G, needs to be highlighted, since it showed good conversion for all substrates, except THIQ.

The mutation effects on $P450_{BM3}$ oxidation of all the substrates showing activity are combined in Table 4.11. The mutations V78I, F87A, I263G, E267V and A328I/L generally promoted conversion. The most dominant activities for these substrates were oxidation at activated positions (C2 of THQ, N1 of Q, and benzylic carbons of the lactam **24**, THQ', THIQ' and THQX), and adding reduced-size amino acids (A/V) at F87 showed enhancement (Figure 4.20). C5,C6 oxidation was promoted by I263G or I263G/A328L for

THQ **13**, the lactam **24** and Q **22** with up to 100% selectivity (TON 2,000), suggesting the active variants might have specific N1 recognition sites to expose C5,C6. C3, Cα–Cβ desaturation and C7,C8 oxidation of the lactam **24**, and C3,C4 oxidation of Q were new activities observed after the introduction of C2-carbonyl group/full aromaticity to THQ scaffold (Figure 4.20).

Table 4.10 The correlation between substrate properties and $P450_{BM3}$ oxidation of quinoline and isoquinoline derivatives.

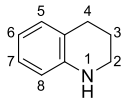
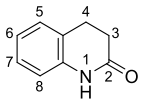
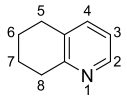
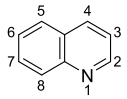
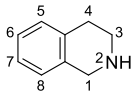
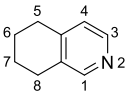
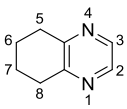
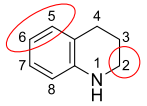
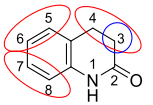
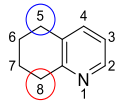
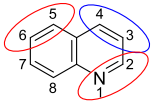
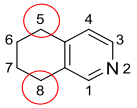
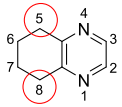
Substrate	***N*-hybridisation**	**aromatic moiety**	***N*-position**	**No. of the 48 library variants showing >50% conversion (TON >1,000)**
 THQ (**13**)	sp^2/sp^3	benzene	N1	30 (RP/H171L/I263G 97% conv., TON 1,940)
 3,4-dihydro-2-quinolinone (**24**)	sp^2 mainly/sp^3	benzene	N1	1 (RP/H171L/I263G 66% conv., TON 1,320)
 THQ' (**38**)	sp^2	pyridine	N1	31 (RP/H171L/I263G 95% conv., TON 1,900)
 Q (**22**)	sp^2	quinoline	N1	8 (RP/H171L/I263G 64% conv., TON 1,280)
 THIQ (**37**)	sp^3	benzene	N2	0 (no activity)
 THIQ' (**42**)	sp^2	pyridine	N2	3 (RP/H171L/I263G 100% conv., TON 2,000)
 THQX (**45**)	sp^2	pyrazine	N1 and N4	6 (RP/H171L/I263G 80% conv., TON 1,600)

Table 4.11 Effect of mutations on $P450_{BM3}$ oxidation of all substrates in Chapter 4. (Major oxidation activity in red; modest and low oxidation activity in blue).

Substrate	Conversion	N1	C2	C3	C4	C5	C6	C7	C8
 THQ (**13**)	F87A A184I A328V/I/L	*No activity*	V78F F87A/V/L A184I E267V	*No activity* (THQ-imine: F87A/L, A328I/F/L <weak promotion>)	*No activity*	F87-unmutated I263G/A328L		*No activity*	
 3,4-dihydro-2-quinolinone (**24**)	V78I A82M F87A I263G A328I	*No activity*	*No activity*	A82M/W I263G/A (weak promotion)	V78I A330P	I263G/A328L		S72H/Y V78I A330W/P	
				F87A (C3,C4 desaturation)					
 THQ' (**38**)	V78I I263G E267V	*No activity*		*No activity*		F87I/A L437LV (modest promotion)	*No activity*	*No activity*	dominant
 Q (**22**)	V78I I263G A328I/L	F87A A328L/I		V78I I263G/A328L (weak promotion)		V78I I263G A330P		*No activity*	
 THIQ' (**42**)	V78I H171L/I263G I263A/E267V	*No activity*	*No activity*	*No activity*	*No activity*	50%	*No activity*	*No activity*	50%
 THQX (**45**)	V78I H171L/I263G I263A/E267V A328L	*No activity*	*No activity*	*No activity*	*No activity*	dominant (C5 = C8)	*No activity*	*No activity*	dominant (C5 = C8)

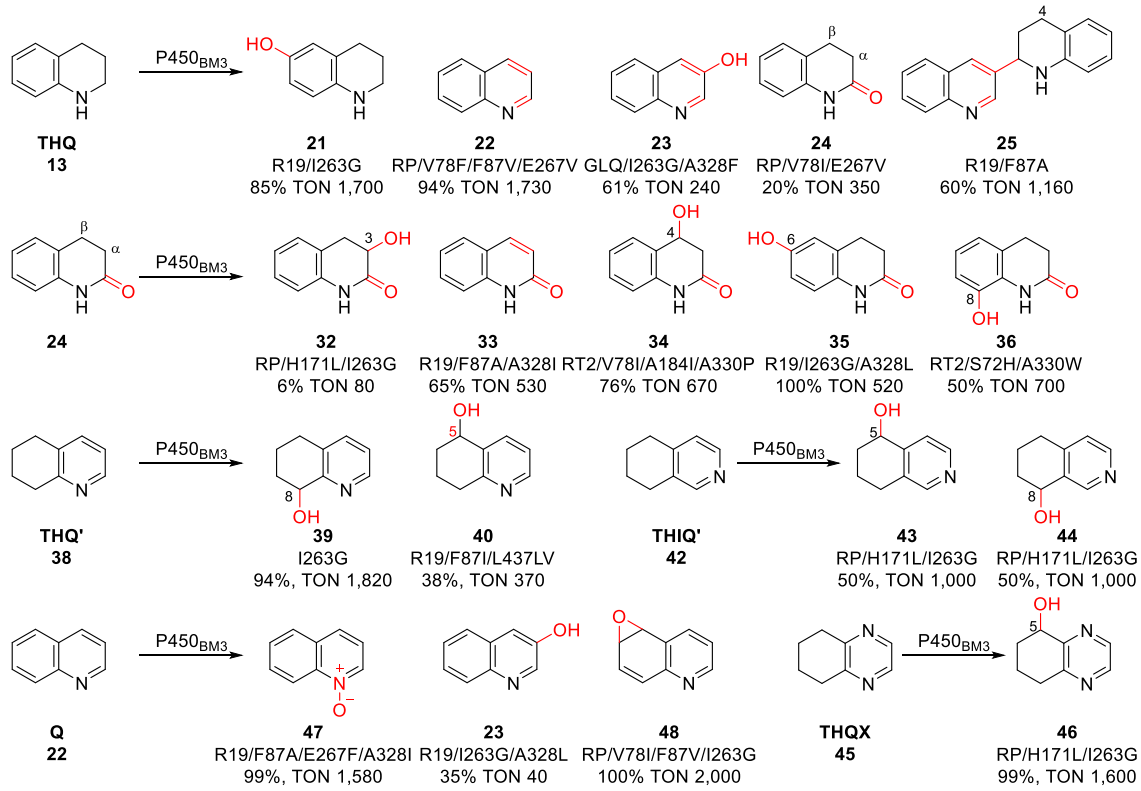


Figure 4.20 P450$_{BM3}$ oxidation of quinoline and isoquinoline derivatives.

The mutations at the B'-, I- and F-helices, the F87 loop, the A328/P329/A330 loop and L437 in the β4-sheet altered the regioselectivity for all. The enantioselectivity for chiral products remain to be determined. Improving selectivity for remote functionalisation of these compounds remains challenging for P450$_{BM3}$. As the dominant oxidation sites were still activated positions and the addition of bulkier mutations (S72H/Y, V78I and A330W) promoted C7,C8 oxidation of the lactam **24**, it was likely that the active sites of most P450$_{BM3}$ variants were so spacious and nonpolar that great substrate mobility assisted the exposure of the activated C–H bonds or nitrogen itself to the ferryl oxygen. The next generation of variant library target for product diversity can be established by introducing or inserting H/Y/W/F/I/L/M/N/Q at the B'-helix, the F87 loop, the A328/P329/A330 loop and L437 in the β4-sheet to RP/H171L/I263G.

Of drug molecules in Figure 4.1 and 4.2, N1, C3, C4, C6, C7 and C8 of THQ, C5 and C7 of the lactam, C2, C3, C4, C6 and C7 of Q were substituted, whereas C2 and C6 of THQ,

C3, C4, C6 and C8 of the lactam, and N1, C3 and C5,C6 of Q were substituted in $P450_{BM3}$ oxidation; substituents at all sites of THIQ in drugs were observed, whilst the current $P450_{BM3}$ variant library showed no activity towards THIQ. This suggests the need of further diversification of these cores by either substrate or protein engineering. Considering THIQ could be hydroxylated by liver microsomes at C1 and C4, the overlays of SF/SB crystal structures of $P450_{BM3}$ with the typical microsomal CYP isozymes in liver, such as 2E1, 1A2, 2D6, 2C9, 2C19 and 3A4, should be analysed with the aid of homology study; the differences of their active sites with $P450_{BM3}$ could be incorporated into $P450_{BM3}$ to 'create' THIQ hydroxylation by protein engineering. Similar strategy was adopted in simulating the oxidation of androstenedione with CYP19A1 by Gly-scanning mutagenesis across the I-helix and the A328/P329/A330 loop of $P450_{BM3}$.[363] Approaches to substrate engineering of THQ and Q oxidation by $P450_{BM3}$ include substituent and protecting group engineering, which are the subjects of Chapters 5 and 6.

Chapter 5 Effect of substituents on the oxidation of quinoline and tetrahydroquinoline derivatives by $P450_{BM3}$

5.1 Introduction

The oxidation of THQ and Q cores by the P450$_{BM3}$ variants generated thus far occurred predominantly at the C2 and C5,C6 positions (Figure 5.1). In contrast, the oxidation of 3,4-dihydro-2-quinolinone showed all sites oxidised. This suggested the introduction of the carbonyl group played a non-trivial role in steering the oxidation around the scaffold. Hence, the effect of substituents on the oxidation pattern of THQ and Q was explored. The THQ and Q derivatives, 2-, 6-, 8-methyl- and 6-methoxy-1,2,3,4-tetrahydroquinolines and 2-, 6-, 8-methyl-quinolines (2/6/8Me-THQs, 6MeO-THQ and 2/6/8Me-Qs in Figure 5.1) were studied. The methyl substituent at C2 may block HAT at C2 of THQ, whilst the C6 and C8 substituents will alter the electron-richness of the C=C bonds of the aromatic ring. The substituents may also alter THQ binding, potentially leading to new products.

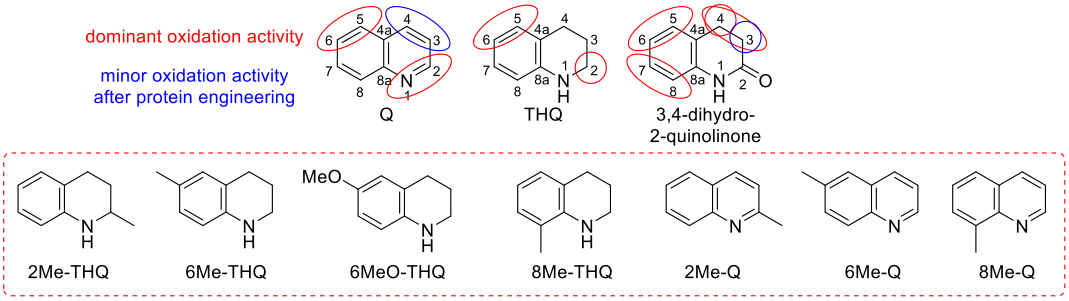


Figure 5.1 Overview of the oxidation activities for THQ, Q and 3,4-dihydro-2quinolinone given by P450$_{BM3}$ variants and the substrates tested in this chapter.

5.2 Substituent effects on the oxidation of the THQ core

5.2.1 Oxidation of 2Me-THQ

2Me-THQ, **52**, was converted by the P450$_{BM3}$ variant library (WY3/4, Appendix 3.9) predominantly to 6-hydroxy-2Me-THQ, **53**, with some of the aromatisation product 2-methyl-quinoline, **54** (Figure 5.2). Minor unidentified peaks in the GC retention time window of dimers were observed. The product 6-hydroxy-2Me-THQ (**53**) was also found to give 6-hydroxy-2Me-Q (**55**, 100% selectivity) in the prolonged incubation of **52** with R19/A184I/A328L. The NMR and MS data of **53**–**55** were consistent with literature.[540–542]

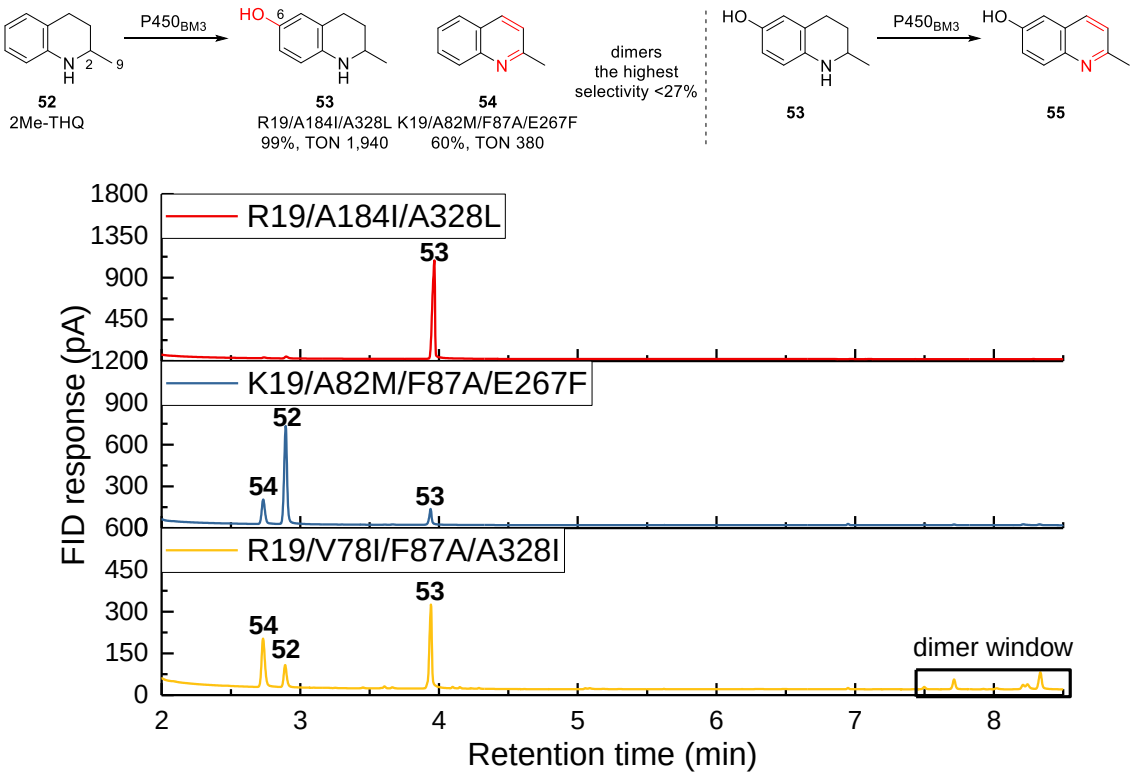


Figure 5.2 The reaction scheme and GC analysis of $P450_{BM3}$ oxidation of 2Me-THQ (**52**).

Within the variant library, 31 out of 48 variants showed >50% conversion (TON >1,000). Wild type $P450_{BM3}$ gave 23% conversion, favouring the formation of **53** (86%, TON 400). The mutations F87V/A, A184I, H171L/I263G and I263G/A328L enhanced the enzyme activity up to 98% conversion (TON 1,960 given by R19/A184I/A328L, Table 5.1 and Figure 5.2). 23 variants favoured C5,C6 oxidation (>86% of **53**). The mutations A184I and I263G/A328L favoured C5,C6 oxidation with R19/A184I/A328L giving 99% of **53** (TON 1,940), whereas this variant gave 39% of the 6-phenol **21** in THQ oxidation. The C2-methyl group suppressed C2 oxidation, giving aromatisation product **54** mainly and the dimers in low proportion. The mutations S72W, E267F, A328I and F87A/I263G promoted the formation of **54,** up to 60% given by K19/A82M/F87A/E267F, which gave 51% of Q in THQ oxidation. A328I improved dimer formation slightly to reach 22% given by R19/F87A/A328I, which gave 58% of dimers for THQ. These suggested that C2-methyl

probably suppressed dimerisation by steric hindrance and its stabilisation for the imine intermediate for aromatisation to yield **54** mainly.

Table 5.1 Conversion and product distribution of $P450_{BM3}$ oxidation of 2Me-THQ (**52**).

Mutant	Conv.	53	54	dimers (minor)
WT	23%	86%	12%	2%
K19/F87V	77%	92%	5%	3%
RP/F87V	91%	93%	4%	2%
RP/H171L/I263G	96%	96%	4%	–
K19/A82M/F87A	85%	75%	20%	4%
K19/A82M/F87A/E267F	32%	31%	60%	9%
R19/I263G/A328L	93%	98%	2%	–
R19/A184I/A328L	98%	99%	1%	–
GV/A184I	83%	95%	2%	3%
R19	79%	94%	6%	–
R19/F87A	97%	71%	17%	12%
R19/F87A/I263G	63%	50%	31%	19%
R19/F87A/A328I	91%	47%	31%	22%
R19/S72W/F87A/A328I	96%	50%	47%	4%

It may be concluded that C2-methyl favoured C5,C6 oxidation and blocked C2-oxidation-initialised dimerisation which was commonly observed in THQ oxidation. The mutation effects on oxidation of 2Me-THQ are summarised in Table 5.2.

Table 5.2 The mutation effects on $P450_{BM3}$ oxidation of 2Me-THQ (**52**).

Conversion	C2 (aromatisation)	C5,C6
F87A/V	S72W	
A184I	F87A/I263G	A184I
H171L/I263G	E267F	I263G/A328L
I263G/A328L	A328I	

5.2.2 Oxidation of 6Me-THQ and 6MeO-THQ

The C2-methyl substituent shifted the selectivity of THQ towards oxidation at C5,C6 and inhibited dimerisation, perhaps due to steric effects flipping the C2 position away from the

heme meanwhile exposing C5,C6. A substituent at C6 was expected to shift the reaction forward C2 attack. For 6Me-THQ, this assumption was roughly true. However, for 6MeO-THQ, unexpected reactions were also observed.

In the oxidation of 6Me-THQ (**56**) with the 48 variant library (WY3/4, Appendix 3.10), only C2 oxidation was observed. The aromatisation product, **57**, the 3-phenol, **58**, the lactam, **59**, and the dimer **60** were purified (Figure 5.3). Prolonged incubation of the preparative scale reactions with K19/F87V/Q403P and GV/A184I yielded **61**–**63**. The NMR and MS data of **57**–**60**, **62** and **63** were consistent with literature.[543–548] The new compound **61** was fully assigned by NMR and MS data (Appendix 4.3, Spectrum 61).

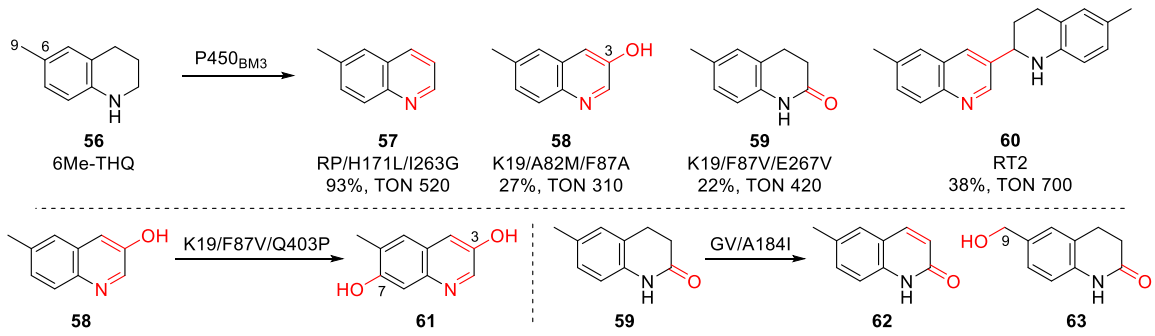


Figure 5.3 The reaction scheme of $P450_{BM3}$ oxidation of 6Me-THQ (**56**).

Within the variant library, 15 out of 48 variants gave >50% conversion (TON >1,000). The wild type enzyme showed 21% conversion (Table 5.3). Similar to oxidation of 2Me-THQ, the mutations F87V and A184I improved the oxidation up to 96% conversion given by K19/F87V/E267V and GV/A184I (TON 1,920, Table 5.3). As for C2 oxidation, the mutations V78I, I263G, E267F and A330P improved the aromatisation activity up to 93% selectivity with impaired conversion; formation of the 3-phenol **58** was increased by A82M and A328L up to 27% and 24% (TON 310 and 360) given by K19/A82M/F87A and R19/F87A/A328L; F87V/E267V raised lactam formation up to 22% (TON 420) given by K19/F87V/E267V; and the mutations F87V, A184I and A264G enhanced dimerisation up to 38% of **60** (TON 700, Table 5.3).

Table 5.3 The conversion and product distribution of $P450_{BM3}$ oxidation of 6Me-THQ (**56**).

Mutant	**conversion**	**57**	**58**	**59**	**60**
WT	21%	69%	–	12%	19%
RP/F87V	**89%**	38%	13%	12%	35%
RP/V78I/F87V	48%	**72%**	4%	1%	24%
K19/F87V	**88%**	36%	15%	19%	29%
K19/F87V/A264G	**88%**	46%	16%	1%	**37%**
K19/F87V/E267V	**96%**	40%	6%	**22%**	30%
K19/A82M/F87A	58%	43%	**27%**	2%	29%
K19/A82M/F87A/E267F	20%	**75%**	10%	–	15%
GVQ	3%	100%	–	–	–
GV/A184I	**96%**	50%	12%	9%	28%
GVQ/A264G	31%	60%	9%	–	31%
RT2	**92%**	48%	3%	11%	**38%**
KU3/A330P	18%	**88%**	–	–	12%
RP/H171L/I263G	28%	**93%**	–	–	7%

To sum up, C6-blockage led to the variant library giving only C2 oxidation with no evidence for C3, C4 and C7,C8 oxidation. Aromatisation activity was predominant across the library in the reactions of low conversion, while dimerisation was hampered. The 6-methyl substituent also shifted the oxidation of the 3-phenol **58** from C5,C6 to C7,C8, probably by its steric effect. Interestingly, methyl oxidation of the lactam **59** was observed but not with **56**. The mutation effects on oxidation of **56** are summarised in Table 5.4.

Table 5.4 The mutation effects on $P450_{BM3}$ oxidation of 6Me-THQ (**56**).

Conversion	**C2 oxidation**			
	aromatisation	**C2,C3-stepwise**	**lactam**	**dimerisation**
F87V A184I	V78I I263G E267F A330P	A82M A328L	F87V/E267V	F87V A184I A264G

6MeO-THQ, **64**, was converted by the 48 variant library (WY7/8, Appendix 3.11) to the aromatisation product **65** (6MeO-Q), dimers and two unidentified products **66**–**69** in the

screening tests (Figures 5.4 & 5.5). Only **65**, **66** and **67** were purified from the preparative scale reaction with I263G after overnight incubation, whereas its screening test showed **65**, **66**, **68** and **69** were products for 8 h incubation. This suggested that the uncharacterised products **68** and **69** were likely to be the acid-labile imine intermediates during the aromatisation step to generate **65** and **67**, explaining why **68** and **69** were not obtained after purification by silica gel column chromatography and prolonged incubation. It also implied that the electron rich 6-methoxy group might stabilise **68** and **69**, and retarded the aromatisation process. The formation of the new dimeric products **66** and **67** involved intermolecular amination. The NMR and MS data of **65** were consistent with literature.[549]

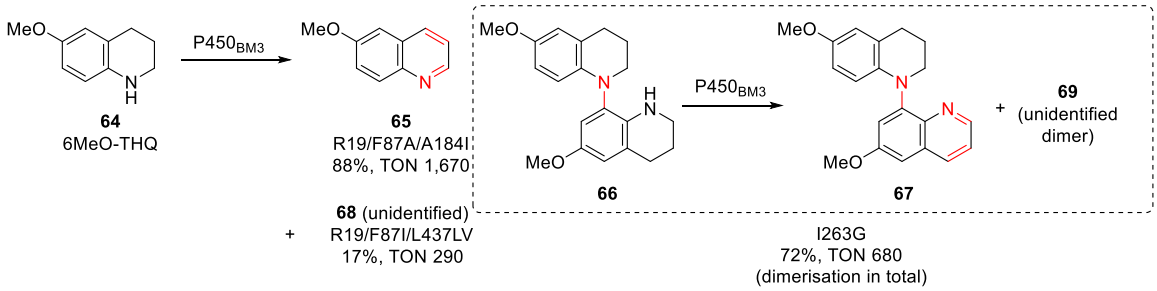


Figure 5.4 The reaction scheme of $P450_{BM3}$ oxidation of 6MeO-THQ (**64**).

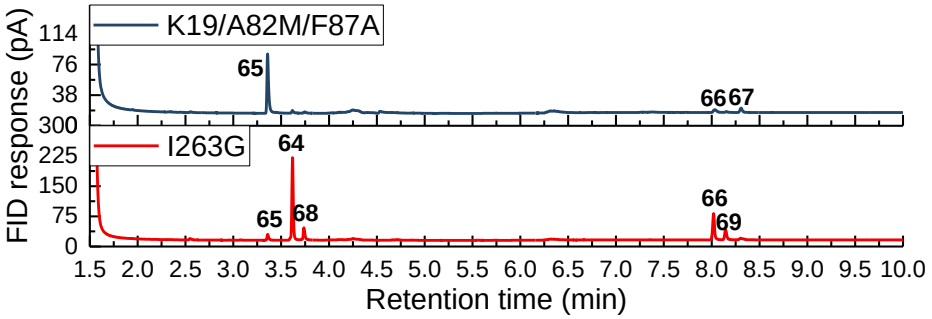


Figure 5.5 GC analysis of the oxidation of 6MeO-THQ (**64**) by the variants K19/A82M/F87A and I263G.

The mass of **66** and **67** were [$2M_{\mathbf{64}}$ – 2H] and [$2M_{\mathbf{64}}$ – 6H] respectively. The mass of **67** and the presence of eight aromatic protons in its ^{1}H NMR spectrum (Figure 5.6) revealed that the dimer consisted of one 6MeO-THQ moiety and one 6MeO-Q moiety. Three CH_2 groups in the aliphatic region, the three mutually coupled aromatic protons, along with the methyl group at δ 3.75, confirmed that all CHs of the 6MeO-THQ moiety were intact.

Therefore, N1 was substituted in this moiety. In the 6MeO-Q moiety, H5' (δ 6.85, d, *J* = 2.8 Hz) and H7' (δ 7.08, d, *J* = 2.8 Hz) shared long-range coupling, thus assigning the N1–C8' linkage of **67**.

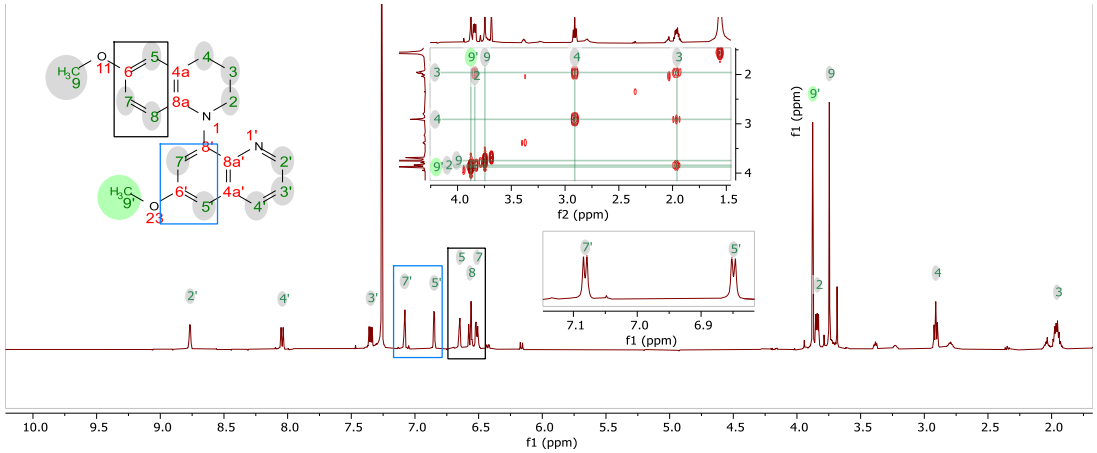


Figure 5.6 The ^{1}H NMR spectrum of **67**.

Based on the assignment of **67**, its precursor **66** which lost two hydrogens during dimerisation, was assigned to the non-aromatised amination product. The six pairs of aliphatic CH_2 groups and five aromatic CH groups in the ^{1}H NMR spectrum (Figure 5.7) showed that **66** consisted of two 6MeO-THQ moieties. The linkage of **66** was fully assigned by tracing the long range coupling pattern of the molecule in its COSY spectrum (Spectrum 63 in Appendix 4.3).

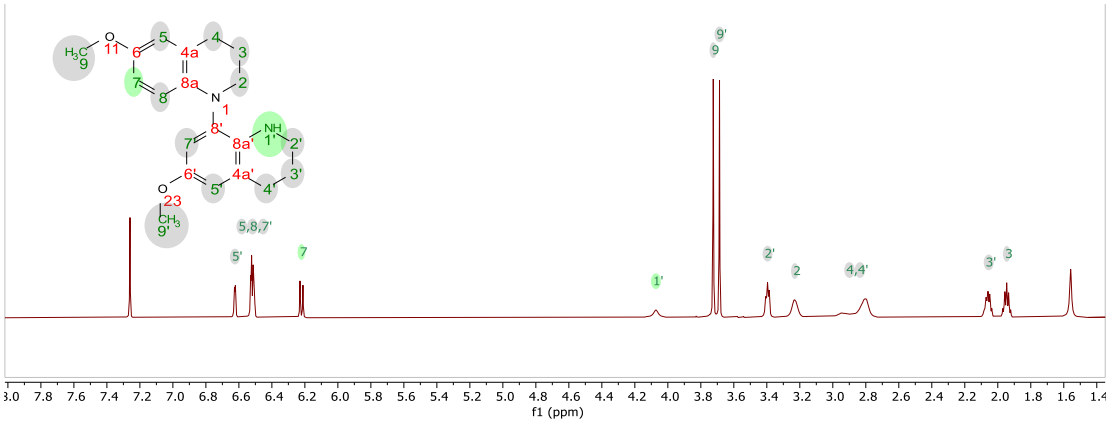


Figure 5.7 The ^{1}H NMR spectrum of **66**.

The formation of the dimer **66** involves intermolecular amination of an aromatic C–H bond. C–H amination by intramolecular nucleophilic attack by a nitrogen on an iminium species generated by loss of OH^- from a cabinolamine[345] cannot apply here, whereas diradical coupling mechanism proposed for the intramolecular amination to synthesise indolactam V by cytochrome P450 oxidases TleB/HinD[550] might rationalise the formation of **66**. Diradical coupling mechanism (Figure 5.8 A) begins with HAT by Compound I from NH to form Compound II and the N1' radical, which has the other three resonant structures (C4a', C6' and C8' radicals). Compound II abstracts NH of another substrate molecule to form the N1 radical. The intermediate of diradical coupling between the N1- and the C8'-radicals aromatises to form **66**. In this mechanism, the ferryl species abstracts two hydrogens from two substrate molecules. The absence of C4a'–N1 or C6'–N1 coupling could result from steric hindrance. The lack of C8–C8' coupling is perhaps because of specific binding of the two substrate molecules inside the active site and thermodynamic control of the N1–C8' coupling process. This mechanism could also be applied to 6Me-THQ, but no such dimer was formed in its oxidation by $P450_{BM3}$.

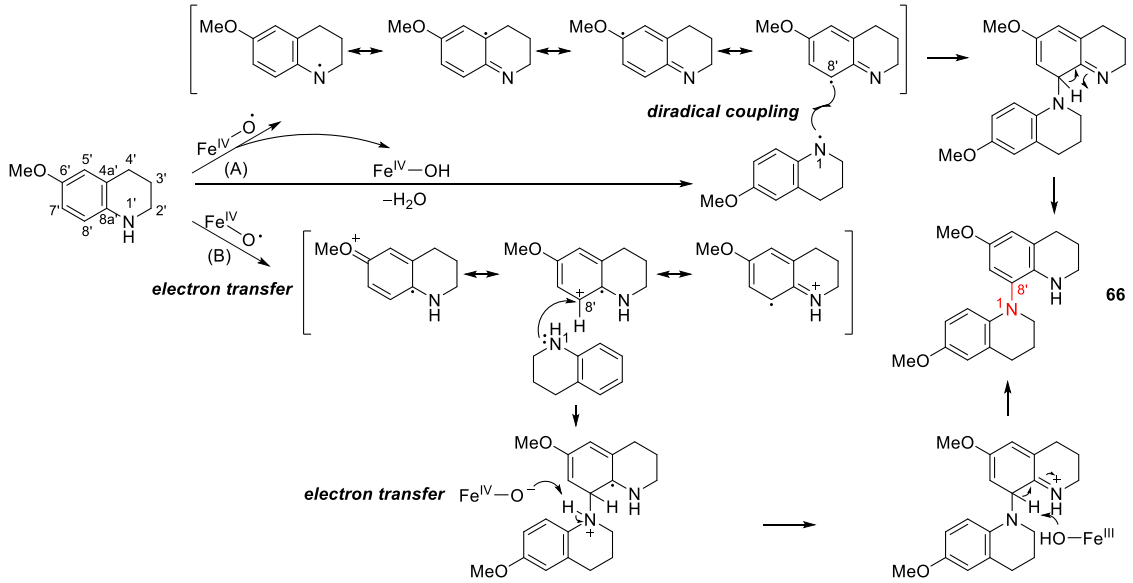


Figure 5.8 Proposed mechanisms for the formation of the C–H amination product **66**.

Noting the highly electron-rich nature of the aromatic ring in **64**, with electron-donating alkyl, methoxy and amine substituents, an electron transfer oxidation mechanism can also be proposed. After one-electron oxidation, the positive charge can be stabilised mainly at C5' and C8' as they are *ortho* to the methoxy and amine substituent, respectively (Figure 5.8 B). The cation radical intermediate is attacked by the nitrogen of a second substrate molecule, and a proton is transferred to the Fe^{IV}–O^{-} species formed after electron transfer. The generated Compound II converts to Fe^{III}–OH via another cycle of electron transfer from the dimeric intermediate. The cation generated is stabilised by the amine nitrogen. The Fe^{III}–OH species then abstracts a proton from C8 to form **66**. In this mechanism, the ferryl species abstracts two electrons and two protons in an oxidative dehydrogenation coupling reaction. The absence of C5' attack could arise from the steric hindrance by 6-methoxy or specific binding of the two substrate molecules.

Table 5.5 Conversion and product distribution of $P450_{BM3}$ oxidation of 6MeO-THQ, **64**.

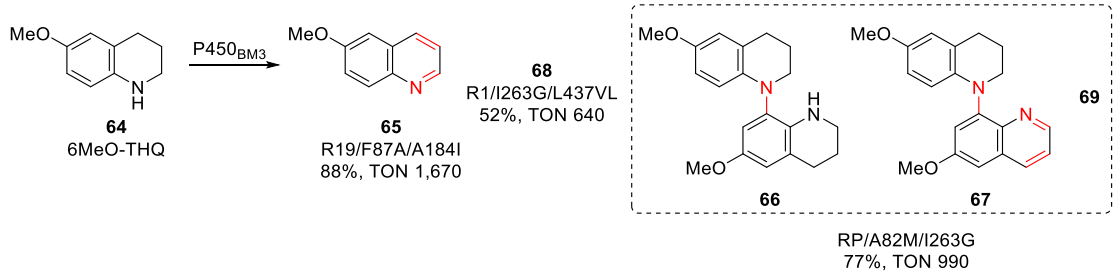
Mutant	**conversion**	**65**	**68**	**66**	**67**	**69**	**dimers (66, 67 & 69)**
RP/A82M/I263A	25%	19%	9%	45%	8%	19%	**72%**
R19	29%	10%	–	64%	–	26%	**90%**
R19/F87A	88%	66%	4%	15%	13%	2%	30%
R19/F87A/A184I	95%	**88%**	–	6%	6%	–	12%
R19/F87I	28%	26%	17%	36%	7%	13%	56%
R19/F87I/L437LV	88%	69%	17%	9%	5%	–	14%
I263G	47%	9%	18%	47%	5%	20%	**72%**
GV/A184I	91%	**87%**	6%	4%	4%	–	8%
RP/A82M/I263G*	64%	19%	3%	46%	14%	17%	**77%**
R1/I263G	54%	12%	27%	45%	15%	–	**60%**
R1/I263G/L437VL*	62%	16%	**52%**	18%	4%	9%	31%

*: 2nd generation variant

Amongst the variant library, 19 out of 48 variants showed >50% conversion (TON >1,000). The wild type enzyme gave negligible conversion. F87A, A184I and L437LV improved conversion and promoted the formation of **65** with R19/F87A/A184I giving the most (88%,

TON 1,670, Figure 5.5). The 2nd generation variant R1/I263G/L437VL gave the most of **68** (52%, TON 640). F87I, I263G and L437VL promoted **68** and retarded the aromatisation process of 6MeO-THQ. For N1–C8' coupling, A82M, I263G/A with the unmutated F87 showed improvement in yielding the dimers (**66**, **67** and **69** up to 90% selectivity given by R19). The 2nd generation variant RP/A82M/I263G showed 77% of the dimers with enhanced conversion (TON 990). The mutation effects are summarised in Table 5.6.

Table 5.6 Mutation effects on $P450_{BM3}$ oxidation of 6MeO-THQ (**64**).



Conversion	**C2-aromatisation (65)**	**Dimerisation of N1-C8' coupling (66, 67 & 69)**	**68**
F87A	F87A	A82M	F87I
A184I	A184I	F87-unmutated	I263G
L437LV	L437LV	I263G/A	L437VL

Both the 6-methyl and the 6-methoxy substituents blocked C5,C6 oxidation of the THQ core. The C6-methyl substituent shifted the enzymatic oxidation activity fully towards C2 aromatisation, whereas the C6-methoxy substituent also introduced N1–C8' coupling due to its enhanced electron richness. However, $P450_{BM3}$ oxidation of 6-hydroxy-THQ which attains similar electron-richness to 6MeO-THQ showed aromatisation only. It was likely that the 6-hydroxy substituent, serving as both hydrogen bond donor and acceptor, formed hydrogen bonds with active site residues to expose the C2 position, whilst a methoxy group was only a hydrogen bond acceptor and loses some interaction with the residue(s), therefore flexibly docking inside the active site. A methoxy group is also bulkier than hydroxyl and methyl groups, which might be another factor affecting the binding orientation.

5.2.3 Oxidation of 8Me-THQ

8Me-THQ (**70**) gave a similar spectrum of products to THQ by the 48 variant library (WY1/2, Appendix 3.12), inculding 6-hydroxy-8Me-THQ (**71**), 8-methyl-quinoline (**72**, 8Me-Q), 3-hydroxy-8Me-Q (**73**), the lactam **74** and the common dimer **75** (Figure 5.9). Further oxidation occurred after prolonged incubation with the variants RP/A82M/I263A, R19/I263G/A328L, K19/A82M/F87A and R19/F87A/A328I, giving the products **76**–**80** (Figure 5.9). C2 and C5,C6 oxidation were observed for 8Me-THQ; C7,C8 oxidation occurred in the oxidation of 3-phenol **73**; benzylic oxidation (C4 and C8-methyl) was observed for the lactam **74**. The NMR and MS data of **71**–**76** matched literature.[274,551–553]

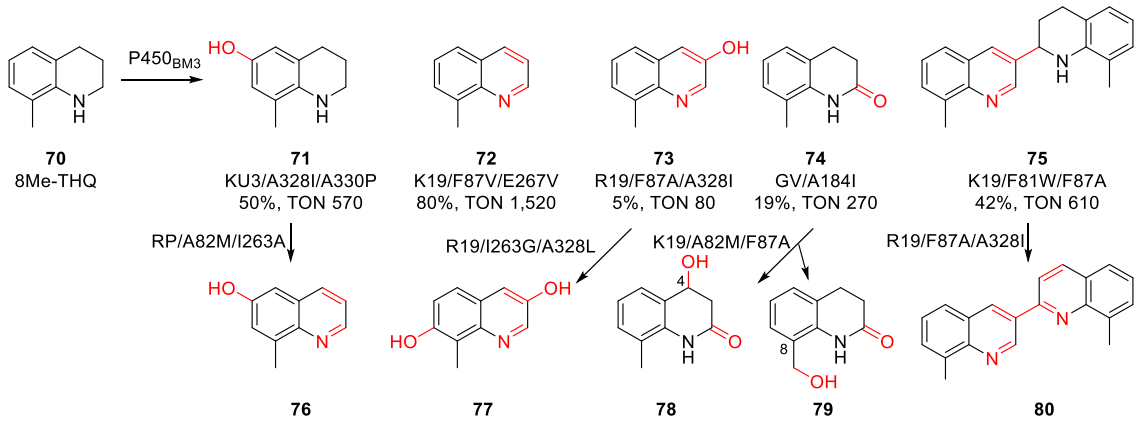


Figure 5.9 The reaction scheme of $P450_{BM3}$ oxidation of 8Me-THQ (**70**).

Out of 48 variants, 29 gave >50% conversion (TON >1,000). The mutations F87A/V, I263G, A264G and E267V improved the conversion up to 95% (TON 1,900, K19/F87V/E267V, Table 5.7). For C5,C6 oxidation, the residue F87 should be unchanged; and the addition of I263G/A328L improved the formation of **71** up to 84% (TON 1,650), given by the 2nd generation variant R19/I263G/A328L which also showed enhancement for C5,C6 oxidation of THQ (79% of **21**, TON 1,390). In combination with the C2-oxidation promoting mutations F87A/V, the aromatisation product **72** was favoured by adding E267V, with K19/F87V/E267V giving 80% of **72**; the minor activity, C2,C3-stepwise oxidation (≤5%), was slightly improved by A328F that the 2nd generation variant K19/F87A/A328F

gave 9% of **73** (TON 80); F81W and A328F improved dimerisation up to 48% (TON 440 of **75**, given by K19/F87A/A328F); A184I and A264G increased the formation of lactam **74** up to 19% given by GV/A184I.

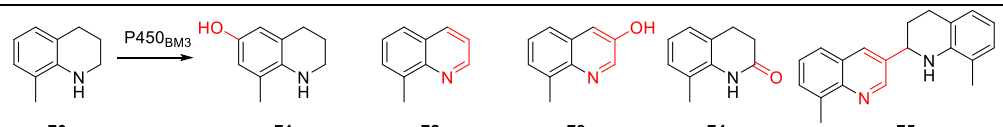
Table 5.7 The conversion and product distribution of $P450_{BM3}$ oxidationof 8Me-THQ (**70**).

Mutant	Conv.	71	72	73	74	75
K19	35%	**36%**	51%	–	2%	11%
K19/F87V	82%	9%	33%	4%	15%	**40%**
K19/F87V/E267V	95%	3%	**80%**	–	7%	10%
K19/F87A/F81W	73%	4%	39%	4%	11%	**42%**
R19	47%	**41%**	44%	0%	2%	14%
R19/F87A	94%	11%	46%	2%	7%	34%
R19/F87A/A328L	83%	**24%**	38%	4%	4%	30%
GV/A184I	70%	9%	33%	1%	**19%**	37%
GVQ	17%	11%	73%	2%	–	14%
GVQ/A264G	65%	7%	50%	3%	10%	19%
RP/H171L/I263G	88%	**47%**	33%	3%	1%	12%
R19/I263G/A328L*	98%	**84%**	14%	2%	–	–
K19/F87A/A328F*	46%	4%	36%	9%	4%	**48%**

*: 2nd generation variant

To conclude, 8Me-THQ was oxidised by $P450_{BM3}$ at C2 and C5,C6 positions. The F87 residue was the switch for both activities. Mutations to small and non-polar amino acids led to C2 oxidation. When it was unchanged, the I263G/A328L couplet favoured C5,C6 oxidation. The mutation effects on 8Me-THQ oxidation are summarised in Table 5.8.

Table 5.8 Mutation effects on $P450_{BM3}$ oxidation of 8Me-THQ (**70**).



70 | **71** R19/I263G/A328L 84%, TON 1,650 | **72** K19/F87V/E267V 80%, TON 1,520 | **73** K19/F87A/A328F 9%, TON 80 | **74** GV/A184I 19%, TON 270 | **75** K19/F81W/F87A 42%, TON 610

Conversion	C5,C6 oxidation	C2 oxidation			
		aromatisation	C2,C3 oxidation	lactam formation	dimerisation
F87A/V I263G A264G E267V	*87F* I263G A328L I263G/A328L	F87V E267V	F87A A328F	F87V A184I A264G	F81W F87V/A

5.2.4 Overall perspective of substituent effects on THQ oxidation

From Table 5.9, it transpired that C6-substitutents decreased the oxidation activity for the THQ core, whereas C2- or C8-methyl did not significantly affect conversion. The oxidation of the substituents was not observed. C2 oxidation was common for all THQs, leading to aromatisation mainly (up to >80% selectivity). C2,C3-stepwise oxidation and lactam formation were minor activities for all THQs (<25% selectivity). C2-blockage shifted the oxidation to C5,C6. C8-blockage made no apparent difference to the oxidation pattern. Both C6 substituents diminished C5,C6 oxidation, while only 6-methoxy showed N1–C8' coupling (C8-amination).

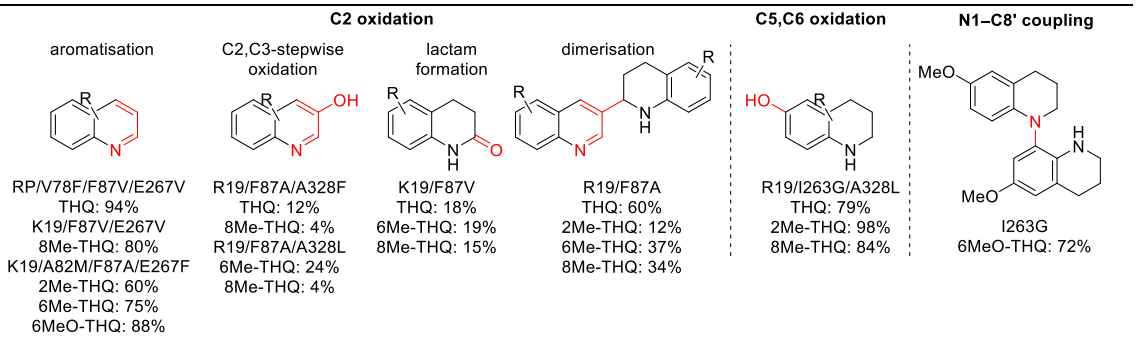
Table 5.9 The summary of the oxidation of THQs by the $P450_{BM3}$ variant library.

substrate	No. of library variants ≥50% conv.	WT conv.	oxidation activity
THQ	30/48 (WY3/4)	10%	C2, C5,C6
2Me-THQ	31/48 (WY3/4)	23%	C2, C5,C6
6Me-THQ	15/48 (WY3/4)	21%	C2
6MeO-THQ	19/48 (WY7/8)	6%	C2, N1,C8'-coupling
8Me-THQ	29/48 (WY1/2) 19/48 (WY3/4)	5%	C2, C5,C6

The mutation effects on oxidation of THQs are summarised in Table 5.10. The 2nd generation variant R19/I263G/A328L favoured C5,C6 oxidation of THQ, 2Me-THQ and 8Me-THQ yielding 79%, 98% and 84% of 6-hydroxy-products, but was unable to oxidise C6-blocked 6Me- and 6MeO-THQs (4% and 6% conversion). The I263G/A328L couplet assisted the exposure of C5,C6 positions of THQs to the ferryl oxygen. The single mutation variant I263G favoured N1–C8' coupling of 6MeO-THQ (72% selectivity). The variants R19/F87A and K19/F87V gave high conversion (69%–97%) and high selectivity of C2 oxidation (70%–100%) for THQ, 6Me-THQ, 6MeO-THQ and 8Me-THQ, showing F87A/V expanded the size of the active site to increase substrate mobility and hence expose the most activated C2 position for oxidation. After forming the carbinolamine intermediates from C2-hydroxylation favoured by F87A/V, other mutations inside the active site also

influenced the downstream product formation processes. The E267V-containning variants RP/V78F/F87V/E267V and K19/F87V/E267V gave 94% and 80% of Q and 8Me-Q, while the E267F-containing K19/A82M/F87A/E267F variant gave 60%, 75% and 88% of 2Me-Q, 6Me-Q and 6MeO-Q respectively, suggesting the key effect of the E267 residue on engineering aromatisation of THQs. The R19/F87A variant favoured C2-oxidation-initialised dimerisation of THQ, 2Me-THQ, 6Me-THQ and 8Me-THQ (60%, 12%, 37% and 34% selectivity). Introducing bulky amino acids Leu or Phe at A328 to R19/F87A slightly improved the yield for 3-phenols of THQ (A328F: 12%), 6Me-THQ (A328L: 24%) and 8Me-THQ (A328L/F: 4%). K19/F87V showed acceptable selectivity for the lactams of THQ, 6Me-THQ and 8Me-THQ (18%, 19% and 15% selectivity).

Table 5.10 The summary of the mutation effects shown in $P450_{BM3}$ oxidation of THQs.



S	conv.	C2				C5,C6	N1–C8'
		aromatisation	3-phenol	lactam	dimer		
THQ	F87A A184I A328V/I/L	V78F F87V E267V	F87A/L A328I/F/ L	F87V/ L A184I	F87A A184I I263G	***87F*** I263G/A328 L	–
2Me-THQ	F87A/V A184I H171L/I263G I263G/A328L	S72W F87A/I263G E267F A328I	–	–	A328I	A184I I263G/A328 L	–
6Me-THQ	F87V A184I	V78I I263G E267F A330P	A82M A328L	F87V/ E267V	F87V A184I A264G	–	–
6MeO-THQ	F87A A184I L437LV	F87A A184I L437LV	–	–	–	–	A82M ***87F*** I263G/ A
8Me-THQ	F87A/V I263G A264G E267V	F87V E267V	F87A A328F	F87V A184I A264G	F81W F87V/ A	***87F*** I263G A328L I263G/A328 L	–

Only the 6-methoxy substituent introduced the new activity N1–C8' coupling in THQ oxidation by the current P450$_{BM3}$ variant library, implying that other substituents, which either significantly alter electron distribution of THQ or introduce H-bonding interaction with the active site residues, should be attempted to achieve oxidation at C3, C4 and C7,C8. Benzylic oxidation (at methyl and C4), which was absent in oxidation of all THQs, was found in the oxidation of the lactam products of THQs most probably due to the introduced carbonyl moiety. The size-reducing mutations F87A/V favouring C2 oxidation of all THQs disclosed that the active sites of the library variants were too spacious. To engineer remote functionalisation of THQs, bulky substituents and mutations capable of developing hydrogen bond could also be introduced to THQ and key residues of P450$_{BM3}$, respectively.

5.3 Substituent effects on the oxidation of the quinoline core

The P450$_{BM3}$ oxidation of quinoline showed lower conversion and turnover than that of THQ; only one quarter of the variant library gave >50% conversion (TON >1,000). The variants showed N1, C3,C4 (minor) and C5,C6 oxidation. C7,C8 oxidation was not observed. Since substituents introduced greater product diversity for THQ oxidation by the variant library, 2-, 6- and 8-methyl-quinolines were selected for the exploration of oxidation at other positions. Moreover, benzylic oxidation would also be expected. This is of interest since the quinolinyl carboxylic acids are useful synthetic intermediates. An similar activity – oxidising the terminal methyl of cholest-4-en-3-one to its carboxylic acid, was reported for two P450s in *Mycobacterium tuberculosis* – CYP125 and CYP142.[554]

5.3.1 Oxidation of 2Me-Q

The variant library (WY3/4, Appendix 3.13) showed similar activity for the oxidation of 2-methyl-quinoline (2Me-Q, **54**) as for quinoline. Oxidation at C3,C4, C5,C6 and 2-methyl to form **81**–**83** were observed after 12 h incubation of the screening reactions (Figure 5.10).

Like Q oxidation, a stable 5,6-arene oxide, **82**, was isolated at 12 h as the only C5,C6-oxidation product of 2Me-Q. No *N*-oxide was found, nor were further oxidation products within 12 h incubation. After 24 h incubation of 2Me-Q, 3-hydroxy-2Me-Q **81** was converted to the 3,6-diphenol **84** by RP/V78I/F87V/H171L/I263G; the 5,6-arene oxide **82** was converted to 5- and 6-phenols **85** and **55** by RP/H171L/I263G, and the *trans*-5,6-diol **86** by RP/H171L/A184I/I263G; the benzylic alcohol **83** was converted to the aldehyde **87** and the carboxylic acid **88** by K19/A82M/F87A. Their NMR and MS data matched literature.[274,555–559]

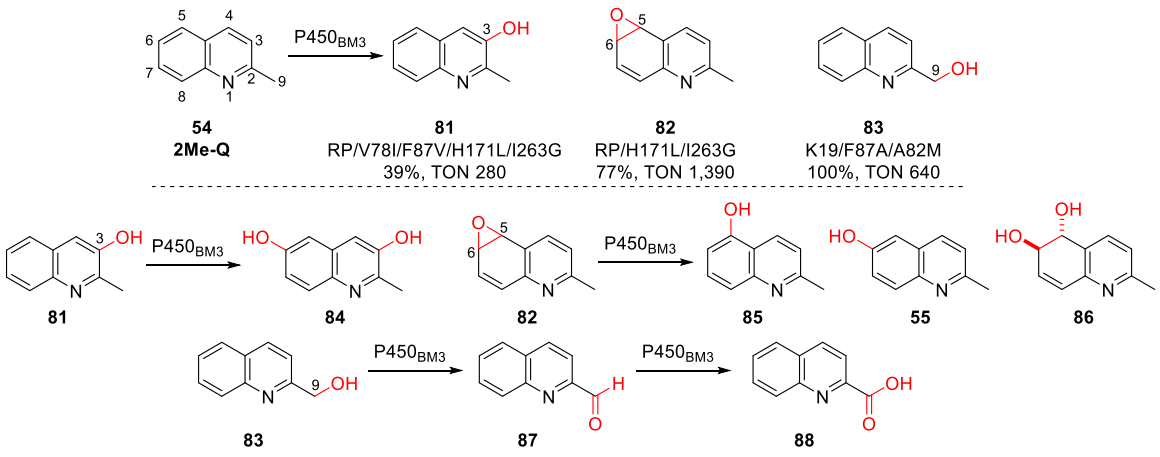


Figure 5.10 The reaction scheme of $P450_{BM3}$ oxidation of 2Me-Q (**54**).

Table 5.11 The conversion and product distribution of $P450_{BM3}$ oxidation of 2Me-Q (**54**).

Mutant	**conv**	**81**	**82**	**83**
R19/F87A	11%	–	21%	79%
R19/F87A/I263G	16%	2%	**58%**	39%
R19/F87A/A328I	31%	–	–	**100%**
R19/F87A/A328L	20%	–	–	**100%**
RP/H171L/I263G	**90%**	1%	**77%**	22%
RP/V78I/F87V/H171L/I263G	36%	**39%**	–	61%

Only the variant RP/H171L/I263G gave >50% conversion of 2Me-Q (90% conversion, TON 1,800). Wild type $P450_{BM3}$ gave no conversion. The combination of H171L/I263G improved the oxidation activity (Table 5.11). The combination V78I/F87V slightly

enhanced C3,C4 oxidation, with RP/H171L/I263G/V78I/F87V showing 39% of **81** (TON 280). C5,C6 oxidation was promoted by I263G, with RP/H171L/I263G giving 77% of **82** (TON 1,390). The mutations F87A and A328I/L increased methyl hydroxylation, which was absent in THQ oxidation, up to 100% selectivity given by R19/F87A/A328L(I).

To conclude, 2-methyl substituent blocked N1-oxidation of Q, increased the yield of the 3-phenol (39% and TON 280 for 2Me-Q; 35% for Q with TON <100), and impaired the general oxidation of Q core in contrast with 8 out of 48 variants showing >50% conversion of Q itself. The mutation effects are summarised in Table 5.12. C2-methyl also influenced further oxidation of the Q core. Unlike the incubation of the 5,6-arene oxide **48** with RP/H171L/I263G which produced the 5-phenol **49** and the *cis*-diepoxide **51**, the incubation of the 5,6-arene oxide **82** with RP/H171L/I263G gave both 5- and 6-phenols due to the stabilisation of the C5-cation intermediate by C2-methyl. In addition, ring-opening of **82** could be engineered by altering the enzyme substrate pocket, since RP/H171L/I263G/A184I gave the hydrolysed product **86** which was absent with RP/H171L/I263G. Substituent effects on such activities need further investigation.

Table 5.12 Mutation effects on $P450_{BM3}$ oxidation of 2Me-Q.

Conversion	C3,C4	C5,C6	methyl
H171L/I263G	V78I F87V	I263G	F87A A328I/L

5.3.2 Oxidation of 6Me-Q

6Me-Q (**57**) was converted by the variant library (WY3/4, Appendix 3.14) to three major products; the *N*-oxide **89**, 5-phenol **90** and the benzylic oxidation product 9-hydroxy-6Me-Q **91** within 12 h incubation of the screening reactions (Figure 5.11). No C3,C4 or C7,C8 oxidation was found. Unlike Q or 2Me-Q, the 5,6-arene oxide of **57** was not directly observed. Within 12 h incubation for either screening or attempted preparative reactions,

the 5-phenol **90** was the only C5,C6-oxidation product, suggesting 6-methyl might accelerate NIH shift of the 5,6-arene oxide of 6Me-Q. Additionally, the further oxidation products **92** and **93** of this 5,6-arene oxide were observed as minor products in the prolonged incubation (24 h) with RT2/V78I/A184I/A330P. As with 2Me-Q oxidation, the benzylic alcohol **91** was oxidised to the aldehyde **94** and the carboxylic acid **95** after 24 h incubation with RP/H171L/I263G. Further oxidation products **92**–**95** were not observable in 12 h incubation. The NMR and MS data matched literature.[558,560–563]

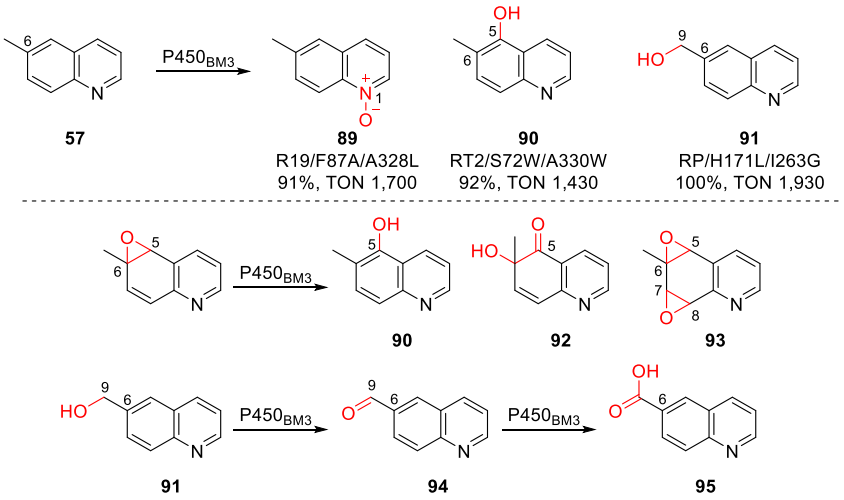


Figure 5.11 The reaction scheme of $P450_{BM3}$ oxidation of 6Me-Q (**57**).

Table 5.13 Conversion and product distribution of $P450_{BM3}$ oxidation of 6Me-Q (**57**).

Mutant	**Conv.**	**89**	**90**	**91**
K19/F87V	**73%**	**92%**	4%	4%
K19/F87V/A328V	**94%**	72%	–	28%
R19	33%	27%	73%	–
R19/F87A	37%	**100%**	–	–
R19/F87A/A328L	**94%**	91%	1%	9%
GVQ/I263G	0%	–	–	–
GVQ/I263G/A328L	61%	–	–	**100%**
RP/H171L/I263G	**97%**	–	–	**100%**
RT2	39%	26%	70%	–
RT2/S72W/A330W	78%	6%	**92%**	2%
KU3/A330P	36%	4%	**90%**	6%

Within the WY3/4 variant library, 13 out of 48 variants gave >50% conversion (TON >1,000). The wild type enzyme gave 20% conversion, including 14% of **89** and 86% of **90**. The mutations F87V, A328L/V and the combination H171L/I263G lifted the conversion to >90% (Table 5.13). N1 oxidation was enhanced by F87V/A, and the variants K19/F87V and R19/F87A gave 92% (TON 1,330) and 100% (TON 740) of **89**. C5,C6 oxidation was favoured by the mutations A330P/W in the F87-unmutated variants, with RT2/S72W/A330W giving the most of **90** (92%, TON 1,430). Methyl oxidation was increased by I263G and A328L to 100% of **91** (TON 1,220) given by GVQ/I263G/A328L.

In contrast with Q itself, 6Me-Q was slightly more active, although its product diversity decreased around the quinoline scaffold. C3,C4 or C7,C8 oxidation was absent in the oxidation of 6Me-Q. The prevalence of high selectivity (up to 100%) for C5,C6 and methyl oxidation showed that the 6-methyl substituent exposed the substituted part to Compound I, instead of shielding C5,C6 position. The mutation effects are summarised in Table 5.14.

Table 5.14 Mutation effects on $P450_{BM3}$ oxidation of 6Me-Q (**57**).

conversion	N1	C5,C6	Methyl
F87V H171L/I263G A328L/V	F87V/A	S72W V78I A330P/W	I263G

5.3.3 Oxidation of 8Me-Q

The C8-methyl substituent gave a different oxidation pattern. 8Me-Q (**72**) was oxidised by the variant library (WY1/2, Appendix 3.15) at C3,C4, C5,C6, C7,C8 and 8-methyl positions (Figure 5.12). Except for the 5-phenol **96**, the products were active substrates for $P450_{BM3}$. Similar to 2Me- and 6Me-Q oxidation, the benzylic alcohol **98** was oxidised to the carboxylic acid **102** by the RP variant in 48 h incubation of **72**. Ring-opening of the 7,8-arene oxide **97** gave 41% of the common NIH shift product **99** and 49% of the methyl

migration product **100** in the RT2/S72G/A330W-catalysed reaction with **97**, whereas the oxidation of **97** with RP/H171L/I263G gave only the diepoxide **101** without any evidence of the phenols **99** and **100**. This implied the ring-opening and NIH shift of the 7,8-arene oxide was catalysed by $P450_{BM3}$ instead of being a spontaneous process. The RT2/S72W/A330W variant gave 2% of **99**, 19% of **100** and 66% of **101** from the oxidation of **97**, indicating S72G favoured the ring-opening process while S72W shifted the preference towards C5,C6 oxidation of **97**. Moreover, further oxidation did occur within 6-hour incubation with the screening variant library. Therefore, control of the reaction time with each variant would maximise the yield of **73**, **97** and **98**. The NMR and MS data of known compounds matched literature.[269,274,564–566]

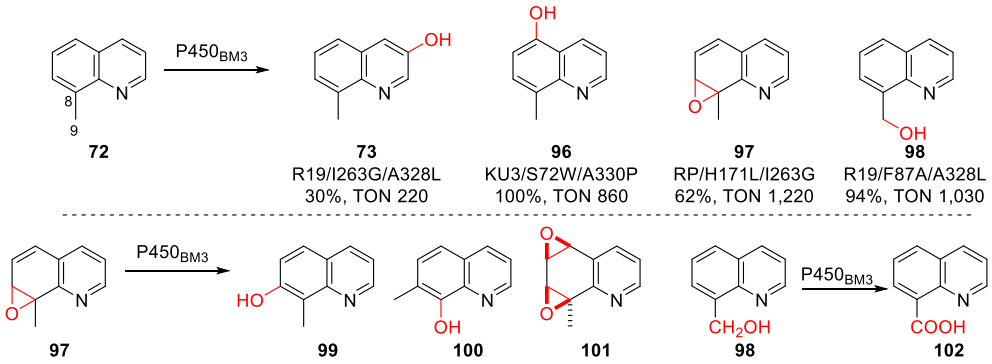


Figure 5.12 The reaction scheme of $P450_{BM3}$ oxidation of 8Me-Q (**72**).

Amongst the variant library, 12 out 48 variants showed >50% conversion (TON >1,000). The wild type enzyme gave no conversion. The mutations I263G and A328I/L/F improved the conversion significantly, with RP/H171L/I263G showing 98% conversion (TON 1,960, Table 5.15). C3,C4 oxidation was slightly increased by the I263G/A328L combination; the 2nd generation variant R19/I263G/A328L gave 30% of **73** (TON 220). As for C5,C6 oxidation, the combinations S72W/A330P(W) enhanced the formation of **96** when F87 was unmutated, and KU3/S72W/A330P gave 100% of **96** (TON 860). The I263G mutation favoured C7,C8 oxidation, with RP/H171L/I263G giving the most (62%, TON 1,220).

Methyl oxidation was substantially promoted by the mutations F87A and A328I/L/F, reaching 94% selectivity, TON 1,030, given by R19/F87A/A328L.

Table 5.15 Conversion and product distribution of $P450_{BM3}$ oxidation of 8Me-Q (**72**).

Mutant	**Conv.**	**73**	**96**	**97**	**98**
RP/H171L/I263G	**98%**	–	26%	**62%**	11%
K19/F87V	45%	–	28%	5%	20%
K19/F87V/A328I	**75%**	–	4%	6%	**81%**
R19	41%	–	63%	11%	0%
R19/F87A	21%	–	30%	4%	61%
R19/F87A/A328F	**68%**	–	4%	2%	89%
R19/F87A/A328L	**55%**	–	3%	3%	**94%**
R19/F87A/A328I	46%	–	0%	6%	89%
KU3/S72W/A330P	43%	–	**100%**	0%	0%
RT2/S72W/A330W	46%	–	**75%**	8%	5%
GVQ/I263G/A328L*	36%	8%	5%	5%	**81**%
R19/I263G/A328L*	37%	**30%**	35%	12%	22%

Table 5.16 Mutation effects on $P450_{BM3}$ oxidation of 8Me-Q (**72**).

conversion	**C3,C4**	**C5,C6**	**C7,C8**	**Methyl**
I263G A328I/L/F	I263G/A328L	F87-unmutated S72W/A330P(W)	I263G	F87A A328L/I/F

To sum up, 8Me-Q was activated at C3,C4, C5,C6, and C7,C8 as well as its methyl group. Like 6Me-Q, 5-phenol **96** was given instead of the 5,6-arene oxide, perhaps due to the stabilisation by the electron-donating 8-methyl substituent. Interestingly, the formation of the stable 7,8-arene oxide can be otherwise explained by its steric hindrance of this substituent inhibiting ring-opening, in stark contrast with the formation of the 5-phenol **90** predominantly observed for 6Me-Q whose 6-methyl should have offered similar effect to stabilise the 5,6-arene oxide intermediate. Hence, both mutations and substituents influenced C5,C6 and C7,C8 oxidation of Qs. It is interesting to notice that the 8-methyl group shielded the nitrogen atom but not the C7,C8 double bond for $P450_{BM3}$ oxidation.

Eventually, oxidation of the Q core at C7,C8 position was achieved by the introduction of 8-methyl substituent. The mutation effects on 8Me-Q oxidation are gathered in Table 5.16.

5.3.4 Overall perspective of the substituent effects on quinoline oxidation

The summary of $P450_{BM3}$ oxidation of quinolines (Table 5.17) showed that 2-methyl suppressed oxidation of Q significantly, whereas 6- and 8-methyls slightly improved the general oxidation activity for the current variant library. RP/H171L/I263G was the only variant showing >90% conversion for all methyl quinolines. Unlike the substituted THQs showing no benzylic oxidation, oxidation at benzylic methyl of 2Me-, 6Me- and 8Me-Qs was discovered as a predominant activity; the other dominant one for all methyl quinolines was C5,C6 oxidation. N1-oxidation was blocked by methyl at C2 and C8; 6-methyl suppressed C3,C4 oxidation; only 8Me-Q gave C7,C8 oxidation (up to 62%). The methyl group in Q core did not block the oxidation at its connecting carbon but steered the substrates to expose its adjacent carbons. For instance, oxidation of 6Me-Q gave high yield of the 5-phenol product from C5,C6 oxidation, and 8Me-Q gave 62% of the stable 7,8-arene oxide as the dominant product in the RP/H171L/I263G-catalysed reaction.

Table 5.17 The oxidation of quinoline and its derivatives by the 48 $P450_{BM3}$ variant libraries.

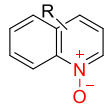
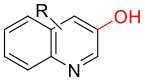
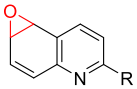
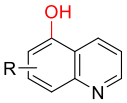
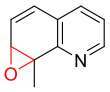
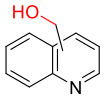
Substrate	No. of library variants ≥50% conv.	WT conv.	Oxidation activity
Q	8/48 (WY1/2)	0%	N1 (99%, TON 1,580) C3,C4 (35%, TON 40) C5,C6 (100%, TON 2,000)
2Me-Q	1/48 (WY3/4)	0%	C3,C4 (39%, TON 280) C5,C6 (77%, TON 1,390) Methyl (100%, TON 640)
6Me-Q	13/48 (WY3/4)	20%	N1 (91%, TON 1,700) C5,C6 (92%, TON 1,400) Methyl (100%, TON 1,930)
8Me-Q	12/48 (WY1/2)	0%	C3,C4 (30%, TON 220) C5,C6 (100%, TON 860) C7,C8 (62%, TON 1,220) Methyl (94%, TON 1,030)

Prolonged incubation (24–48 h) of these substrates with the library variants provided a spectrum of multi-functionalised products which were not discovered in all screening reactions of 8 h incubation: 3-phenols were further oxidised to form 3,6- and 3,7-diphenols; arene oxides were converted to diepoxides or the downstream phenols; hydroxymethyl products were further functionalised to their aldehydes and carboxylic acids. In addition, aromatic oxidation at C5,C6 yielded 5,6-arene oxides for Q and 2Me-Q but 5-phenols for 6Me-Q and 8Me-Q; C3,C4 oxidation gave only 3-phenols for Q, 2Me-Q and 8Me-Q; C7,C8 oxidation of 8Me-Q produced 7,8-arene oxide, the longer incubation of which gave the NIH product 7-phenol and the 8-methyl-migration product 8-phenol (roughly in 1 : 1 ratio) with the particular variant RT2/S72G/A330W. This observation confirmed that ring-opening of arene oxides was influenced by both the intrinsic property of substrate (*e.g.* the directing effect of the methyl substituent) and the mutations in each $P450_{BM3}$ variant.

The mutation effects on Q oxidation are summarised in Table 5.18. I263G and its combination H171L/I263G, along with bulky mutations at A328, enhanced the oxidation activity for all Qs. F87A/A328I favoured N1-oxidation of Q and 6Me-Q, and shifted the preference to methyl oxidation for 2Me-Q and 8Me-Q; R19/F87A/A328I gave ≥98% of *N*-oxides of Q and 6Me-Q, and ≥89% of the hydroxymethyl products of 2Me-Q and 8Me-Q. The I263G/A328L combination showed enhancement for C3,C4 oxidation of Q and 8Me-Q (35% and 30% given by R19/I263G/A328L, respectively), whereas V78I/F87V/I263G improved C3,C4 oxidation up to 39% for 2Me-Q given by RP/H171L/I263G/V78I/F87V. RT2/S72W/A330W produced ≥75% of 5-phenols of 6Me-Q and 8Me-Q, while the RP/H171L/I263G variant gave >75% of 5,6-arene oxides of Q and 2Me-Q. RP/H171L/I263G also gave the most of the 7,8-arene oxide for 8Me-Q (62%) and the hydroxymethyl product for 6Me-Q (100%). The diversity in oxidation patterns of 2Me-/6Me-/8Me-Qs and Q by RP/H171L/I263G suggested that 2-methyl was not as effective in

reorienting the binding of Q moiety inside the active site as 6- and 8-methyls. The Q/2Me-Q/6Me-Q/8Me-Q-bound crystal structures of RP/H171L/I263G, along with the ligand-protein docking experiments between Qs and RP/H171L/I263G, will reveal more information on how to diversify the oxidation of quinoline core, especially for creating the new oxidation activity at C7,C8, by both substituent and protein engineering.

Table 5.18 The mutation effects on $P450_{BM3}$ oxidation of quinoline and its methyl derivatives.

 R19/F87A/A328I Q: 98% 6Me-Q: 100%	 R19/I263G/A328L Q: 35% 8Me-Q: 30% RP/V78I/F87V/H171L/I263G 2Me-Q: 39%	 RP/H171L/I263G Q: 79% 2Me-Q: 77%	 RT2/S72W/A330W 6Me-Q: 92% 8Me-Q: 75%	 RP/H171L/I263G 8Me-Q: 62%	 R19/F87A/A328I 2Me-Q: 100% 8Me-Q: 89% RP/H171L/I263G 6Me-Q: 100%

S	Conversion	N1	C3,C4	C5,C6	C7,C8	Methyl
Q	V78I I263G A328I/L	F87A A328L/I	V78I I263G/A328L	V78I I263G A330P	–	–
2Me-Q	H171L/I263G	–	V78I F87V	I263G	–	F87A A328I/L
6Me-Q	F87V H171L/I263G A328L/V	F87V/A	–	S72W V78I A330P/W	–	I263G
8Me-Q	I263G A328I/L/F	–	I263G/A328L	F87-unmutated S72W/A330P(W)	I263G	F87A A328L/I/F

Oxidation of 3-hydroxy-Qs showed that the V78I/F87V combination favoured the formation of 3,6-diphenols given by RP/V78I/F87V for 3-hydroxy-Q and by RP/H171L/I263G/V78I/F87V for 3-hydroxy-2Me-Q, whereas R19/I263G/A328L containing the I263G/A328L couplet only gave 3,7-diphenols for 3-hydroxy-6Me-Q and 3-hydroxy-8Me-Q. Multi-substituent effects on oxidation of the Q core can be further studied based on this observation. To complete the full landscape of substituent effects on Q oxidation, 3-/4-/5-/7-methyl quinolines should also be tested with the current variant library, although all sites of Q core have already been proven oxidisable. Retarding or

accelerating the ring-opening process of the arene oxides and altering the enzymatic regio-control of NIH shift/methyl migration will also be possible exploring directions.

5.4 Summary

In contrast with $P450_{BM3}$ oxidation of THQ (Figure 5.13) which gave C2 oxidation (100%, favoured by the mutations F87A/V) and C5,C6 oxidation (85% given by R19/I263G, favoured by the I263G/A328L couplet with unmutated 87F), the introduction of 2-/6-methyls improved C5,C6 oxidation up to 100% selectivity of 6-hydroxy-2Me-THQ given by R19/A184I/A328L and gave only C2 oxidation for 6Me-THQ across the variant library. The bulky and electron rich 6-methoxy substituent gave rise to a new amination activity, N1–C8' coupling, favoured by I263G/A and unmutated 87F with up to 90% selectivity given by R19. 8-Methyl made little difference in product profile of THQ. The selectivity of each product from C2 oxidation of THQ (aromatisation, C2,C3-oxidation, lactam formation and dimerisation) was not improved after the introduction of methyl and methoxy substituents. Methyl group of THQs was blocked for any oxidation activity.

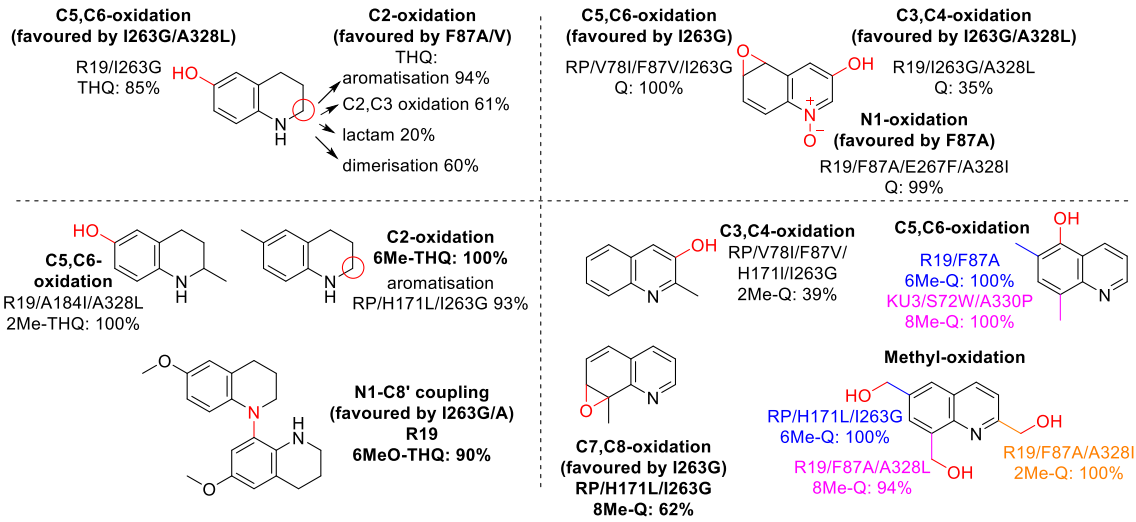


Figure 5.13 The summary of $P450_{BM3}$ oxidation of THQs and Qs.

As for oxidation of Q itself (Figure 5.13), showing activity at N1 (99% of *N*-oxide given by R19/F87A/E267F/A328I), C3,C4 (35% of 3-phenol given by R19/I263G/A328L) and

C5,C6 (100% of 5,6-arene oxide given by RP/V78I/F87V/I263G), 2-methyl was found to show higher selectivity of 3-hydroxy-2Me-Q (39% by RP/V78I/F87V/H171L/I263G); 6- and 8-methyl substituents gave 5-phenols instead of the 5,6-arene oxides up to 100% selectivity by R19/F87A and KU3/S72W/A330P from oxidation at C5,C6; the introduction of 8-methyl led to C7,C8 oxidation with RP/H171L/I263G giving the most of 7,8-arene oxide of 8Me-Q (62%); methyl oxidation of 2Me-, 6Me- and 8Me-Qs with up to 100% selectivity was given by several $P450_{BM3}$ variants (Figure 5.13).

Comparing oxidation of THQ derivatives and methyl quinolines, N1-oxidation was observed for Q and 6Me-Q and favoured by F87A, and 6MeO-THQ (N1–C8' coupling) was promoted by I263G/A; C2 oxidation was common for THQs and favoured by F87A/V but not shown in Q oxidation; oxidation at C3, C4, C7,C8 and methyl was absent for THQs but all observable in oxidation of Qs; no arene oxide product was formed in THQ oxidation, whereas 5,6-/7,8-arene oxides and their rearrangement product, the phenols, were given in biotransformation of Qs and could be engineered by mutating the residues S72, I263 and A330. The sp^2 nitrogen atom in Qs, which is more sterically rigid and less electron rich than the nitrogen atom of THQs, might be the crux of higher oxidation diversity but lower activity. As 41% of the common NIH-shift product 7-hydroxy-8-methylquinoline and 49% of the methyl-migration product 7-methyl-8-quinolinol was given by RT2/S72G/A330W in oxidation of 7,8-arene oxide of 8Me-Q but 2% and 19% given by RT2/S72W/A330W, engineering $P450_{BM3}$ in combination with the strategy of enhanced delocalisation of the nitrogen atom of THQ core might even produce the unfavoured phenols (5-/7-phenols of THQ). Therefore, in Chapter 6, a handful of protecting groups are introduced to block/delocalise the nitrogen atom of THQ, exploring for oxidation at C3, C4, and C7,C8 of THQ core, which remained inaccessible in $P450_{BM3}$ biotransformation after the introduction of methyl and methoxy substituents.

Chapter 6 The role of protecting groups in $P450_{BM3}$ oxidation of cyclic amines

6.1 Introduction

The results in Chapters 4 and 5 showed that the P450$_{BM3}$-catalysed oxidation of THQs was restricted to the activated C2 (Nα) or C5,C6 positions, probably due to electron-donating property of the lone pair on the nitrogen atom. No oxidation at C3, C4 or C7,C8 was observed. Therefore, the effect of modifying groups that delocalise this lone pair on enzymatic activity and selectivity was investigated in this chapter. Common protecting groups with a carbonyl or sulfonyl group, *e.g.* acyl (Ac), *t*-butoxycarbonyl (Boc), mesyl (Ms), tosyl (Ts), and isopropylsulfonyl (Ips), would reduce the activating/directing effect of the nitrogen while altering the steric demand and the hydrogen-bonding characteristics of the substrate. This combination of substrate engineering with enzyme evolution might lead to different product profiles. *N*-Boc pyrrolidine and piperidine were also explored here.

Previous reports on P450-catalysed oxidation of simple cyclic amines, such as azetidines, pyrrolidines and piperidines, were mostly based on P450pyr (Figure 6.1 A).[423–426] Li *et al.* found that protected cyclic amines were hydroxylated by P450pyr at non-activated C–H bonds, *e.g.*, up to 98% yield and 98% *ee* to 3*R*-hydroxy- and 96% *ee* to 3*S*-hydroxy-pyrrolidines were obtained after the introduction of "docking/protecting" groups (Bz, Cbz, phenoxycarbonyl, Boc, Ac and methoxycarbonyl) to the nitrogen atom of pyrrolidine.[468] P450$_{BM3}$ has been engineered to catalyse intramolecular amination of *N*-substituted THIQ, affording a novel synthetic pathway to the imidazolidine-4-one core (Figure 6.1 B).[345]

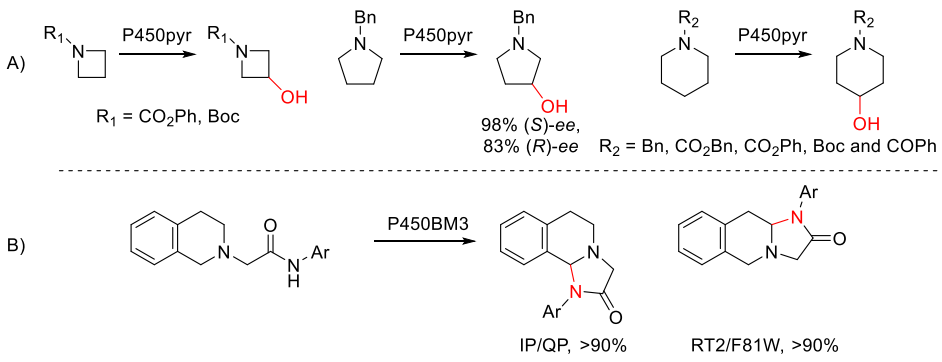


Figure 6.1 Previous research on P450 oxidation of simple cyclic amines.[345,423–426]

Protecting group engineering has been proved viable for high regio- and enantioselectivity of remote functionalisation of pyrrolidine. The work described in this chapter takes this systematic approach, changing both the substrate and the enzyme, in order to explore regiodiversity control in $P450_{BM3}$ catalysis. One major objective was to discover oxidation at positions other than C2 and C5,C6 of THQ. With regards to oxidation of the aromatic ring, if the arene oxide mechanism was followed, initial arene oxide formation at the C5,C6 and C7,C8 bonds would be expected to give 6-hydroxy- and 8-hydroxy-THQs. Formation of the less favoured 5- or 7-hydroxy derivatives would indicate a role for active site residues in the epoxide ring opening process,[436] or a change in mechanism to, for example, direct hydroxylation relying only on close proximity of the C–H bond to the ferryl oxygen.

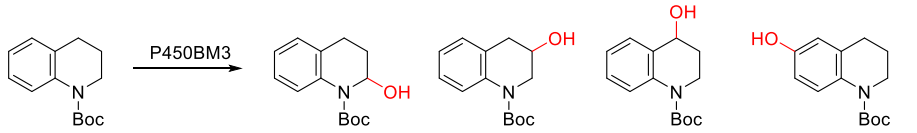
6.2 $P450_{BM3}$ oxidation of the protected THQs

N-Boc, *N*-Ac, *N*-Ts, *N*-Ms and *N*-Ips-THQs were synthesised according to general protocols described in Chapter 2. Due to the low solubility of *N*-Ts, *N*-Ms and *N*-Ips-THQ in aqueous solution, the final concentration of substrates in screening reactions was lowered to 1 mM. The addition of cyclodextrin into each reaction was tested but showing no improvement. Low solubility hampered preparative scale reactions with *N*-Ts-THQ, but *N*-Ms- and *N*-Ips-THQs were sufficiently soluble for product purification and characterisation.

6.2.1 Oxidation of *N*-Boc-THQ

The screening reactions of *N*-Boc-THQ (**103**) were carried out using 2 mM substrate with 1 μM enzyme; total conversion of substrate corresponded to a TON of 2,000. The presence of the bulky Boc group did not retard substrate oxidation; only the wild type and 4 variants gave <50% conversion (TON <1,000) of *N*-Boc-THQ. Preparative scale reactions with R19/F87A/A328G/P329G/A330G, RP/H171L/I263G and I263G gave the C2, C3, C4 and C5,C6 oxidation products **104**–**107** (Table 6.1). C7,C8 oxidation was unidentified.

Table 6.1 Conversion and product distribution of $P450_{BM3}$ oxidation of **103**.



N-Boc-THQ **103**

104 R19/F87A/I263G 85%, TON 1,700

105 R19/A330W 6%, TON 100

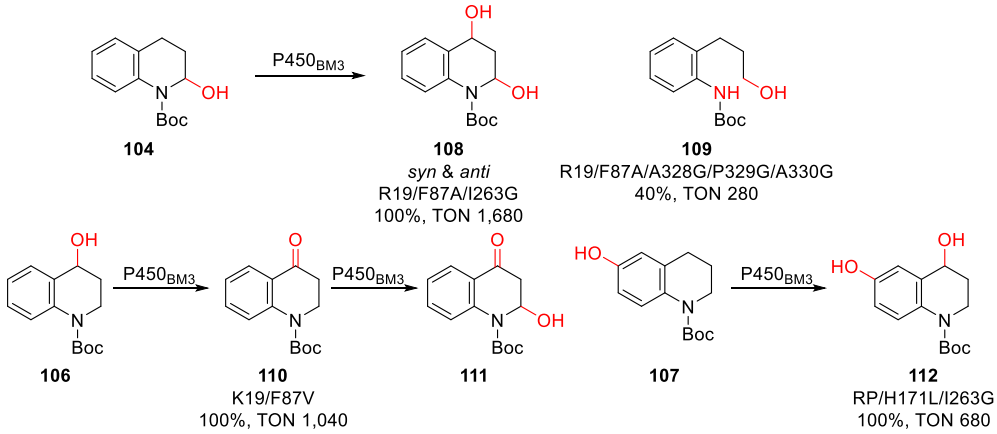
106 RT2/V78I/A184I/A330P 100%, TON 2,000

107 GVQ/V78L/I263G 44%, TON 860

Mutant	**Conv.**	**Selectivity**			
		2-OH: 104	**3-OH: 105**	**4-OH: 106**	**6-OH: 107**
R19	98%	2%	–	98%	–
R19/A330W	81%	9%	**6%**	81%	4%
R19/F87A	100%	47%	–	53%	–
R19/F87A/A184I	100%	82%	–	18%	–
R19/F87A/I263G	100%	**85%**	–	15%	–
K19/F87A/I263G	100%	67%	–	29%	4%
R19/F87A/A328G/P329G/A330G	99%	51%	5%	44%	–
KU3/A184I/A330P	48%	–	–	**100%**	–
RT2/V78I/A184I/A330P	100%	–	–	**100%**	–
I263G	83%	–	–	75%	25%
RP/H171L/I263G	100%	–	–	66%	34%
GVQ/I263G	94%	15%	1%	52%	31%
GVQ/V78L/I263G	98%	8%	2%	47%	**44%**

Clearly, introduction of the Boc group had diversified the product profile compared to THQ which only showed oxidation at C2 and C5,C6. The most common products across the library were 2-hydroxy-*N*-Boc-THQ (**104**, 85% with R19/F87A/I263G, TON 1,700) and 4-hydroxy-*N*-Boc-THQ (**106**, 100% with RT2//V78I/A184I/A330P, TON 2,000). The wild type enzyme also gave 100% of the C4 oxidation product **106** but with a lower TON of 400. Unlike unprotected THQ, the C2 alcohol was stable to iminium formation, and products from subsequent reactions of an iminium species, *e.g.* dimer formation, were not observed. This was consistent with the delocalisation of the nitrogen lone pair into the protecting group, thus disfavouring loss of the C2 alcohol group. The GVQ/V78L/I263G mutant showed the highest selectivity (44%) for 6-hydroxy-*N*-Boc-THQ, **107** (TON 860), and 3-hydroxy-*N*-Boc-THQ (**105**) was formed at 6% (TON 100) by the R19/A330W variant.

Table 6.2 Conversion and production distribution of further oxidation of *N*-Boc-THQ (**103**).



Mutant	**conv.**	*6 h*	**104**	*16 h*	**104**	**108**	**109**
R19/F87A/A328G/P329G/A330G	99%		51%		16%	21%	14%
R19/F87A/A184I	100%		82%		0%	82%	–
R19/F87A/I263G	100%		85%		0%	84%	1%
Mutant	**conv.**	*6 h*	**106**	*16 h*	**106**	**110**	
K19/F87V	100%		90%		43%	47%	
Mutant	**conv.**	*6 h*	**107**	*16 h*	**107**	**112**	
GVQ/V78L/I263G	98%		44%		11%	33%	
RP/H171L/I263G	100%		34%		0%	34%	

Longer reaction times (16 h *vs*. 6 h) afforded an assortment of further oxidation products (Table 6.2). The time-course of the reaction with R19/F87A/A328G/P329G/A330G showed that the 2-hydroxy product **104** was further converted to 2,4-dihydroxy-*N*-Boc-THQ **108** (*syn* : *anti* = 7.5 : 10 by ^{1}H NMR, 21% regioselectivity, TON 420) and the ring-opening alcohol **109** (14%, TON 280), which was likely formed by ring opening of the carbinolamine **104** and subsequent reduction of the aldehyde by the reductase domain of P450$_{BM3}$. The mutants R19/F87A/A184I and R19/F87A/I263G fully converted **104** to **108** showing ≥99% selectivity (82% and 84% in the prolonged incubation of **103**, TON 1,640 and 1,680 respectively). The benzylic alcohol **106** was oxidised to the ketone **110** by most library variants (100% selectivity, TON 1,040 given by K19/F87V) and the ketone **110** could also be further oxidised to the 2-hydroxy-4-ketone **111** after 24 h incubation, whilst the 6-hydroxy derivative **107** (44%, TON 860, 98% conversion) was only oxidised at the

benzylic position to give 4,6-dihydroxy-*N*-Boc-THQ, **112** (100% selectivity, TON 680 given by RP/H171L/I263G). Interestingly, the benzylic C4-alcohol did not give **112**.

The mutation effects on oxidation of **103** are summarised in Table 6.3. Variants containing the A184I/A330P couplet without a mutation at F87 favoured C4 oxidation (100% **106**, TON 2,000). The F87A mutation and its combination with A184I and I263G promoted C2 oxidation, with up to 85% of the C2-alcohol **104** for the R19/F87A/I263G variant (Table 6.1). The bulky substitutions V78L and A330W seemed to play a role in generating the C3-alcohol **105**. Combination of V78L/W/F, A328L/W/F, P329L/W/F and A330W/L/F added into the base variant R19 will be worth preparing to obtain higher selectivity of **105**. C5,C6 oxidation was favoured by I263G and slightly improved by V78L. However, since 6-hydroxy-THQ was readily formed with 85% selectivity and TON 1,700 with THQ itself, the lower selectivity is not a significant issue. Overall, the results showed that Boc-protection of THQ led to different regiodiversity of oxidation, *e.g.* high selectivity for C4 oxidation compared to none for THQ and the first observation of C3 oxidation. Although no C7,C8 oxidation was discovered, other protecting groups could have different effects.

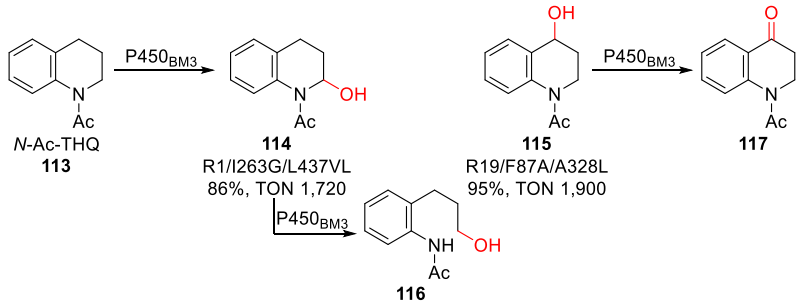
Table 6.3 Mutation effects on $P450_{BM3}$ oxidation of *N*-Boc-THQ (**103**).

C2	C3	C4	C5,C6
F87A A184I I263G	V78L A330W A328G/P329G/A330G	A184I/A330P	V78L I263G

6.2.2 Oxidation of *N*-Ac-THQ

Under the same screening condition used for the Boc-protected form, *N*-Ac-THQ (**113**) was found to be oxidised by $P450_{BM3}$ at C2 and C4, whilst the wild type was inactive (Table 6.4). R19/F87A-based variants showed the highest selectivities; R19/F87A/I263G formed 64% (TON 630) of 2-hydroxy-*N*-Ac-THQ (**114**) and R19/F87A/A328L gave (95%, TON 1,900) of 4-hydroxy-*N*-Ac-THQ (**115**).

Table 6.4 The conversion and product distribution of 16-hour $P450_{BM3}$ biotransformation of *N*-Ac-THQ.



Mutant	Conv.	Selectivity		Further oxidation (conversion)	
		2-OH: 114	4-OH: 115	116	117
GVQ	89%	8%	92%	90%	21%
GVQ/A330W	95%	6%	94%	92%	22%
K19/F87V	95%	5%	95%	100%	35%
R19	47%	13%	87%	83%	4%
R19/F87A	100%	13%	87%	100%	11%
R19/F87A/I263G	49%	64%	36%	55%	–
I263G	93%	29%	71%	80%	3%
RP/H171L/I263G	89%	31%	69%	100%	5%
R19/F87I	44%	7%	93%	56%	7%
R19/F87I/L437LV	17%	31%	69%	48%	10%
R1/I263G	100%	49%	51%	23%	6%
R1/I263G/L437LV*	100%	68%	32%	2%	9%
R1/I263G/L437VL*	100%	**86%**	14%	13%	16%

As with *N*-Boc-THQ, the C2 alcohol was stable during screening for 8 h. Prolonged reactions only gave the ring-opening alcohol **116** from **114**, and the C4-ketone **117** from **115**. No C5,C6 oxidation, which was prevalent for THQ itself, was found.

The acyl derivative was not as active a substrate as the Boc analogue; only half of the variants gave >50% conversion. The F87A/I263G combination and the L437LV insertion mutation tended to favour C2 oxidation (Table 6.5). The addition of L437LV and L437VL into R1/I263G pushed the selectivity of **114** up to 86% (TON 1,720 given by the 2nd generation variant R1/I263G/L437VL in Table 6.4). Variants without an F87 mutation, or those with F87V/I, gave more of the benzylic oxidation product **115** (Table 6.5). However, these products were formed with high selectivity and TON with the Boc-protected form,

and no new oxidation sites were obtained. Therefore, oxidation of the *N*-acyl derivative was not investigated further.

Table 6.5 The mutation effects on $P450_{BM3}$ oxidation of *N*-Ac-THQ (**113**).

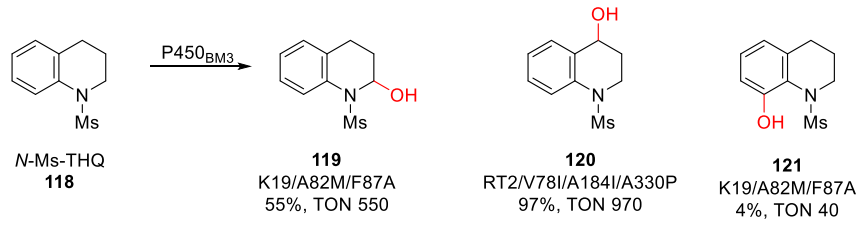
conversion	C2	C4
F87A/V	F87A/I263G L437LV L437VL	F87V/I

6.2.3 Oxidation of *N*-Ms-THQ

On account of the low solubility of the mesyl derivative *N*-Ms-THQ (**118**), screening reactions were carried out with 1 mM substrate and 1 μM enzyme. C2 and C4 oxidation to **119** and **120** were by far the most common activity (Table 6.6). The wild type gave only the 4-hydroxy derivative **120** at 11% conversion. Due to the low solubility, preparative scale reactions were conducted by sequential addition of 1 mM aliquots of the substrate at 4-hour intervals. Under these conditions, 8-hydroxy-*N*-Ms-THQ, **121**, was purified as a minor product from the reaction with K19/F87A/A82M. This was the first evidence for C7,C8 oxidation of the THQ core. Although 6MeO-THQ showed N1–C8' coupling (amination) due to the electron-donating property and bulky size of 6-methoxy group, the coupling products were formed via either double HAT from the NH groups or electron transfer at C8, instead of direct oxygenation at C7,C8 double bond.

Within the screening library, 34 out of 48 variants converted more than half of the substrate (TON >500). F87A/V enhanced the activity (Table 6.6), while A82M/F87A and F87A/I263G favoured C2 oxidation to **119**, which mirrored the pattern for *N*-Ac-THQ. Unfortunately, the 8-hydroxy derivative **121** was not readily detectable at screening scale, making it difficult to draw conclusions on mutations that promoted its formation.

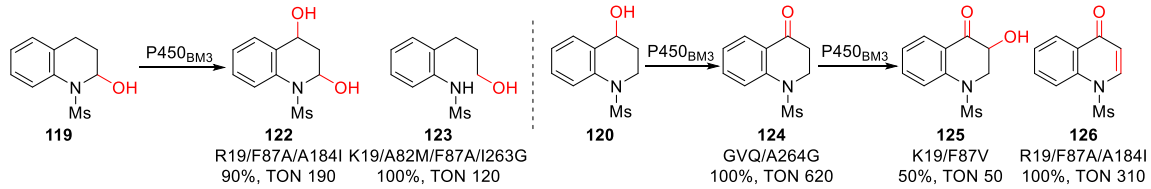
Table 6.6 Conversion and product distribution of $P450_{BM3}$-catalysed oxidation of *N*-Ms-THQ (**118**).



N-Ms-THQ **118** | **119** K19/A82M/F87A 55%, TON 550 | **120** RT2/V78I/A184I/A330P 97%, TON 970 | **121** K19/A82M/F87A 4%, TON 40

Mutant	**Conversion**	**Selectivity**	
		119	**120**
GVQ	**100%**	8%	**92%**
K19/F87V	**100%**	11%	**89%**
RP/F87V	**93%**	7%	**93%**
K19/F87A/I263G	22%	**70%**	30%
K19/F87A/A82M	100%	55%	41%
K19/F87A/A82M/I263G	33%	**74%**	26%
R19/F87A	**100%**	23%	73%
R19/F87A/I263G	57%	**66%**	34%

Table 6.7 Conversion and product distribution of further oxidation of *N*-Ms-THQ by $P450_{BM3}$.



119 | **122** R19/F87A/A184I 90%, TON 190 | **123** K19/A82M/F87A/I263G 100%, TON 120 | **120** | **124** GVQ/A264G 100%, TON 620 | **125** K19/F87V 50%, TON 50 | **126** R19/F87A/A184I 100%, TON 310

Mutant	**Conv.**	**119**	**122**	**123**	**120**	**124**	**125**	**126**
	24 h				*36 h*			
R19/F87A	100%	5%	6%	12%	68%	6%	–	–
R19/F87A/A184I	100%	2%	**19%**	2%	15%	31%	–	**31%**
K19/F87V	100%	0%	11%	–	30%	49%	**5%**	**5%**
K19/A82M/F87A	100%	10%	17%	27%	36%	5%	–	–
K19/A82M/F87A/I263G	33%	39%	–	35%	26%	–	–	–
GVQ/A264G	100%	0%	7%	–	31%	61%	–	1%

Longer reaction times resulted in a variety of further oxidation products (Table 6.7). The C2-alcohol **119** was oxidised to the 2,4-diol **122** and the ring-opening alcohol **123**, and the C4-alcohol **120** to the ketone **124** (100% selectivity from **120** for all variants, TON up to 620 given by GVQ/A264G). The product distribution in Table 6.5 showed that the A184I

mutation favoured the formation of **122** to **123** (19% and 2%, TON 190 and 20 given by R19/F87A/A184I), while the I263G mutation promoted **123** (100% from **119**, TON 120 given by K19/A82M/F87A/I263G). Interestingly, this ketone was found to be further oxidised with some variants. In the oxidation of *N*-Ms-THQ (**118**) with the variant R19/F87A/A184I, the C2–C3 desaturation product quinolin-4(*1H*)-one **126** constituted 31% of the products (TON 310) after 36-hour incubation. K19/F87V gave 5% of a new product, the C3-hydroxylation product **125** (TON 50), and 5% of **126** in oxidation of **118**.

The similarity between the activity pattern of *N*-Ms-THQ (Table 6.8) and *N*-Ac-THQ, which were different from that of *N*-Boc-THQ, suggested that the size of the protecting group had an important role in product activity. Even though no big change was found and further work are required, the evidence of C7,C8 oxidation and the oxidation of the ketone **124** at the C3 position supported the substrate engineering strategy.

Table 6.8 The mutation effects on $P450_{BM3}$ oxidation of *N*-Ms-THQ (**118**).

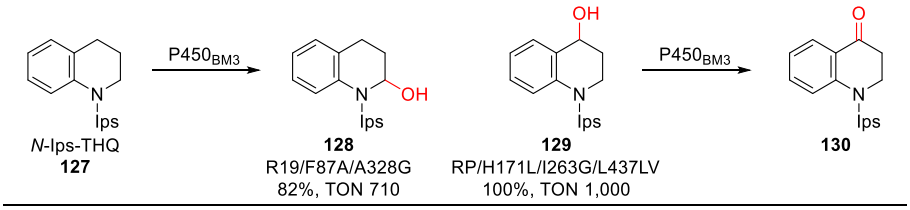
Conversion	C2	C4	C7,C8
F87A/V	A82M/F87A F87A/I263G	F87V	A82M/F87A

6.2.4 Oxidation of *N*-Ips-THQ

The isopropylsulfonyl (Ips) group is bulkier than mesyl and its use as a protecting group was explored against the 48-variant library (WY5/6, Appendix 3.19) at 1 mM substrate concentration. However, C2 and C4 were the only two sites oxidised (Table 6.9). The wild type enzyme was inactive. Further oxidation of the C4 alcohol was found to form the C4-ketone **130**. Within the screening library, 19 out of 48 variants showed >50% conversion (TON >500). F87A promoted enzymatic activity and biased selectivity slightly towards C2. The effect of side chain volume at residue 328 in R19/F87A was instructive, with A328G favouring C2 oxidation while A328L/F enhanced C4 oxidation. There were also activity-

enhancing combinations, *e.g.* in the RP/H171L/I263G series, the insertion mutation L437LV improved the enzymatic activity without any change for the oxidation site of the substrate. These effects and trends were valuable information for enzyme engineering but it seemed that Ips was not bulky enough to induce C3 and C7,C8 oxidation.

Table 6.9 The conversion and product distribution of $P450_{BM3}$ oxidation of *N*-Ips-THQ (**127**).



Mutant	Conversion	Selectivity	
		128	**129**
R19	30%	–	100%
R19/F87A	61%	28%	72%
R19/F87A/A184I	100%	43%	57%
R19/F87A/I263G	93%	17%	83%
R19/F87A/A328G	87%	**82%**	18%
R19/F87A/A328L	99%	1%	**99%**
R19/F87A/A328F	100%	15%	85%
RP/H171L/I263G	33%	–	**100%**
RP/H171L/I263G/L437LV	100%	–	**100%**

conversion	C2	C4
F87A, A184I, I263G, L437LV	F87A/A184I F87A/A328G	I263G F87A/A328L/F

6.2.5 The role of protecting group in $P450_{BM3}$ oxidation of THQ

Substrate engineering of THQ by the use of different protecting groups provided oxidation at positions not accessible with unprotected THQ, in particular high selectivity for C4 oxidation, and evidence of C3 and C7,C8 oxidation products (Figure 6.2). The C2-alcohol was also stabilised to iminium formation and the subsequent reactions found with THQ. Unprotected THQ and the 2-, 6- and 8-methyl-substituted derivatives were oxidised at C2 and C5,C6 (Chapters 4 & 5). Combination of protecting group engineering and mutations at residues A82, F87, I263, A328 and A330 led to different regiochemistries, including low

selectivity for C3 and C7,C8 oxidation. The introduction of bulky amino acids W/Y/F/L/I/H/M at these sites might improve the regioselectivity for C3 and C7,C8 oxidation. The enantioselectivity for C3 and C4 oxidation will also be of interest.

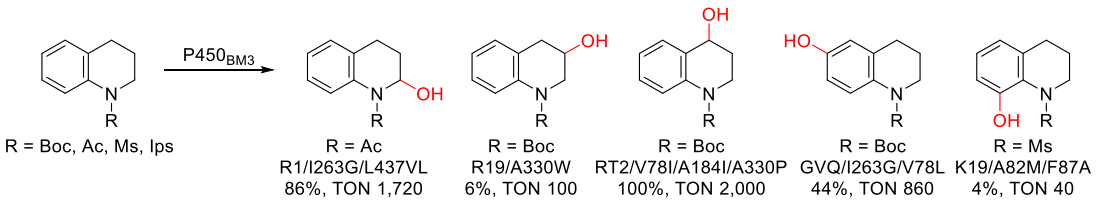


Figure 6.2 General reaction scheme of $P450_{BM3}$ oxidation of *N*-protected-THQs.

6.3 $P450_{BM3}$ oxidation of the protected THIQs

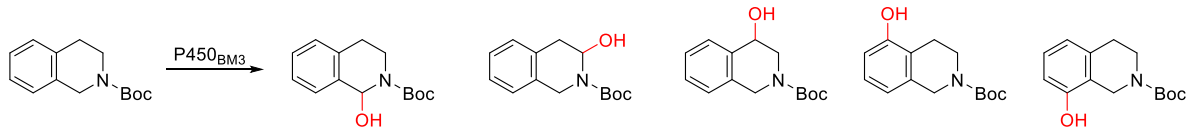
In contrast to THQ, all methylene C–H bonds in THIQ are activated and should be oxidised if they are accessible to the ferryl oxygen. Unprotected THIQ was tested with the variant library. However, unlike with THQ, difficulties were encountered, both in the extraction of organics from the reaction mixtures and GC analysis. Therefore, oxidation of the unprotected substrate was not explored further, focusing instead on the Boc-, Ac-, Ts-, Ms- and Ips-protected forms. As found with THQ, *N*-Ts-THIQ was insoluble in aqueous solution to show any conversion. The other four THIQ derivatives showed interesting product diversity and selectivity variations with the $P450_{BM3}$ variant library.

6.3.1 Oxidation of *N*-Boc-THIQ

Screening of *N*-Boc-THIQ (**131**) for oxidation revealed that it was a good substrate for the variant library, with only 6 variants giving less than 50% conversion (TON <1,000) using 2 mM substrate and 1 μM enzyme. Both aliphatic and aromatic positions were accessible for oxidation to form 1-, 3-, 4-, 5- and 8-hydroxy-*N*-Boc-THIQ (**132**–**136**, Table 6.10). The benzylic, Nα carbon, C1, is the most activated methylene group in **131** but, interestingly, few variants showed a high percentage of oxidation at this position. The F87I mutation and the combinations F87A/A82M and F87A/A328G showed preference for C1 oxidation; the

highest selectivity was 63% (TON 1,200) of **132** given by K19/F87A/A82M. The side-chain volume at residue 328 had a dominant effect, switching the preference of R19/F87A/A328G from 54% C1 oxidation giving **132** to 94% selectivity of the R19/F87A/A328L variant for C4 oxidation to give **134** (TON 1,800). Notably, the R19/F87A/A328G variant also formed 34% of the C3 (Nα) oxidation product 3-hydroxy-(**133**) compared to 21% for R19/F87A. The A264G mutation increased the selectivity for **133** to 51% with R19/F87A/A264G/A328G. The addition of A82M and I263G also promoted **133** by the GVQ base variant. Combinations of A184I, I263A and A328L were required for aromatic oxidation but they led to low conversions; R19/I263A/A328L gave 21% of 5-hydroxy-(**135**) and 33% of 8-hydroxy-(**136**) at just 23% conversion.

Table 6.10 The conversion and product distribution of $P450_{BM3}$ oxidation of *N*-Boc-THIQ (**131**).



131 | **132** K19/A82M/F87A 63%, TON 1,130 | **133** R19/F87A/A264G/A328G 51%, TON 960 | **134** R19/F87A/A328L 94%, TON 1,800 | **135** R19/A184I/A328L 21%, TON 100 | **136** R19/A184I/A328L 33%, TON 150

Mutant	**Conversion**	**Selectivity**				
		1-OH: 132	**3-OH: 133**	**4-OH: 134**	**5-OH: 135**	**8-OH: 136**
K19/A82M/F87A	90%	**63%**	1%	36%	–	–
K19/A82M/F87A/E267F	88%	**63%**	1%	35%	–	–
K19/A82M/F87A/I263G	57%	**63%**	7%	30%	–	–
GVQ	98%	32%	6%	62%	–	–
GVQ/I263G	98%	29%	28%	43%	–	–
GVQ/A82M/I263G	53%	37%	39%	24%	–	–
R19/F87A/A264G/A328G	94%	35%	**51%**	14%	–	–
R19/F87A/A328G	98%	54%	34%	12%	–	–
R19/F87A	100%	23%	21%	56%	–	–
R19/F87A/A328L	96%	2%	4%	**94%**	–	–
R19/A330W	89%	14%	3%	**82%**	1%	–
RP/H171L/I263G	81%	15%	5%	76%	2%	1%
R19/F87I/L437LV	43%	18%	7%	73%	2%	1%
R19	100%	38%	3%	58%	-	1%
R19/F87I	99%	45%	2%	54%	-	-
R19/A328L/I263A	23%	21%	3%	22%	**21%**	**33%**
R19/A328L/A184I	8%	47%	-	28%	7%	18%

Aromatic oxidation of *N*-Boc-THIQ could proceed via the 5,6-, 6,7- and 7,8-arene oxides (Figure 6.3). Upon epoxide ring-opening, the most stable carbocations would have the positive charge on the ring junction carbons. Therefore, both of the phenols from each arene oxide should be formed in equal amount if the enzyme does not affect ring opening. If all three arene oxides were formed in equal proportions, twice the amount of the 6- and 7-phenols ought to be formed compared to the 5- and 8-phenols, which was contradictory to the experimental observation. The discovery of the 5- and 8-phenol as the only aromatic oxidation products indicated that either the ring opening of the arene oxide intermediate was biased by the enzyme, *e.g.* stabilisation of the secondary carbocations by a side chain, or the mechanism was more akin to hydrogen atom abstraction, or the oxygen atom insertion step was more concerted and the site of oxidation was determined by proximity of the C–H bond to the ferryl oxygen.

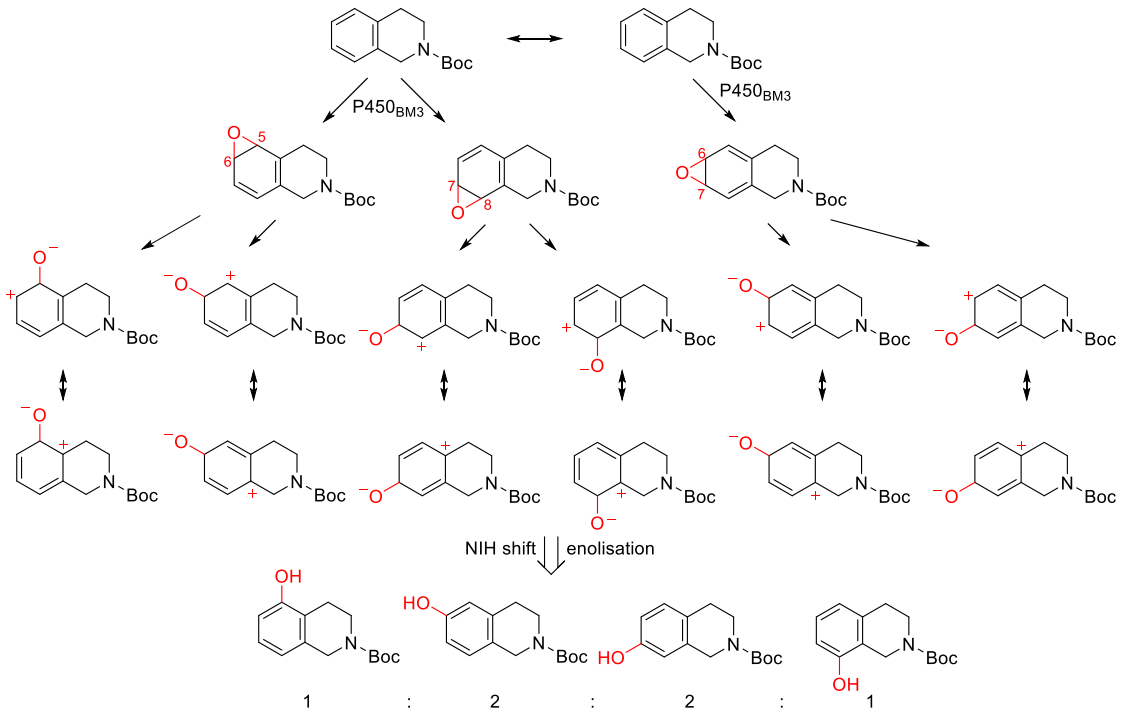


Figure 6.3 NIH shift products of P450-catalysed aromatic oxidation of *N*-Boc-THIQ.

The observation of the less favoured NIH shift 5- and 8-phenol products was interesting, but both the conversion and selectivity were rather low (Table 6.10). The results from

variant screening indicated that insertion mutations at L437 such as the L437LV led to some aromatic oxidation. Therefore, different insertions at L437 were combined with the I263G mutation in the R1/I263G mutant which showed high conversion and a small amount of aromatic oxidation products. As shown in Table 6.11, the L437LV insertion biased the selectivity towards the 5-phenol **135** (20%) whilst L437LH gave more 8-phenol **136** (20%). These selectivities were comparable to the highest values observed with the R19/A328L/I263A variant. It is reasonable to propose that further increases in selectivity for **135** and **136** could be obtained in follow-up work by mutagenesis at A184, I263 and A328 of the R1/I263G/L437LV variant. The mutation effects were also summarised in Table 6.11.

Table 6.11 Conversion and product distribution of *N*-Boc-THIQ (**131**) oxidised by the 2nd generation $P450_{BM3}$ variants. (R1 = R47L/Y51F/H171L)

Mutant	**Conversion**	**Selectivity**				
		132	**133**	**134**	**135**	**136**
R1/I263G	100%	22%	4%	73%	–	–
R1/I263G/L437LV	78%	–	2%	68%	20%	10%
R1/I263G/L437VL	87%	3%	3%	65%	15%	14%
R1/I263G/L437LM	57%	19%	2%	60%	10%	9%
R1/I263G/L437LF	76%	5%	3%	68%	12%	12%
R1/I263G/L437LS	73%	4%	5%	75%	7%	10%
R1/I263G/L437LH	44%	6%	2%	55%	17%	20%

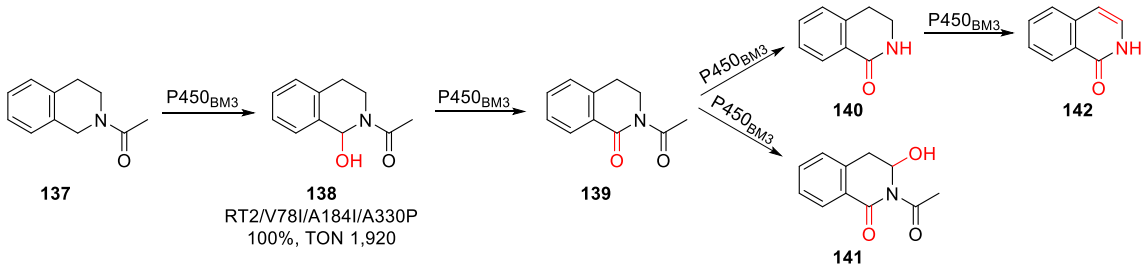
C1	**C3**	**C4**	**5- and 8-phenols**
F87I F87A/A82M F87A/A328G	A328G A264G	A328L A330W	I263A/A328L I263G/L437LX

6.3.2 Oxidation of *N*-Ac-THIQ

Only C1 oxidation was observed in the oxidation of *N*-Ac-THIQ (**137**) by the variant library (WY5/6, Appendix 3.21). Further oxidation of the C1-alcohol **138** at longer reaction times gave *N*-acyl-3,4-dihydroisoquinolinone **139**, deprotection of **139** to 3,4-dihydro-isoquinolinone **140**, 3-hydroxy-*N*-acyl-3,4-dihydroisoquinoinone **141**, and isoquinolinone

142 from desaturation of **140** across the C3–C4 bond (Table 6.12). The mechanism of *N*-de-acylation is not clear although acyl protecting groups are more readily lost than, for example, Boc for which there was no evidence for deprotection during enzymatic turnover. Although an oxidative mechanism could not be ruled out, de-acylation of **139** to form **140** could also occur by nucleophilic attack by the ferric peroxy species.

Table 6.12 The conversion and further oxidation of $P450_{BM3}$ oxidation of *N*-Ac-THIQ (**137**).



Mutant	Conversion (major further oxidation products)
WT	38% (64% **139**)
I263G	69% (28% **138**)
GV/A184I	72% (63% **141**)
GVQ	60% (40% **141**)
GVQ/A330W	72% (29% **139** and 29% **141**)
K19/F87V	70% (25% **138**, 20% **139**, 19% **140** and 23% **141**)
K19/F81W/F87A	84% (19% **139**, 32% **141** and 22% **142**)
R19/F87A/A184I	69% (25% **138**, 26% **141** and 22% **142**)
RT2/V78I/A184I/A330P	96% (70% **141**)

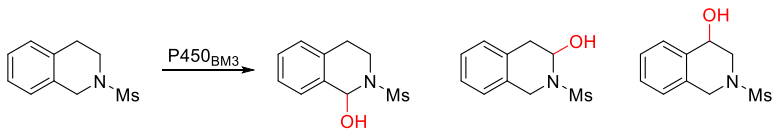
The variant library was less active for the oxidation of *N*-Ac-THIQ compared to the Boc analogue, with just 14 out of 48 variants showed higher than 50% conversion (TON >1,000). The wild type showed modest conversion (38% conversion, TON 760) and further oxidation (*e.g.* 64% selective for **139** in product distribution of 16-hour incubation) even before the substrate was fully consumed, suggesting that 1-hydroxy-(**138**) was an even better substrate for $P450_{BM3}$ than **137**. F81W, F87V, A184I, A330P and A330W promoted activity. A184I favoured the further oxidation of **138** and **139** to form **141**.

It was unexpected that an acyl group restricted the product scope to C1 oxidation. The small methyl group might lead to multiple binding orientations and greater mobility of the substrate within the active site, such that C1, the most activated position in the substrate, was preferentially attacked. The oxidation of *N*-Ac-3,4-dihydroisoquinolinone (**139**) and 3,4-dihydroisoquniolinone (**140**) indicated the possibility of P450-catalysed oxidation of fused-ring lactams to various drug fragment-like products.

6.3.3 Oxidation of *N*-Ms-THIQ

The variant library primarily converted *N*-Ms-THIQ (**143**) into C1, C3 and C4 hydroxylation products **144**–**146** (Table 6.13), in marked contrast to *N*-Ac-THIQ (**137**) which only showed initial C1 oxidation. No oxidation of the aromatic ring was found.

Table 6.13 The conversion and product distribution of $P450_{BM3}$ oxidation of *N*-Ms-THIQ (**143**).



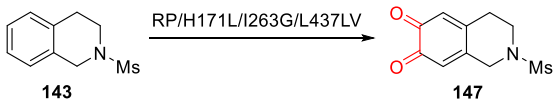
143 | **144** RT2/V78I/A184I/A330P 93%, TON 930 | **145** RP/H171L/I263G 44%, TON 440 | **146** GVQ/V78L/I263G 51%, TON 400

Mutant	**Conversion**	**Selectivity**		
		1-OH: 144	**3-OH: 145**	**4-OH: 146**
RT2/V78I/A184I/A330P	100%	**93%**	2%	1%
R19/F87A/A328G	51%	86%	5%	8%
RT2	74%	82%	2%	14%
GVQ	36%	66%	2%	28%
K19/F87V/Q403P	94%	64%	2%	33%
K19/F87V	48%	63%	3%	32%
RP/H171L/I263G	100%	31%	**44%**	16%
GVQ/V78L/I263G	78%	31%	13%	**51%**
GVQ/I263G	68%	33%	21%	**44%**
R19/F87A/A184I	70%	48%	10%	39%
R19/F87A	25%	51%	14%	32%

Conversion	**C1**	**C3**	**C4**	**aromatic**
A184I I263G Q403P	V78I A328G	I263G	V78L F87V/I263G	L437LV

N-Ms-THIQ was not a good substrate for the enzyme library; only 8 variants provided >50% conversion (TON >500). The mutations V78I/L, A184I, I263G, A328G and Q403P promoted substrate conversion and RP/H171L/I263G showed full conversion (TON 1,000, Table 6.13). The V78I and A328G mutations favoured C1 oxidation with the variant RT2/V78I/A184I/A330P showing 93% of **144** (TON 930), whereas the I263G mutation favoured C3 hydroxylation (up to 44% of **145** given by RP/H171L/I263G); however, when combined with F87V, C4 hydroxylation was enhanced instead, and this selectivity was further increased with V78L (51% of **146**, TON 400 given by GVQ/V78L/I263G).

Although C1 hydroxylation was common for *N*-Ms-THIQ, C3 and C4 oxidation were observed with up to *ca.* 50% selectivity with the library. This suggested that the sulfonyl group was materially different from the carbonyl, either because of increased hydrogen-bonding with the sulfonyl or the longer N–S bond compared to a N–C bond. There were subtle but significant differences between the two protecting groups which could be explored in future. No aromatic oxidation product was observed except for a preparative scale reaction over a long reaction time with the variant RP/H171L/I263G/L437LV that gave the orthoquinone **147** (Figure 6.4). However, no precursor, *e.g.* 6- or 7-hydroxy-*N*-Ms-THIQ, was recovered. Nevertheless, isolation of **147** indicated that aromatic oxidation of **143** was possible. The mutation effects were summarised in Table 6.13.



143 **147**

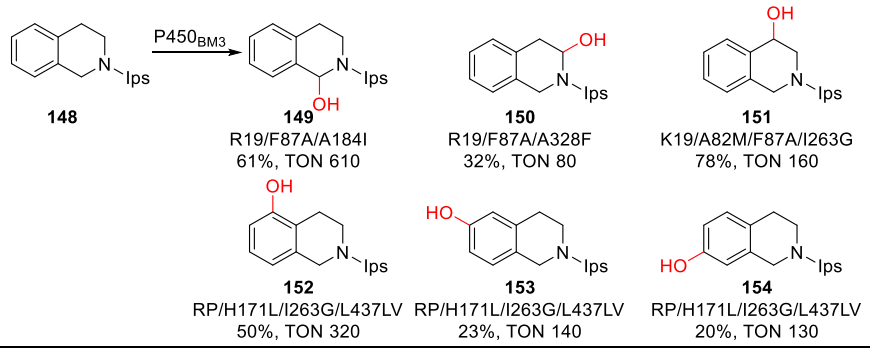
Figure 6.4 The reaction scheme of oxidation of *N*-Ms-THIQ (**143**) with RP/H171L/I263G/L437LV.

6.3.4 Oxidation of *N*-Ips-THIQ

The wild type showed no activity towards *N*-Ips-THIQ (**148**). The mutant R19/F87A/A184I was chosen for a preparative scale reaction which gave full substrate conversion (TON 1,000) and afforded products arising from oxidation of the methylene groups, i.e. 1-, 3-,

and 4-hydroxy-*N*-Ips-THIQ, **149**–**151** (Table 6.14). Preparative scale reactions with the variant RP/H171L/I263G/L437LV showed a TON of 590, yielding the aromatic oxidation products 5-, 6-, and 7-hydroxy-*N*-Ips-THIQs, **152**–**154**. Therefore, the change from *N*-Ms to *N*-Ips enabled the generation of aromatic oxidation products for sulfonyl groups.

Table 6.14 The conversion and product distribution for oxidation of *N*-Ips-THIQ (**148**) by $P450_{BM3}$.



Mutant	**Conversion**	**Selectivity for aliphatic oxidation products**		
		1-OH: 149	**3-OH: 150**	**4-OH: 151**
GVQ	**100%**	**58%**	6%	31%
K19/F87V	72%	32%	11%	48%
K19/F87V/A264G	**100%**	49%	3%	32%
R19/F87A	26%	48%	19%	18%
R19/F87A/A328G	**100%**	**51%**	17%	28%
R19/F87A/A328F	26%	12%	**32%**	45%
R19/F87A/A328L	30%	18%	5%	**70%**
R19/F87A/A184I	**100%**	**61%**	13%	21%
R19/F87A/I263G	**100%**	40%	12%	33%
K19/F87A/A82M	76%	33%	7%	46%
K19/F87A/A82M/I263G	20%	–	8%	**78%**
		5-OH: 152	**6-OH** & **7-OH: 153** & **154**	
I263G	19%	24%	18%	
RP/H171L/I263G	12%	36%	21%	
RP/H171L/I263G/L437LV	63%	**50%**	**43%**	
R19/I263G/A328L	10%	18%	**45%**	
RT2/S72W/A330W	90%	2%	2%	

Within the screening library, 17 out of 48 variants provided higher than 50% conversion (TON >500). Methylene oxidation required the F87A/V mutations. The A184I, I263G and A328G mutation promoted conversion, up to 100% (Table 6.14). Amongst the F87V-based

variants, the mutation A264G enhanced conversion and C1 hydroxylation. In the R19/F87A-series, A184I and I263G separately enhanced C1 and C4 oxidation without sacrificing turnover, whilst A328F/L respectively promoted C3/C4 oxidation, but impairing conversion. A82M also favoured C4 hydroxylation.

Aromatic oxidation was observed with variants with no mutation at F87. In addition, the I263G mutation was of critical importance. The two phenols **153** and **154** co-eluted on the GC under all tested conditions; as such only their total contribution to the product profile was determined. Addition of the L437LV insertion mutation promoted the formation of the 5-phenol **152**, whilst A328L favoured formation of the 6- and 7-phenols **153** and **154**, albeit at the expense of reduced conversion. RT2/S72W/A330W was the only other variant to give trace amounts of these three phenols, suggesting S72 and A330 could be target residues for further engineering. Further oxidation was found in prolonged reactions but at far lower extents than with acyl. The mutation effects are summarised in Table 6.15.

Table 6.15 Mutation effects on $P450_{BM3}$ oxidation of *N*-Ips-THIQ (**148**).

Conversion	**C1**	**C3**	**C4**	**Aromatic oxidation (5-, 6- and 7-phenols)**
F87A/V A184I I263G A328G	F87V/A264G F87A/A184I	F87A/A328F	F87A/I263G F87A/A328L A82M	*87F* I263G A328L L437LV

6.3.5 The effect of protecting group on $P450_{BM3}$ oxidation of THIQ

Unlike with THQ, the $P450_{BM3}$ variant library did not show readily detectable oxidation of THIQ. Most of the variants showed no activity. On the other hand, substrate engineering via the introduction of a protecting group revealed that every C–H and C=C bond was accessible to oxidation by $P450_{BM3}$ variants. The effect of varying the protecting group was striking (Figure 6.5); C1 and C4 hydroxylation could be obtained with very high yields and

selectivity (≥94%), C3 hydroxylation with modest selectivity (51%), and the 8-phenol with reasonable selectivity (33%), with Ac and Boc as protecting groups. The Ips protecting group shifted the selectivity to afford the 5-, 6,- and 7-phenols from aromatic oxidation, at up to 51% for the 5-phenol and 20–30% for the 6- and 7-phenols, the latter two were not observed at all with Boc. The Ac protecting group only gave C1 oxidation and further oxidation products that were also of potential interest in the synthesis of diversified compounds. Further oxidation reactions were less evident to absent with *N*-Boc- or *N*-Ips-THIQ. Hence, the size of the protecting group was a significant factor in turnover activity, product selectivity and chemoselectivity. The results suggested that other bulky protecting groups, *e.g.* triflyl (Tf) or carboxybenzyl (Cbz), could lead to altered product selectivity.

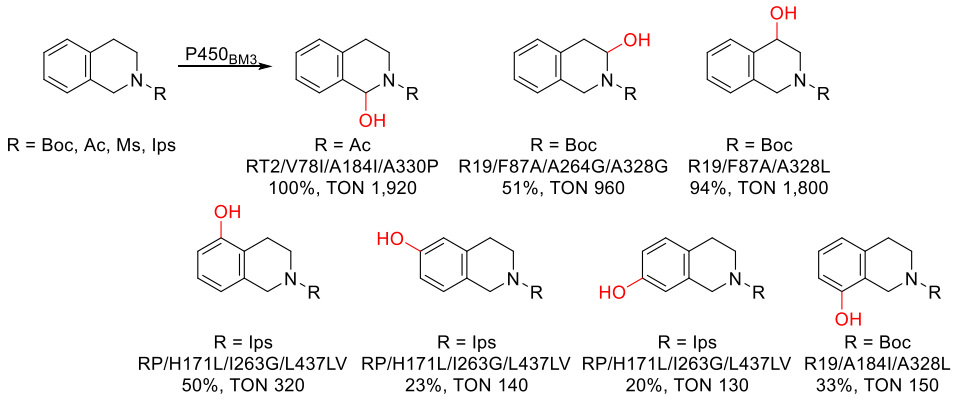


Figure 6.5 General reaction scheme of $P450_{BM3}$ oxidation of *N*-protected-THIQs.

Oxidation at the C3 position, even the activated position in THIQ, remained challenging. This mirrored the observation with THQ for which C3 is an unactivated position and its oxidation could not be obtained with any degree of selectivity. Further screening, perhaps coupled with crystal structure determination, will be required to understand the low selectivity for this position. Further work will also be required to determine the absolute configuration of chiral products and the enantioselectivity of the variant library.

In contrast with oxidation of *N*-protected-THQs, protecting group engineering of THIQ successfully diversified the product selectivity of the $P450_{BM3}$ variants. For instance, the

RP/H171L/I263G variant gave predominantly the 4-hydroxy-products of all protected THQs (Boc: 66%, Ac: 69%, Ms: 82%, and Ips: 100%), whereas it gave 76% of 4-hydroxy-*N*-Boc-THIQ, 100% of 1-hydroxy-*N*-Ac-THIQ, 20% of 3-hydroxy-*N*-Ms-THIQ, and 57% of 5-/6-/7-hydroxy-*N*-Ips-THIQs. This suggested that the protecting groups of the THIQ core interacted with the active site residues in a different manner from those of the THQ core, and the directing effect of the nitrogen atom was effectively shielded in the THIQ core by the introduction of protecting groups. Protein-ligand docking experiments and substrate-bound crystal structures with RP/H171L/I263G will reveal whether the substrate pocket topology changes significantly by altering the nitrogen atom position (N1/N2) and the *N*-protecting group (Boc/Ac/Ms/Ips), and assist the design of new variants with higher selectivity for C3 and aromatic oxidation of the THQ and the THIQ cores which remain in low to modest levels (≤51%) thus far.

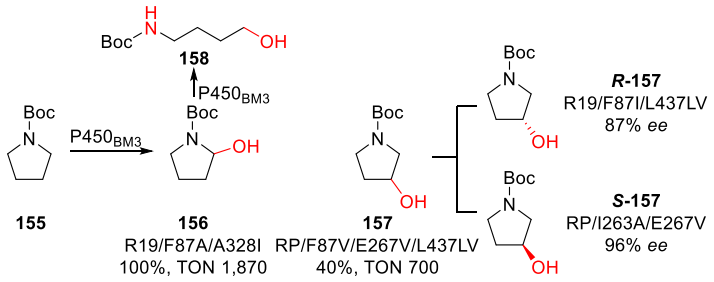
6.4 P450$_{BM3}$ oxidation of protected single-ring cyclic amines

Protected single-ring cyclic amines were tested to compare the effect of the protecting groups on substrate oxidation with THQ and THIQ. Therefore, the *N*-acyl, *N*-mesyl, *N*-tosyl and *N*-Boc derivatives of pyrrolidine and piperidine were screened for oxidation with the P450$_{BM3}$ variant library. As with THQ and THIQ, the *N*-tosyl derivatives were too insoluble to give meaningful results. The *N*-Ac and *N*-Ms-derivatives were converted to ring-opening and more water-soluble products which hampered extraction and analysis, likely due to the small size of the protecting groups and the spacious nature of substrate pocket of the P450$_{BM3}$ variants favouring Nα oxidation. Only the *N*-Boc derivatives showed reasonable extraction to give interpretable data, and only the results for *N*-Boc-pyrrolidine and *N*-Boc-piperidine oxidation are reported here.

6.4.1 Oxidation of *N*-Boc-pyrrolidine

In the P450$_{BM3}$ biotransformation of *N*-Boc-pyrrolidine (**155**) at a substrate concentration of 2 mM and enzyme concentration of 1 μM, the wild type enzyme was found to be inactive whilst 40 of the 48 variants in the screening library showed >50% conversion (TON >1,000). Product purification from preparative scale reactions and characterisation by NMR and MS data showed that the Nα- and Nβ-hydroxylation products **156** and **157** were readily formed, and the α-alcohol **156** underwent ring-opening and reduction of the resultant aldehyde to form the terminal alcohol **158** (Table 6.16).

Table 6.16 Conversion and product distribution of P450$_{BM3}$ oxidation of *N*-Boc pyrrolidine (**155**).



Mutant	Conversion	Selectivity		
		156 & **158**	**157**	***enantiomeric excess***
R19/F87I	89%	93%	7%	75% *ee* to *R*
R19/F87I/L437LV*	100%	93%	7%	87% *ee* to *R*
R19/F87A	89%	100%	–	–
R19/F87A/A328F*	60%	87%	13%	86% *ee* to *R*
GVQ	50%	100%	–	–
GVQ/I263G	83%	92%	8%	34% *ee* to *S*
RP	97%	100%	–	–
RP/H171L	96%	100%	–	–
RP/H171L/I263G	99%	81%	19%	89% *ee* to *S*
RP/F87V	99%	96%	4%	30% *ee* to *R*
RP/E267V	94%	97%	3%	44% *ee* to *S*
RP/I263A/E267V	95%	75%	12%	96% *ee* to *S*
RP/F87V/E267V	96%	84%	16%	66% *ee* to *R*
RP/V78F/F87V/E267V	71%	6%	20%	61% *ee* to *R*
RP/F87V/E267V/L437LV	87%	60%	40%	76% *ee* to *R*

GC analysis showed that Nα-oxidation was favoured across the variant library. For most variants, the α-alcohol **156** was further converted to the linear alcohol **158**. β-Hydroxylation of **155** to form **157** was promoted by the mutations V78F, F87I/V, I263G, E267V, A328F and L437LV (Table 6.16), although the highest selectivity for **157** was a modest 40%. The enantiomers of a commercial racemic mixture of the β-alcohol **157** were readily resolved by chiral-phase GC (Figure 6.6).

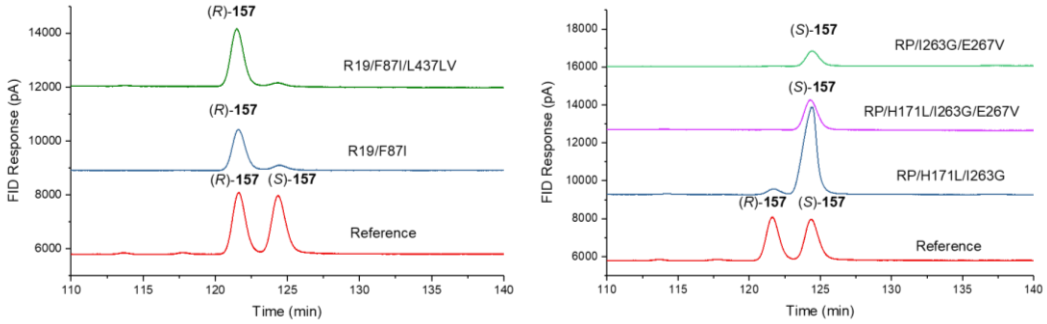


Figure 6.6 The chiral GC analysis of the screening reactions of **155** with $P450_{BM3}$.

Analysis of the screening reactions showed high enantioselectivity within the variant library (Figure 6.6 and Table 6.16). Amongst the mutations, F87I/V, A328F and L437LV favoured the *R*-enantiomer with R19/F87A/A328F showing 86% *ee*, whilst the I-helix mutations I263G/A and E267V in the RP-based variants preferred the *S*-enantiomer, with RP/H171L/I263G yielding 89% *ee* for *S*-**157** at 19% β-selectivity and RP/I263A/E267V giving 96% *ee* at 12% selectivity. The E267V mutation increased both the β-selectivity and preference of RP/F87V for the *R*-enantiomer from 4% **157** at 30% *ee* to 16% **157** and 66% *ee* for the RP/F87V/E267V while maintaining a high conversion. Addition of the L437LV insertion mutation raised the proportion of **157** further, to 40%, while increasing the *ee* for *R*-**157** to 76%. Li *et al.*[468] reported much higher regioselectivity of **157** (96%–100%) given by *Sphingomonas* sp. HXN-200 strain and the biotransformation can reach gram-scale with 85%–98% yield of **157**, but the highest enantioselectivity they achieved was no higher than 23% *ee* for *R*-**157** (9%–23% *ee*). Further engineering of P450pyr led to *N*-benzyl

pyrrolidine oxidation to give 83% *ee* to *R*- and 98% *ee* to *S*-enantiomer of 3-hydroxy-*N*-benzyl pyrrolidine (100% selectivity).[425] Further screening of the $P450_{BM3}$ library studied here and additional mutagenesis, will be required for higher regioselectivity and stereoselectivity of oxidation at the β-position. RP/F87V/E267V/L437LV and RP/H171L/I263G and would be excellent starting templates for a site-saturation mutagenesis study.

6.4.2 Oxidation of *N*-Boc-piperidine

N-Boc-piperidine (**159**, 2 mM) was screened against the 48-variant library (1 μM enzyme) to afford α-, β- and γ-oxidation products (Table 6.17). A time course study with the variant R19/F87A/A328I showed that α-hydroxylation product **160**, was rapidly converted to the ring-opening alcohol product **163** and the hydroxy-enamine **164** within 6 hours. Further oxidation of the γ-hydroxylation product, 4-hydroxy-*N*-Boc-piperidine **162**, afforded the γ-ketone **165**. Unexpectedly, when **165** was screened against the variant library, **162** was found to be the only product, i.e. the ketone was reduced to the alcohol by the reductase domain of the enzymes without any evidence of C–H bond oxidation.

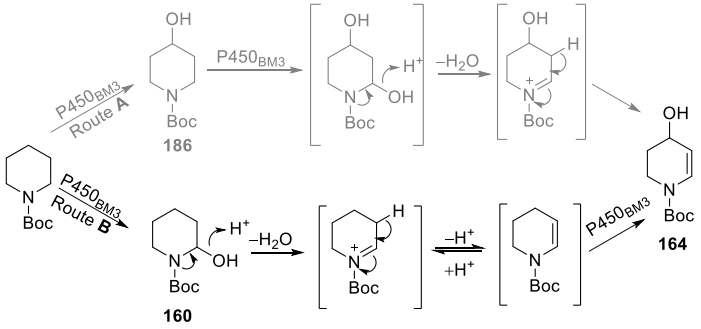
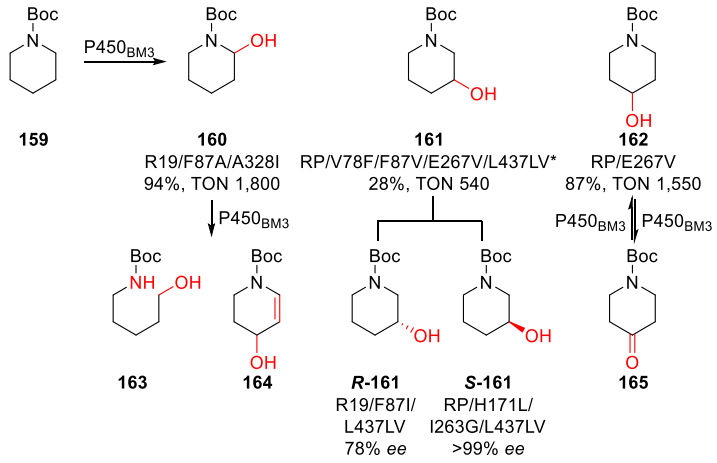


Figure 6.7 The proposed mechanisms of the formation of **164**.

The multiply functionalised product **164** could be formed either from **160** or **162** (Figure 6.7). 2-Hydroxy-(**160**) loses the hydroxide to form the iminium species which is in equilibrium with its enamine tautomer, thus being hydroxylated at the activated allylic C4 position (Route B). Alternatively, the γ-oxidation product 4-hydroxy-(**162**) could undergo

an γ-hydroxylation/iminium-enamine series of reactions (Route A), or the desaturation reaction could proceed via the abstraction of two hydrogen atoms (from C2 and C3) without the involvement of a 2,4-dihydroxy intermediate. Screening of **162** against the variant library did not give **164**, suggesting that **164** was formed via Route B.

Table 6.17 The conversion and product distribution of $P450_{BM3}$ oxidation of *N*-Boc-piperidine (**159**).



Mutant	Conv.	Selectivity			
		2-OH: 160	161	*enantiomeric excess*	162
R19/F87A	87%	82%	1%	-	17%
R19/F87I	89%	27%	8%	16% *ee* to *R*	**65%**
R19/F87I/L437LV*	100%	25%	**19%**	**78% *ee* to *R***	56%
GVQ	93%	90%	1%	-	9%
GVQ/N70S	64%	75%	4%	60% *ee* to *S*	11%
GVQ/I263G	89%	78%	2%	-	20%
RP	94%	94%	1%	-	5%
RP/H171L	88%	93%	1%	-	6%
RP/H171L/I263G	73%	23%	2%	-	75%
RP/H171L/I263G/L437LV*	97%	-	6%	**>99% *ee* to *S***	**94%**
RP/F87V	94%	58%	2%	-	40%
RP/E267V	89%	9%	4%	-	**87%**
RP/F87V/E267V	94%	16%	7%	56% *ee* to *S*	**77%**
RP/V78F/F87V/E267V	68%	12%	**26%**	50% *ee* to *S*	**62%**
RP/F87V/E267V/L437LV	78%	6%	13%	24% *ee* to *S*	**82%**
RP/V78F/F87V/E267V/L437LV*	97%	2%	**28%**	28% *ee* to *S*	**70%**
RT2/F81W/A328I	62%	59%	2%	52% *ee* to *R*	23%
RT2/A82M/A330P	87%	38%	2%	32% *ee* to *R*	60%
RT2/V78I/A184I/A330P	86%	65%	1%	40% *ee* to *S*	30%

The variant library showed high activity for *N*-Boc-piperidine oxidation. Only the wild type and four variants showed <50% conversion (TON <1,000). The ring-opening alcohol **163** was the only product formed by wild type $P450_{BM3}$. The C2 and C4 alcohols were the preferred product for most variants. C4 (γ) oxidation to give **162** was favoured by the F87V and F87I mutations close to the heme, and the I-helix mutations I263G and E267V, at up to 94% for the RP/H171L/L263G/L437LV variant (97% conversion, TON 1,860). These F87V, F87I and E267V mutations also slightly improved β (C3) oxidation to **161**. Two other mutations, V78F and L437LV also promoted β oxidation. Further mutagenesis integrated V78F and L437LV into RP/F87V/E267V, yielding slightly higher regioselectivity for **161** (28%, TON 540) at high conversion (97%).

The enantioselectivity of the variant library for β-oxidation were determined by reference to commercial racemic and enantiomerically pure samples of 3-hydroxy-*N*-Boc-piperidine **161**. The data are demonstrated in Table 6.13. The insertion mutation L437LV had a pivotal effect, increasing the bias of F87I towards the *R*-enantiomer from 16% to 78% *ee* for the variant RP/F87I/L437LV (19% β-selectivity), and that of I263G towards *S*-**161** to >99% *ee* for RP/H171L/I263G/L437LV (6% β-selectivity).

Expanded screening also showed that the mutations N70S, A82M, A328I and A330P might assist in altering enantioselectivity for β (C3) oxidation of *N*-Boc-piperidine **159**. Although the increases were small for each mutation, their effect mirrored observations with *N*-Boc-THQ and *N*-Boc-THIQ where mutations at these residues as well as V78, I263 and P329, biased the selectivity slightly towards C3 (β) oxidation. Moreover, the reversible converting reaction between **162** and **165** can be exemplified to test whether the reductase domain of $P450_{BM3}$ (BMR) catalyses the reduction of **165** and the terminal aldehydes forming from the carbinolamines. The heme iron of the selected enzyme can be pre-processed by the saturation of the inhibitory molecules or the alteration of the conservative

cysteine ligand, to hinder the common P450 activity without impairing the electron transfer process too much. Under such prerequisites, the ketone **165** and NADPH will be added into the enzyme solution for biotransformation. If **162** is produced, BMR is proven to catalyse the reduction.

6.4.3 Summary of $P450_{BM3}$ oxidation of *N*-Boc-pyrrolidine and piperidine

Smaller size of the simple cyclic amines pyrrolidine and piperidine, along with less bulky protecting groups Ms and Ac, exposed Nα mainly for $P450_{BM3}$ to oxidise. The bulkier Ts-protected forms suffered solubility issues. An *N*-phenyl group in Chapter 3 also only gave α oxidation for the cyclic amine cores. The Boc protecting group balanced the solubility and the steric hindrance around the nitrogen atom, rendering *N*-Boc-pyrrolidine and piperidine viable substrates. Such observation suggests the bulkier-size protecting groups of no significant influence on substrate solubility, *e.g.* Cbz, could be tested for remote functionalisation by $P450_{BM3}$.

In the oxidation of *N*-Boc pyrrolidine and piperidine, wild type gave either no conversion or low conversion (14%, TON 280) with only Nα oxidation. It was notable that R19/F87I, R19/F87I/L437LV, RP/F87V/E267V/L437LV, RP/V78F/F87V/E267V and RP/F87V/E267V gave modest increases in β-hydroxylation products for both *N*-Boc-pyrrolidine and piperidine. The mutations V78F, F87I, E267V and L437LV altered the regio- and enantioselectivity of β oxidation of both substrates suggesting they might shape the substrate pocket with a specific binding region for the Boc group. Site-saturation mutagenesis at V78, F87, E267 and L437 based on the variants R19 and RP, assisted by molecular modelling, will expand the vision of engineering remote functionalisation.

The engineering of β oxidation for *N*-Boc-piperidine is more difficult than its pyrrolidine analogue, as this also requires inhibition of γ oxidation. Such requisite calls for accurate

control of the substrate binding orientation. Bulky amino acids F/W/Y/H/I/L are worth introducing at A82, F87, I263, E267, A330 and L437, which played important roles in engineering γ oxidation, to improve β hydroxylation.

6.5 Protecting group effects on $P450_{BM3}$ oxidation of cyclic amines

Across the oxidation of protected THQ, THIQ, pyrrolidine and piperidine, Boc groups diversified oxidation activity most, whereas Boc, Ips and Ms groups showed oxidation at all available sites of the benzene motif (Figure 6.8). The effects of the Boc group on selectivity, its maintenance of substrate solubility and its easy deprotection procedure made it the most desirable protecting group. Other protecting groups of similar properties, *e.g.* Cbz, could be investigated in future. The chiral protecting groups should also be attempted.

The alternation of the regiospecificity in the oxidation of the protected THQs and THIQs echoed with the previous research on $P450_{BM3}$ oxidation of fatty acids.[567] The wild type enzyme showed 100% selectivity for epoxidation at C17=C18 double bond of eicosapentaenoic acid (5 C=C double bonds), 20% of epoxidation at C14=C15 double bond and 80% of hydroxylation at C18 of arachidonic acid (4 C=C double bonds), and 41%, 36% and 23% of hydroxylation at C17, C18 and C19 of eicosatrienoic acid (3 C=C double bonds).[567] The number of the double bonds shifted the oxidation activity of these linear fatty acids of same length, which resembled the selectivity engineering property of different protecting groups shown here.

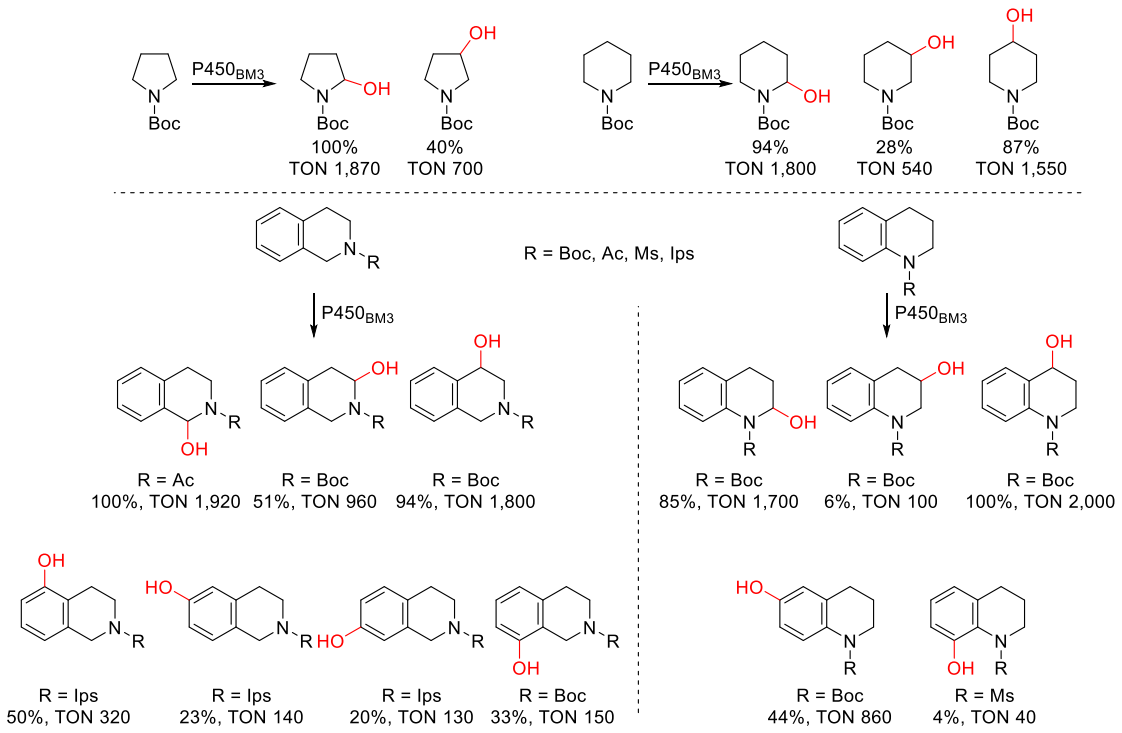


Figure 6.8 Summary of $P450_{BM3}$ oxidation of *N*-protected piperidine, THQs and THIQs.

For all tested substrates, β oxidation, i.e. C3 of pyrrolidine, piperidine and THQ motifs and C4 of THIQ motif, was observed. For oxidation at non-activated β positions, the variant library and 2nd generation variants showed limited to modest selectivity (6%–51%). For the THQ motif, the Ms-derivative gave 4% C7,C8 oxidation, and C4 oxidation was favoured for all protected THQs contrasting with oxidation of methyl-/methoxyl-THQs & THQ itself.

Oxidation of protected THIQs, compared with THIQ itself (inactive) and THIQ' (benzylic oxidation only), showed great diversity with the protecting groups Boc and Ips. In addition to C1, C3 and C4 oxidaiton, the 5-, 6-, 7- and 8-phenols were formed from these two protected forms. Moreover, *N*-Boc-THIQ and *N*-Ips-THIQ shared the key residues I263, A328 and L437, the mutations of which could enhance or alter aromatic oxidation of the THIQ core, but with different preference for aromatic oxidation sties: Boc favoured the 5-phenol (21%) and 8-phenol (33%); Ips gave the 5-phenol (50%), 6-phenol (23%) and 7-phenol (20%). Both site-saturation mutagenesis and insertion mutations (either before or after) around these sites could be attempted at the R1 template, to engineer aromatic

oxidation of the THIQ core. The substrate-bound crystal structures of the active variants would be of interest to understand the enzyme-substrate interactions.

Bulky protecting groups (Boc/Ips), bulky amino acids (A330W, 87F, A328L, A184I, A82M, *etc.*) and insertion mutations (L437LH, L437LV, L437VL, *etc.*) tended to increase the product diversity of oxidation of the THQ/THIQ/pyrrolidine/piperidine cores, which implied that the substrate pocket of the current $P450_{BM3}$ library variants was too commodious. Greater substrate mobility inside the enzyme active site favoured oxidation of the most activated, Nα position. Therefore, protein engineering of remote functionalisation of cyclic amines could focus on altering substrate pocket topology by adding and inserting mutations of bulky side-chains or capable of developing hydrogen bond.

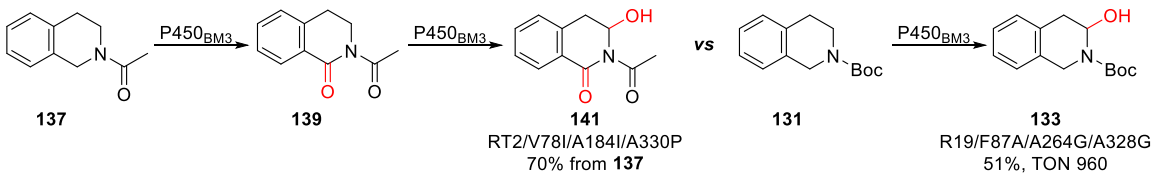


Figure 6.9 The comparison between C3 oxidation of the lactam **139** and the amine **131** by $P450_{BM3}$.

C3 of THQ, THIQ, pyrrolidine and piperidine remained the most inaccessible oxidation sites for $P450_{BM3}$. Notably, hydroxylation of the lactam **139** showed high regioselectivity at C3 (70%), whereas the highest selectivity of 3-alcohol directly from the protected THIQs was 51% with the Boc-protected form (Figure 6.9). This led to the exploration of oxidation of lactam motifs in Chapter 7, searching for good diversity of oxidation pattern and high regioselectivity which complement the oxidation of cyclic amines.

Chapter 7 Remote functionalisation of lactams

7.1 Introduction

The results in previous chapters indicated that β-oxidation of cyclic amines remained a significant challenge for P450$_{BM3}$ engineering; the highest β-selectivity for pyrrolidine- and piperidine-containing substrates did not exceed 40% except for THIQ for which the β-position was also benzylic. Transition metal catalysts[568,569] rarely give high selectivity for amine functionalisation at non-activated β C–H bonds (Figure 7.1); a general catalyst for β C–H activation of cyclic amines thus remains a sought-after target.

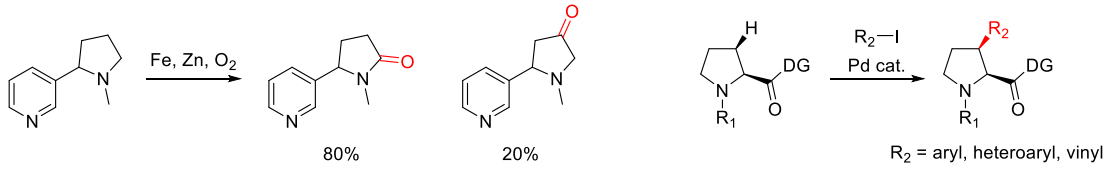


Figure 7.1 Examples of β-functionalisation of cyclic amines catalysed by transition metal catalysts.[568,569]

The effect of substituents and protecting group on the oxidation of cyclic amines described in Chapters 5 & 6 indicated the importance of altering the electronic structure of the cyclic amine core, changing hydrogen bonding interactions with the active site residues, and modulating/screening the effect of the lone pair on nitrogen. For the THQ core, a 6-methoxy substituent gave C8 amination, a new activity, more likely due to its strong electron-donating property; *N*-protected THQ and the lactam of THQ were oxidised at all available sites with the lactam showing high C7,C8 oxidation (73% of 8-phenol), whereas THQ itself was found to give C2 and C5,C6 oxidation only (Figure 7.2). For its regioisomer THIQ, oxidation of protected THIQs showed high diversity, giving >90% selectivity at C1/C4 and modest selectivity (20%–51%) for the 3-alcohol, 5-, 6-, 7- and 8-phenols. C3 oxidation of protected THIQs reached 51% selectivity by changing the protecting group, but the lactam of *N*-Ac-THIQ increased C3 hydroxylation up to 70%. These suggested that the asymmetric *N*-protected lactams, with a new H-bond acceptor introduced, might provide alternative routes for multiply functionalised nitrogen heterocyclic compounds.

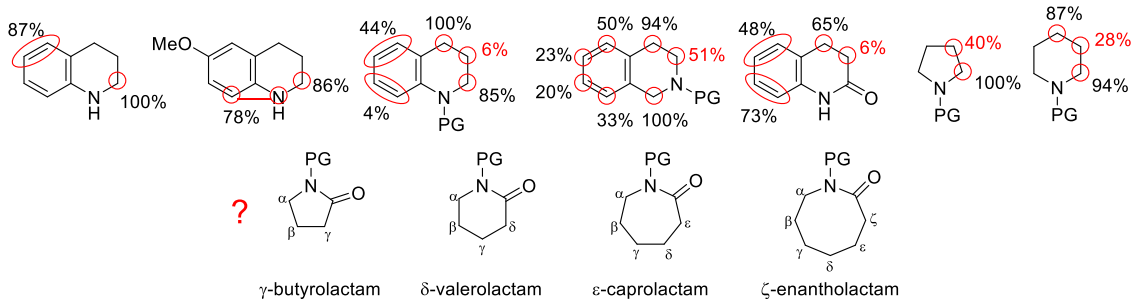


Figure 7.2 The selectivity patterns for $P450_{BM3}$ oxidation of molecules of THQ core to reveal lactams as available substrates.

Lactams can be interesting targets for P450-catalysed C–H activation as the asymmetric amide contains activated carbon atoms at the α-position to the nitrogen and carbonyl group. They also present hydrogen bonding donors (NH in the unprotected lactams) and acceptors that are part of the cyclic structure for interaction with substrate pocket residues, potentially providing different binding orientations from *N*-protected amines. Single and multiple oxy-functionalisation at different C–H bonds of lactams also provide alternative routes to functionalised cyclic amines via hydride reduction (Figure 7.3).[570,571]

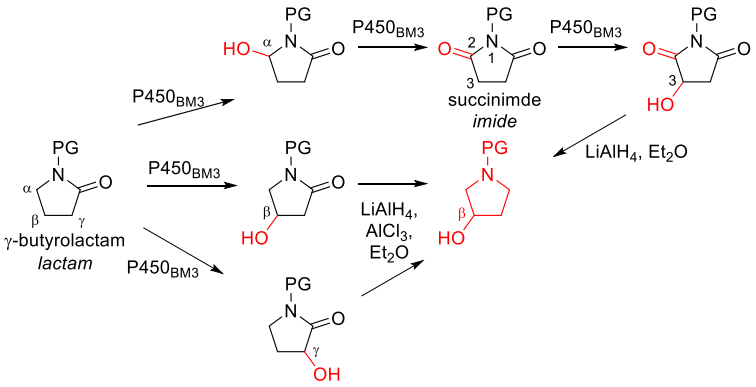


Figure 7.3 An example of functionalisation of lactam and routes to functionalised cyclic amines.[570,571]

Moreover, lactams are ubiquitous cores in drugs and alkaloids with a wide variety of bioactivities (Figure 7.4). Stereoselective introduction of substituents on the peripheral carbons of lactams is of great interest as well as utility in drug discovery and synthesis. Direct C–H bond oxidation by biohydroxylation of lactams to provide synthetic intermediates has been studied extensively for a broad range of lactam species including monocyclic, fused-ring, and spirocyclic lactams (Figure 7.5). Whole collections of

microorganisms are often screened for lactam oxidation. Of these, *Beauveria bassiana* ATCC 7159,[431,432] *Cunninghamella elegans*,[433] and *Streptomyces antibioticus* ATCC 14890,[434] are some of the most successful. Engineered bacterial P450 enzymes have also been explored, including $P450_{pyr}$[424,428,429] and $P450_{BM3}$.[225]

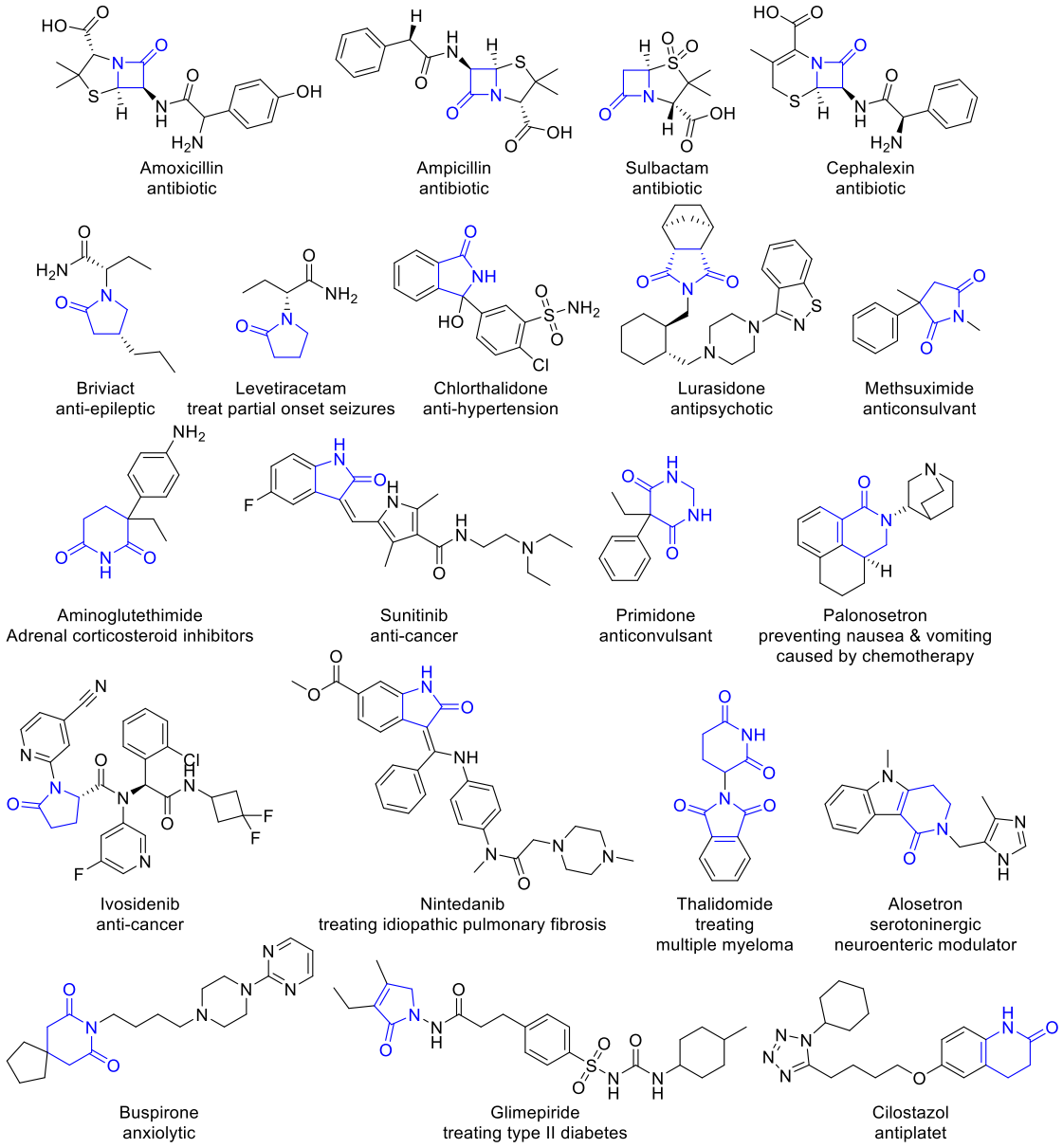


Figure 7.4 Examples of drugs and alkaloids possessing lactam and imide cores.

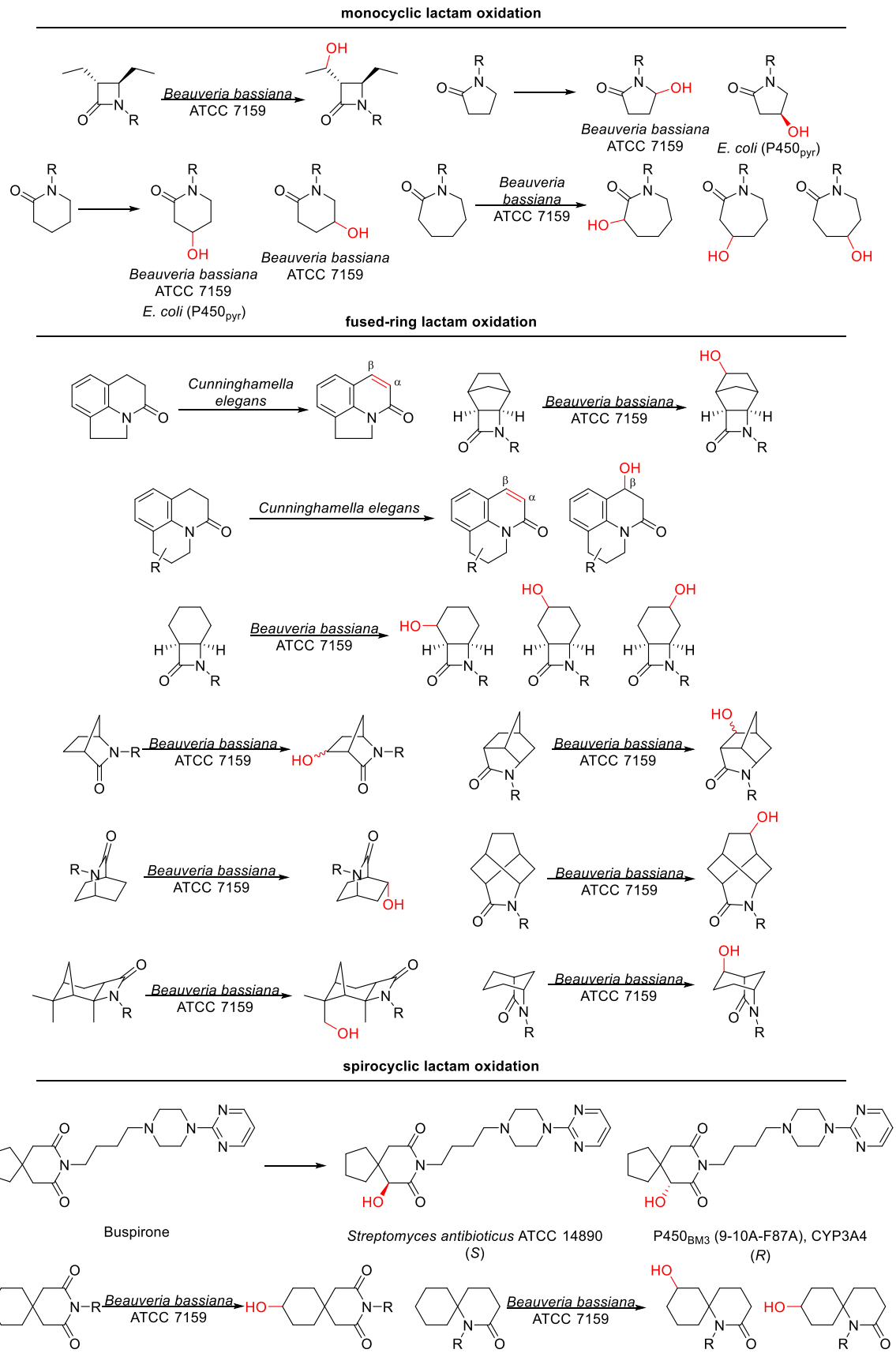


Figure 7.5 A selection of biohydroxylation of monocyclic,[424,428,429,431,432] fused-ring[432,433,456] and spirocyclic lactams[225,432,434] by *Beauveria bassiana* ATCC7159, *Cunninghamella elegans*, P450pyr and $P450_{BM3}$.

For single-ring lactam oxidation, *Beauveria bassiana* ATCC 7159[431,432] and *E. coli* harbouring wild-type and engineered $P450_{pyr}$[424,428,429] oxidised γ-butyrolactam, δ-valerolactam and ε-caprolactam at both activated and non-activated carbons. *Cunninghamella elegans*[433] gave α,β-desaturation and β-benzylic hydroxylation products for the 3,4-dihydroquinolin-2(*1H*)-one core. *B. bassiana* generally hydroxylated fused- and bridged-ring lactams at the auxiliary rings and exocyclic carbons,[432,456] most of which were non-activated positions. The spirocyclic drug buspirone was oxidised by *Streptomyces antibioticus* ATCC 14890[434] mainly to *S*-6-hydroxy-buspirone, whilst the $P450_{BM3}$ variant 9-10A-F87A[225] provided mostly *R*-6-hydroxy-buspirone.

Previous studies have demonstrated the feasibility of using biocatalysts to obtain remote functionalisation of lactams, but not yet offering generalised systems with the ability to control and engineer product selectivity. The work in this chapter focused on exploring whether engineered $P450_{BM3}$ could provide such systems for C(sp^3)–H activation of nitrogen heterocycles. In addition to the single-ring compounds γ-butyrolactam, δ-valerolactam, ε-caprolactam and ζ-enantholactam, spirolactams and spiroimides were studied with *N*-Boc, *N*-vinyl, *N*-Ph or *N*-Bn protecting groups for $P450_{BM3}$ oxidation.

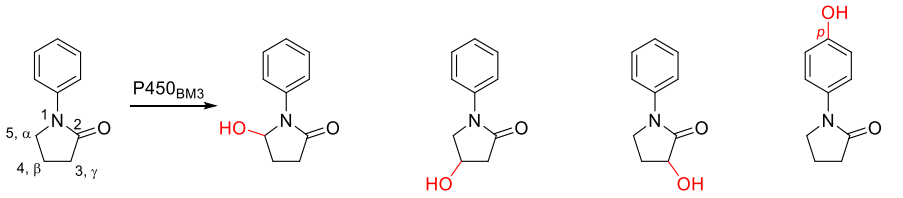
7.2 $P450_{BM3}$ oxidation of γ-butyrolactam (pyrrolidin-2-one)

In this section, *N*-protected derivatives of γ-butyrolactam were tested against the 48 variant $P450_{BM3}$ library (Appendix 3.26 & 3.27) at 2 mM substrate concentration and 1 μM enzyme in 200 mM phosphate buffer, pH 8.0. Phenyl and benzyl protecting groups were used.

7.2.1 Oxidation of *N*-phenyl-γ-butyrolactam

N-Phenyl-γ-butyrolactam (**166**) was oxidised at both rings, yielding α-, β-, and γ-hydroxylation (to N) products **167**–**169** and the *p*-phenol **170** (Table 7.1). Unlike *N*-Ph-pyrrolidine, there was no evidence of any ring-opening or Povarov reaction products.

Table 7.1 The conversion and product distributions of $P450_{BM3}$-catalysed reactions yielding **167**–**170**.



$P450_{BM3}$ variant	**Conversion**	**Selectivity**			
		5-OH: 167	**4-OH: 168**	**3-OH: 169**	***p*-OH: 170**
KU3/A330P	60%	93%	2%	5%	–
KU3/S72W/A330P	94%	97%	3%	–	–
RP/H171L/I263G/F87V/V78I	64%	92%	1%	5%	3%
RT2/H171L/I263G/A330W	100%	83%	1%	2%	14%
R47L/Y51F/I263R	65%	76%	10%	2%	16%
RP/H171L/I263G	100%	70%	11%	2%	16%
RP/H171L/I263G/A184I	70%	73%	9%	3%	16%
R1/I263G/L437LV*	97%	27%	–	61%	11%
R1/V78I/I263G/L437LI*	78%	44%	–	56%	–
R1/I263G/L437VL*	100%	51%	2%	48%	–
RP/A82M/I263G*	63%	59%	17%	12%	12%
R1/I263G	94%	67%	12%	21%	–
Activity enhancer		A330P	A82M/I263G	I263G/L437LV	I263G/R

Although the Nβ- and Nγ-alcohols (**168** and **169**) were observed with a handful of variants in the screening library, their combined percentages never exceeded 30%. Amongst the 25 variants of >50% conversion (TON >1,000), only the I263G variants RP/H171L/I263G, RP/H171L/I263G/A184I, RP/H171L/I263G/V78I/F87V, RT2/H171L/I263G/A330W and R47L/Y51F/I263R gave some of **168**–**170** (Table 7.1). The I263G sub-library (Appendix 3.26), which was developed for cyclic amine functionalisation and based on RP/H171L/I263G and R1/I263G with mutations introduced at V78, A82, F81 and L437, was thence screened, from which it was found that L437 insertion mutations improved Nγ-selectivity to 61% (TON 1,200) of 3-hydroxy-(**169**) with R1/I263G/L437LV, whilst the

A82M mutation slightly improved the β-selectivity to a modest 17% (TON 220) of 4-hydroxy-(**168**) for the RP/A82M/I263G variant.

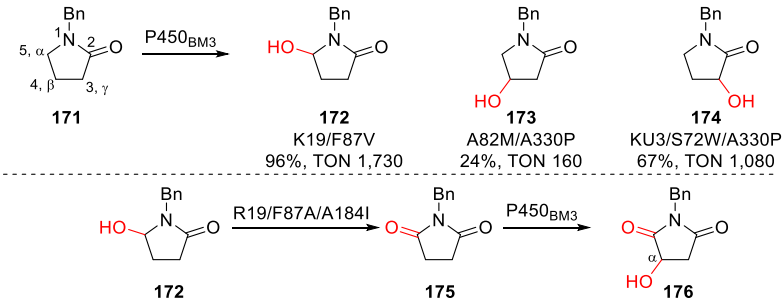
α-Oxidation to form **167** was promoted by the A330P mutation. Therefore, all C–H bonds of the lactam ring in **166** were oxidised by $P450_{BM3}$. Selectivity for Nα oxidation was high (97% of **167**), there was moderate selectivity for Nγ (carbonyl Cα) oxidation (61% of **169**), while the unactivated Nβ (C4) position was least favoured, at a maximum selectivity of 17% for **168**. Since removal of the phenyl protecting group was not straightforward, use of the more readily removed benzyl protecting group was investigated.

7.2.2 Oxidation of *N*-benzyl-γ-butyrolactam

The oxidation of *N*-benzyl γ-butyrolactam (**171**) gave the Nα-, Nβ- and Nγ-alcohols **172**–**174**, and further oxidation of the Nα-alcohol **172** to the imide **175** (Table 7.2, Appendix 3.27). The 36 h incubation with R19/F87A/A184I afforded the α-hydroxy-imide **176**, which was not observable in the screening reactions as they were incubated for 8 h.

Of the 48 variants in the library, 18 were found to convert more than half of the substrate (TON >1,000). The mutations S72W, A184I and A264G increased conversion. Nα-hydroxylation of **171** to *N*-benzyl-5-hydroxy-pyrrolidinone **172**, and of the imide **175** to **176**, showed >90% selectivity for 40 library variants. F81W, F87A and A184I enhanced formation of the imide **175**. For Nβ-oxidation, the A82M/A330P combination was the only that produced more than 20% of *N*-benzyl-4-hydroxypyrrolidinone, **173**, but the conversion was low (32%). Addition of S72W, V78I, or A184I to A330P-based variants increased the selectivity of the 3-hydroxy-product, **174**, to 67% given by the variant KU3/A330/S72W.

Table 7.2 The conversion and product distribution of $P450_{BM3}$ oxidation of *N*-benzyl-γ-butyrolactam, **171**.



Mutant	Conv.	Selectivity			
		5-OH: 172	4-OH: 173	3-OH: 174	imide: 175
A82M/A330P	32%	28%	24%	47%	–
KU3/A330P	48%	68%	4%	27%	–
KU3/A330P/S72W	80%	25%	8%	67%	–
RT2/A330P/V78I/A184I	85%	41%	3%	56%	–
R19	44%	100%	–	–	–
R19/F87A	25%	73%	–	–	27%
R19/F87A/A184I	83%	41%	–	–	59%
K19/F87A/F81W	61%	70%	–	–	30%
GVQ/A264G	76%	97%	–	–	3%
Activity enhancer		87F A330P	A82M/ A330P	S72W	A184I

The observation that different mutations were required to enhance Nβ- and Nγ-oxidation of **166** and **171** suggested the viability of altering the selectivity by varying the protecting group. It was also significant that there was no evidence of oxidation of the aromatic ring or the activated benzylic position of the benzyl protecting group in **171** whereas oxidation of the phenyl protecting group was observed for **166**. The benzyl protecting group also led to higher, though still modest (24%) selectivity for oxidation at the non-activated C4(β) position, supporting its use in further engineering with other amide and lactam substrates.

7.3 $P450_{BM3}$ oxidation of δ-velarolactam (piperidin-2-one)

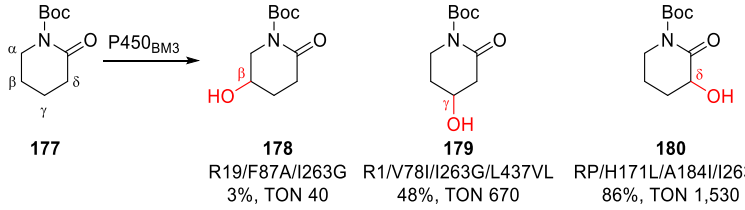
The effect of Boc, benzyl and tosyl as protecting groups was investigated with δ-velarolactam (piperidin-2-one). The *N*-tosyl derivative was insoluble in phosphate buffer,

leading to low conversion; its low volatility also hampered GC analysis which gave broad peaks. Therefore, its oxidation was not investigated further.

7.3.1 $P450_{BM3}$ oxidation of *N*-Boc-δ-velarolactam

Only two variants of the 48-variant library (WY2/9, Appendix 3.28), R19/F87A/I263G and RP/H171L/A184I/I263G, showed >50% conversion (73% and 89%, TON 1,460 and 1,780, respectively) of *N*-Boc-δ-velarolactam, **177** (Table 7.3). Interestingly, Nα-oxidation was not observed with any variant; C3(Nδ) hydroxylation was the most common activity with the highest yield of **180** (86%, TON 1,530) given by RP/H171L/A184I/I263G. In addition to **180**, R19/F87A/I263G also gave 17% (TON 250) of the Nγ hydroxylation product **179**.

Table 7.3 The conversion and product distribution of $P450_{BM3}$ oxidation of *N*-Boc-δ-velarolactam, **177**.



177 | **178** R19/F87A/I263G 3%, TON 40 | **179** R1/V78I/I263G/L437VL 48%, TON 670 | **180** RP/H171L/A184I/I263G 86%, TON 1,530

Mutant	**Conversion**	**Selectivity**		
		β-OH: 178	**γ-OH: 179**	**δ-OH: 180**
R19/F87A/I263G	73%	3%	17%	80%
RP/H171L/A184I/I263G	89%	–	14%	86%
RP/H171L/I263G/L437LV*	81%	–	18%	81%
R1/I263G/L437LV*	79%	–	16%	84%
R1/V78I/I263G/L437LV*	61%	–	18%	82%
R1/V78I/I263G/L437VL*	70%	–	48%	52%
R19/F87I	7%	–	100%	–
R19/F87A	15%	–	–	100%
R19/F87A/I263G/A264G	14%	–	–	100%
K19/F87V	5%	–	62%	38%
K19/F87V/I263G	16%	–	10%	90%
Activity enhancer			F87I/V L437LV	F87A I263G

The I263G sub-library was then screened and the mutations L437VL and V78I were identified to slightly increase γ-hydroxylation to form **179** (48%, TON 670 for R1/V78I/I263G/L437VL). Of the remaining variants, R19/F87I converted only 7% of the substrate but **179** was the only product it gave, suggesting the F87I mutation might increase γ-hydroxylation which needs further confirmation by repeating the 1 mL screening reaction with 2 mM substrate and 10 μM enzyme. The variant library gave little (<5%) of the Nβ oxidation product 3-hydroxy-*N*-Boc-piperidin-2-one (**178**). The F87V mutation also promoted Nγ-hydroxylation (62% of **179** at 5% conversion given by K19/F87V), but this was reversed by the addition of I263G as K19/F87V/I263G gave 90% of **180** (Table 7.3).

7.3.2 Oxidation of *N*-benzyl-δ-velarolactam

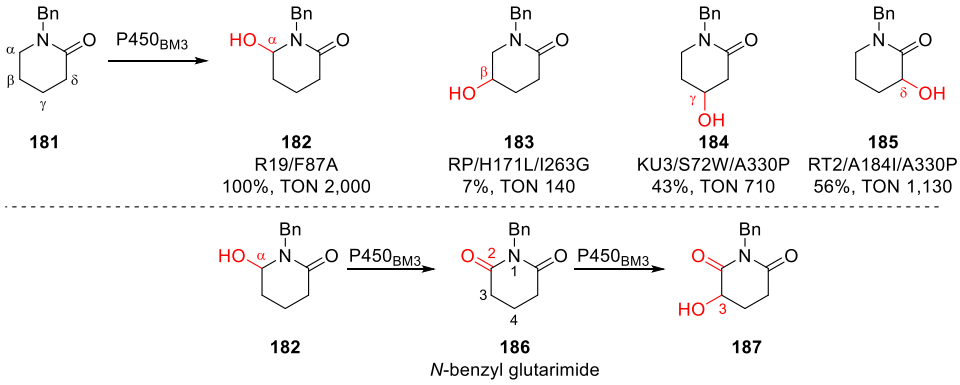
N-Benzyl-δ-velarolactam, **181**, was a much better substrate compared to the *N*-Boc form **177**, with 30 variants out of 48 (TFA/B plates, Appendix 3.29) giving >50% conversion. All mono-hydroxylation products of the lactam ring were formed (Table 7.4).

With the R19/F87A variant, **181** was oxidised with total selectivity and 100% conversion (TON 2,000) to the Nα hydroxylation product **182**; on prolonged reaction **182** was oxidised to the imide **186** and the 3-hydroxy-imide **187**. Similar to oxidation of cyclic amines, the mutations F87A/V were found to generally favour Nα oxidation of all the benzyl protected lactams due to Ala/Val creating space above heme and allowing greater substrate mobility.

The base variants RT2, RP, and R19/F87A gave 100% conversion, whereas wild type enzyme was inactive, suggesting R47L/Y51F might enhance the enzyme activity. V78F and L437LV slightly improved the yield for β-hydroxylation, with the 2nd generation variant RP/H171L/I263G/L437LV giving the most of **183** (19%, TON 360, Table 7.4). The mutations favouring γ oxidation to give **184** were S72W, A82M/A330P and I263R/G; the highest selectivity was 43% given by KU3/S72W/A330P (TON 710). The δ-alcohol **185** is

another precursor to 3-hydroxypiperidine. The mutations A184I, I263A/E267V, A330P, and L437LV favoured δ-oxidation, with the RT2/A184I/A330P variant yielding the most of **185** (56% selective, TON 1,130). Interestingly, this 2nd generation variant RP/H171L/I263G/L437LV demonstrated an evenly distributed product profile, with 35% of **182**, 19% of **183**, 14% of **184** and 31% of **185**, which is a good template variant for engineering β- and δ-oxidation via mutating/inserting residues around L437.

Table 7.4 The conversion and product distribution of $P450_{BM3}$ oxidation of *N*-benzyl-δ-velarolactam, **181**.



Mutant	Conv.	Selectivity			
		α-OH: 182	β-OH: 183	γ-OH: 184	δ-OH: 185
R19/F87A	100%	100%	–	–	–
RP/F87V	100%	100%	–	–	–
RP	100%	93%	3%	3%	–
RT2	94%	87%	6%	7%	–
RP/H171L/I263G/L437LV*	94%	35%	19%	14%	31%
RT2/V78F	30%	74%	14%	11%	–
RP/H171L	100%	85%	7%	8%	–
RP/H171L/I263G	100%	62%	7%	31%	–
R47L/Y51F/I263R	50%	57%	–	40%	2%
RT2/A330P	87%	57%	3%	11%	29%
RT2/A330P/A82M	95%	24%	1%	38%	38%
RT2/A330P/A184I	100%	23%	2%	18%	56%
KU3/A330P/S72W	83%	22%	–	43%	35%
K19/F87A/A184I/A328I	86%	59%	–	8%	33%
RP/I263A/E267V	100%	62%	5%	3%	29%
Activity enhancer		F87A	V78F L437LV	I263G/R	A82M A184I A330P

The insertion mutation L437VL improved γ oxidation of the Boc protected **177**, while L437LV showed improved β- and δ-oxidation of **181**. This perhaps suggested that the L437 turn in the β4 sheet interact with the protecting group, either Boc or benzyl herein, to tune the substrate binding orientation. Hence, site-saturation mutagenesis at L437 region (including insertion mutations before/after L437) should be carried out with R1/I263G and RP/H171L/I263G as templates to engineer remote functionalisation of these two δ-velarolactams **177** and **181**.

7.4 $P450_{BM3}$ oxidation of ε-caprolactams

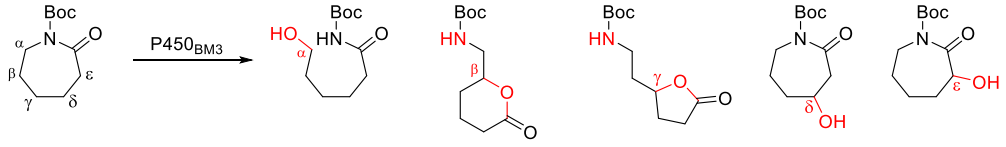
The seven-membered lactam ε-caprolactam with vinyl, Boc and benzyl protecting groups were screened for oxidation. *N*-Vinyl-ε-caprolactam provided mainly the deprotected ε-caprolactam and epoxidation of the vinyl group, with no evidence for any hydroxylation of the lactam ring. Only the Boc and benzyl derivatives will be discussed here.

7.4.1 Oxidation of *N*-Boc-ε-caprolactam

The variants K19/F87V and R19/F87A were selected from initial screening for preparative scale reactions, from which five products were characterised (Table 7.5). These arose from oxidation from every available carbon position in the lactam ring – the ring-opening alcohol **189** derived from Nα-hydroxylation, the lactones **190** and **191** derived from the β- and γ-alcohol respectively, the δ-alcohol **192** and the ε-alcohol **193**. Lactones **190** and **191** had the same retention time on the GC under all conditions tested. The proportions of these relative to other GC-detectable products were estimated from NMR spectra of crude extracts and then combined with the integrated GC peak areas to calculate the product selectivity. Time-course monitoring of the reaction with the K19/F87V variant showed no evidence of peaks with different retention times that could be assigned to the β- or γ-alcohol, indicating that these intermediates underwent rapid rearrangement to form the lactones **190**

and **191**, probably due to the formation of conformationally favoured 5- and 6-membered ring lactones. The enzyme might also play a role in this fast rearrangement of the lactam to the lactone. By contrast, the δ- (**192)** and ε- (**193**) alcohols did not undergo rearrangement to the 4-membered (β-) and 3-membered (α-) ring lactones.

Table 7.5 Conversion and product distribution of $P450_{BM3}$ oxidation of *N*-Boc ε-caprolactam (**188**).



188		**189**	**190**	**191**	**192**	**193**
	R19/F87A	42%	–	22%	3%	33%
	K19/F87V	4%	10%	51%	8%	27%

$P450_{BM3}$ Variant	**Conversion**	**Selectivity**			
		189	**190 & 191**	**δ-OH: 192**	**ε-OH: 193**
GVQ/I263G	100%	27%	16%	1%	55%
GVQ/A82M/I263G	51%	100%	–	–	–
RP/H171L/I263G	86%	–	90%	–	10%
RP/I263A/E267V	61%	–	94%	–	6%
R19/F87I	34%	53%	42%	5%	1%
R19/F87I/L437LV	67%	–	93%	7%	–
K19/F87V (NMR analysis)	64%	4%	61%	8%	27%
K19/F87V/E267V	25%	–	70%	17%	13%
K19/F87A/I263G	100%	71%	13%	1%	15%
R19/F87A	85%	42%	22%	3%	33%
R19/F87A/I263G	100%	90%	8%	1%	1%
R19/F87A/I263G/A264G	77%	–	23%	2%	76%
Activity enhancer		A82M	I263G/A	E267V	A264G

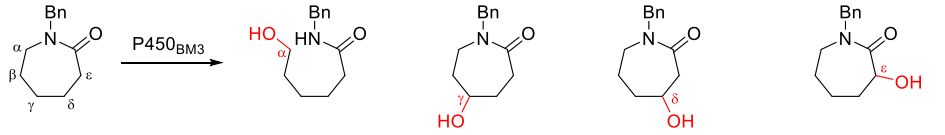
Across the 48-variant screening library, 19 variants showed >50% conversion (TON >1,000); four variants, K19/F87A/I263G, R19/F87A/A184I, R19/F87A/I263G and GVQ/I263G gave full conversion (Table 7.5). The mutations I263G/A in the F87-unmutated variants, and the F87I/L437LV combination, favoured the formation of lactone **191** via initial γ-oxidation (93%), whilst the combination of F87V with E267V slightly increased δ-hydroxylation to 17%. The R19/F87A/I263G variant gave 90% of the Nα oxidation product **189**, but addition of the A264G mutation shifted the selectivity to Nε-

hydroxylation; R19/F87A/I263G/A264G gave the most of **193** (76% selective, TON 1,170), which has potential application in the synthesis of β- and α,α,β-functionalised azepanes.

7.4.2 Oxidation of *N*-benzyl-ε-caprolactam

The benzyl protected form **194** was oxidised by the 48-variant library (WY7/8) and the I263G sub-library (Appendix 3.31) at the Nα-position to the ring-opening alcohol **195**, the γ-alcohol **196**, the δ-alcohol **197**, and the ε-alcohol **198** (Table 7.6). Unlike *N*-Boc-ε-caprolactam (**188**), no ring rearrangement to lactones was observed.

Table 7.6 Conversion and product distribution of $P450_{BM3}$ oxidation of *N*-benzyl ε-caprolactam (**194**).



194 | **195** K19/F87V 100%, TON 1,740 | **196** RP/I263G 92%, TON 1,840 | **197** RP/H171L/I263G 9%, TON 180 | **198** RT2/V78I/A184I/A330P 93%, TON 1,050

Mutant	**Conversion**	**Selectivity**			
		195	**196**	**197**	**198**
GV/A184I	46%	100%	–	–	–
GVQ	71%	100%	–	–	–
K19/F87V	87%	100%	–	–	–
R19/F87A	84%	100%	–	–	–
RP/H171L	95%	45%	44%	–	10%
RP/I263G	100%	–	92%	5%	–
RP/H171L/I263G	95%	–	91%	9%	–
RP/H171L/A184I/I263G	96%	–	86%	10%	–
RT2	92%	48%	44%	–	7%
RT2/V78I/A184I/A330P	56%	2%	3%	2%	93%
R19	42%	64%	30%	–	7%
R19/S72W/F87A/A328I	19%	24%	5%	8%	61%
Activity enhancer		F87A/V	I263G	I263G	V78I

N-Benzyl-ε-caprolactam was a reasonable substrate for the screening library, with 15 out of 48 variants converted more than 50% of substrate (TON >1,000). The R47L/Y51F couplet boosted the oxidation activity. The I263G mutation shifted the selectivity to 92% for the γ-alcohol **196**, together with 5% of the δ-alcohol **197**. The introduction of H171L to

the RP/I263G-based variants yielded some **197** (up to 10% given by RP/H171L/A184I/I263G). The triple combination of V78I/A184I/A330P promoted 93% ε-hydroxylation to give **198**. S72W also promoted **198**, but with impaired conversion.

Compared with *N*-Boc-ε-caprolactam (**188**), the oxidation pattern of *N*-benzyl ε-caprolactam (**194**) also provided high selectivity for γ- and ε-oxidation products across the variant library. Selectivity for oxidation of the β- and δ-C–H bonds remained low. However, the less electron-withdrawing benzyl protecting group stopped rearrangement to lactones. The effect of mutations also changed with the protecting group. Further substrate and enzyme engineering are required to shift the oxidation selectivity towards Nβ and Nδ.

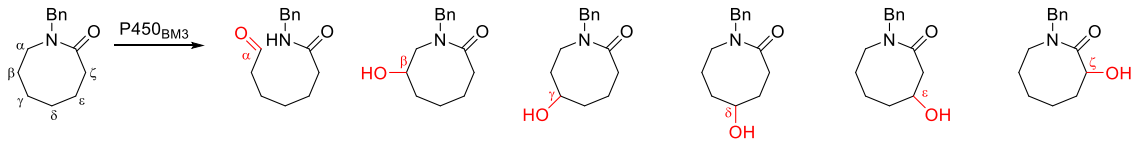
7.5 Oxidation of *N*-benzyl-ζ-enantholactam

N-Benzyl-ζ-enantholactam (**199**) was screened against a 24-variant library (WY9, Appendix 3.32). GC analysis showed products arising from oxidation at all C–H bonds, with moderately high selectivity (~70%) for the aldehyde, γ- and δ-alcohols, 30–40% of the β- and ε-alcohols, and low selectivity (16%) for the ζ-alcohol (Table 7.7).

Two variants, R19/F87I and GV/A184I, completed the reaction within 1.5 hours (100% conversion, TON 2,000). Another 3 variants, K19/F87V, R19/F87A and R19/F87A/A184I, also indicated >50% conversion in 1.5 hours. After 8 h incubation, 5 variants out of 24 gave >50% conversion, with F87I/V/A and A184I showing activity enhancement. The mutation A330W favoured the Nβ alcohol **201** (56% at only 5% conversion, given by R19/A330W, Table 7.7). The base variant RT2 gave 30% (TON 230) of Nβ oxidation. The mutation F87I was crucial for γ-oxidation; R19/F87I was the only variant showing >50% yield of **202**. The mutations A82M, A184I and Q403P, and the combination I263G/A328L enhanced the formation of the δ-hydroxylation product **203** at up to 78% selectivity (given by K19/F87V/Q403P). The combination of I263G/A328L and the mutation A328V

improved ε-hydroxylation. The GVQ/I263G/A328L variant gave only two products, 53% of δ-(**203**) and 47% of ε-(**204**) perhaps due to the influence of the I263G/A328L couplet on the binding orientation of the substrate. ζ-Hydroxylation was least favoured; A328V slightly improved its selectivity to 16% given by K19/F87V/A328V. In oxidation of *N*-benzyl-ζ-enantholactam (**199**), the mutations F87V/I no longer favoured Nα oxidation, and the mutations A82M, A184I, I263G, A328V/L, A330W and Q403P altered substrate binding inside the active site favouring remote functionalisation.

Table 7.7 Conversion and product distribution of $P450_{BM3}$ oxidation of *N*-benzyl ζ-enantholactam (**199**).



Mutant	**Conv.**	**Selectivity**					
		200	**201**	**202**	**203**	**204**	**205**
GV/A184I	100%	5%	5%	29%	55%	6%	–
GVQ	31%	84%	–	–	–	16%	–
GVQ/I263G/A328L	20%	–	–	–	53%	47%	–
K19/F87V	75%	37%	8%	17%	29%	9%	–
K19/F87V/A328V	44%	–	3%	5%	38%	38%	16%
K19/F87V/Q403P	28%	–	2%	14%	78%	6%	–
K19/A82M/F87A/A330W	57%	–	15%	24%	51%	8%	3%
R19/F87A	88%	78%	–	5%	5%	11%	–
R19/F87A/A184I	100%	19%	5%	16%	53%	7%	–
R19/F87I	100%	2%	–	75%	23%	–	–
R19/A330W	5%	–	56%	15%	23%	5%	–
RT2	38%	–	30%	17%	43%	10%	–
GV/A184I/I263G*	12%	–	–	27%	70%	1%	1%
K19/A82M/F87A/I263G/A264G*	17%	–	3%	9%	84%	4%	1%
K19/A82M/F87A/A264G*	22%	–	8%	6%	62%	10%	14%
K19/A82M/F87A/A264G/A328G*	20%	–	80%	5%	9%	3%	3%
Activity enhancer		F87V/A	A328G A330W	F87I	A264G Q403P	A328L/V	A264G A328V

The product diversity observed with GV/A184I, K19/A82M/F87A/A330W, R19/F87A and R19/F87A/A184I made them good candidates for further selectivity engineering. The substrate was then screened against the Gly-sub-library (developed by Wenyu Chen and Aaron Leung), with Gly introduced at the I-helix and the A328/P329/A330 loop of the aforementioned four variants (Appendix 3.32). As for the selectivity improvement of remote functionalisation of **199**, β-hydroxylation was promoted to 80% selectivity though with low conversion (20%), given by K19/A82M/F87A/A264G/A328G; δ-hydroxylation was increased to 84% selectivity with low yield again (17%), shown by K19/A82M/F87A/I263G/A264G (Table 7.7). The I-helix mutations I263G and A264G promoted Nδ and Nζ oxidation respectively, and A328G was found improving Nβ oxidation.

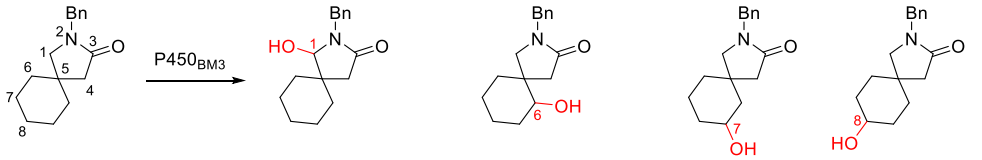
In summary, conversion of **199** was improved by F87A/V/I and A184I; A328G and A330W favoured Nβ oxidation (up to 80%); F87I lifted Nγ oxidation (up to 75%); A184I, I263G and Q403P increased Nδ oxidation (up to 84%); A328V and I263G/A328L improved Nε oxidation (up to 47%); A264G and A328V raised Nζ oxidation slightly (up to 16%). The stereoselectivity of these products needs to be determined. Protein engineering can be carried out on the RT2 base variant by introducing the identified mutations and their combinations. Protecting group engineering may also be informative, but less electron-withdrawing protecting groups may be better choices since these seem to reduce the ring-rearrangement of the hydroxy-lactams to 5- and 6-membered ring lactones. Such extent of oxidation diversity has never been observed in other lactams, which might be justified as the flexibility and bulky size of the eight-membered ring and the bulky benzyl group restricted the movement of the substrate inside the active site, where the addition of the mutations shifted the exposed C–H bonds.

7.6 $P450_{BM3}$ oxidation of spirolactams

7.6.1 Oxidation of *N*-benzyl-2-azaspiro[4.5]decan-3-one

The screening reactions of *N*-benzyl-2-azaspiro[4.5]decan-3-one (**206**) by the 24-variant library (WY9, Appendix 3.33) were carried out for 3 hours in order to minimise any further oxidation. The substrate was oxidised at the Nα carbon C1 and all three positions (C6, C7, C8) of the carbocyclic ring to form the corresponding alcohols **207**–**210** (Table 7.8). There was no evidence for oxidation at C4 of the lactam ring.

Table 7.8 Conversion and product profile of $P450_{BM3}$ oxidation of *N*-benzyl-2-azaspiro-[4.5]decan-3-one.



206 | **207** R19/S72P/A330W 90%, TON 1,170 | **208** R19/A328G/P329G/A330G 35%, TON 690 | **209** GVQ/V78L/I263G 70%, TON 330 | **210** R19/I263G 81%, TON 1,280

Mutant	**Conversion**	**Selectivity**			
		207	**208**	**209**	**210**
R19	90% (16 h)	22%	5%	1%	72%
R19/F87I	20% (3 h)	–	21%	30%	49%
	67% (16 h)	1%	24%	30%	45%
R19/F87A	55% (3 h)	46%	–	19%	32%
R19/F87A/A184I	91% (3 h)	14%	–	22%	57%
R19/F87A/A328G/P329G/A330G	9% (3 h)	76%	4%	5%	15%
R19/A328G/P329G/A330G*	99% (16 h)	27%	35%	–	38%
GV/A184I	95% (3 h)	6%	3%	18%	70%
GVQ	2% (3 h)	62%	–	27%	11%
GVQ/V78L/I263G	24% (3 h)	–	6%	70%	24%
K19/F87V/I263G	20% (3 h)	–	12%	63%	26%
R19/I263G*	79%	–	–	18%	81%
R19/S72V/A330W*	56%	85%	–	–	15%
R19/S72P/A330W*	65%	90%	–	–	10%
R19/P329G/A330W*	92%	82%	2%	–	16%
R19/A330W	8%	60%	–	–	40%
Activity enhancer		S72P/V A330W	87F A328G/P329 G/A330G	V78L I263G	I263G F87V/ A184I

Within the library, 5 variants gave higher than 50% conversion (TON >1,000). The mutation A184I was found to promote substrate oxidation and accelerate the biotransformation – the variants GV/A184I and R19/F87A/A184I showed >90% conversion within 3 hours (TON >1,800, Table 7.8). The larger side chain for F87I slightly promoted C6 oxidation on the carbocyclic ring to form **208**. When F87 was not mutated, the 8-hydroxy-product **210** was favoured, with 72% selectivity given by R19. Addition of the A328G/P329G/A330G triplet switched the activity towards C6 hydroxylation from 5% given by R19 to 35% given by R19/A328G/P329G/A330G. C7 oxidation was favoured by F87I and the combination of F87V/I263G with GVQ/V78L/I263G giving 70% of **209**, and C8 oxidation by A184I.

The expanded variant library based on R19 and GVQ with non-polar amino acids introduced at the active site residues S72, A328, P329, A330 and all I-helix residues (developed mainly by Yuan Zhang) was screened with **206**. The R19/I263G variant gave 81% of **210** compared to 72% for R19, and the mutations S72V, S72P, P329G and A330W favoured α-oxidation (Table 7.8).

In terms of oxidation of **206**, C4(γ) oxidation was not observed. C6 oxidation was a minor activity. This suggested that C4 and C6 were far away from the ferryl oxygen, possibly due to the presence of the C3 carbonyl group. Exploration of mutations at S72, A328, P329 and A330, which can alter the hydrogen bonding network inside the active site, might resolve this issue to generate some C4(γ) hydroxylation product.

7.6.2 Oxidation of *N*-benzyl-2-azaspiro[4.6]undecane-3-one

With 2-azaspiro[4.6]undecane-3-one, **211**, the unprotected substrate was screened against the variant library. Three variants, K19/F87V, GV/A184I and K19/A82M/F87A/A330W

converted more than 60% of the substrate into the C6 and C8 hydroxylation products **212** and **213** (Figure 7.6). The C6(α)-hydroxylation product was favoured.

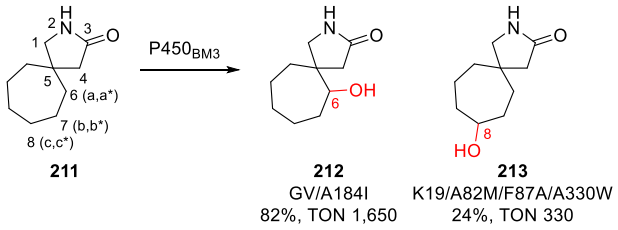


Figure 7.6 The reaction scheme of $P450_{BM3}$ oxidation of 2-azaspiro[4.6]undecan-3-one (**211**).

The protected form **214** was converted in 3-hour incubation by the WY9 library into C1, C7(b), C7(b*), C8(c) and C8(c*) hydroxylation products **215**–**217** (Figure 7.7), without any evidence of C6 hydroxylation. The similarity of the polarities for the C7 and the C8 diastereomers made them very difficult to separate; **216** had to be characterised as a mixture. Even so, the relative stereochemistry of **216** and **217** were tentatively assigned by the distinct coupling patterns between C1–H and C1–H' (Figure 7.8 and 7.9). In their ^{1}H NMR spectra, both 5*R*,7*R*-/5*S*,7*S*-**216** and 5*R*,8*R*-/5*S*,8*S*-**217** showed a singlet for the Nα CH_2 group (C1), whereas the Nα CH_2 groups in 5*R*,7*S*-/5*S*,7*R*-**216** and 5*R*,8*S*-/5*S*,8*R*-**217** were a double doublet and a quartet, respectively. 5*R*,7*R*-/5*S*,7*S*-**216** also showed a quartet for the benzylic CH_2 (C12) at δ 4.43 ppm, but 5*R*,8*R*-/5*S*,8*S*-**217** showed a singlet for hydrogens at C12. This suggested that c/c*-OH was too remote to influence the splitting pattern of benzylic CH_2. Prolonged incubation of the preparative reaction using GV/A184I also generated their corresponding ketones **218** and **219**; determination of their configuration at C5 would lead to the absolute stereochemistry and enantioselectivity of **216** and **217**. The respective nOe spectra are needed for further confirmation of the stereochemistry of the diastereomers of **216** and **217**.

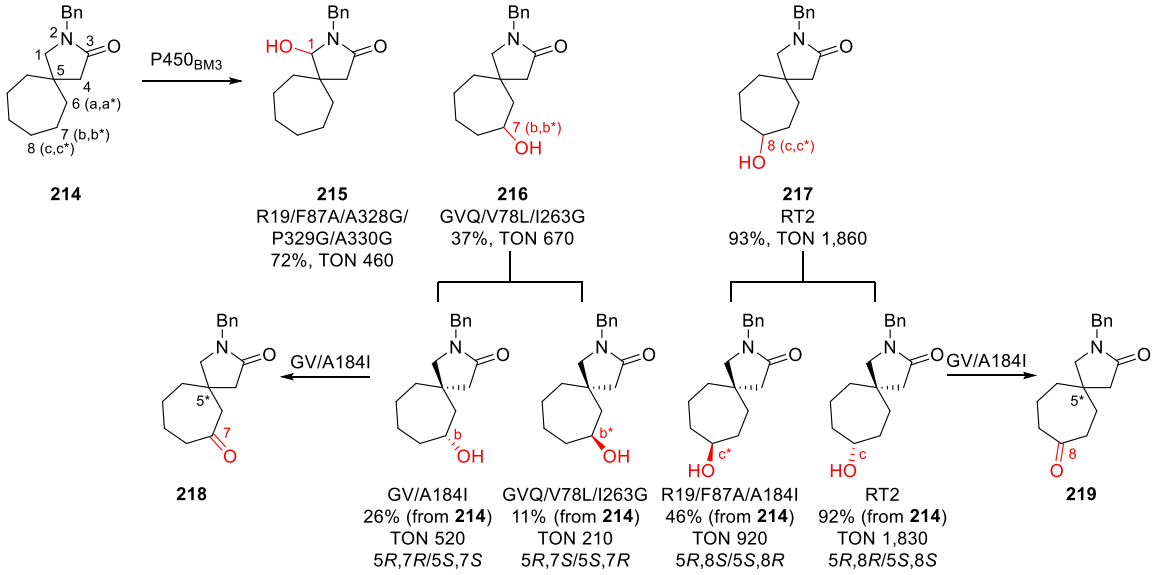


Figure 7.7 The reaction scheme of $P450_{BM3}$ oxidation of *N*-benzyl 2-azaspiro[4.6]undecan-3-one (**214**).

The dominant diastereomeric pair of **216** consisted of 5*R*,7*R*- and 5*S*,7*S*-7-hydroxy-2-azaspiro[4.6]undecane-3-one, and 5*R*,8*R*- and 5*S*,8*S*-**217** were prevalently formed across the variant library. Even though their absolute stereochemistry needs further study to clarify, the coincidence of the favourable relative stereochemistry indicated that the Compound I might tend to abstract the hydrogen atoms on the same side as the C5–C4 bond. This also implied that amino acid residues close to the porphyrin ring anchored the carbonyl group to differentiate each symmetric pair of C–H bonds of the seven-membered ring. The lack of any C6 oxidation, in contrast with the oxidation of **211** mainly giving C6 oxidation, also suggested that the protecting group of the nitrogen atom might tilt the substrate binding orientation significantly inside the active site.

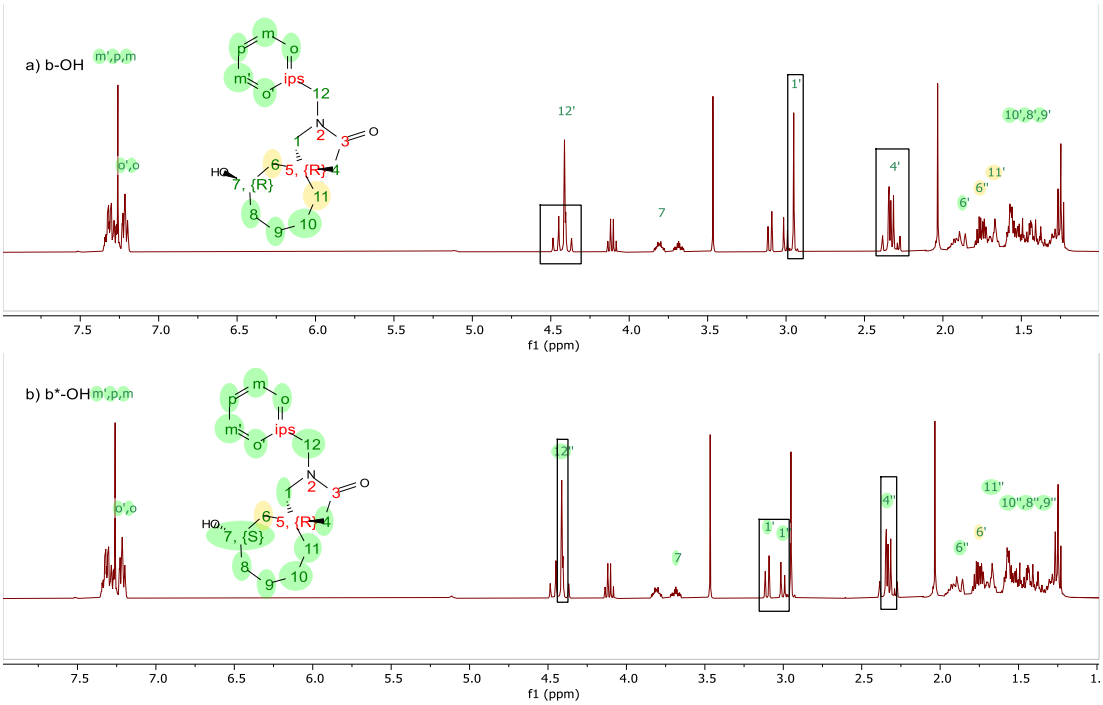


Figure 7.8 The ^{1}H NMR spectrum of **216** (b-OH and b*-OH).

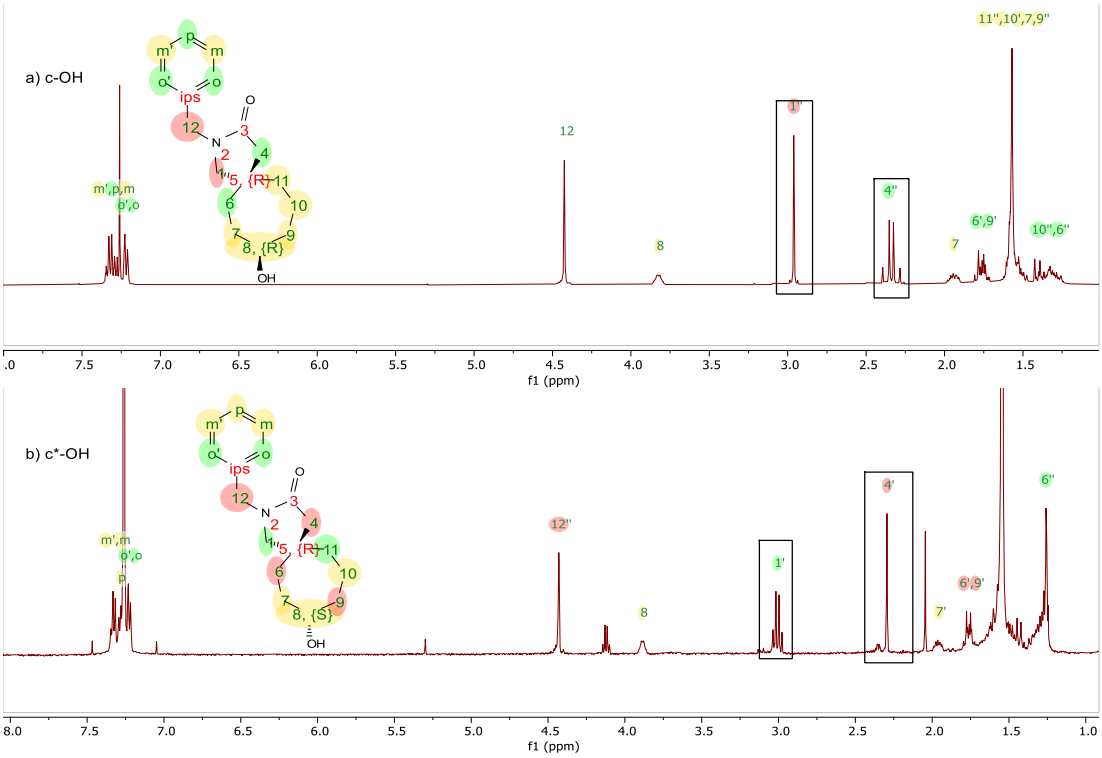


Figure 7.9 The ^{1}H NMR of **217** (c-OH and c*-OH).

In terms of conversion, 10 out of 24 variants (WY9, Appendix 3.33) converted half of the amount of substrate (TON >1,000), with RT2, GV/A184I and R19/F87A/A184I showing full conversion (TON 2,000). The mutations F87V/I and A184I enhanced the general

oxidation activities and all of the high-conversion variants showed C8 hydroxylation as their dominant activity (>50% selectivity, TON >850). Only the variant R19/F87A/A328G/P329G/A330G gave >50% of the α-hydroxylation product **215** (72%, TON 460), revealing the importance of the A328/P329/A330 region in flipping regioselectivity. The 2nd generation variant R19/P329G/A330W even gave 44% of the 6-hydroxy-product **220** (Figures 7.10 and 7.11).

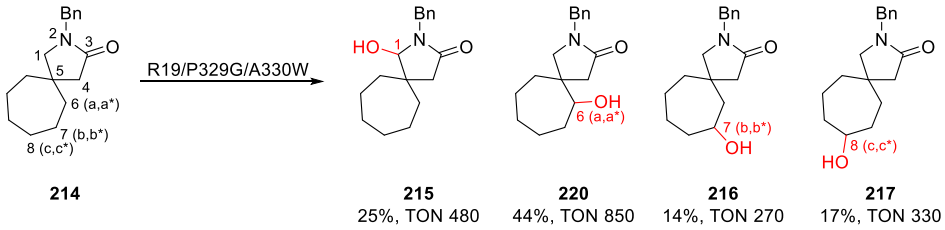


Figure 7.10 The reaction scheme of the R19/P329G/A330W-catalysed oxidation of **214**.

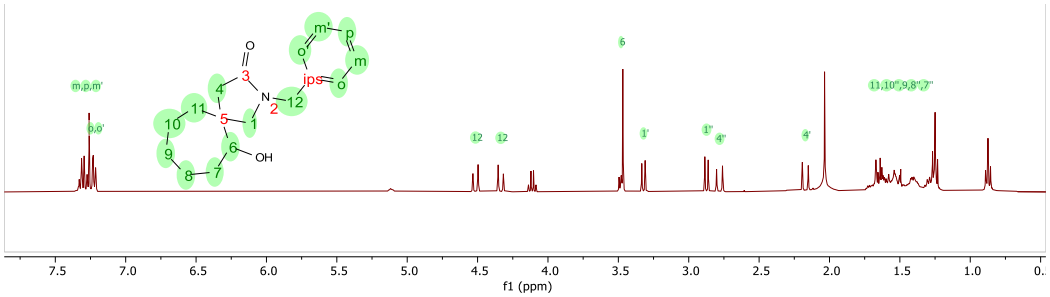


Figure 7.11 The ^{1}H NMR of **220**.

The combinations V78L/I263G, I263A/A328L and F87V/A184I tuned the activity modestly to C7 oxidation; A184I and I263A/A328L favoured the b-alcohol **216** (>99% *de*, TON 210 given by R19/I263A/A328L), whilst F87I slightly improved the yield of the b*-alcohol (8 : 10 *dr*, TON 90 given by R19/F87I; Table 7.9). C8 oxidation was the dominant activity observed for most screening reactions (up to 93% given by RT2). The mutation F87V itself preferred to form the c-alcohol (10 : 1 *dr*, TON 1,350), whilst F87A and F87A/A184I favoured the formation of the c*-alcohol (12 : 10 and 11 : 10 *dr*, TON 470 and 920 shown by R19/F87A and R19/F87A/A184I). Additionally, RT2 strongly favoured the formation of the c-alcohol **217**.

Table 7.9 The conversion and product distribution of $P450_{BM3}$ oxidation of *N*-benzyl-2-azaspiro[4.6]undecan-3-one (**214**).

Mutant	**Conv.**	**Selectivity**				
		215	**216**	***dr* (b*/b)**	**217**	***dr* (c*/c)**
GV/A184I	100%	–	28%	1/10	71%	1/10
RT2	100%	–	7%	6/10	93%	96% *de* to c
K19/F87V	88%	2%	15%	2/10	83%	1/10
K19/F87V/A328V	79%	–	11%	2/10	86%	93% *de* to c
RP/V78I/E267V	87%	–	14%	2/10	83%	1/10
GVQ/V78L/I263G	91%	–	37%	4/10	58%	4/10
R19/F87I	88%	–	12%	8/10	87%	6/10
R19/F87A	57%	13%	10%	6/10	75%	1 2/10
R19/F87A/A184I	100%	1%	10%	2/10	89%	1 1/10
R19/F87A/A328G/P329G/A330G	32%	72%	12%	>99% *de* to b	11%	3/10
R19/I263A/A328L	39%	–	27%	>99% *de* to b	64%	94% *de* to c
R19/A330W	11%	10%	–	–	63%	>99% *de* to c
Activity enhancer		A328G/P329G/A330G	V78L A184I A328L		RT2	

Most variants showing oxidation at the introduced β-spiro cycles indicated that the size of the active site was currently too spacious for the γ-butyrolactam core itself, and that the introduction of the bulkier or the H-bond donating amino acids at the active site residues would possibly improve the β oxidation of γ-butyrolactam derivatives. Also, bulkier benzyl group indicated slightly higher oxidation at β- and γ-oxidation which suggested that bulkier protecting groups like Cbz should be tested for γ-butyrolactam and its spiro-lactams to improve the contacting efficiency between the active-site residues and the substrates.

7.6.3 Oxidation of 8-azaspiro[4.5]decanes and its imide derivatives

The successful example of $P450_{BM3}$ oxidation of **186** stimulated the investigation of its spiro-derivatives, 8-azaspiro[4.5]decane **221** and 8-azaspiro[4.5]decane-7,9-dione **222**

(imide). Firstly, both non-protected substrates **221** and **222** were screened against the WY9 library to acquire background knowledge that **221** was inactive, whilst **222** was mainly oxidised by the library at α C–H to form **223** with the variant K19/A82M/F87A/A330W showing highest yield (82% selective, TON 1,120, Figure 7.12). Obviously, the reduction of **223** will lead to the formation of its β-hydroxy-piperidine derivative.

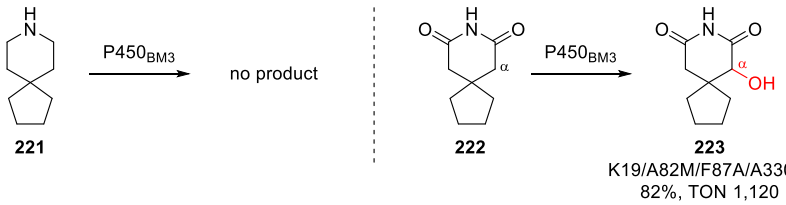


Figure 7.12 The reaction schemes of $P450_{BM3}$ oxidation of 8-azaspiro[4.5]decane (**221**) and 8-azaspiro[4.5]decane-7,9-dione (**222**).

Secondly, *N*-Boc-8-azaspiro[4.5]decane (**224**) was screened, and the 48-variant library (TFA1/B1, Appendix 3.35) produced two major products and a couple of minor products. The variant RP/F87V was scaled up for product purification, leading to 32% of 1-alcohol **225**, 27% of 2-alcohol **226**, 17% of 2-ketone **227** and 20% of *syn*-1,3-diol **228** being purified after overnight incubation (Figure 7.13).

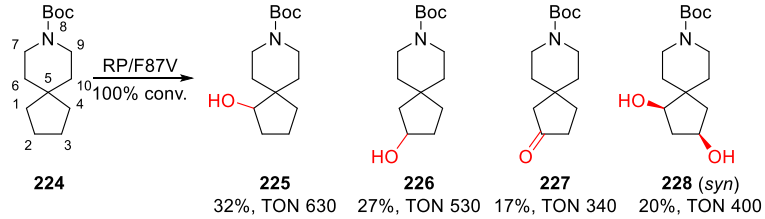


Figure 7.13 The reaction scheme of the RP/F87V-catalysed oxidation of *N*-Boc-8-azaspiro[4.5]decane.

The mono-hydroxylation products **225** and **226** were the dominant products. The mutations R47L/Y51F, F87V/I/A and I263G promoted general enzymatic activities, for example, the R47L/Y51F variant gave 95% (TON 1,900), in contrast with the totally inactive wild type enzyme. F87A and E267V promoted the formation of **225**; with R19/F87A showing 86% selectivity (TON 1,620) and RP/E267V giving 100% (TON 260), whilst I263G, E267G and A328I favoured **226** (85%, TON 660 given by RP/E267G, 98%, TON 960 given by

GVQ/I263G and 97%, TON 780 given by RT2/F81W/A328I, Table 7.10). There was no evidence for any α- or β-oxidation.

Table 7.10 Conversion and product distribution of $P450_{BM3}$ oxidation of *N*-Boc 8-azaspiro[4.5]decane.

Mutant	**conv.**	**225**	**226**	**227**	**228**
RP	96%	58%	41%	1%	
RP/F87V	98%	32%	27%	17%	20%
RP/E267V	13%	100%			
RP/E267G	39%	15%	85%		
RP/F87V/E267V	96%	42%	44%	4%	8%
GVQ	21%	100%			
GVQ/I263G	49%		98%	2%	
R19/F87I	92%	18%	79%	3%	
R19/F87A	94%	86%	11%		1%
R19/F87A/A328I	82%	48%	49%	2%	
R47L/Y51F	95%	44%	55%	1%	
RT2	98%	40%	59%	1%	
RT2/F81W	69%	57%	42%	1%	
RT2/F81W/A328I	40%		97%	2%	
Activity enhancer		F87A/V E267V	I263G E267G A328I	F87V	F87V

Due to the lack of β oxidation of the 8-azaspiro[4.5]decane core, the production of α-alcohol of **222** and the good enzymatic activity towards *N*-benzyl-δ-velarolactam in contrast with the *N*-Boc- or *N*-Ts forms, *N*-benzyl-8-azaspiro[4.5]decane-7,9-dione (**229**) was screened against the WY9 variant library (Appendix 3.36), also targeting for α-hydroxylation and remote functionalisation.

The variants R19/F87I and GV/A184I were used for the biotransformation of **229** on preparative scale. The variant R19/F87I gave 42% C6(α) hydroxylation **230**, 16% of its ring-rearranged lactone **233**, 32% of 2-alcohol **231** and 5% of the *syn*-2,6-diol **232** (2*S*,5*S*,6*S* or/and 2*R*,5*R*,6*R*). GV/A184I also produced the 6,10-diol **234** and its ring-

rearranged lactone **235** (Figure 7.14). The α-alcohol **230** was reduced by $LiAlH_4$ into the β-hydroxy-amine **236** as one example of the methodology.

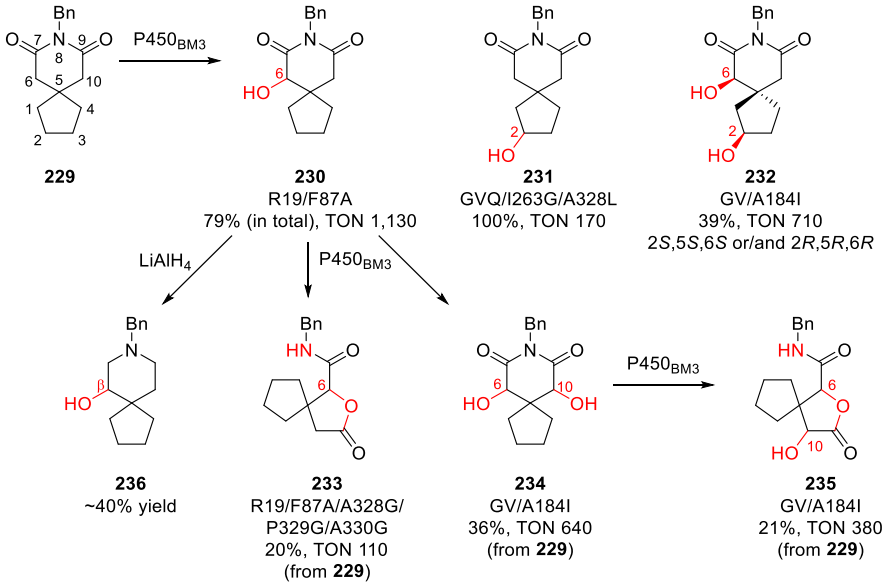


Figure 7.14 Reaction scheme of $P450_{BM3}$ oxidation of *N*-benzyl-8-azaspiro[4.5]decane-7,9-dione (**229**).

The formation of **233**, **234** and **235** was concurrent with the oxidation of **229** to **230**, which meant that the $P450_{BM3}$ enzymes might recognise **230** as a better substrate than **229**. Such observation also elucidated the dilemma of raising the proportion of **230** in the product profile; suppression of further oxidation should be considered whilst adding mutations to improve α (C6) oxidation. The lack of C1 oxidation was in stark contrast to oxidation of **224**, which suggested that the two carbonyl groups might interact with the active-site residues to steer away the C1–H and C4–H for both **229**, **230** and **231**.

A third of the 24 variant library showed higher than 50% conversion (TON >1,000) after 3 h incubation and the mutations V78L, F87A/V and A184I promoted the general oxidation activity. 15 variants favoured C6 oxidation including the formation of **230**, **233**, **234** and **235**, and F81W, F87A, L188Q and A328V/G favoured such activity (Table 7.11). F87V/A, A328I and I263G diversified further oxidation of **230**, while A328V/G favoured the ring-rearrangement of **230** only. The variants that gave high proportions of **230** (>60%

selectivity) also coincided with low conversion ranging from 10% to 30% (TTN 200–600, Table 7.11); mutations which improved conversion also increased further oxidation to some extent. The variants R19/I263A/A328L and GVQ/I263G/A328L gave 100% selectivity of **231** though with inhibited conversion (8% and 3%); nevertheless, this showed that the I263 and the A328 residues affected C2 oxidation. The mutations F87V and A184I increased the proportion of **232**, and GV/A184I gave the most (39%).

Table 7.11 The conversion and selectivity of $P450_{BM3}$ oxidation of **229**.

Mutant	**Conversion**	**Selectivity**						
		230	**233**	**234**	**235**	**C6**	**231**	**232**
R19/F87I	36%	42%	16%	–	–	58%	32%	5%
R19/F87A	71%	46%	13%	7%	13%	79%	5%	–
R19/F87A/I263G/A264G	90%	10%	4%	8%	–	22%	22%	20%
R19/F87A/A328G	21%	74%	21%	–	–	95%	5%	–
R19/F87A/A328G/P329G/A330G	28%	64%	20%	–	–	84%	16%	–
R19/F87A/A184I	61%	54%	15%	9%	4%	82%	6%	12%
GV/A184I	91%	15%	5%	14%	21%	55%	6%	39%
GVQ	5%	98%	2%	–	–	100%	–	–
GVQ/V78L/I263G	63%	16%	6%	17%	9%	48%	33%	20%
GVQ/I263G/A328L	8%	–	–	–	–	–	100%	–
R19/I263G/A328L	3%	–	–	–	–	–	100%	–
K19/F87V	68%	35%	11%	–	15%	61%	5%	33%
K19/F87V/I263G	65%	15%	5%	19%	8%	48%	25%	28%
K19/F87V/A328V	19%	72%	20%	–	–	92%	8%	–
K19/F87V/Q403P	64%	40%	13%	–	15%	68%	5%	–
K19/F81W/F87A	14%	72%	23%	–	–	95%	5%	–
Activity enhancer		F87A/V					I263G/ A328L	

To sum up, compared with *N*-benzyl glutarimide (**186**), the oxidation of the glutarimide ring in **229** was more diversified that multi-functionalisation and ring-rearranged cyclisation were commonly observed for **229**. The lack of piperidine ring oxidation for **224** and the lack of C1 oxidation for **229** also suggested that the backbone modification of the amine core can direct the selectivity shift, perhaps via introducing H-bonding interactions

and altering the substrate size in this case, without any evolution of the existed enzyme library. The successful example of reducing **230** into **236** also laid the foundation of generating multi-functionalised cyclic amines, *e.g.* the reduction of **232** and **234**. The comparison between oxidation of **224** and **229** also indicated that the mutation F81W and the A328/P329/A330 region were important for C2 hydroxylation of **224** but maintaining C6 mono-hydroxylation of **229**. More mutagenesis and substrate-bound crystal structures could be applied to understand the difference, and other substrates such as *N*-Boc-8-azaspiro[4.5]decane-7,9-dione and *N*-benzyl-8-azaspiro[4.5]decane ought to be screened for more precise comparison. The absolute stereochemistry of the products has to be determined.

7.7 Summary and outlook

Monocyclic lactams and their spirocyclic derivatives were found to be excellent substrates for engineered $P450_{BM3}$ enzymes. The reactions with high conversion and the *N*-benzyl-protected lactams were normally completed within 4 hours (TON 2,000) and further oxidation usually occurred over prolonged incubation. The versatility of engineered $P450_{BM3}$ was reflected by the wide range of products generated from the studied reaction where nearly all C–H bonds of these cores were hydroxylated. The highest selectivities for remote functionalisation and oxidation at α-to-carbonyl (Figure 7.15) showed that benzyl was the preferred protecting group for remote functionalisation of lactams in contrast with Boc/Ph/H.

For the monocyclic lactams, although oxidation at some sites of these cores are still in low selectivity after protecting group and protein engineering (Figure 7.15), the reduction of the mono-alcohol products by $LiAlH_4$ will give >75% selectivity for the mono hydroxy-amines (pyrrolidine, piperidine, azepane and azocane) at all available sites. The absolute

stereochemistry of these products has to be determined, which provides wider scope for engineering the stereochemistry of both the lactam- and the amino-alcohols.

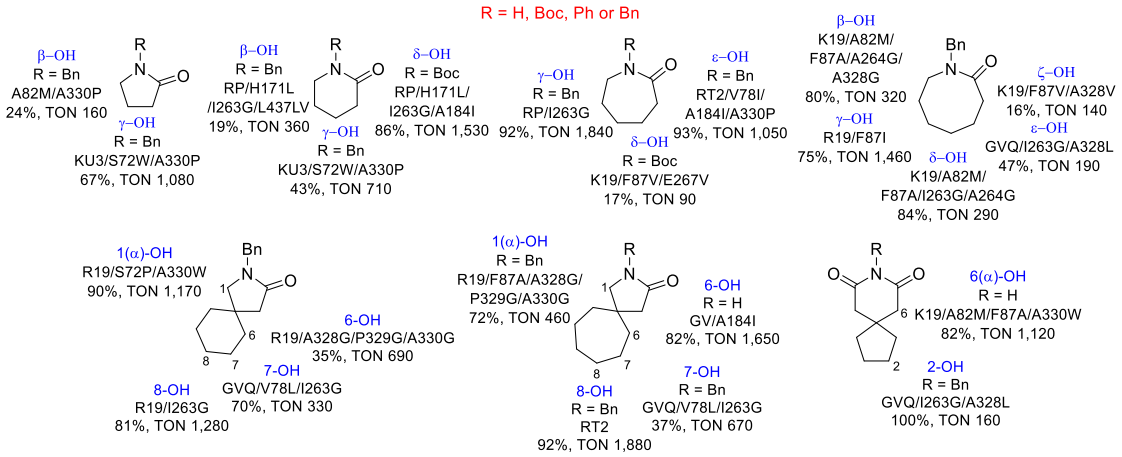


Figure 7.15 The highest P450$_{BM3}$ oxidation selectivities discovered for the lactams and imides studied in the present work.

In terms of the effects of the protecting groups, the Boc group favoured Nδ oxidation of δ-velarolactam (up to 86%) and showed highest oxidation activity (17%) at Nδ oxidation of ε-caprolactam. The oxidation of the non-protected 2-azaspiro[4.6]undecane-3-one and 8-azaspiro[4.5]decane-7,9-dione were found to show mainly C6 oxidation (up to 82% for both). Apart from these sites, the benzyl-protected monocyclic and spirocyclic lactams showed the highest regioselectivity for remote functionalisation (Figure 7.15). Overall, phenyl itself was oxidised, competing with the oxidation of the lactam core; Boc showed diversity in lactam oxidation, but its electron-withdrawing effect on the nitrogen atom, together with the lactam carbonyl group, facilitated ring-rearrangement of the hydroxy-lactam products to afford 5-/6-membered lactones; benzyl, compared with Boc, sped up the reaction without sacrificing oxidation diversity and selectivity for remote functionalisation. Therefore, benzyl would be the suitable protecting group for further exploration of lactam functionalisation by engineered P450$_{BM3}$.

Nβ oxidation remained difficult to achieve for the γ-butyrolactam, δ-velarolactam and ε-carprolactam cores even with *N*-benzyl, but was achieved to 80% for *N*-Bn-ζ-

enantholactam. This observation, along with the modest to high selectivity for oxidation at the Nβ carbocyclic ring of the spiro-lactams, suggested that the active sites of the $P450_{BM3}$ variants were too spacious to restrain substrate binding to expose only the non-activated C–H bonds. Furthermore, the less bulky mutations F87A/V (locating immediately above the heme) generally favouring Nα oxidation supported this hypothesis. S72W and A330W promoted remote functionalisation of lactams, implying that hydrogen bonding might steer the movement of the substrate by anchoring its carbonyl group. Therefore, to engineer for the Nβ oxidation, bulky amino acids capable of developing hydrogen bonds (W/H/Y/M/S/T/Q/N) should be introduced at or inserted before/after the key residues, such as S72, V78, A82, A184, A330 and L437, based on the RT2 variant which disfavoured Nα oxidation and gave evenly-distributed products from remote functionalisation.

In this chapter, remote functionalisation was commonly found after the introduction of the carbonyl group into Nα of the cyclic amine scaffolds, suggesting complex cyclic amine derivatives with substituents capable of developing hydrogen bonds, *e.g.* with ester substituents, might be worth conducting for the obtainment of hydroxy-products inaccessible by classic synthesis. Expanded screening would be useful for the substrates which was only screened against the WY9 library. The absolute stereochemistry of the hydroxy products should be determined so that enantioselectivity engineering would be carried out. As suggested in Chapter 3, integrating the topology features of P450pyr, which only showed Nβ oxidation of γ-butyrolactam and Nγ oxidation of δ-velarolactam, into $P450_{BM3}$ could also be helpful for promoting remote functionalisation of the lactams.

Chapter 8 Conclusion and outlook

8.1 Summary

The engineered $P450_{BM3}$ variants (246 variants tested in total) showed both high product diversity as well as acceptable to good regioselectivity for the oxidation of the cores of pyrrolidine, piperidine, quinoline (Q), tetrahydroquinoline (THQ), tetrahydroisoquinoline (THIQ), γ-butyrolactam, δ-velarolactam, ε-caprolactam and ζ-enantholactam derivatives (Figure 8.1). The wild type enzyme showed little to no activity for most of these substrates. Screening with constantly updated 48-variant sub-libraries, together with new variants designed from observed selectivity trends, led to remote functionalisation of the studied nitrogen heterocycles. Product profiles were affected by (a) the position and nature (Me *vs*. MeO) of substituents, (b) modification of the cores (cyclic amines, lactams, and imides), and (c) the properties of the *N*-protecting group (Ph, Bn, Ac, Boc, Ms, Ips, and Ts). Biotransformations *in vivo* and *in vitro* reached space-time yields of 1 g/L/day.

The enzyme library oxidised THQ at the C2 and C5,C6 positions, with C2 oxidation leading to dimer formation via the enamine/iminium equilibrium. Methyl substitution at C2, C6 and C8 suppressed oxidation at the *ipso* carbon but otherwise had little effect on the oxidation site; whereas an electron-rich MeO-substituent at C6 introduced a new activity – C8-amination giving the N1–C8' coupling dimers for which a diradical coupling mechanism was proposed. Quinoline (Q) oxidation gave the *N*-oxide, the 3-OH, and the 5,6-arene oxide. Methyl substituents had greater effects; >90% selectivity for benzylic oxidation of 2Me-, 6Me- and 8Me-Qs was observed, and the C2- and C8-Me substituents suppressed *N*-oxide formation. Interestingly, methyl substituents in Q directed oxidation to its vicinity; the 2-Me increased C3,C4 oxidation, the 6-Me gave more C5,C6 oxidation and promoted cleavage of the 5,6-oxide to yield the 5-OH, and the 8-Me substituent led to C7,C8 oxidation which gave the expected 7-OH alcohol as well as the 8-OH via an NIH shift of the methyl group.

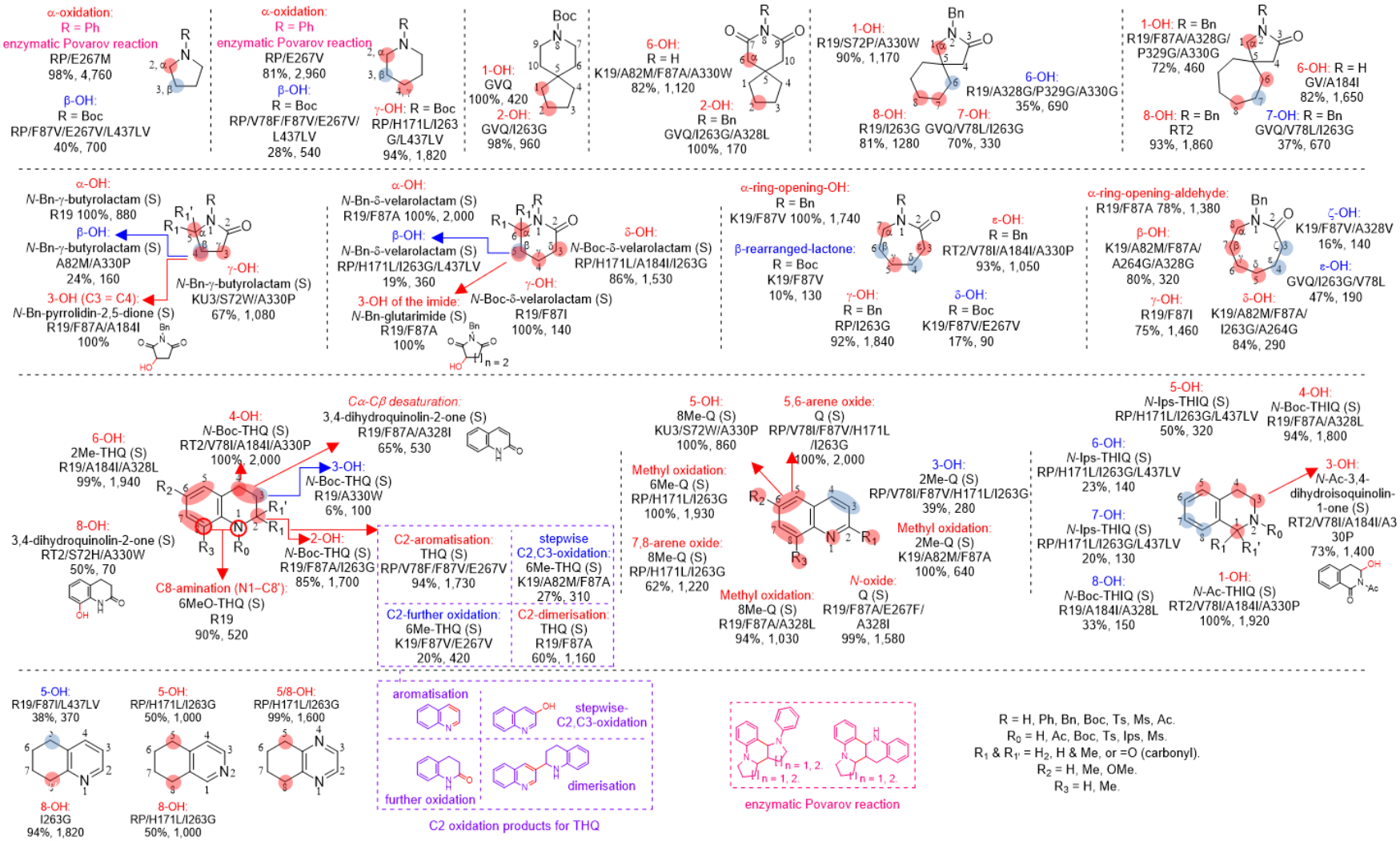


Figure 8.1 The summary of the oxidation of all the cyclic amines and lactams tested in this thesis by engineered $P450_{BM3}$.

Lactam and imides showed different product scopes to their amine analogues. With both Boc and Bn as protecting group, Nα oxidation was readily suppressed. The asymmetric lactams showed rich product diversity, *e.g. N*-Bn-ζ-enantholactam and *N*-Bn-spiro-lactams, indicating the flexibility and evolvability of the $P450_{BM3}$ active site. Both the lactam carbonyl and the hydroxyl group introduced by P450-catalysed remote oxidation are synthetic handles for the synthesis of fragment-like, functionally-diversified cyclic nitrogen compounds. Alcohol derivatives of lactams and imides are readily reduced to the corresponding amine analogues.

The size and electron-withdrawing nature of N-protecting groups altered the activity and selectivity of substrate oxidation. For pyrrolidine and piperidine cores, both phenyl and Boc-protected forms gave mainly C2 (Nα) oxidation; the *N*-phenyl derivatives formed dimers via the Povarov reaction – the first observation of this reaction with an enzyme – whereas the Nα-alcohols for the *N*-Boc derivatives were stable. *N*-Bn-protected cyclic amines were not converted at all, perhaps because Bn, in contrast with Ph and Boc, cannot delocalise the nitrogen lone pair which could bind to the heme iron and inhibit catalysis. For lactam cores, the C5(γ) hydroxylation product of *N*-Boc-ε-caprolactam rearranged to a lactone due to the electron-withdrawing nature of Boc, while the γ-alcohol of *N*-Bn-ε-caprolactam was stable. For THQ, Boc-, Ac-, Ips- and Ms-protecting groups promoted C4 oxidation which was not observed with unprotected THQ. For THIQ, the Boc- and Ips-derivatives showed diversified oxidation of the benzene motif of THIQ whereas *N*-Ac- and *N*-Ms-THIQ did not show oxidation of the benzene ring.

A combination of substrate engineering and protein engineering led to good regiodiversity of cyclic amine, lactam and imide oxidation. Not all sites were oxidised in all tested substrates, and the preference for Nα oxidation of small cyclic amines and lactams remained difficult to eliminate. Of the mutations, the results showed that (a) the F87A and

F87V mutations opened up the active site, leading to greater substrate mobility that the most activated position (Nα) was preferentially oxidised; (b) the R47L/Y51F combination increased activity as the non-polar residues Leu and Phe would favour the entry and binding of hydrophobic molecules such as *N*-protected amines, lactams and imides; (c) the bulky and polar substitutions S72W/H and A330W diversified lactam oxidation, perhaps due to hydrogen bonding interactions with the substrate; (d) I263G and A264G, located close to the sixth water ligand of the heme iron, enhanced the oxidation activity, with the R47L/Y51F/I401P/H171L/I263G (RP/H171L/I263G) variant showing good activity for most of the tested substrates; (e) the insertion mutation L437LV in the β4-sheet favoured remote functionalisation in several cases. These observations suggest a $P450_{BM3}$ variant library for remote functionalisation of cyclic amines can be established by introducing bulky and polar amino acids W/H/Y/N/Q at the A328/P329/A330 loop and the B'-helix, insertion mutations either side of L437, the I263G and A264G mutations in the I-helix, and L/I or unmutated F at residue 87, to the base variants RP/H171L/I263G, R19 and RT2.

The research in this thesis filled in the blank of P450 oxidation of simple cyclic amine molecules by a relatively systematic approach. Although the evolved variant library presented herein showed modest selectivity for remote sites, the work built the foundation of further 'training' of the $P450_{BM3}$ enzymes to gain better oxidation specificity. The efforts exerted on increasing the scale of biotransformation to industrial standard provided a handy tool for medicinal chemists to plot their plan of synthesising amine drugs. In addition, a variant library consisting of the 12 base variants RP/H171L/I263G, R1/I263G/L437LV, R1/I263G/L437VL, R19/F87I, R19/A184I/A328L, GV/A184I, GVQ/V78L/I263G, RT2/S72W/A330W, KU3/A330P, RT2/V78I/A184I/A330P, K19/F87V and K19/A82M/F87A showed quantifiable evidence for nearly all target activities, which established the 1st generation of cyclic amine-focused variant library capable of giving

remote functionalisation. The balance between the promiscuity of substrate recognition and the specificity of oxidation sites remained ever-changing in P450 bioengineering, whereas this piece of work pointed a possible direction to investigate further.

8.2 Future work and outlook

A high priority in future work should be to determine the absolute stereochemistry of the alcohol products by X-ray crystallography of derivatives with a heavy atom such as Br, by MicroED, or spectroscopic methods such as advanced Mosher ester analysis. Chiral-phase GC and LC methods for determining enantiomeric ratios will establish correlations for enantioselectivity engineering. Other substituted cyclic amines, lactams and their fused-ring, bicyclic and spirocyclic derivatives can be tested against the designed variant library in the overall drive towards product diversity with high selectivity while utilising a relatively small number of variants.

Another approach to active site redesign is to compare the active sites of $P450_{BM3}$ and P450pyr which has been found to give remote functionalisation of cyclic amines and lactams. This idea is also inspired by the funnel-shaped active site of the cholesterol-bound crystal structure of CYP125A1, as the bulky side-chains of the active site amino acids did restrict the open space above the heme iron only enough to expose the terminal methyl group of the alkyl branch, which significantly increased the oxidation specificity.[48] Grafting the features of P450pyr (*e.g.*, the shrinking-sized active site and the hydrophobic and bulky side-chains vicinal to the heme iron) onto $P450_{BM3}$ will increase the remote functionalisation of cyclic amines, and expand the product range accessible by this highly active single-polypeptide enzyme. The methodology can be applied to many more P450 isozymes originated from other organisms, to facilitate the study of the chemical functions and biological properties of the entire CYP superfamilies.

The work described in this thesis, whereby a small library of enzyme variants possessing diverse substrate pocket topology was screened against a range of related compounds to identify relevant residues for further mutagenesis, has provided a large body of activity and selectivity data. Future efforts may apply machine learning or deep learning to this body of data to design mutations to enhance the activity and stereoselectivity of C–H activation by $P450_{BM3}$. Specific oxidation at difficult sites of macromolecules and real drugs by P450s will also be of great interests; and the structure of plant, viral, fungal and other bacterial P450s capable of oxidising substrate at non-activated carbons should be investigated to guide the engineering and active-site-grafting work of $P450_{BM3}$. Crystal structure determination and computational methods, including docking and MD simulations, would add further data and insight in key enzyme–substrate interactions and the dynamics of substrate mobility within the active site.

Reference

1 R. W. Estabrook, *Drug Metab. Dispos.*, 2003, **31**, 1461–1473.
2 H. S. Mason, W. L. Fowlks and E. Peterson, *J. Am. Chem. Soc.*, 1955, **77**, 2914–2915.
3 O. Hayaishi, M. Katagiri and S. Rothberg, *J. Am. Chem. Soc.*, 1955, **77**, 5450–5451.
4 H. S. Mason, in *Science*, 1957, vol. 125, pp. 1185–1188.
5 M. Klingenberg, *Arch. Biochem. Biophys.*, 1958, **75**, 376–386.
6 T. Omura and R. Sato, *J. Biol. Chem.*, 1962, **237**, 1375–1376.
7 S. Yoshioka, S. Takahashi, H. Hori, K. Ishimori and I. Morishima, *Eur. J. Biochem.*, 2001, **268**, 252–259.
8 R. Perera, M. Sono, J. A. Sigman, T. D. Pfister, Y. Lut and J. H. Dawson, *Proc. Natl. Acad. Sci. U. S. A.*, 2003, **100**, 3641–3646.
9 A. W. Munro, K. J. McLean, J. L. Grant and T. M. Makris, *Biochem. Soc. Trans.*, 2018, **46**, 183–196.
10 M. D. Driscoll, K. J. McLean, C. Levy, N. Mast, I. A. Pikuleva, P. Lafite, S. E. J. Rigby, D. Leys and A. W. Munro, *J. Biol. Chem.*, 2010, **285**, 38270–38282.
11 H. Ogura, C. R. Nishida, U. R. Hoch, R. Perera, J. H. Dawson and P. R. Ortiz De Montellano, *Biochemistry*, 2004, **43**, 14712–14721.
12 A. J. Dunford, K. J. McLean, M. Sabri, H. E. Seward, D. J. Heyes, N. S. Scrutton and A. W. Munro, *J. Biol. Chem.*, 2007, **282**, 24816–24824.
13 D. W. Nebert, D. R. Nelson, M. J. Coon, R. W. Estabrook, R. Feyereisen, Y. Fujii-kuriyama, F. J. Gonzalez, F. P. Guengerich, I. C. Gunsalus, E. F. Johnson, J. C. Loper, R. Sato, M. R. Waterman and D. J. Waxman, *DNA Cell Biol.*, 1991, **10**, 1–14.
14 D. R. Nelson, L. Koymans, T. Kamataki, J. J. Stegeman, R. Feyereisen, D. J. Waxman, M. R. Waterman, O. Gotoh, M. J. Coon, R. W. Estabrook, I. C. Gunsalus and D. W. Nebert, *Pharmacogenetics*, 1996, 6, 1–42.
15 D. R. Nelson, in *Cytochrome P450 Protocols*, Humana Press, New Jersey, 2013, vol. 53, pp. 15–24.
16 D. R. Nelson, *Biochim. Biophys. Acta - Proteins Proteomics*, 2018, **1866**, 141–154.
17 D. R. Nelson, *Hum. Genomics*, 2009, **4**, 59–65.
18 D. R. Nelson, *Biochim. Biophys. Acta - Proteins Proteomics*, 2011, **1814**, 14–18.
19 D. C. Lamb, A. H. Follmer, J. V. Goldstone, D. R. Nelson, A. G. Warrilow, C. L. Price, M. Y. True, S. L. Kelly, T. L. Poulos and J. J. Stegeman, *Proc. Natl. Acad. Sci.*, 2019, **116**, 12343–12352.
20 Q. Cheng, C. D. Sohl, F. K. Yoshimoto and F. P. Guengerich, *J. Biol. Chem.*, 2012, **287**, 29554–29567.
21 C. Yamashita, Y. Aoyama, M. Noshiro and Y. Yoshida, *J. Biochem.*, 2001, **130**, 849–856.
22 S. E. Bulun, S. Sebastian, K. Takayama, T. Suzuki, H. Sasano and M. Shozu, *J. Steroid Biochem. Mol. Biol.*, 2003, **86**, 219–224.
23 A. Conley, *Reproduction*, 2001, **121**, 685–695.
24 N. Nakayama, A. Takemae and H. Shoun, *J. Biochem.*, 1996, **119**, 435–440.
25 T. Fukuda, Y. Imai, M. Komori, M. Nakamura, E. Kusunose and M. Kusunose, *J. Biochem.*, 1993, **113**, 7–12.
26 K. K. Wu and J. Y. Liou, *Biochem. Biophys. Res. Commun.*, 2005, **338**, 45–52.
27 S. Hara, A. Miyata, C. Yokoyama, H. Inoue, R. Brugger, F. Lottspeich, V. Ullrich and T. Tanabe, *J. Biol. Chem.*, 1994, **269**, 19897–19903.
28 O. Pylypenko, F. Vitali, K. Zerbe, J. A. Robinson and I. Schlichting, *J. Biol. Chem.*, 2003, **278**, 46727–46733.
29 Y. Yasutake, Y. Fujii, T. Nishioka, W. K. Cheon, A. Arisawa and T. Tamura, *J. Biol. Chem.*, 2010, **285**, 31193–31201.
30 I. G. Denisov and S. G. Sligar, in *Cytochrome P450*, Springer International Publishing, Cham, 2015, vol. 53, pp. 69–109.
31 M. J. Honeychurch, H. A. O. Hill and L. L. Wong, *FEBS Lett.*, 1999, **451**, 351–353.
32 O. Bangcharoenpaurpon, A. I. K. Rizos, P. M. Champion, D. Jollie and S. G. Sligar, *J. Biol. Chem.*, 1986, **261**, 8089–8092.
33 S. Nagano, J. R. Cupp-Vickery and T. L. Poulos, *J. Biol. Chem.*, 2005, **280**, 22102–22107.
34 S. Nagano and T. L. Poulos, *J. Biol. Chem.*, 2005, **280**, 31659–31663.
35 M. Sharrock, P. G. Debrunner, C. Schulz, J. D. Lipscomb, V. Marshall and I. C. Gunsalus, *Biochim. Biophys. Acta - Protein Struct.*, 1976, **420**, 8–26.
36 M. A. Carrondo, I. Bento, P. M. Matias and P. F. Lindley, *J. Biol. Inorg. Chem.*, 2007, **12**, 429–442.
37 I. Schlichting, J. Berendzen, K. Chu, A. M. Stock, S. A. Maves, D. E. Benson, R. M. Sweet, D. Ringe, G. A. Petsko and S. G. Sligar, *Science (80-.).*, 2000, **287**, 1615–1622.
38 D. E. Benson, K. S. Suslick and S. G. Sligar, *Biochemistry*, 1997, **36**, 5104–5107.

39 T. L. Poulos and Y. Madrona, *Biotechnol. Appl. Biochem.*, 2013, **60**, 128–133.
40 R. Davydov, R. Perera, S. Jin, T. C. Yang, T. A. Bryson, M. Sono, J. H. Dawson and B. M. Hoffman, *J. Am. Chem. Soc.*, 2005, **127**, 1403–1413.
41 T. L. Poulos, B. C. Finzel and A. J. Howard, *J. Mol. Biol.*, 1987, **195**, 687–700.
42 P. M. Kells, H. Ouellet, J. Santos-Aberturas, J. F. Aparicio and L. M. Podust, *Chem. Biol.*, 2010, **17**, 841–851.
43 D. Ghosh, J. Griswold, M. Erman and W. Pangborn, *Nature*, 2009, **457**, 219–223.
44 M. Akhtar, D. Corina, S. Miller, A. Z. Shyadehi and J. N. Wright, *Biochemistry*, 1994, **33**, 4410–4418.
45 M. Akhtar, V. C. O. Njar and J. Neville Wright, *J. Steroid Biochem. Mol. Biol.*, 1993, **44**, 375–387.
46 J. C. Hackett, R. W. Brueggemeier and C. M. Hadad, *J. Am. Chem. Soc.*, 2005, **127**, 5224–5237.
47 F. P. Guengerich and A. W. Munro, *J. Biol. Chem.*, 2013, **288**, 17065–17073.
48 K. J. McLean, P. Lafite, C. Levy, M. R. Cheesman, N. Mast, I. A. Pikuleva, D. Leys and A. W. Munro, *J. Biol. Chem.*, 2009, **284**, 35524–35533.
49 J. D. Lipscomb, S. G. Sligar, M. J. Namtvedt and I. C. Gunsalus, *J. Biol. Chem.*, 1976, **251**, 1116–1124.
50 J. P. Clark, C. S. Miles, C. G. Mowat, M. D. Walkinshaw, G. A. Reid, S. N. Daff and S. K. Chapman, *J. Inorg. Biochem.*, 2006, **100**, 1075–1090.
51 S. G. Sligar, J. D. Lipscomb, P. G. Debrunner and I. C. Gunsalus, *Biochem. Biophys. Res. Commun.*, 1974, **61**, 290–296.
52 B. Prasad, D. J. Mah, A. R. Lewis and E. Plettner, *PLoS One*, , DOI:10.1371/journal.pone.0061897.
53 S. P. De Visser, F. Ogliaro, N. Harris and S. Shaik, *J. Am. Chem. Soc.*, 2001, **123**, 3037–3047.
54 M. Filatov and S. Shaik, *J. Phys. Chem. A*, 1998, 102, 3835–3846.
55 D. Kumar, B. Karamzadeh, G. N. Sastry and S. P. De Visser, *J. Am. Chem. Soc.*, 2010, **132**, 7656–7667.
56 S. Shaik, D. Kumar, S. P. de Visser, A. Altun and W. Thiel, *Chem. Rev.*, 2005, **105**, 2279–2328.
57 G. Guroff, J. Renson, S. Udenfriend, J. W. Daly, D. M. Jerina and B. Witkop, *Science (80-.).*, 1967, **157**, 1524–1530.
58 C. K. Chang and F. Ebina, *J. Chem. Soc. Chem. Commun.*, 1981, 778–779.
59 J. W. Daly, D. M. Jerina and B. Witkop, *Experientia*, 1972, **28**, 1129–1149.
60 P. C. Nair, R. A. McKinnon and J. O. Miners, *Drug Metab. Rev.*, 2016, **48**, 434–452.
61 T. H. L. P. Oulos, 1999, **96**, 1863–1868.
62 J. Cupp-Vickery, R. Anderson and Z. Hatziris, *Proc. Natl. Acad. Sci. U. S. A.*, 2000, **97**, 3050–3055.
63 M. R. Wester, J. K. Yano, G. A. Schoch, C. Yang, K. J. Griffin, C. D. Stout and E. F. Johnson, *J. Biol. Chem.*, 2004, **279**, 35630–35637.
64 I. F. Sevrioukova and T. L. Poulos, *Biochemistry*, 2015, **54**, 4083–4096.
65 D. Ghosh, J. Lo, D. Morton, D. Valette, J. Xi, J. Griswold, S. Hubbell, C. Egbuta, W. Jiang, J. An and H. M. L. Davies, *J. Med. Chem.*, 2012, **55**, 8464–8476.
66 C. J. C. Whitehouse, S. G. Bell and L.-L. Wong, *Chem. Soc. Rev.*, 2012, **41**, 1218–1260.
67 I. G. Denisov, T. M. Makris, S. G. Sligar and I. Schlichting, *Chem. Rev.*, 2005, **105**, 2253–2277.
68 P. Jean, J. Pothier, P. M. Dansette, D. Mansuy and A. Viari, *Proteins Struct. Funct. Genet.*, 1997, **28**, 388–404.
69 O. Gotoh, *J. Biol. Chem.*, 1992, **267**, 83–90.
70 O. Pylypenko and I. Schlichting, *Annu. Rev. Biochem.*, 2004, **73**, 991–1018.
71 C. A. Hasemann, R. G. Kurumbail, S. S. Boddupalli, J. A. Peterson and J. Deisenhofer, *Structure*, 1995, **3**, 41–62.
72 K. G. Ravichandran, S. S. Boddupalli, C. A. Hasemann, J. A. Peterson and J. Deisenhofer, *Science (80-.).*, 1993, **261**, 731–736.
73 S. H. White, A. S. Ladokhin, S. Jayasinghe and K. Hristova, *J. Biol. Chem.*, 2001, **276**, 32395–32398.
74 O. S. Andersen and R. E. Koeppe, *Annu. Rev. Biophys. Biomol. Struct.*, 2007, **36**, 107–130.
75 B. C. Monk, T. M. Tomasiak, M. V. Keniya, F. U. Huschmann, J. D. A. Tyndall, J. D. O'Connell, R. D. Cannon, J. G. McDonald, A. Rodriguez, J. S. Finer-Moore and R. M. Stroud, *Proc. Natl. Acad. Sci. U. S. A.*, 2014, **111**, 3865–3870.
76 SAKAGUCHI and M., *Front. Biotransformation*, 1993, **8**, 59–73.
77 T. Omura and A. Ito, 1991, vol. 206, pp. 75–81.
78 C. Von Wachenfeldt, T. H. Richardson, J. Cosme and E. F. Johnson, *Arch. Biochem. Biophys.*, 1997, **339**, 107–114.
79 J. Cosme and E. F. Johnson, *J. Biol. Chem.*, 2000, **275**, 2545–2553.
80 E. F. Johnson and C. D. Stout, *J. Biol. Chem.*, 2013, **288**, 17082–17092.
81 P. A. Williams, J. Cosme, V. Sridhar, E. F. Johnson and D. E. McRee, *Mol. Cell*, 2000, **5**, 121–131.
82 P. A. Williams, J. Cosme, V. Sridhar, E. F. Johnson and D. E. McRee, *J. Inorg. Biochem.*, 2000, **81**, 183–190.
83 I. G. Denisov, A. Y. Shih and S. G. Sligar, *J. Inorg. Biochem.*, 2012, **108**, 150–158.

84 V. Cojocaru, K. Balali-Mood, M. S. P. Sansom and R. C. Wade, *PLoS Comput. Biol.*, 2011, **7**, e1002152.
85 K. Berka, M. Paloncýová, P. Anzenbacher and M. Otyepka, *J. Phys. Chem. B*, 2013, **117**, 11556–11564.
86 J. L. Baylon, I. L. Lenov, S. G. Sligar and E. Tajkhorshid, *J. Am. Chem. Soc.*, 2013, **135**, 8542–8551.
87 S. Sansen, J. K. Yano, R. L. Reynald, G. A. Schoch, K. J. Griffin, C. D. Stout and E. F. Johnson, *J. Biol. Chem.*, 2007, **282**, 14348–14355.
88 C. Ozalp, E. Szczesna-Skorupa and B. Kemper, *Biochemistry*, 2006, **45**, 4629–4637.
89 K. Nakayama, A. Puchkaev and I. A. Pikuleva, *J. Biol. Chem.*, 2001, **276**, 31459–31465.
90 T. L. Poulos, B. C. Finzel and A. J. Howard, *Biochemistry*, 1986, **25**, 5314–5322.
91 H. Li and T. L. Poulos, *Nat. Struct. Biol.*, 1997, **4**, 140–146.
92 Y. T. Lee, E. C. Glazer, R. F. Wilson, C. D. Stout and D. B. Goodin, *Biochemistry*, 2011, **50**, 693–703.
93 W. Yang, S. G. Bell, H. Wang, W. Zhou, M. Bartlam, L. L. Wong and Z. Rao, *Biochem. J.*, 2011, **433**, 85–93.
94 A. Y. Lu, K. W. Junk and M. J. Coon, *J. Biol. Chem.*, 1969, **244**, 3714–3721.
95 L. O. Narhi and A. J. Fulco, *J. Biol. Chem.*, 1987, **262**, 6683–6690.
96 E. L. Rylott, R. G. Jackson, J. Edwards, G. L. Womack, H. M. B. Seth-Smith, D. A. Rathbone, S. E. Strand and N. C. Bruce, *Nat. Biotechnol.*, 2006, **24**, 216–219.
97 H. M. B. Seth-smith, S. J. Rosser, A. Basran, E. R. Travis, E. R. Dabbs, S. Nicklin and N. C. Bruce, *Appl. Environ. Microbiol.*, 2002, **68**, 4764–4771.
98 T. Omura, E. Sanders, R. W. Estabrook, D. Y. Cooper and O. Rosenthal, *Arch. Biochem. Biophys.*, 1966, **117**, 660–673.
99 I. C. Gunsalus, J. D. Lipscomb, V. Marshall, H. Frauenfelder, E. Münck and E. Greenbaum, *Biochem. J.*, 1971, **125**, 7–8.
100 G. A. Roberts, G. Grogan, A. Greter, S. L. Flitsch and N. J. Turner, *J. Bacteriol.*, 2002, **184**, 3898–3908.
101 D. J. B. Hunter, G. A. Roberts, T. W. B. Ost, J. H. White, S. Müller, N. J. Turner, S. L. Flitsch and S. K. Chapman, *FEBS Lett.*, 2005, **579**, 2215–2220.
102 G. A. Roberts, A. Celik, D. J. B. Hunter, T. W. B. Ost, J. H. White, S. K. Chapman, N. J. Turner and S. L. Flitsch, *J. Biol. Chem.*, 2003, **278**, 48914–48920.
103 R. De Mot and A. H. A. Parret, *Trends Microbiol.*, 2002, **10**, 502–508.
104 L. Liu, R. D. Schmid and V. B. Urlacher, *Appl. Microbiol. Biotechnol.*, 2006, **72**, 876–882.
105 A. Modi and J. H. Dawson, *Monooxygenase, Peroxidase and Peroxygenase Properties and Mechanisms of Cytochrome P450*, Springer International Publishing, Cham, 2015, vol. 851.
106 F. Hannemann, A. Bichet, K. M. Ewen and R. Bernhardt, *Biochim. Biophys. Acta - Gen. Subj.*, 2007, **1770**, 330–344.
107 P. R. O. De Montellano, *Cytochrome P450: Structure, mechanism, and biochemistry: Third edition*, 2005.
108 E. O. D. Johnson and L. L. Wong, *Catal. Sci. Technol.*, 2016, **6**, 7549–7560.
109 A. Rojubally, *Linking cytochrome P450cam (CYP101) to its redox partner putidaredoxin and probing new reactions of the P450cam system*, 2008.
110 K. A. Gentry, M. Zhang, S. C. Im, L. Waskell and A. Ramamoorthy, *Chem. Commun.*, 2018, **54**, 5780–5783.
111 M. Wang, D. L. Roberts, R. Paschke, T. M. Shea, B. S. S. Masters and J.-J. P. Kim, *Proc. Natl. Acad. Sci.*, 1997, **94**, 8411–8416.
112 U. H. N. Dürr, L. Waskell and A. Ramamoorthy, *Biochim. Biophys. Acta - Biomembr.*, 2007, **1768**, 3235–3259.
113 I. Hanukoglu, *Adv. Mol. Cell Biol.*, 1996, **14**, 29–56.
114 T. D. Porter, *J. Biochem. Mol. Toxicol.*, 2002, **16**, 311–316.
115 T. Iyanagi and H. S. Mason, *Biochemistry*, 1973, **12**, 2297–2308.
116 T. Iyanagi, R. Makino and F. K. Anan, *Biochemistry*, 1981, **20**, 1722–1730.
117 D. D. Oprians and M. J. Coon, *J Biol Chem.*, 1982, **257**, 8935–8944.
118 D. D. Oprians, L. D. Gorskyb and M. J. Coon, *J. Biol. Chem.*, 1982, **258**, 8684–8691.
119 W. Baer-Dubowska and H. Szaefer, *Expert Opin. Drug Metab. Toxicol.*, 2013, **9**, 927–941.
120 T. Iyanagi, C. Xia and J.-J. P. Kim, *Arch. Biochem. Biophys.*, 2012, **528**, 72–89.
121 P. Durairaj, J. S. Hur and H. Yun, *Microb. Cell Fact.*, 2016, **15**, 1–16.
122 A. Ramamoorthy, C. Barnaba, K. Gentry and N. Sumangala, *F1000Research*, 2017, **6**, 1–10.
123 H. Yamazaki, M. Nakamura, T. Komatsu, K. Ohyama, N. Hatanaka, S. Asahi, N. Shimada, F. P. Guengerich, T. Shimada, M. Nakajima and T. Yokoi, *Protein Expr. Purif.*, 2002, **24**, 329–337.
124 J. Y. L. Chiang, *Arch. Biochem. Biophys.*, 1981, **211**, 662–673.
125 N. Kimmich, A. Das, I. Sevrioukova, Y. Meharenna, S. G. Sligar and T. L. Poulos, *J. Biol. Chem.*, 2007, **282**, 27006–27011.
126 D. B. Hawkes, G. W. Adams, A. L. Burlingame, P. R. Ortiz De Montellano and J. J. De Voss, *J. Biol. Chem.*, 2002, **277**, 27725–27732.

127 Y. Madrona, S. A. Hollingsworth, S. Tripathi, J. B. Fields, J. C. N. Rwigema, D. J. Tobias and T. L. Poulos, *Biochemistry*, 2014, **53**, 1435–1446.
128 C. R. Nishida and P. R. Ortiz De Montellano, *Biochem. Biophys. Res. Commun.*, 2005, **338**, 437–445.
129 K. Kojoh, H. Matsuzawa and T. Wakagi, *Eur. J. Biochem.*, 1999, **264**, 85–91.
130 E. Fukuda, H. Kino, H. Matsuzawa and T. Wakagi, *Eur. J. Biochem.*, 2001, **268**, 5639–5646.
131 A. V. Puchkaev and P. R. Ortiz De Montellano, *Arch. Biochem. Biophys.*, 2005, **434**, 169–177.
132 A. V. Puchkaev, T. Wakagi and P. R. Ortiz de Montellano, *J. Am. Chem. Soc.*, 2002, **124**, 12682–12683.
133 C. J. Jackson, D. C. Lamb, T. H. Marczylo, A. G. S. Warrilow, N. J. Manning, D. J. Lowe, D. E. Kelly and S. L. Kelly, *J. Biol. Chem.*, 2002, **277**, 46959–46965.
134 S. L. Kelly and D. E. Kelly, *Philos. Trans. R. Soc. B Biol. Sci.*, , DOI:10.1098/rstb.2012.0476.
135 A. J. Warman, O. Roitel, R. Neeli, H. M. Girvan, H. E. Seward, S. A. Murray, K. J. McLean, M. G. Joyce, H. Toogood, R. A. Holt, D. Leys, N. S. Scrutton and A. W. Munro, *Biochem. Soc. Trans.*, 2005, **33**, 747–753.
136 L. O. Narhi and A. J. Fulco, *J. Biol. Chem.*, 1986, **261**, 7160–7169.
137 R. T. Ruettinger, L. P. Wen and A. J. Fulco, *J. Biol. Chem.*, 1989, **264**, 10987–10995.
138 A. W. Munro, D. G. Leys, K. J. McLean, K. R. Marshall, T. W. B. Ost, S. Daff, C. S. Miles, S. K. Chapman, D. A. Lysek, C. C. Moser, C. C. Page and P. L. Dutton, *Trends Biochem. Sci.*, 2002, **27**, 250–257.
139 A. J. Fulco, *Annu. Rev. Pharmacol. Toxicol.*, 1991, **31**, 177–203.
140 T. W. B. Ost, J. Clark, C. G. Mowat, C. S. Miles, M. D. Walkinshaw, G. A. Reid, S. K. Chapman and S. Daff, *J. Am. Chem. Soc.*, 2003, **125**, 15010–15020.
141 A. Daiber, H. Shoun and V. Ullrich, *J. Inorg. Biochem.*, 2005, **99**, 185–193.
142 K. Nakahara, T. Tanimoto, K. I. Hatano, K. Usuda and H. Shoun, *J. Biol. Chem.*, 1993, **268**, 8350–8355.
143 J. E. Froehlich, A. Itoh and G. A. Howe, *Plant Physiol.*, 2001, **125**, 306–317.
144 A. Itoh and G. A. Howe, *J. Biol. Chem.*, 2001, **276**, 3620–3627.
145 S. M. C. Lau, P. A. Harder and D. P. O'Keefe, *Biochemistry*, 1993, **32**, 1945–1950.
146 Y. Shibata, K. Matsui, T. Kajiwara and A. Hatanaka, *Biochem. Biophys. Res. Commun.*, 1995, 207, 438–443.
147 J. M. Hagel and P. J. Facchini, *Plant Cell Physiol.*, 2013, **54**, 647–672.
148 R. K. and R. Croteau, 2010, **5**, 1–23.
149 B. Hamberger, T. Ohnishi, B. Hamberger, A. Séguin and J. Bohlmann, *Plant Physiol.*, 2011, **157**, 1677–1695.
150 M. D. Andersen, P. K. Busk, I. Svendsen and B. L. Møller, *J. Biol. Chem.*, 2000, **275**, 1966–1975.
151 M. Mizutani and F. Sato, *Arch. Biochem. Biophys.*, 2011, **507**, 194–203.
152 M. Nafisi, S. Goregaoker, C. J. Botanga, E. Glawischnig, C. E. Olsen, B. A. Halkier and J. Glazebrook, *Plant Cell*, 2007, **19**, 2039–2052.
153 T. Nomura, H. Magome, A. Hanada, N. Takeda-Kamiya, L. N. Mander, Y. Kamiya and S. Yamaguchi, *Plant Cell Physiol.*, 2013, **54**, 1837–1851.
154 S. Takahashi, Y. S. Yeo, Y. Zhao, P. E. O'Maille, B. T. Greenhagen, J. P. Noel, R. M. Coates and J. Chappell, *J. Biol. Chem.*, 2007, **282**, 31744–31754.
155 K. M. Ewen, F. Hannemann, S. Iametti, A. Morleo and R. Bernhardt, *J. Mol. Biol.*, 2011, **413**, 940–951.
156 K. M. Ewen, M. Kleser and R. Bernhardt, *Biochim. Biophys. Acta - Proteins Proteomics*, 2011, **1814**, 111–125.
157 S. G. Sligar, T. M. Makris and I. G. Denisov, *Biochem. Biophys. Res. Commun.*, 2005, **338**, 346–354.
158 P. J. Loida and S. G. Sligar, *Biochemistry*, 1993, **32**, 11530–11538.
159 T. M. Makris, R. Davydov, I. G. Denisov, B. M. Hoffman and S. G. Sligar, *Drug Metab. Rev.*, 2002, **34**, 691–708.
160 M. Girhard, P. J. Bakkes, O. Mahmoud and V. B. Urlacher, in *Cytochrome P450*, Springer International Publishing, Cham, 2015, pp. 451–520.
161 J. B. Van Beilen, W. A. Duetz, A. Schmid and B. Witholt, *Trends Biotechnol.*, 2003, **21**, 170–177.
162 Z. Li, Y. Jiang, X. F. P. Guengerich, L. Ma, S. Li and W. Zhang, *J. Biol. Chem.*, 2020, **295**, 833–849.
163 V. B. Urlacher and M. Girhard, *Trends Biotechnol.*, 2019, **37**, 882–897.
164 K. Auclair and V. Polic, 2015, pp. 209–228.
165 A. de Raadt, H. Griengl and H. Weber, *ChemInform*, 2010, **33**, no-no.
166 S. Negretti, A. R. H. Narayan, K. C. Chiou, P. M. Kells, J. L. Stachowski, D. A. Hansen, L. M. Podust, J. Montgomery and D. H. Sherman, *J. Am. Chem. Soc.*, 2014, **136**, 4901–4904.
167 O. Shoji, T. Fujishiro, H. Nakajima, M. Kim, S. Nagano, Y. Shiro and Y. Watanabe, *Angew. Chemie - Int. Ed.*, 2007, **46**, 3656–3659.
168 T. Fujishiro, O. Shoji and Y. Watanabe, *Tetrahedron Lett.*, 2011, **52**, 395–397.
169 O. Shoji, C. Wiese, T. Fujishiro, C. Shirataki, B. Wünsch and Y. Watanabe, *J. Biol. Inorg. Chem.*, 2010, **15**, 1109–1115.

170 O. Shoji, T. Kunimatsu, N. Kawakami and Y. Watanabe, *Angew. Chemie - Int. Ed.*, 2013, **52**, 6606–6610.
171 U. T. Bornscheuer and M. Pohl, *Curr. Opin. Chem. Biol.*, 2001, **5**, 137–143.
172 H. Zhao, L. Giver, Z. Shao, J. A. Affholter and F. H. Arnold, *Nat. Biotechnol.*, 1998, **16**, 258–261.
173 F. H. Arnold, *Cold Spring Harb. Symp. Quant. Biol.*, 2009, **74**, 41–46.
174 P. A. Romero and F. H. Arnold, *Nat. Rev. Mol. Cell Biol.*, 2009, **10**, 866–876.
175 G. D. Roiban and M. T. Reetz, *Chem. Commun.*, 2015, **51**, 2208–2224.
176 V. B. Urlacher, A. Makhsumkhanov and R. D. Schmid, *Appl. Microbiol. Biotechnol.*, 2006, 70, 53–59.
177 A. Seifert, S. Vomund, K. Grohmann, S. Kriening, V. B. Urlacher, S. Laschat and J. Pleiss, *ChemBioChem*, 2009, **10**, 853–861.
178 E. Weber, A. Seifert, M. Antonovici, C. Geinitz, J. Pleiss and V. B. Urlacher, *Chem. Commun.*, 2011, **47**, 944–946.
179 K. Zhang, B. M. Shafer, M. D. Demars, H. A. Stern and R. Fasan, *J. Am. Chem. Soc.*, 2012, **134**, 18695–18704.
180 J. B. Y. H. Behrendorff, W. Huang and E. M. J. Gillam, *Biochem. J.*, 2015, **467**, 1–15.
181 C. Brieke, M. Tarnawski, A. Greule and M. J. Cryle, *J. Inorg. Biochem.*, 2018, **185**, 43–51.
182 S. Kille, F. E. Zilly, J. P. Acevedo and M. T. Reetz, *Nat. Chem.*, 2011, **3**, 738–743.
183 H. Venkataraman, S. B. A. de Beer, L. A. H. van Bergen, N. van Essen, D. P. Geerke, N. P. E. Vermeulen and J. N. M. Commandeur, *ChemBioChem*, 2012, **13**, 520–523.
184 S. B.A. de Beer, L. A.H. van Bergen, K. Keijzer, V. Rea, H. Venkataraman, C. Fonseca Guerra, F. Matthias Bickelhaupt, N. P.E. Vermeulen, J. N.M. Commandeur and D. P. Geerke, *Curr. Drug Metab.*, 2012, **13**, 155–166.
185 X. Ren, J. A. Yorke, E. Taylor, T. Zhang, W. Zhou and L. L. Wong, *Chem. - A Eur. J.*, 2015, **21**, 15039–15047.
186 M. A. Noble, C. S. Miles, S. K. Chapman, D. A. Lysek, A. C. Mackay, G. A. Reid, R. P. Hanzlik and A. W. Munro, *Biochem. J.*, 1999, **339**, 371–379.
187 Q.-S. S. Li, J. Ogawa, R. D. Schmid and S. Shimizu, *FEBS Lett.*, 2001, **508**, 249–252.
188 B. M. A. Lussenburg, L. C. Babel, N. P. E. Vermeulen and J. N. M. Commandeur, *Anal. Biochem.*, 2005, **341**, 148–155.
189 W. C. Huang, A. C. G. Westlake, J. D. Maréchal, M. G. Joyce, P. C. E. Moody and G. C. K. Roberts, *J. Mol. Biol.*, 2007, **373**, 633–651.
190 Q. S. Li, U. Schwaneberg, M. Fischer, J. Schmitt, J. Pleiss, S. Lutz-Wahl and R. D. Schmid, *Biochim. Biophys. Acta - Protein Struct. Mol. Enzymol.*, 2001, **1545**, 114–121.
191 A. Li, C. G. Acevedo-Rocha, L. D'Amore, J. Chen, Y. Peng, M. Garcia-Borràs, C. Gao, J. Zhu, H. Rickerby, S. Osuna, J. Zhou and M. T. Reetz, *Angew. Chemie - Int. Ed.*, 2020, 12499–12505.
192 S. J. Sadeghi, Y. T. Meharenna, A. Fantuzzi, F. Valetti and G. Gilardi, *Faraday Discuss.*, 2000, **116**, 135–153.
193 M. Fairhead, S. Giannini, E. M. J. Gillam and G. Gilardi, *J. Biol. Inorg. Chem.*, 2005, **10**, 842–853.
194 F. Sabbadin, R. Hyde, A. Robin, E.-M. Hilgarth, M. Delenne, S. Flitsch, N. Turner, G. Grogan and N. C. Bruce, *ChemBioChem*, 2010, **11**, 987–994.
195 F. Sabbadin, G. Grogan and N. C. Bruce, 2013, pp. 239–249.
196 R. A. George and J. Heringa, *Protein Eng.*, 2002, **15**, 871–879.
197 X. Chen, J. L. Zaro and W. C. Shen, *Adv. Drug Deliv. Rev.*, 2013, **65**, 1357–1369.
198 P. Hlavica, *Biotechnol. Adv.*, 2009, **27**, 103–121.
199 M. S. Shet, C. W. Fisher, M. P. Arlotto, C. H. L. Shackleton, P. L. Holmans, C. A. Martinwixtrom, Y. Saeki and R. W. Estabrook, *Arch. Biochem. Biophys.*, 1994, **311**, 402–417.
200 G. Schröder, E. Unterbusch, M. Kaltenbach, J. Schmidt, D. Strack, V. De Luca and J. Schröder, *FEBS Lett.*, 1999, **458**, 97–102.
201 L. Didierjean, L. Gondet, R. Perkins, S. M. C. Lau, H. Schaller, D. P. O'Keefe and D. Werck-Reichhart, *Plant Physiol.*, 2002, **130**, 179–189.
202 M. Nodate, M. Kubota and N. Misawa, *Appl. Microbiol. Biotechnol.*, 2006, **71**, 455–462.
203 V. R. Dodhia, A. Fantuzzi and G. Gilardi, *J. Biol. Inorg. Chem.*, 2006, **11**, 903–916.
204 J. Schückel, E. L. Rylott, G. Grogan and N. C. Bruce, *ChemBioChem*, 2012, **13**, 2758–2763.
205 H. Hirakawa and T. Nagamune, *ChemBioChem*, 2010, **11**, 1517–1520.
206 T. Haga, H. Hirakawa and T. Nagamune, *PLoS One*, 2013, **8**, 1–11.
207 J. A. Peterson and S. S. Boddupalli, *Arch. Biochem. Biophys.*, 1992, **294**, 654–661.
208 X. Fang and J. R. Halpert, *Drug Metab. Dispos.*, 1996, **24**, 1282 LP – 1285.
209 E. G. Hrycay and S. M. Bandiera, *Arch. Biochem. Biophys.*, 2012, **522**, 71–89.
210 N. P. Niraula, B. K. Kanth, J. K. Sohng and T. J. Oh, *Enzyme Microb. Technol.*, 2011, **48**, 181–186.
211 I. Matsunaga, A. Ueda, N. Fujiwara, T. Sumimoto and K. Ichihara, *Lipids*, 1999, **34**, 841–846.
212 M. Girhard, S. Schuster, M. Dietrich, P. Dürre and V. B. Urlacher, *Biochem. Biophys. Res. Commun.*,

2007, **362**, 114–119.
213 R. W. Estabrook, K. M. Faulkner, M. S. Shet and C. W. Fisher, *Methods Enzymol.*, 1996, **272**, 44–51.
214 K. M. Faulkner, M. S. Shet, C. W. Fisher and R. W. Estabrook, *Proc. Natl. Acad. Sci. U. S. A.*, 1995, **92**, 7705–7709.
215 M. P. Mayhew, V. Reipa, M. J. Holden and V. L. Vilker, *Biotechnol. Prog.*, 2000, **16**, 610–616.
216 V. Reipa, M. P. Mayhew, M. J. Holden and V. L. Vilker, *Chem. Commun.*, 2002, **2**, 318–319.
217 H. B. Gray and J. R. Winkler, *Annu. Rev. Biochem.*, 1996, **65**, 537–561.
218 V. V. Shumyantseva, Y. D. Ivanov, N. Bistolas, F. W. Scheller, A. I. Archakov and U. Wollenberger, *Anal. Chem.*, 2004, **76**, 6046–6052.
219 S. Cosnier, *Biosens. Bioelectron.*, 1999, **14**, 443–456.
220 W. Schuhmann, H. Wohlschläger, J. Huber, H. L. Schmidt and H. Stadler, *Anal. Chim. Acta*, 1995, **315**, 113–122.
221 M. Antonini, P. Ghisellini, L. Pastorino, C. Paternolli and C. Nicolini, *IEE Proc. Nanobiotechnology*, 2003, **150**, 31–34.
222 Y. Guo and S. Dong, *Anal. Chem.*, 1997, **69**, 1904–1908.
223 B. Munge, C. Estavillo, J. B. Schenkman and J. F. Rusling, *ChemBioChem*, 2003, 4, 82–89.
224 C. Estavillo, Z. Lu, I. Jansson, J. B. Schenkman and J. F. Rusling, *Biophys. Chem.*, 2003, **104**, 291–296.
225 M. Landwehr, L. Hochrein, C. R. Otey, A. Kasrayan, J.-E. E. Bäckvall and F. H. Arnold, *J. Am. Chem. Soc.*, 2006, **128**, 6058–6059.
226 J. Michizoe, H. Ichinose, N. Kamiya, T. Maruyama and M. Goto, *J. Biosci. Bioeng.*, 2005, **99**, 12–17.
227 T. Mouri, T. Shimizu, N. Kamiya, M. Goto and H. Ichinose, *Biotechnol. Prog.*, 2009, 25, 1372–1378.
228 V. I. Tishkov and V. O. Popov, *Biomol. Eng.*, 2006, **23**, 89–110.
229 A. Andreadeli, D. Platis, V. Tishkov, V. Popov and N. E. Labrou, *FEBS J.*, 2008, 275, 3859–3869.
230 S. C. Maurer, K. Kühnel, L. A. Kaysser, S. Eiben, R. D. Schmid and V. B. Urlacher, *Adv. Synth. Catal.*, 2005, **347**, 1090–1098.
231 T. Kubo, M. W. Peters, P. Meinhold and F. H. Arnold, *Chem. - A Eur. J.*, 2006, **12**, 1216–1220.
232 J. R. Falck, Y. K. Reddy, D. C. Haines, K. M. Reddy, U. M. Krishna, S. Graham, B. Murry and J. A. Peterson, *Tetrahedron Lett.*, 2001, **42**, 4131–4133.
233 M. E. Ener, Y. T. Lee, J. R. Winkler, H. B. Gray and L. Cheruzela, *Proc. Natl. Acad. Sci. U. S. A.*, 2010, **107**, 18783–18786.
234 N. H. Tran, D. Nguyen, S. Dwaraknath, S. Mahadevan, G. Chavez, A. Nguyen, T. Dao, S. Mullen, T. A. Nguyen and L. E. Cheruzel, *J. Am. Chem. Soc.*, 2013, **135**, 14484–14487.
235 K. Jensen, J. B. Johnston, P. R. O. de Montellano and B. L. Møller, *Biotechnol. Lett.*, 2012, **34**, 239–245.
236 Y. S. Kim, M. Hara, K. Ikebukuro, J. Miyake, H. Ohkawa and I. Karube, *Biotechnol. Tech.*, 1996, **10**, 717–720.
237 M. Hara, S. Iazvovskaia, H. Ohkawa, Y. Asada and J. Miyake, *J. Biosci. Bioeng.*, 1999, **87**, 793–797.
238 K. Jensen, P. E. Jensen and B. L. Møller, *Trends Plant Sci.*, 2012, **17**, 60–63.
239 S. Kumar, Y. Zhao, L. Sun, S. S. Negi, J. R. Halpert and B. K. Muralidhara, *Mol. Pharmacol.*, 2007, **72**, 1191–1199.
240 K. Schroer, M. Kittelmann and S. Lütz, *Biotechnol. Bioeng.*, 2010, **106**, 699–706.
241 I. Neunzig, M. Widjaja, F. T. Peters, H. H. Maurer, A. Hehn, F. Bourgaud and M. Bureik, *Appl. Biochem. Biotechnol.*, 2013, **170**, 1751–1766.
242 G. Di Nardo and G. Gilardi, *Int. J. Mol. Sci.*, 2012, **13**, 15901–15924.
243 A. Li, A. Ilie, Z. Sun, R. Lonsdale, J.-H. H. Xu and M. T. Reetz, *Angew. Chemie - Int. Ed.*, 2016, **55**, 12026–12029.
244 S. Wu and Z. Li, *ChemCatChem*, 2018, **10**, 2164–2178.
245 J. A. McIntosh, C. C. Farwell and F. H. Arnold, *Curr. Opin. Chem. Biol.*, 2014, **19**, 126–134.
246 Y. Ensari, G. de Almeida Santos, A. J. Ruff and U. Schwaneberg, *Enzyme Microb. Technol.*, 2020, 138.
247 M. Ahsan, M. Patil, H. Jeon, S. Sung, T. Chung and H. Yun, *Catalysts*, 2018, **8**, 400.
248 H. Zhou, B. Wang, F. Wang, X. Yu, L. Ma, A. Li and M. T. Reetz, *Angew. Chemie Int. Ed.*, 2019, **58**, 764–768.
249 J. Alonso-Gutierrez, R. Chan, T. S. Batth, P. D. Adams, J. D. Keasling, C. J. Petzold and T. S. Lee, *Metab. Eng.*, 2013, **19**, 33–41.
250 C. J. Paddon, P. J. Westfall, D. J. Pitera, K. Benjamin, K. Fisher, D. McPhee, M. D. Leavell, A. Tai, A. Main, D. Eng, D. R. Polichuk, K. H. Teoh, D. W. Reed, T. Treynor, J. Lenihan, H. Jiang, M. Fleck, S. Bajad, G. Dang, D. Dengrove, D. Diola, G. Dorin, K. W. Ellens, S. Fickes, J. Galazzo, S. P. Gaucher, T. Geistlinger, R. Henry, M. Hepp, T. Horning, T. Iqbal, L. Kizer, B. Lieu, D. Melis, N. Moss, R. Regentin, S. Secrest, H. Tsuruta, R. Vazquez, L. F. Westblade, L. Xu, M. Yu, Y. Zhang, L. Zhao, J. Lievense, P. S. Covello, J. D. Keasling, K. K. Reiling, N. S. Renninger and J. D. Newman, *Nature*, 2013, **496**, 528–532.
251 Q. Wang, M. L. Hillwig and R. J. Peters, *Plant J.*, 2011, **65**, 87–95.

252 Y. Wu, M. L. Hillwig, Q. Wang and R. J. Peters, *FEBS Lett.*, 2011, **585**, 3446–3451.
253 J. Guo, Y. J. Zhou, M. L. Hillwig, Y. Shen, L. Yang, Y. Wang, X. Zhang, W. Liu, R. J. Peters, X. Chen, Z. K. Zhao and L. Huang, *Proc. Natl. Acad. Sci. U. S. A.*, 2013, **110**, 12108–12113.
254 E. O. Fukushima, H. Seki, S. Sawai, M. Suzuki, K. Ohyama, K. Saito and T. Muranaka, *Plant Cell Physiol.*, 2013, **54**, 740–749.
255 Y. Yan, A. Kohli and M. A. G. Koffas, *Appl. Environ. Microbiol.*, 2005, **71**, 5610–5613.
256 E. Leonard, Y. Yan, K. H. Lim and M. A. G. Koffas, *Appl. Environ. Microbiol.*, 2005, **71**, 8241–8248.
257 E. Leonard, Y. Yan and M. A. G. Koffas, *Metab. Eng.*, 2006, **8**, 172–181.
258 M. D. Mikkelsen, L. D. Buron, B. Salomonsen, C. E. Olsen, B. G. Hansen, U. H. Mortensen and B. A. Halkier, *Metab. Eng.*, 2012, **14**, 104–111.
259 K. M. Hawkins and C. D. Smolke, *Nat. Chem. Biol.*, 2008, **4**, 564–573.
260 E. Fossati, A. Ekins, L. Narcross, Y. Zhu, J. P. Falgueyret, G. A. W. Beaudoin, P. J. Facchini and V. J. J. Martin, *Nat. Commun.*, 2014, **5**, 3283.
261 E. Matsumura, M. Matsuda, F. Sato and H. Minami, *Nat. Prod. Phytochem. Bot. Metab. Alkaloids, Phenolics Terpenes*, 2013, **105**, 3–24.
262 Fumihiko Sato, Takayuki Inui and Tomoya Takemura, *Curr. Pharm. Biotechnol.*, 2007, **8**, 211–218.
263 Y. Miura and A. J. Fulco, *J. Biol. Chem.*, 1974, 249, 1880–1888.
264 R. S. Hare and A. J. Fulco, *Biochem. Biophys. Res. Commun.*, 1975, 65, 665–672.
265 N. English, V. Hughes and C. R. Wolf, *J. Biol. Chem.*, 1994, **269**, 26836–26841.
266 C. N. A. Palmer, E. Axen, V. Hughes and C. R. Wolf, *J. Biol. Chem.*, 1998, **273**, 18109–18116.
267 S. S. Boddupalli, R. W. Estabrook and J. A. Peterson, *J. Biol. Chem.*, 1990, **265**, 4233–4239.
268 L. O. Narhi, B. H. Kim, P. M. Stevenson and A. J. Fulco, *Biochem. biophys. Res. Commun.*, 1983, **116**, 851–858.
269 D. Appel, S. Lutz-Wahl, P. Fischer, U. Schwaneberg and R. D. Schmid, *J. Biotechnol.*, 2001, **88**, 167–171.
270 C. K. J. Chen, T. K. Shokhireva, R. E. Berry, H. Zhang and F. A. Walker, *J. Biol. Inorg. Chem.*, 2008, **13**, 813–824.
271 Y. Lu and L. he Mei, *J. Zhejiang Univ. Sci. B.*, 2007, **8**, 27–32.
272 S. Pflug, S. M. Richter and V. B. Urlacher, *J. Biotechnol.*, 2007, **129**, 481–488.
273 S. Schneider, M. G. Wubbolts, G. Oesterhelt, D. Sanglard and B. Witholt, *Biotechnol. Bioeng.*, 1999, **64**, 333–341.
274 Y. Li and L. L. Wong, *Angew. Chemie Int. Ed.*, 2019, **58**, 9551–9555.
275 P. K. Chowdhary, M. Alemseghed and D. C. Haines, *Arch. Biochem. Biophys.*, 2007, **468**, 32–43.
276 C. R. Otey, M. Landwehr, J. B. Endelman, K. Hiraga, J. D. Bloom and F. H. Arnold, *PLoS Biol.*, 2006, **4**, 789–798.
277 S. Eiben, H. Bartelmäs and V. B. Urlacher, *Appl. Microbiol. Biotechnol.*, 2007, **75**, 1055–1061.
278 D. Roccatano, T. S. Wong, U. Schwaneberg and M. Zacharias, *Biopolymers*, 2005, **78**, 259–267.
279 H. Li, K. Darwish and T. L. Poulos, *J. Biol. Chem.*, 1991, **266**, 11909–11914.
280 J. S. Miles, A. W. Munro, B. N. Rospendowski, W. E. Smith, J. McKnight and A. J. Thomson, *Biochem. J.*, 1992, **288**, 503–509.
281 A. W. Munro, J. G. Lindsay, J. R. Coggins, S. M. Kelly and N. C. Price, *FEBS Lett.*, 1994, **343**, 70–74.
282 S. Govindaraj and T. L. Poulos, *Biochemistry*, 1995, **34**, 11221–11226.
283 S. Govindaraj and T. L. Poulos, *Protein Sci.*, 1996, **5**, 1389–1393.
284 T. Oster, S. S. Boddupalli and J. A. Peterson, *J. Biol. Chem.*, 1991, **266**, 22718–22725.
285 T. D. Porter and C. B. Kasper, *Biochemistry*, 1986, **25**, 1682–1687.
286 S. D. Black, *Biochem. Biophys. Res. Commun.*, 1994, **203**, 162–168.
287 I. Sevrioukova, G. Truan and J. A. Peterson, *Biochemistry*, 1996, **35**, 7528–7535.
288 S. Govindaraj and T. L. Poulos, *J. Biol. Chem.*, 1997, **272**, 7915–7921.
289 A. W. Munro, *Biochem. Soc. Trans.*, 1993, **21**, 2682.
290 A. W. Munro, J. Gordon Linday, J. R. Coggins, N. C. Price and S. M. Kelly, *Biochem. Biophys. Acta*, 1996, **1296**, 127–137.
291 A. P. Jamakhandi, B. C. Jeffus, V. R. Dass and G. P. Miller, *Arch. Biochem. Biophys.*, 2005, **439**, 165–174.
292 H.-C. Chen and R. P. Swenson, *Biochemistry*, 2008, **47**, 13788–13799.
293 A. W. Munro, S. Daff, J. R. Coggins, J. G. Lindsay and S. K. Chapman, *Eur. J. Biochem.*, 1996, **239**, 403–409.
294 S. D. Black and S. T. Martin, *Biochemistry*, 1994, **33**, 12056–12062.
295 A. J. Fulco, B. H. Kim, R. S. Matson, L. Owers Narhi and R. T. Ruettinger, *Mol. Cell. Biochem.*, 1983, **53**–**54**, 155–161.
296 T. Kitazume, D. C. Haines, R. W. Estabrook, B. Chen and J. A. Peterson, *Biochemistry*, 2007, **46**, 11892–

11901.
297 R. Neeli, H. M. Girvan, A. Lawrence, M. J. Warren, D. Leys, N. S. Scrutton and A. W. Munro, *FEBS Lett.*, 2005, **579**, 5582–5588.
298 V. E. V. Ferrero, L. Andolfi, G. Di Nardo, S. J. Sadeghi, A. Fantuzzi, S. Cannistraro and G. Gilardi, *Anal. Chem.*, 2008, **80**, 8438–8446.
299 B. Rowlatt, J. A. Yorke, A. J. Strong, C. J. C. Whitehouse, S. G. Bell and L. L. Wong, *Protein Cell*, 2011, **2**, 656–671.
300 G. Gilardi, Y. T. Meharenna, G. E. Tsotsou, S. J. Sadeghi, M. Fairhead and S. Giannini, *Biosens. Bioelectron.*, 2002, **17**, 133–145.
301 A. Fantuzzi, Y. T. Meharenna, P. B. Briscoe, F. Guerlesquin, S. J. Sadeghi and G. Gilardi, *Biochim. Biophys. Acta - Bioenerg.*, 2009, **1787**, 234–241.
302 M. Su, S. Chakraborty, Y. Osawa and H. Zhang, *J. Biol. Chem.*, 2020, **295**, 1637–1645.
303 C. J. C. Whitehouse, W. Yang, J. A. Yorke, H. G. Tufton, L. C. I. Ogilvie, S. G. Bell, W. Zhou, M. Bartlam, Z. Rao and L.-L. Wong, *Dalt. Trans.*, 2011, **40**, 10383.
304 A. B. Carmichael and L. L. Wong, *Eur. J. Biochem.*, 2001, **268**, 3117–3125.
305 J. Catalano, K. Sadre-Bazzaz, G. A. Amodeo, L. Tong and A. McDermott, *Biochemistry*, 2013, **52**, 6807–6815.
306 T. W. . Ost, C. S. Miles, J. Murdoch, Y.-F. Cheung, G. A. Reid, S. K. Chapman and A. W. Munro, *FEBS Lett.*, 2000, **486**, 173–177.
307 A. Hegde, D. C. Haines, M. Bondlela, B. Chen, N. Schaffer, D. R. Tomchick, M. Machius, H. Nguyen, P. K. Chowdhary, L. Stewart, C. Lopez and J. A. Peterson, *Biochemistry*, 2007, **46**, 14010–14017.
308 Q. S. Li, J. Ogawa, R. D. Schmid and S. Shimizu, *Appl. Environ. Microbiol.*, 2001, **67**, 5735–5739.
309 D. C. Haines, D. R. Tomchick, M. Machius and J. A. Peterson, *Biochemistry*, 2001, **40**, 13456–13465.
310 Z. Cong, O. Shoji, C. Kasai, N. Kawakami, H. Sugimoto, Y. Shiro and Y. Watanabe, *ACS Catal.*, 2015, **5**, 150–156.
311 R. A. Luirink, S. J. Dekker, L. Capoferri, L. F. H. Janssen, C. L. Kuiper, M. E. Ari, N. P. E. Vermeulen, J. C. Vos, J. N. M. Commandeur and D. P. Geerke, *J. Inorg. Biochem.*, 2018, **184**, 115–122.
312 C. G. Acevedo-Rocha, C. G. Gamble, R. Lonsdale, A. Li, N. Nett, S. Hoebenreich, J. B. Lingnau, C. Wirtz, C. Fares, H. Hinrichs, A. Deege, A. J. Mulholland, Y. Nov, D. Leys, K. J. McLean, A. W. Munro and M. T. Reetz, *ACS Catal.*, 2018, **8**, 3395–3410.
313 L. Richards, A. Lutz, D. K. Chalmers, A. Jarrold, T. Bowser, G. W. Stevens and S. L. Gras, *Biotechnol. Reports*, 2019, **24**, e00372.
314 K. Neufeld, S. M. Zu Berstenhorst and J. Pietruszka, *Anal. Biochem.*, 2014, **456**, 70–81.
315 K. Neufeld, B. Henßen and J. Pietruszka, *Angew. Chemie Int. Ed.*, 2014, **53**, 13253–13257.
316 A. Rentmeister, T. R. Brown, C. D. Snow, M. N. Carbone and F. H. Arnold, *ChemCatChem*, 2011, **3**, 1065–1071.
317 C. F. Butler, C. Peet, A. E. Mason, M. W. Voice, D. Leys and A. W. Munro, *J. Biol. Chem.*, 2013, **288**, 25387–25399.
318 C. F. Oliver, S. Modi, M. J. Sutcliffe, W. U. Primrose, L. Y. Lian and G. C. K. Roberts, *Biochemistry*, 1997, **36**, 1567–1572.
319 M. J. Cryle, N. J. Matovic and J. J. de Voss, *Org. Lett.*, 2003, **5**, 3341–3344.
320 M. J. Cryle and J. J. De Voss, *Chem. Commun.*, 2004, **4**, 86–87.
321 M. J. Cryle and J. J. De Voss, *ChemBioChem*, 2008, **9**, 261–266.
322 W. T. Sulistyaningdyah, J. Ogawa, Q. S. Li, C. Maeda, Y. Yano, R. D. Schmid and S. Shimizu, *Appl. Microbiol. Biotechnol.*, 2005, **67**, 556–562.
323 R. J. Sowden, S. Yasmin, N. H. Rees, S. G. Bell and L. L. Wong, *Org. Biomol. Chem.*, 2005, **3**, 57–64.
324 S. Eiben, L. Kaysser, S. Maurer, K. Kühnel, V. B. Urlacher and R. D. Schmid, *J. Biotechnol.*, 2006, **124**, 662–669.
325 M. Dietrich, T. A. Do, R. D. Schmid, J. Pleiss and V. B. Urlacher, *J. Biotechnol.*, 2009, **139**, 115–117.
326 R. J. F. Branco, A. Seifert, M. Budde, V. B. Urlacher, M. J. Ramos and J. Pleiss, *Proteins Struct. Funct. Genet.*, 2008, **73**, 597–607.
327 Y. Watanabe, S. Laschat, M. Budde, O. Affolter, Y. Shimada and V. B. Urlacher, *Tetrahedron*, 2007, **63**, 9413–9422.
328 A. M. Sawayama, M. M. Y. Chen, P. Kulanthaivel, M. S. Kuo, H. Hemmerle and F. H. Arnold, *Chem. - A Eur. J.*, 2009, **15**, 11723–11729.
329 J. Reinen, S. Ferman, E. Vottero, N. P. E. Vermeulen and J. N. M. Commandeur, *J. Biomol. Screen.*, 2011, **16**, 239–250.
330 E. Vottero, V. Rea, J. Lastdrager, M. Honing, N. P. E. Vermeulen and J. N. M. Commandeur, *J. Biol. Inorg. Chem.*, 2011, **16**, 899–912.
331 A. Seifert and J. Pleiss, *Proteins Struct. Funct. Bioinforma.*, 2009, **74**, 1028–1035.

332 P. Meinhold, M. W. Peters, A. Hartwick, A. R. Hernandez and F. H. Arnold, *Adv. Synth. Catal.*, 2006, **348**, 763–772.
333 C. J. C. C. Whitehouse, S. G. Bell, H. G. Tufton, R. J. P. P. Kenny, L. C. I. I. Ogilvie and L.-L. L. Wong, *Chem. Commun.*, 2008, **1**, 966–968.
334 S. H. Ryu, B. Y. Park, S. Y. Kim, S. H. Park, H. J. Jung, M. Park, K. D. Park, T. Ahn, H. S. Kang and C. H. Yun, *Drug Metab. Dispos.*, 2014, **42**, 1493–1497.
335 Y. T. Chang and G. H. Loew, *J. Biomol. Struct. Dyn.*, 1999, **16**, 1189–1203.
336 L. D. Syntrivanis, L. L. Wong and J. Robertson, *European J. Org. Chem.*, 2018, **2018**, 6369–6378.
337 I. Geronimo, C. A. Denning, W. E. Rogers, T. Othman, T. Huxford, D. K. Heidary, E. C. Glazer and C. M. Payne, *Biochemistry*, 2016, **55**, 3594–3606.
338 J. C. Lewis, S. M. Mantovani, Y. Fu, C. D. Snow, R. S. Komor, C. H. Wong and F. H. Arnold, *ChemBioChem*, 2010, **11**, 2502–2505.
339 A. Shehzad, S. Panneerselvam, M. Linow, M. Bocola, D. Roccatano, J. Mueller-Dieckmann, M. Wilmanns and U. Schwaneberg, *Chem. Commun.*, 2013, **49**, 4694–4696.
340 Y. Ji, A. M. Mertens, C. Gertler, S. Fekiri, M. Keser, D. F. Sauer, K. E. C. Smith and U. Schwaneberg, *Chem. - A Eur. J.*, 2018, **24**, 16865–16872.
341 Q.-S. Li, U. Schwaneberg, P. Fischer and R. D. Schmid, *Chem. – A Eur. J.*, 2000, **6**, 1531–1536.
342 L. L. Wu, C. L. Yang, F. C. Lo, C. H. Chiang, C. W. Chang, K. Y. Ng, H. H. Chou, H. Y. Hung, S. I. Chan and S. S. F. Yu, *Chem. - A Eur. J.*, 2011, 17, 4774–4787.
343 K. Kühnel, S. C. Maurer, Y. Galeyeva, W. Frey, S. Laschat and V. B. Urlacher, *Adv. Synth. Catal.*, 2007, **349**, 1451–1461.
344 S. C. Maurer, H. Schulze, R. D. Schmid and V. Urlacher, *Adv. Synth. Catal.*, 2003, 345, 802–810.
345 X. Ren, J. A. O'Hanlon, M. Morris, J. Robertson and L. L. Wong, *ACS Catal.*, 2016, **6**, 6833–6837.
346 C. H. Yun, K. H. Kim, D. H. Kim, H. C. Jung and J. G. Pan, *Trends Biotechnol.*, 2007, **25**, 289–298.
347 T. J. Volz, D. A. Rock and J. P. Jones, *J. Am. Chem. Soc.*, 2002, **124**, 9724–9725.
348 M. J. Cryle and J. J. De Voss, *Angew. Chemie - Int. Ed.*, 2006, **45**, 8221–8223.
349 T. K. Hyster and F. H. Arnold, *Isr. J. Chem.*, 2015, **55**, 14–20.
350 M. B. Murataliev, L. N. Trinh, L. V. Moser, R. B. Bates, R. Feyereisen and F. A. Walker, *Biochemistry*, 2004, **43**, 1771–1780.
351 E. Stjernschantz, B. M. A. Van Vugt-Lussenburg, A. Bonifacio, S. B. A. De Beer, G. Van Der Zwan, C. Gooijer, J. N. M. Commandeur, N. P. E. Vermeulen and C. Oostenbrink, *Proteins Struct. Funct. Genet.*, 2008, **71**, 336–352.
352 D. C. Haines, A. Hegde, B. Chen, W. Zhao, M. Bondlela, J. M. Humphreys, D. A. Mullin, D. R. Tomchick, M. MacHius and J. A. Peterson, *Biochemistry*, 2011, **50**, 8333–8341.
353 R. Agudo, G. D. Roiban and M. T. Reetz, *ChemBioChem*, 2012, **13**, 1465–1473.
354 S. Bähr, S. Brinkmann-Chen, M. Garcia-Borràs, J. M. Roberts, D. E. Katsoulis, K. N. Houk and F. H. Arnold, *Angew. Chemie - Int. Ed.*, 2020, 15507–15511.
355 C. J. C. Whitehouse, W. Yang, J. A. Yorke, B. C. Rowlatt, A. J. F. Strong, C. F. Blanford, S. G. Bell, M. Bartlam, L.-L. Wong and Z. Rao, *ChemBioChem*, 2010, **11**, 2549–2556.
356 C. J. C. Whitehouse, S. G. Bell and L. L. Wong, *Chem. - A Eur. J.*, 2008, **14**, 10905–10908.
357 S. A. Loskot, D. K. Romney, F. H. Arnold and B. M. Stoltz, *J. Am. Chem. Soc.*, 2017, **139**, 10196–10199.
358 T. Klaus, A. Seifert, T. Häbe, B. M. Nestl and B. Hauer, *Catalysts*, , DOI:10.3390/catal9030252.
359 J. B. Wang, A. Ilie and M. T. Reetz, *Adv. Synth. Catal.*, 2017, **359**, 2056–2060.
360 H. Venkataraman, S. B. A. D. Beer, D. P. Geerke, N. P. E. Vermeulen and J. N. M. Commandeur, *Adv. Synth. Catal.*, 2012, **354**, 2172–2184.
361 J. A. O'Hanlon, X. Ren, M. Morris, L. L. Wong and J. Robertson, *Org. Biomol. Chem.*, 2017, **15**, 8780–8787.
362 W. C. Huang, P. M. Cullis, E. L. Raven and G. C. K. Roberts, *Metallomics*, 2011, **3**, 410–416.
363 W. Chen, M. J. Fisher, A. Leung, Y. Cao and L. L. Wong, *ACS Catal.*, 2020, **10**, 8334–8343.
364 C. J. C. Whitehouse, S. G. Bell, W. Yang, J. A. Yorke, C. F. Blanford, A. J. F. Strong, E. J. Morse, M. Bartlam, Z. Rao and L. L. Wong, *ChemBioChem*, 2009, **10**, 1654–1656.
365 A. Hopkins, J. Lanfear, C. Lipinski and L. Beeley, *Annu. Rep. Med. Chem.*, 2005, **40**, 339–348.
366 C. G. Wermuth, *J. Med. Chem.*, 2004, **47**, 1303–1314.
367 R. MacArron, M. N. Banks, D. Bojanic, D. J. Burns, D. A. Cirovic, T. Garyantes, D. V. S. Green, R. P. Hertzberg, W. P. Janzen, J. W. Paslay, U. Schopfer and G. S. Sittampalam, *Nat. Rev. Drug Discov.*, 2011, **10**, 188–195.
368 P. J. Hajduk and J. Greer, *Nat. Rev. Drug Discov.*, 2007, **6**, 211–219.
369 D. A. Erlanson, S. W. Fesik, R. E. Hubbard, W. Jahnke and H. Jhoti, *Nat. Rev. Drug Discov.*, 2016, **15**, 605–619.
370 D. W. Fry, A. J. Kraker, A. McMichael, L. A. Ambroso, J. M. Nelson, W. R. Leopold, R. W. Connors

and A. J. Bridges, *Science (80-.).*, 1994, **265**, 1093–1095.
371 S. Wilhelm, C. Carter, M. Lynch, T. Lowinger, J. Dumas, R. A. Smith, B. Schwartz, R. Simantov and S. Kelley, *Nat. Rev. Drug Discov.*, 2006, **5**, 835–844.
372 A. J. Souers, J. D. Leverson, E. R. Boghaert, S. L. Ackler, N. D. Catron, J. Chen, B. D. Dayton, H. Ding, S. H. Enschede, W. J. Fairbrother, D. C. S. Huang, S. G. Hymowitz, S. Jin, S. L. Khaw, P. J. Kovar, L. T. Lam, J. Lee, H. L. Maecker, K. C. Marsh, K. D. Mason, M. J. Mitten, P. M. Nimmer, A. Oleksijew, C. H. Park, C. M. Park, D. C. Phillips, A. W. Roberts, D. Sampath, J. F. Seymour, M. L. Smith, G. M. Sullivan, S. K. Tahir, C. Tse, M. D. Wendt, Y. Xiao, J. C. Xue, H. Zhang, R. A. Humerickhouse, S. H. Rosenberg and S. W. Elmore, *Nat. Med.*, 2013, **19**, 202–208.
373 S. Thaisrivongs, P. K. Tomich, K. D. Watenpaugh, K. T. Chong, J. W. Howe, C. P. Yang, J. W. Strohbach, S. R. Turner, J. P. McGrath, M. J. Bohanon, J. C. Lynn, A. M. Mulichak, P. A. Spinelli, R. R. Hinshaw, P. J. Pagano, J. B. Moon, M. J. Ruwart, K. F. Wilkinson, B. D. Rush, G. L. Zipp, R. J. Dalga, F. J. Schwende, G. M. Howard, G. E. Padbury, L. N. Toth, Z. Zhao, K. A. Koeplinger, T. J. Kakuk, S. L. Cole, R. M. Zaya, R. C. Piper and P. Jeffrey, *J. Med. Chem.*, 1994, **37**, 3200–3204.
374 N. Thornberry and A. Weber, *Curr. Top. Med. Chem.*, 2007, **7**, 557–568.
375 J. Das, P. Chen, D. Norris, R. Padmanabha, J. Lin, R. V. Moquin, Z. Shen, L. S. Cook, A. M. Doweyko, S. Pitt, S. Pang, D. R. Shen, Q. Fang, H. F. de Fex, K. W. McIntyre, D. J. Shuster, K. M. Gillooly, K. Behnia, G. L. Schieven, J. Wityak and J. C. Barrish, *J. Med. Chem.*, 2006, **49**, 6819–6832.
376 H. Riechers, H. P. Albrecht, W. Amberg, E. Baumann, H. Bernard, H. J. Böhm, D. Klinge, A. Kling, S. Müller, M. Raschack, L. Unger, N. Walker and W. Wernet, *J. Med. Chem.*, 1996, **39**, 2123–2128.
377 B. L. De Corte, *J. Med. Chem.*, 2005, **48**, 1689–1696.
378 Y. Yamamura, H. Ogawa, T. Chihara, K. Kondo, T. Onogawa, S. Nakamura, T. Mori, M. Tominaga and Y. Yabuuchi, *Science (80-.).*, 1991, **252**, 572–574.
379 K. J. Duffy, M. G. Darcy, E. Delorme, S. B. Dillon, D. F. Eppley, C. Erickson-Miller, L. Giampa, C. B. Hopson, Y. Huang, R. M. Keenan, P. Lamb, L. Leong, N. Liu, S. G. Miller, A. T. Price, J. Rosen, R. Shah, T. N. Shaw, H. Smith, K. C. Stark, S. S. Tian, C. Tyree, K. J. Wiggall, L. Zhang and J. I. Luengo, *J. Med. Chem.*, 2001, **44**, 3730–3745.
380 G. Bollag, J. Tsai, J. Zhang, C. Zhang, P. Ibrahim, K. Nolop and P. Hirth, *Nat. Rev. Drug Discov.*, 2012, **11**, 873–886.
381 V. Velvadapu, B. T. Farmer and A. B. Reitz, in *The Practice of Medicinal Chemistry*, Elsevier, 2015, pp. 161–180.
382 B. C. Doak, C. J. Morton, J. S. Simpson and M. J. Scanlon, *Aust. J. Chem.*, 2013, **66**, 1465–1472.
383 P. J. Hajduk, D. J. Augeri, J. Mack, R. Mendoza, J. Yang, S. F. Betz and S. W. Fesik, *J. Am. Chem. Soc.*, 2000, **122**, 7898–7904.
384 H. Jhoti, G. Williams, D. C. Rees and C. W. Murray, *Nat. Rev. Drug Discov.*, 2013, **12**, 644.
385 R. J. Hall, P. N. Mortenson and C. W. Murray, *Prog. Biophys. Mol. Biol.*, 2014, **116**, 82–91.
386 D. C. Ress, M. Congreve, C. W. Murray and R. Carr, *Nat. Rev. Drug Discov.*, 2004, **3**, 660–672.
387 E. Vitaku, D. T. Smith and J. T. Njardarson, *J. Med. Chem.*, 2014, **57**, 10257–10274.
388 M. Aldeghi, S. Malhotra, D. L. Selwood and A. W. E. Chan, *Chem. Biol. Drug Des.*, 2014, **83**, 450–461.
389 P. Kittakoop, C. Mahidol and S. Ruchirawat, *Curr. Top. Med. Chem.*, 2014, **14**, 239–252.
390 C. Zhang, C. K. De, R. Mal and D. Seidel, *J. Am. Chem. Soc.*, 2008, **130**, 416–417.
391 K. R. Campos, *Chem. Soc. Rev.*, 2007, **36**, 1069–1084.
392 A. McNally, C. K. Prier and D. W. C. MacMillan, *Science (80-.).*, 2011, **334**, 1114–1117.
393 E. A. Mitchell, A. Peschiulli, N. Lefevre, L. Meerpoel and B. U. W. Maes, *Chem. - A Eur. J.*, 2012, **18**, 10092–10142.
394 P. Jain, P. Verma, G. Xia and J.-Q. Yu, *Nat. Chem.*, 2017, **9**, 140–144.
395 W. Chen, L. Ma, A. Paul and D. Seidel, *Nat. Chem.*, 2018, **10**, 165–169.
396 J. B. Roque, Y. Kuroda, J. Jurczyk, L.-P. Xu, J. S. Ham, L. T. Göttemann, C. A. Roberts, D. Adpressa, J. Saurí, L. A. Joyce, D. G. Musaev, C. S. Yeung and R. Sarpong, *ACS Catal.*, 2020, **10**, 2929–2941.
397 A. Trowbridge, S. M. Walton and M. J. Gaunt, *Chem. Rev.*, 2020, **120**, 2613–2692.
398 G. Kumar, S. Pradhan and I. Chatterjee, *Chem. - An Asian J.*, 2020, 651–672.
399 P. Beak, A. Basu, D. J. Gallagher, Y. S. Park and S. Thayumanavan, *Acc. Chem. Res.*, 1996, **29**, 552–560.
400 I. Coldham and D. Leonori, *Org. Lett.*, 2008, **10**, 3923–3925.
401 Z. Li and C. J. Li, *Org. Lett.*, 2004, 6, 4997–4999.
402 Z. Li, D. S. Bohle and C.-J. Li, *Proc. Natl. Acad. Sci.*, 2006, **103**, 8928–8933.
403 Z. Li and C. J. Li, *J. Am. Chem. Soc.*, 2005, 127, 6968–6969.
404 Z. Li, P. D. MacLeod and C. J. Li, *Tetrahedron Asymmetry*, 2006, **17**, 590–597.
405 X. Z. Shu, Y. F. Yang, X. F. Xia, K. G. Ji, X. Y. Liu and Y. M. Liang, *Org. Biomol. Chem.*, 2010, **8**, 4077–4079.
406 X.-Z. Shu, X.-F. Xia, Y.-F. Yang, K.-G. Ji, X.-Y. Liu and Y.-M. Liang, *J. Org. Chem.*, 2009, **74**, 7464–

7469.
407 N. Shankaraiah, R. A. Pilli and L. S. Santos, *Tetrahedron Lett.*, 2008, **49**, 5098–5100.
408 H. N. T. Yoshimitsu, Y. Arano, *Synfacts*, 2005, **2005**, 0254–0254.
409 H. Prokopcová, S. D. Bergman, K. Aelvoet, V. Smout, W. Herrebout, B. Van der Veken, L. Meerpoel and B. U. W. Maes, *Chem. - A Eur. J.*, 2010, **16**, 13063–13067.
410 J. W. Beatty and C. R. J. Stephenson, *Acc. Chem. Res.*, 2015, **48**, 1474–1484.
411 L. R. Reddy, B. V. S. Reddy and E. J. Corey, *Org. Lett.*, 2006, **8**, 2819–2821.
412 R. Fan, D. Pu, F. Wen and J. Wu, *J. Org. Chem.*, 2007, **72**, 8994–8997.
413 N. R. Paz, D. Rodríguez-Sosa, H. Valdés, R. Marticorena, D. Melián, M. B. Copano, C. C. González and A. J. Herrera, *Org. Lett.*, 2015, **17**, 2370–2373.
414 E. A. Wappes, S. C. Fosu, T. C. Chopko and D. A. Nagib, *Angew. Chemie Int. Ed.*, 2016, **55**, 9974–9978.
415 H. Zhang and K. Muñiz, *ACS Catal.*, 2017, **7**, 4122–4125.
416 L. M. Lutete, I. Kadota and Y. Yamamoto, *J. Am. Chem. Soc.*, 2004, **126**, 1622–1623.
417 Z. Liu and J. F. Hartwig, *J. Am. Chem. Soc.*, 2008, **130**, 1570–1571.
418 L. D. Julian and J. F. Hartwig, *J. Am. Chem. Soc.*, 2010, **132**, 13813–13822.
419 A. Takemiya and J. F. Hartwig, *J. Am. Chem. Soc.*, 2006, **128**, 6042–6043.
420 B. Sundararaju, M. Achard, G. V. M. Sharma and C. Bruneau, *J. Am. Chem. Soc.*, 2011, **133**, 10340–10343.
421 N. Kaloğlu, *Tetrahedron*, 2019, **75**, 2265–2272.
422 J. J. Topczewski, P. J. Cabrera, N. I. Saper and M. S. Sanford, *Nature*, 2016, **531**, 220–224.
423 D. Chang, H. J. Feiten, K. H. Engesser, J. B. Van Beilen, B. Witholt and Z. Li, *Org. Lett.*, 2002, **4**, 1859–1862.
424 W. Zhang, W. L. Tang, Z. Wang and Z. Li, *Adv. Synth. Catal.*, 2010, **352**, 3380–3390.
425 S. Q. Pham, G. Pompidor, J. Liu, X. D. Li and Z. Li, *Chem. Commun.*, 2012, **48**, 4618–4620.
426 W. L. Tang, Z. Li and H. Zhao, *Chem. Commun.*, 2010, **46**, 5461–5463.
427 A. Li, J. Liu, S. Q. Pham and Z. Li, *Chem. Commun.*, 2013, **49**, 11572–11574.
428 D. Chang, B. Witholt and Z. Li, *Org. Lett.*, 2000, **2**, 3949–3952.
429 S. Q. Pham, P. Gao and Z. Li, *Biotechnol. Bioeng.*, 2013, **110**, 363–373.
430 Y. Yi and Z. Li, *Chimia (Aarau).*, 2015, **69**, 136–141.
431 H. L. Holland, T. A. Morris, P. J. Nava and M. Zabic, *Tetrahedron*, 1999, **55**, 7441–7460.
432 G. J. Grogan and H. L. Holland, *The biocatalytic reactions of Beauveria spp.*, 2000, vol. 9.
433 T. A. Crabb and S. L. Soilleux, *Tetrahedron*, 1986, **42**, 5407–5413.
434 R. L. Hanson, W. L. Parker, D. B. Brzozowski, T. P. Tully, M. Liu, A. Kotnis and R. N. Patel, *Tetrahedron Asymmetry*, 2005, **16**, 2711–2716.
435 G. Reign, H. McMahon, M. Ishizaki, T. Ohara, K. Shimane, Y. Esumi, C. Green, C. Tyson and S. Ninomiya, *Carcinogenesis*, 1996, **17**, 1989–1996.
436 T. S. Dowers, D. A. Rock, D. A. Rock, B. N. S. Perkins and J. P. Jones, *Drug Metab. Dispos.*, 2004, **32**, 328–332.
437 S. B. Karki and J. P. Dinnocenzo, *Xenobiotica*, 1995, **25**, 711–724.
438 D. Kim and F. P. Guengerich, *Annu. Rev. Pharmacol. Toxicol.*, 2005, **45**, 27–49.
439 L. Peterlin Masic, *Curr. Drug Metab.*, 2011, **12**, 35–50.
440 L. R. Hall and R. P. Hanzlik, *J. Biol. Chem.*, 1990, **265**, 12349–12355.
441 L. Constantino, E. Rosa and J. iley, *Biochem. Pharmacol.*, 1992, **44**, 651–658.
442 L. R. Hall, R. T. Iwamoto and R. P. Hanzlik, *J. Org. Chem.*, 1989, **54**, 2446–2451.
443 C. L. Shaffer, S. Harriman, Y. M. Koen and R. P. Hanzlik, *J. Am. Chem. Soc.*, 2002, **124**, 8268–8274.
444 K. M. Roberts and J. P. Jones, *Chem. - A Eur. J.*, 2010, **16**, 8096–8107.
445 F. P. Guengerich, C.-H. Yun and T. L. Macdonald, *J. Biol. Chem.*, 1996, **271**, 27321–27329.
446 E. Baciocchi, O. Lanzalunga, A. Lapi and L. Manduchi, *J. Am. Chem. Soc.*, 1998, **120**, 5783–5787.
447 G. Galliani, M. Nali, B. Rindone, S. Tollari, M. Rocchetti and M. Salmona, *Xenobiotica*, 1986, **16**, 511–517.
448 L. T. Burka, F. Peter Guengerich, R. J. Willard, T. L. Macdonald, F. P. Guengerich, R. J. Willard and T. L. Macdonald, *J. Am. Chem. Soc.*, 1985, **107**, 2549–2551.
449 P. R. O. De Montellano, H. S. Beilan and K. L. Kunze, *J Biol Chem*, 1981, **256**, 6708–6713.
450 J. A. Hinson, S. D. Nelson and J. R. Gillette, *Mol. Pharmacol.*, 1979, **15**, 419–427.
451 J. R. M. and D. J. J. J. A. HINSON, *Mol. Pharmacol.*, 1975, **11**, 462–469.
452 M. J. Cryle, J. E. Stok and J. J. De Voss, *Aust. J. Chem.*, 2003, **56**, 749–762.
453 S. Ghassabian, T. Rawling, F. Zhou, M. R. Doddareddy, B. N. Tattam, D. E. Hibbs, R. J. Edwards, P. H. Cui and M. Murray, *Biochem. Pharmacol.*, 2012, **84**, 215–223.
454 K. Oguri, Y. Tanimoto, M. Mishima and H. Yoshimura, *Xenobiotica*, 1989, **19**, 171–178.
455 L. LabbÈ, Z. Abolfathi, È. Lessard, H. Pakdel, P. Beaune and J. Turgeon, *Xenobiotica*, 2003, **33**, 13–25.

456 R. Furstoss, A. Archelas, B. Waegell, J. Le Petit and L. Deveze, *Tetrahedron Lett.*, 1980, **21**, 451–454.
457 F. P. Guengerich, M. V Martin, C. D. Sohl and Q. Cheng, *Nat. Protoc.*, 2009, **4**, 1245–1251.
458 M. Bietti, A. Cuppoletti, C. Dagostin, C. Florea, C. Galli, P. Gentili, H. Petride and C. R. Caia, *European J. Org. Chem.*, 1998, **1998**, 2425–2429.
459 B. Chiavarino, R. Cipollini, M. E. Crestoni, S. Fornarini, F. Lanucara and A. Lapi, *J. Am. Chem. Soc.*, 2008, **130**, 3208–3217.
460 R. K. Zhang, K. Chen, X. Huang, L. Wohlschlager, H. Renata and F. H. Arnold, *Nature*, 2019, **565**, 67–72.
461 J. Zhang, X. Huang, R. K. Zhang and F. H. Arnold, *J. Am. Chem. Soc.*, 2019, **141**, 9798–9802.
462 Y. Seto and F. P. Guengerich, *J. Chromatogr. B Biomed. Sci. Appl.*, 1993, **619**, 71–77.
463 F. P. Guengerich, O. Okazaki, Y. Seto and T. L. Macdonald, *Xenobiotica*, 1995, **25**, 689–709.
464 Y. Seto and F. P. Guengerich, *J. Biol. Chem.*, 1993, **268**, 9986–9997.
465 K. Kato, S. Jingu, N. Ogawa and S. Higuchi, *Biomed. Chromatogr.*, 2002, **16**, 25–30.
466 B. Ho and N. Castagnoli, *J. Med. Chem.*, 1980, **23**, 133–139.
467 H. MASUMOTO, K. TAKEUCHI, S. OHTA and M. HIROBE, *Chem. Pharm. Bull. (Tokyo).*, 1989, **37**, 1788–1794.
468 Z. Li, H. J. Feiten, D. Chang, W. A. Duetz, J. B. Van Beilen and B. Witholt, *J. Org. Chem.*, 2001, **66**, 8424–8430.
469 S. Sharma, Yamini and P. Das, *New J. Chem.*, 2019, **43**, 1764–1769.
470 A. Cartier, E. Levernier, A. L. Dhimane, T. Fukuyama, C. Ollivier, I. Ryu and L. Fensterbank, *Adv. Synth. Catal.*, 2020, 2254–2259.
471 P. Liu, H. Chen, S. Daniel, D. Hang, L. Zhao, H. Wang and Z. Zeng, *J. Fluor. Chem.*, 2013, **156**, 327–332.
472 Y. Ma, X. Yao, L. Zhang, P. Ni, R. Cheng and J. Ye, *Angew. Chemie - Int. Ed.*, 2019, **58**, 16548–16552.
473 M. Buswell, I. Fleming, U. Ghosh, S. Mack, M. Russell and B. P. Clark, *Org. Biomol. Chem.*, 2004, **2**, 3006.
474 M. Fochi, L. Caruana and L. Bernardi, *Synth.*, 2014, **46**, 135–157.
475 X. Jiang and R. Wang, *Chem. Rev.*, 2013, **113**, 5515–5546.
476 Y. H. Shen, Y. Q. Su, J. M. Tian, S. Lin, H. L. Li, J. Tang and W. D. Zhang, *Helv. Chim. Acta*, 2010, **93**, 2393–2396.
477 D. Tan, G. Chou and Z. Wang, *Chem. Nat. Compd.*, 2014, **50**, 329–332.
478 P. D. Brown, A. C. Willis, M. S. Sherburn and A. L. Lawrence, *Angew. Chemie - Int. Ed.*, 2013, **52**, 13273–13275.
479 G. Wittig and H. Sommer, *Justus Liebigs Ann. Chem.*, 1955, **594**, 1–14.
480 G. A. Swan and J. D. Wilcock, *J. Chem. Soc. Perkin Trans. 1*, 1974, 885–891.
481 J. B. P. A. Wijnberg, J. J. J. de Boer and W. N. Speckamp, *Recl. des Trav. Chim. des Pays-Bas*, 1978, **97**, 227–231.
482 G. H. Kerr, O. Meth-Cohn, E. B. Mullock and H. Suschitzky, *J. Chem. Soc. Perkin Trans. 1*, 1974, 1614.
483 G. D. Khandelwal, G. A. Swan and R. B. Roy, *J. Chem. Soc. Perkin Trans. 1*, 1974, **53**, 891–896.
484 M. Buswell and I. Fleming, *Chem. Commun.*, 2003, **34**, 202–203.
485 D. Anastasiou, E. Campi, H. Chaouk, G. Fallon, W. Jackson, Q. Mccubbin and A. Trnacek, *Aust. J. Chem.*, 1994, **47**, 1043.
486 G. Rao and M. Periasamy, *Synlett*, 2015, **26**, 2231–2236.
487 G. Q. Xu, J. T. Xu, Z. T. Feng, H. Liang, Z. Y. Wang, Y. Qin and P. F. Xu, *Angew. Chemie - Int. Ed.*, 2018, **57**, 5110–5114.
488 S. Honzawa, T. Sugihara, M. Uchida and T. Tashiro, *Heterocycles*, 2017, **95**, 994.
489 X.-L. Yu, L. Kuang, S. Chen, X.-L. Zhu, Z.-L. Li, B. Tan and X.-Y. Liu, *ACS Catal.*, 2016, 6182–6190.
490 L. Jia, S. Gao, J. Xie and M. Luo, *Adv. Synth. Catal.*, 2016, **358**, 3840–3846.
491 F. Hong, H. Li, D. Zhu, Z. Xia, H. Zhang, H. Wang and Z. Zeng, *J. Fluor. Chem.*, 2014, **168**, 61–68.
492 G. Zolotnitsky, U. Cogan, N. Adir, V. Solomon, G. Shoham and Y. Shoham, *Proc. Natl. Acad. Sci.*, 2004, **101**, 11275–11280.
493 L. Fielding, S. Rutherford and D. Fletcher, *Magn. Reson. Chem.*, 2005, **43**, 463–470.
494 A. B. Northrup and D. W. C. MacMillan, *J. Am. Chem. Soc.*, 2002, **124**, 6798–6799.
495 A. B. Northrup, I. K. Mangion, F. Hettche and D. W. C. MacMillan, *Angew. Chemie Int. Ed.*, 2004, **43**, 2152–2154.
496 I. K. Mangion, A. B. Northrup and D. W. C. MacMillan, *Angew. Chemie Int. Ed.*, 2004, **43**, 6722–6724.
497 S. P. Brown, M. P. Brochu, C. J. Sinz and D. W. C. MacMillan, *J. Am. Chem. Soc.*, 2003, **125**, 10808–10809.
498 M. P. Brochu, S. P. Brown and D. W. C. MacMillan, *J. Am. Chem. Soc.*, 2004, **126**, 4108–4109.
499 T. D. Beeson and D. W. C. MacMillan, *J. Am. Chem. Soc.*, 2005, **127**, 8826–8828.

500 T. D. Beeson, A. Mastracchio, J.-B. Hong, K. Ashton and D. W. C. MacMillan, *Science (80-.).*, 2007, **316**, 582–585.
501 A. B. Northrup and D. W. C. MacMillan, *J. Am. Chem. Soc.*, 2002, **124**, 2458–2460.
502 R. M. Wilson, W. S. Jen and D. W. C. MacMillan, *J. Am. Chem. Soc.*, 2005, **127**, 11616–11617.
503 J. F. Austin, S. G. Kim, C. J. Sinz, W. J. Xiao and D. W. C. MacMillan, *Proc. Natl. Acad. Sci. U. S. A.*, 2004, **101**, 5482–5487.
504 S. P. Brown, N. C. Goodwin and D. W. C. MacMillan, *J. Am. Chem. Soc.*, 2003, **125**, 1192–1194.
505 T. J. Osberger, D. C. Rogness, J. T. Kohrt, A. F. Stepan and M. C. White, *Nature*, 2016, **537**, 214–219.
506 J. C. Lo, D. Kim, C. M. Pan, J. T. Edwards, Y. Yabe, J. Gui, T. Qin, S. Gutiérrez, J. Giacoboni, M. W. Smith, P. L. Holland and P. S. Baran, *J. Am. Chem. Soc.*, 2017, **139**, 2484–2503.
507 A. Gesell, M. Rolf, J. Ziegler, M. L. D. Chávez, F. C. Huang and T. M. Kutchan, *J. Biol. Chem.*, 2009, **284**, 24432–24442.
508 N. Ikezawa, K. Iwasa and F. Sato, *J. Biol. Chem.*, 2008, **283**, 8810–8821.
509 A. B. Northrup, *Science (80-.).*, 2004, **305**, 1752–1755.
510 V. G. Dumas, L. A. Defelipe, A. A. Petruk, A. G. Turjanski and M. A. Marti, *Proteins Struct. Funct. Bioinforma.*, 2014, **82**, 1004–1021.
511 J. J. Li, T. S. Mei and J. Q. Yu, *Angew. Chemie - Int. Ed.*, 2008, **47**, 6452–6455.
512 Q. Yu, N. Zhang, J. Huang, S. Lu, Y. Zhu, X. Yu and K. Zhao, *Chem. - A Eur. J.*, 2013, **19**, 11184–11188.
513 N. R. Deprez and M. S. Sanford, *J. Am. Chem. Soc.*, 2009, 131, 11234–11241.
514 D. Li, N. Xu, Y. Zhang and L. Wang, *Chem. Commun.*, 2014, **50**, 14862–14865.
515 D. Shabashov and O. Daugulis, *J. Org. Chem.*, 2007, **72**, 7720–7725.
516 Q. Liu, Q. Li, Y. Ma and Y. Jia, *Org. Lett.*, 2013, **15**, 4528–4531.
517 V. Sridharan, P. A. Suryavanshi and J. Carlos Menéndez, *Chem. Rev.*, 2011, **111**, 7157–7259.
518 A. R. Katritzky, S. Rachwal and B. Rachwal, *Tetrahedron*, 1996, **52**, 15031–15070.
519 S. N. Pandeya and A. Tyagi, *Int. J. Pharm. Pharm. Sci.*, 2011, **3**, 52–61.
520 T. Suzuki, S. Fujita, S. Narimatsu, Y. Masubuchi, M. Tachibana, S. Ohta and M. Hirobe, *FASEB J.*, 1992, **6**, 771–776.
521 R. S. Obach and D. K. Dalvie, *Drug Metab. Dispos.*, 2006, **34**, 1310–1316.
522 R. E. Martin, J. D. Aebi, B. Hornsperger, H. J. Krebs, B. Kuhn, A. Kuglstatter, A. M. Alker, H. P. Märki, S. Müller, D. Burger, G. Ottaviani, W. Riboulet, P. Verry, X. Tan, K. Amrein and A. V. Mayweg, *J. Med. Chem.*, 2015, **58**, 8054–8065.
523 H. J. Son, S. H. Han, J. A. Lee, C. S. Lee, J. W. Seo, D. Y. Chi and O. Hwang, *Eur. J. Pharmacol.*, 2016, **771**, 152–161.
524 J. R. Cabrero-Antonino, R. Adam, K. Junge, R. Jackstell and M. Beller, *Catal. Sci. Technol.*, 2017, **7**, 1981–1985.
525 S. Murahashi, T. Oda, T. Sugahara and Y. Masui, *J. Org. Chem.*, 1990, **55**, 1744–1749.
526 K. W. Anderson, T. Ikawa, R. E. Tundel and S. L. Buchwald, *J. Am. Chem. Soc.*, 2006, **128**, 10694–10695.
527 W. Zhou, L. Zhang and N. Jiao, *Tetrahedron*, 2009, **65**, 1982–1987.
528 A. V. Aksenov, I. V. Aksenova, I. V. Malikova and N. A. Aksenov, *Russ. J. Org. Chem.*, 2009, **45**, 1416–1417.
529 A. Z. Shyadehi, D. C. Lamb, S. L. Kelly, D. E. Kelly, W. H. Schunck, J. N. Wright, D. Corinat and M. Akhtart, *J. Biol. Chem.*, 1996, **271**, 12445–12450.
530 E. Poupon and E. Gravel, *Chem. - A Eur. J.*, 2015, **21**, 10604–10615.
531 P. R. Ortiz de Montellano, in *Cytochrome P450*, Springer International Publishing, Cham, 2015, pp. 111–176.
532 I. M. Bell, J. M. Erb, R. M. Freidinger, S. N. Gallicchio, J. P. Guare, M. T. Guidotti, R. A. Halpin, D. W. Hobbs, C. F. Homnick, M. S. Kuo, E. V. Lis, D. J. Mathre, S. R. Michelson, J. M. Pawluczyk, D. J. Pettibone, D. R. Reiss, S. Vickers, P. D. Williams and C. J. Woyden, *J. Med. Chem.*, 1998, **41**, 2146–2163.
533 S. Kaiser, S. P. Smidt and A. Pfaltz, *Angew. Chemie Int. Ed.*, 2006, **45**, 5194–5197.
534 T. Putkonen, A. Tolvanen, R. Jokela, S. Caccamese and N. Parrinello, *Tetrahedron*, 2003, **59**, 8589–8595.
535 L.-W. Hsin, L.-T. Chang and H.-L. Liou, *Synlett*, 2008, **2008**, 2299–2302.
536 D. R. Boyd, R. J. H. Davies, L. Hamilton and J. J. McCullough, *J. Chem. Soc. Perkin Trans. 1*, 1992, 31.
537 G. Tangherlini, D. V. Kalinin, D. Schepmann, T. Che, N. Mykicki, S. Ständer, K. Loser and B. Wünsch, *J. Med. Chem.*, 2019, **62**, 893–907.
538 T. Rodrigues, D. Reker, J. Kunze, P. Schneider and G. Schneider, *Angew. Chemie Int. Ed.*, 2015, **54**, 10516–10520.
539 S. K. Agarwal, D. R. Boyd, R. J. H. Davies, L. Hamilton, D. M. Jerina, J. J. McCullough and H. P. Porter, *J. Chem. Soc. Perkin Trans. 1*, 1990, 1969.
540 M. KAWASE and Y. KIKUGAWA, *Chem. Pharm. Bull. (Tokyo).*, 1981, **29**, 1615–1623.

541 R.-G. Xing, Y.-N. Li, Q. Liu, Y.-F. Han, X. Wei, J. Li and B. Zhou, *Synthesis (Stuttg).*, 2011, **2011**, 2066–2072.
542 K. M. Solntsev, C. E. Glower, L. M. Tolbert and D. Huppert, *J. Am. Chem. Soc.*, 2005, **127**, 8534–8544.
543 K. H. He, F. F. Tan, C. Z. Zhou, G. J. Zhou, X. L. Yang and Y. Li, *Angew. Chemie - Int. Ed.*, 2017, **56**, 3080–3084.
544 US Patent and Trademark Office, US20050250820, 2005.
545 Y. Hwang, Y. Park, Y. B. Kim, D. Kim and S. Chang, *Angew. Chemie - Int. Ed.*, 2018, **57**, 13565–13569.
546 Z. Jia, Q. Yang, L. Zhang and S. Luo, *ACS Catal.*, 2019, **9**, 3589–3594.
547 J. Wu, S. Xiang, J. Zeng, M. Leow and X. W. Liu, *Org. Lett.*, 2015, **17**, 222–225.
548 US2017275277 (A1), 2017.
549 A. E. Wendlandt and S. S. Stahl, *J. Am. Chem. Soc.*, 2014, **136**, 11910–11913.
550 F. He, T. Mori, I. Morita, H. Nakamura, M. Alblova, S. Hoshino, T. Awakawa and I. Abe, *Nat. Chem. Biol.*, 2019, **15**, 1206–1213.
551 S. Chen, Q. Wan and A. K. Badu-Tawiah, *Angew. Chemie*, 2016, **128**, 9491–9495.
552 P. A. Claret and A. G. Osborne, *Spectrosc. Lett.*, 1977, **10**, 35–42.
553 T. Tsuritani, Y. Yamamoto, M. Kawasaki and T. Mase, *Org. Lett.*, 2009, **11**, 1043–1045.
554 H. Ouellet, J. B. Johnston and P. R. O. de Montellano, *Trends Microbiol.*, 2011, **19**, 530–539.
555 V. A. Mamedov, V. L. Mamedova, V. V. Syakaev, D. E. Korshin, G. Z. Khikmatova, E. V. Mironova, O. B. Bazanova, I. K. Rizvanov and S. K. Latypov, *Tetrahedron*, 2017, **73**, 5082–5090.
556 J. A. Weitgenant, J. D. Mortison and P. Helquist, *Org. Lett.*, 2005, **7**, 3609–3612.
557 H. Y. Choi and D. Y. Chi, *J. Am. Chem. Soc.*, 2001, **123**, 9202–9203.
558 G. F. Zha, W. Y. Fang, J. Leng and H. L. Qin, *Adv. Synth. Catal.*, 2019, **361**, 2262–2267.
559 K. Paridala, S. M. Lu, M. M. Wang and C. Li, *Chem. Commun.*, 2018, **54**, 11574–11577.
560 C. Sen and S. C. Ghosh, *Adv. Synth. Catal.*, 2018, **360**, 905–910.
561 US Patent and Trademark Office, US5112817 (A), 1992.
562 K. A. Korvinson, H. K. Akula, C. T. Malinchak, D. Sebastian, W. Wei, T. A. Khandaker, M. R. Andrzejewska, B. Zajc and M. K. Lakshman, *Adv. Synth. Catal.*, 2020, **362**, 166–176.
563 K. J. Liu, S. Jiang, L. H. Lu, L. L. Tang, S. S. Tang, H. S. Tang, Z. Tang, W. M. He and X. Xu, *Green Chem.*, 2018, **20**, 3038–3043.
564 Y. Xu, M. C. Young, C. Wang, D. M. Magness and G. Dong, *Angew. Chemie Int. Ed.*, 2016, **55**, 9084–9087.
565 J. P. Abell and H. Yamamoto, *J. Am. Chem. Soc.*, 2009, **131**, 15118–15119.
566 M. N. Wenzel, P. K. Owens, J. T. W. Bray, J. M. Lynam, P. M. Aguiar, C. Reed, J. D. Lee, J. F. Hamilton, A. C. Whitwood and I. J. S. Fairlamb, *J. Am. Chem. Soc.*, 2017, **139**, 1177–1190.
567 J. H. Capdevila, S. Wei, C. Helvig, J. R. Falck, Y. Belosludtsev, G. Truan, S. E. Graham-Lorence and J. A. Peterson, *J. Biol. Chem.*, 1996, **271**, 22663–22671.
568 D. H. R. Barton, J. Boivin, D. Gaudin and K. Jankowski, *Tetrahedron Lett.*, 1989, **30**, 1381–1382.
569 D. P. Affron, O. A. Davis and J. A. Bull, *Org. Lett.*, 2014, **16**, 4956–4959.
570 J. Wang, S. D. Cady, V. Balannik, L. H. Pinto, W. F. DeGrado and M. Hong, *J. Am. Chem. Soc.*, 2009, **131**, 8066–8076.
571 D. Willcox, B. G. N. Chappell, K. F. Hogg, J. Calleja, A. P. Smalley and M. J. Gaunt, *Science (80-.).*, 2016, **354**, 851–857.